MOLECULAR AND CELLULAR BASIS OF CHILDHOOD-ONSET NEURODEGENERATIVE DISORDERS

By

AHMAD ALZAHRANI

A thesis submitted to the University of Birmingham for the degree of DOCTOR OF PHILOSOPHY

Institute of Cancer and Genomic Sciences

College of Medical and Dental Sciences

University of Birmingham

April 2023

Abstract

The neuronal ceroid lipofuscinoses (NCL) are a group of inherited progressive neurodegenerative diseases with variable ages of onset and a group of inherited lysosomal storage disorders that affect the brain and retina. One of the NCL disease genes is CLN7, which encodes a lysosomal membrane protein. The function of the CLN7 protein requires further study to discover how it functions in the lysosomal membrane and at synapses. Mutations in *Drosophila* CLN7 leads to developmental abnormalities in synapses but it is not clear how CLN7 operates at the synapse. One method of investigating CLN7 function is to identify its partner proteins in membrane complexes. Proximity labelling using BioID was used *Drosophila* cells *in vitro* to proteins neighbouring CLN7. CLN7 was seen to interact with multiple proteins, in particular with many related to cytoskeleton function, with proteins present at the *Drosophila* neuromuscular junction where CLN7 is also resident, and with glial proteins. However, the BioID technique proved impossible to apply *in vivo* in *Drosophila*. Therefore, I used a second-generation proximity labelling variant technique, TurboID, in both *Drosophila* S2 cells and *in vivo* in both *Drosophila* larval and adult stages. TurboID proximity labelling identified numerous CLN7-interacting proteins related to the cytoskeleton, synapse and plasma membrane. Several of these overlapped with the previous experiments. My experiments have identified key protein partners for CLN7 that will help discover how CLN7 functions at the synapse to regulate neural development.

For the role of CLN7 in *Drosophila* growth and development, I have shown that CLN7 mutant flies are larger than controls with potential dysregulation of mTORC signalling underpinning the dysregulation of growth and neurodevelopment.

Acknowledgement

Alhamdulillah, always and forever, praise be to Allah, who blessed me and provided me with his help and mercy.

Firstly, I would like to thank my supervisor, Richard Tuxworth, for his help and advice during my study period. He guided and supported me during very difficult moments in my academic life. Thank you, Richard, for your patience and for standing by me (as I was a unique case in your lab team). Your support is greatly appreciated.

Additionally, I extend my gratitude to the wonderful people I met in our office and lab. Whether it was through their assistance or a simple chat and some joking, their presence made my study time more enjoyable.

I would like to thank the amazing people whom I met in Birmingham. In particular, Uncle Abdurahman, the wonderful Arabic man, stood by me when I arrived in Birmingham. He always invites me to his home, and I am truly grateful for his kindness and generosity. Additionally, I want to express my gratitude to my best friend in Birmingham, Ahmed Farhan. Ahmed has a very kind heart, and I appreciate all the time we've spent together—especially the tasty breakfasts on Saturday mornings. Moreover, I cannot forget my Saudi best friend, Hakeem. Our afternoon breaks for some gossip have been delightful. Thank you, Hakeem, and I wish you a lovely life.

I thank Kyle, as I started my project with him and followed his advice. Additionally, I would like to thank Naser, Jamming, Uncar, and Matt, as well as all the kind people who provided me with amazing explanations and excellent solutions when I faced some unusual problems.

My nephew Laith and niece Ethar are very lovely and wonderful kids. They always ask me about the return date to Saudi Arabia. Thanks to you all for our Telegram chats, and a special greeting to your beautiful sister (a little Thana).

Last but most importantly, my Mum, you do not know how much I love and admire you. You mean everything to me and my life. I cannot thank you enough for your love, care, inspiration, direction, and lovely and kind advice. Many thanks to all my family members for their help, kindness, and support.

Contents

LIST OF FIGURES

LIST OF TABLES

LIST OF ABBREVIATIONS

Abbreviation	Meaning
LAMP	Lysosomal-associated membrane protein
v-ATPase	Vascular H^+ ATPase
TOR	Target of rapamycin
mTORC1	Mammalian target of rapamycin complex 1
NCLs	Neuronal ceroid lipofuscinoses
TFEB	Transcriptional factor EB
ATP	Adenosine triphosphate
TPC	Two pore channels
MCOLN1	Mucolipin TRP Cation Channel 1
LMPs	Lysosomal membrane proteins
SCARB2	Scavenger receptor class B member 2
LSDs	Lysosomal storage disorders
NPC	Niemann-Pick type C
GBA	Glucocerebrosidase
CMA	Chaperone-mediated autophagy
AMPK	Adenosine monophosphate-activated protein kinases
PKA	protein kinase A
LC3	microtubule-associated protein light chain 3
GTP	Guanosine triphosphate
ER	Endoplasmic reticulum
UPR	Unfolded protein response
NMJ	Neuromuscular junction
Ach	Acetylcholine
AChE	Acetylcholinesterase
AChRs	Acetylcholine receptors
SV	Synaptic vesicles
nAchRs	Nicotinic acetylcholine receptors
AP	Action potential
mAP	Membrane action potential
PSDs	Postsynaptic densities
CNS	Central nerve system
PNS	Peripheral nerve system
CLN	Ceroid lipofuscinosis neuronal
CLEAR	Coordinated lysosomal expression and regulation
TPP1	Tripeptidyl-peptidase 1
Cath-D	Cathepsin D
MFSD8	Major facilitator superfamily domain containing 8
vLINCL	variant late infantile neuronal ceroid lipofuscinosis
FPP	fingerprint profiles
RLP	rectilinear profiles
LINCL	late infantile neuronal ceroid lipofuscinosis
CB	Cerebellar

Les	Late endosomes
PKB	Protein kinase B
MEF	Mouse embryonic fibroblast
SILAC	Stable Isotope Labelling by Amino acids in Cell culture
KO	Knock out.
Aga	Aspartylglucosaminidase
Siae	Sialate O-acetylesterase
Gns	N-acetylglucosamine-6-sulfatase
Naaa	N-acetylethanolaminehydrolyzing acid amidase
Cpq	carboxypeptidase Q
Prcp	Lysosomal Pro-X carboxypeptidase
Dpp2	dipeptidyl peptidase 2
Pcyox1	includes prenyl cysteine oxidase
NPc2	Niemann Pick type C2 protein
Psap	Prosaposin
SCMAS	Subunit c of mitochondrial ATPsae synthase
IGF	insulin/insulin-like growth factor
ILPs	insulin-like peptides
IPC	insulin producing cell
DILP	Drosophila insulin-like peptide
InR	insulin-like receptor
PIP2	phosphatidylinositol-4,5-bisphophate
PTEN	Phosphate and tensin homolog
PIP3	PI-3,4,5-triphosphate
AMPK	AMP-activated protein kinase
IRS	Insulin receptor substrates
AMPK	Adenosine 5’-monophosphate-activated protein kinases
PTEN	Phosphate and tension homology deleted on chromosome ten
TSC	Tuberous sclerosis complex
ULK1	Unc-51 like autophagy activating kinase 1
PKCa	Protein kinase C- alpha
DDM	n-Dodecyl-beta-Maltoside Detergent
SMALPs	Styrene Maleic-Acid Lipid Particles

1.INTRODUCTION

1.1. Lysosomes

1.1.1. Lysosomal organelles

Lysosomes are considered the primary degradative compartments found in eukaryotic cells. Depending on the cell type, species and context, the lysosomes have different sizes, shapes, numbers, and functions. Hundreds of lysosomes between 0.1 µm and 1 µm in diameter are found in most metazoan animal cells while yeast and plant cells enclose just one or a few lysosomes [1]. The lysosome is enclosed by a single phospholipid bilayer of 7-10 nm thickness which includes numerous transmembrane proteins. 80% of the lysosomal membrane proteins are lysosome-associated membrane protein 1 (LAMP1) and LAMP2 [1]. LAMP and other proteins are heavily glycosylated and form the glycocalyx. This provides a protective coat against auto-digestion of the limiting membrane by the lytic enzymes resident within the lysosomal lumen, which are active at low pH (pH 4.5 – 5.5) of the lysosome internal environment. The lysosome luminal acidity is activated by the pumping of protons by the vascular H^+ ATPase (v-ATPase) which is supported by an opposite flow of other ions such as Cl^-, Na^+, and K^+ [1-3]. The lysosome acidity provides an ideal environment for the luminal hydrolase function and facilitates the degradation of macromolecules to produce amino acids, monosaccharides and free fatty acids which are then transferred to the cytoplasm of the cell through special permeases (Figure1.1 and Figure 1.2) [1, 3].

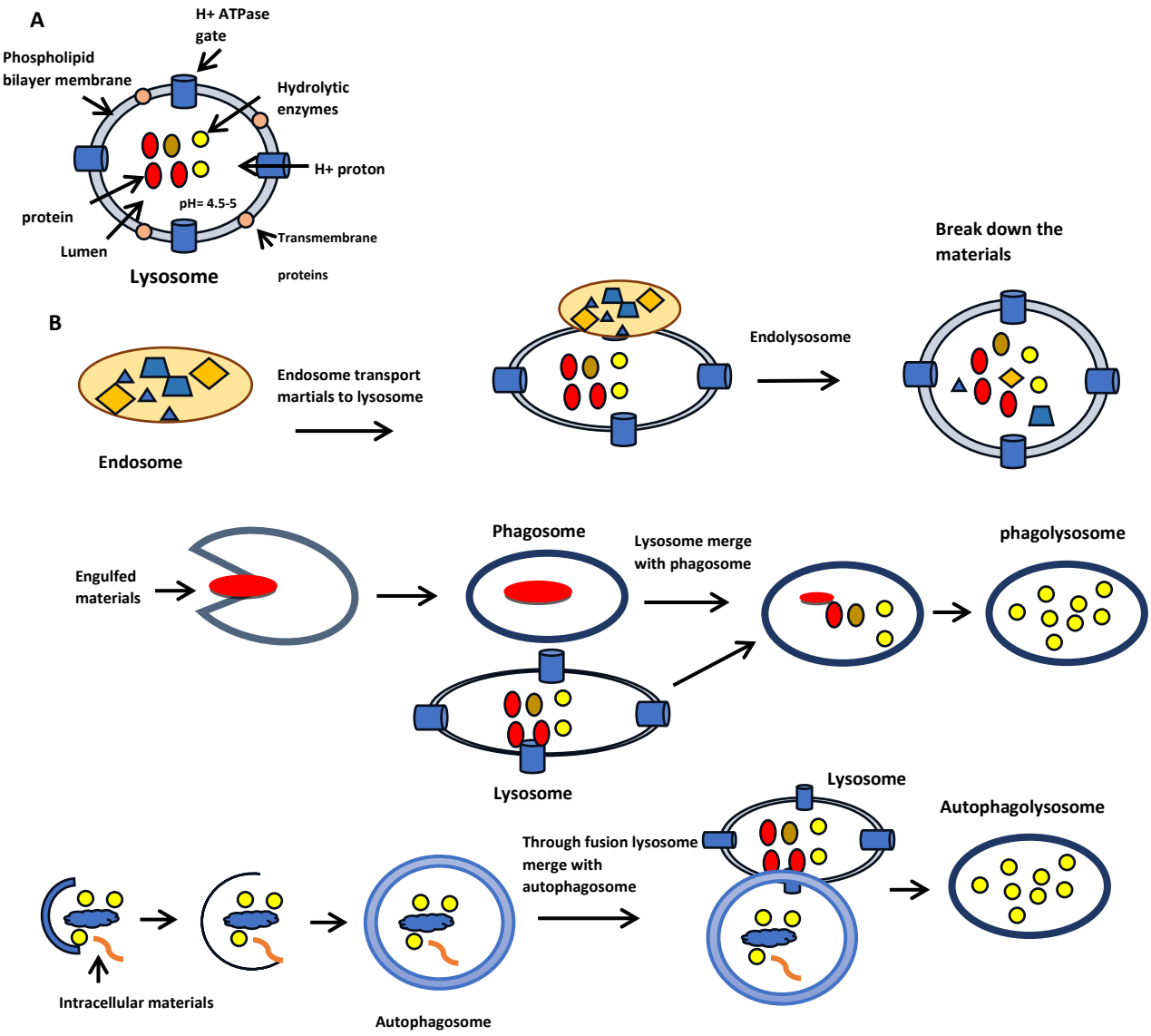

Figure 1. 1: The lysosome structure and function.

A schematic diagram of lysosomal structure and function diagram including **(A)** the structure of lysosome as it correlated by double membrane layer (phospholipid bilayer). It includes membrane proteins, in addition to H+ ATPase gates to pump H+ proton to the lysosomal lumen to keep its acidity at pH 4.5- 5. Hydrolytic enzyme inside the lysosome including nucleases, protases, lipases, glucosidases, and acid phosphatases to breakdown the macromolecules. **(B)** Indicate to the breakdown macromolecule inside the lysosome as with endosome the materials taken to the lysosome for breakdown. In the case of a phagosome, materials including microorganisms, senescent cells, or apoptotic cells are engulfed and then transported to fuse with the lysosome. The phagosome has membrane-bound proteins that recruit and fuse with the lysosome to form a phagolysosome. An autophagosome is a double-layer membrane that engulfs intracellular materials (the target contents) and transports this autophagic cargo to the lysosome to form an autophagolysosome.

1.1.2. Lysosome function

Lysosomes are intracellular hydrolytic organelles that degrade several macromolecules and whole damaged organelles. Acid hydrolases include protease, lipases, glycosidases, nuclease, sulfatases, and acid phosphatases which digest all the macromolecule classes comprising lipids, nucleic acids, proteins, and carbohydrates [1, 4]. Phagocytosis and macropinocytosis and clathrin and caveolin-dependent and -independent endocytosis are used to import macromolecules from the extracellular space to feed the lysosomal system for the degradation process [1, 3]. Damaged or misfolded proteins cytoplasmic macromolecules and the entire organelles are taken to the lysosome via autophagy (Figure 1.1) [3-5]. Consequently, lysosomal processing is important for removing toxic cellular components, terminating signal transduction processes, elimination of worn-out organelles and maintaining metabolic homeostasis [6]. However, lysosome functions are essential for cellular health maintenance [4, 7].

Not only is the lysosome important for degradation and recycling, but it also acts as a nexus for integrating cellular growth and stress signalling and responses. Multiple signalling pathways converge on the lysosome including protein kinases and phosphatases, ion and nutrient transporters and transcription factors and transcriptional regulators [1, 8]. The lysosome has an essential role in the nutrient sensing and metabolic regulation through its physical and functional association with the master target of rapamycin complex 1 (m TORC1) [1, 4]. mTORC1 is a protein kinase complex that is built around the ancient serine-threonine kinase mTOR [9]. It has been identified that the lysosome plays a critical role in the main inputs to mTORC1. The mTORC1 complex is recruited to the surface of the lysosomes in amino acid and growth factor-rich conditions where it activates downstream

programmes and lead to cell growth and proliferation. In contrast, under conditions of cellular stress, including oxidative stress or starvation, the mTORC1 complex dissociated from the lysosomal surface and the cell activates stress response pathways. Hence, mTORC1 works as a nutrient sensor on the lysosomal surface and is affected by dynamic changes in energetic state of the cell. In addition, several adaptive lysosomal responses like biogenesis, reformation, and autophagy are regulated by mTORC1 [4, 10, 11].

Ras homologue enriched in brain (Rheb) is a GTP-binding protein [12], that activates the mTORC1 on the lysosomal surface through two mechanisms. First, mTORC1 is translocated to the lysosome under the stimulation of Rags and nutrients. Second, Rheb from its GDP-bound form to a GTP-bound form in response to growth factors. When amino acids are sufficient, mTORC1 is translocated from the cytoplasm to the lysosome [13]. Additionally, amino acids activate Ragulator, which regulates Rag GTPase to recruit mTORC1 to the lysosome. Rag and Ragulator are components of the lysosome nutrient sensing machinery (LYNUS). Rag forms a heterodimeric complex containing Rag A or B with Rag C or D [13]. In contrast, Ragulator acts as a guanine nucleotide exchange factor (GEF) and consists of a pentameric complex with subunits LAMTOR1-5. Additionally, in response to amino acids, the signalling adaptor p62 and E3 ubiquitin play a role in recruiting mTORC1 to the lysosome. Active Rags facilitate the recruitment of mTORC1 to Rheb on the lysosomal surface[13].

When growth factors are stimulated, PI3K produces PIP3 in the plasma membrane, which leads to the activation of protein kinase B (Akt) [14]. Akt, a serine/threonine kinase [15], Tuberous sclerosis complex 2 (TSC2) is then phosphorylated and inhibited by the serine/threonine kinase Akt, which works as the Rheb GTPase activation protein (GAP) at the surface of the lysosome [14]. However, Rheb, which binds and activates mTORC1, is

regulated by TSC1, TSC2, and TBC1. The activation of TSC1 and TSC2 leads to the inhibition of Rheb, which in turn inhibits mTORC1 activity [16]. On the other hand, inhibition of the TSC complex activity leads to the activation of Rheb-GTP, which directly binds and stimulates mTORC1 at the surface of the lysosome [13].

Guanine nucleotide exchange in Rag is stimulated by amino acids [13], and Rag senses amino acids to activate mTORC1, possibly through v-ATPase. As amino acids are sensed in the lysosomal lumen via v-ATPase, this leads to the activation of Rag through Ragulator. In this process, Rag activation requires ATP hydrolysis by the v-ATPase [17]. Another mechanism involves proton-assisted amino acid transport (PAT1), which pumps amino acids out of the lysosome lumen and interacts with Rag, leading to the activation of mTORC1 [18]. Leucine, which is sensed via glutaminolysis, acts as an activator of Rag. Additionally, leucine activates glutamate dehydrogenase (GDH), which produces alpha-ketoglutarate. Alpha-ketoglutarate activates Rag via an unknown mechanism [13, 19].

Hence, mTORC1-mediated signals are stimulated by the lysosomal surface which appears to play a role as a metabolic signalling centre that incorporates nutritional information from the interior of the lysosome and the cytoplasm, leading to the balanced regulation between biosynthetic and catabolic. How this process is regulated by lysosomal membrane proteins is not fully understood and needs further studies [1, 4].

1.1.3. Lysosomal acidification

Lysosomal acidification is reported to be dysregulated in all neuronal ceroid lipofuscinoses (NCLs) except CLN2 and CLN8 [20]. Endocytic organelle acidification is important for the degradation and clearance of endogenous and exogenous materials which are distributed to

the lysosome through the pathways of endosomes and autophagosomes. The acidity of lysosome is adjusted by V-ATPase which is a multi-subunit protein compound including a lysosomal membrane-anchored V0-sector and a cytosolic V1-sector. Most intracellular organelles are acidified by the v-ATPase by pumping protons across the membrane into the vesicular lumen. By hydrolysing ATP, the V1-sector produces energy that is used to facilitate proton transport from the cytoplasm to the vesicular lumen through the lysosomal membrane (Figure 1.1) [21]. Cell surface receptor recycling, protein degradation by lysosomal hydrolases, the dissociation of receptor-ligand complexes, neurotransmitter loading, and synaptic vesicle recycling all depend on lysosomal pH. In addition, it has been shown that intracellular pH changes lead to alterations in organelle morphology, movement, and function [2, 21]. Lysosomal pH dysregulation leads to the disruption of endocytic function, autophagic degradation, and the biogenesis and transport of macromolecules, causing metabolic disorders, immunological diseases, and proteinopathic neurodegenerative diseases. Inflammatory diseases might occur because lysosomal acidity deficiency affects mitochondrial function [22]. Additionally, pH deficiency causes disorders in many lysosomal enzymes and impairs the clearance of several substrates, including protein aggregates, contributing to many diseases, including lysosomal storage disorders (LSDs) [6].

1.1.4. Lysosomal exocytosis

Lysosomal exocytosis is the process of secretion of lysosomal content, which is observed by the translocation of lysosomal membrane proteins markers to the plasma membrane. Through this process, the lysosomes fuse with the plasma membrane via a Ca^{2+}-regulated

mechanism which leads to lysosomal content being released into the extracellular matrix [23, 24]. The lysosomal exocytosis process plays an important role in the repair of the plasma membrane, in addition to the secretion of lysosomal content. In cases of injury to the plasma membrane, the lysosomes move to the injured site and fuse to the plasma membrane [23-25]. The lysosomal exocytosis process is important in the mechanisms of defence against the infection of bacteria, and it has been found that this process affects a specific type of muscular dystrophy [23, 24]. Transcriptional factor EB (TFEB) regulates lysosomal exocytosis by controlling both lysosomal docking and fusion with the plasma membrane through the regulation of gene expression. The lysosomal nonselective cation channel (MCOLN1) is mutated in mucolipidosis IV (MLIV), which is considered a type of LSD. The lysosomal exocytosis is decreased in MLIV cells. MCOLN1 regulates intralysosomal Ca release, which affects the lysosomal exocytosis. It has been shown that TFEB regulates the gene encoding MCOLN1, indicating the effect of TFEB on lysosomal exocytosis [26]. Moreover, the Coordinated Lysosomal Expression and Regulation gene network (CLEAR) has been discovered to be regulated by TFEB. CLEAR appears to regulate several lysosomal functions, including lysosomal exocytosis, which enhances the effect of TFEB on lysosomal exocytosis [27].

TFEB upregulates the expression of genes whose protein products increase lysosomal dynamics and lead to a mucolipin 1-mediated rise in intracellular Ca^{2+}. In addition, osteoclast differentiation and bone resorption are affected by TFEB mediated regulation of the lysosomal exocytosis process [4, 7, 23].

1.1.5. Roles of lysosomal Ion in signalling, exocytosis, and membrane repair

Numerous ion channels in the lysosomal membrane transport ions, including Na^+, K^+, Ca^{2+} and Cl^- and their movement across lysosomal channels creates a resting lysosomal membrane potential that supports the maintenance of the proton gradient established by the v-ATPase. It regulates the Ca^{2+} release during lysosomal exocytosis and amino acid transport regulation from the lysosomal lumen during starvation. Consequently, the lysosomal membrane potential is a part of lysosomal function [28].

The two-pore channels 1 and 2 (TPC1 and TPC2) establish the lysosomal membrane potential in addition to 12-transmembrane-spanning Na^+ channels that regulate the large Na^+ currents. The Na^+ cation is found at a high level in the lysosomal lumen and the lysosomal membrane potential can be affected by its movement to the cytoplasm [28] [29]. TPC1 and TPC2 activity is regulated by nutrients and these complexes are inhibited by active mTORC1 and high levels of ATP. During starvation, the removal of inhibition of TPC1 and TPC2 combined with the increase in Na^+ currents out of the lysosome caused by decreased levels of ATP and inactivation of mTORC1, Resulting in lysosomal membrane depolarization [23, 29]. During starvation, arginine and lysine, two cationic amino acids, are released from the lysosome lumen as a result of the lysosomal membrane depolarisation. During famine, this flow of amino acids is crucial for sustaining energy levels [29].

Phosphatidylinositol 3, 5-bisphosphate (PI (3,5) P_2) is a phosphoinositide found in the endo-lysosomal system [30, 31]. In addition, the mucolipin TRP cation channel 1 (MCOLN1), which is a Fe^{2+}, Ca^{2+} and Zn^{2+}-permeable channel, selectively localises to the membrane of lysosomes. Lysosomal exocytosis is stimulated by Ca^{2+}, which is released from the lysosomal lumen by MCOLN1 and that Ca^{2+}flux is important for the fusion of lysosomes with other

organelles, including endosomes and phagosomes. Lysosomal exocytosis is important for several processes, including the function of immune cells during parasitic attacks, bone resorption by osteoclasts, the function of melanocytes for skin pigmentation and fertilization. MCOLN1 mutations leads to the inherited lysosomal storage disorder, mucolipidosis type IV. An imbalance in lysosomal levels of PI (3,5) P_2 can cause lysosomal enlargement and lead to neurodegeneration [1, 30, 31].

1.1.6. Transcription regulation of lysosomal function

Lysosomal functions are regulated by transcriptional control, and coordinated transcriptional control regulates several lysosomal genes, including hydrolysis, lysosomal membrane permeases, and the proteins associated with the lysosome [1].

Lysosomal functions are regulated by the MiT/TFE transcriptional factor family, which contains TFEB, a basic helix-loop-helix transcription factor that binds to genes including the CLEAR element network [32]. Additionally, activated TFEB, activation of which depends on nutrient status, regulates autophagy [32]. During nutrient-replete conditions, mTORC1 binds to TFEB at the lysosomal surface, causing the isolation of 14-3-3 binding and cytoplasmic localization [33, 34]. Under starvation conditions, the lysosomal calcium channel MCOLN1 releases calcium, which activates Ca-dependent phosphate and calcineurin. This leads to the dephosphorylation of TFEB, ultimately activating the target genes [32].

It has been investigated that TFEB stimulates the expression of several proteins that regulate autophagy processes, including the initiation of autophagosome formation, elongation, substrate capture, and autophagosome trafficking. Additionally, TFEB is involved in fusion of autophagosomes with lysosomes [35, 36]. Consequently, A key player in cellular

catabolism, TFEB encourages cells to use autophagy to choose and seize substrates, which are then degraded by the lysosome [35, 36].

Rag GTPase is also an important component of the TFEB regulation. RagD mutations inhibit TFEB nuclear translocation under starved conditions of amino acids [37]. Conversely, dominant-negative Rag GTPase, promotes the accumulation of TFEB in the nucleus [34]. TFE3 and MITF, both sub-members of the MiT/TFE family, mediate a nutrient-dependent lysosomal response in a similar manner [33]. Alongside mTORC1, other growth-regulating kinases, including MEK/ERK and Glycogen Synthase Kinase 3 (GSK3), have an impact on MiT/TFE [36].

The zinc-finger transcription factor ZSCAN3 is found at the promoters of multiple lysosomal genes and is involved in the suppression of lysosomal gene expression, which leads to inhibition during nutrient-replete conditions [32]. ZKSCAN3 is found in the nucleus under full nutrient conditions. However, during starvation or mTORC1 inhibition, ZKSCAN3 is driven out of the nucleus [1, 32]. This leads to the catabolic processes that mediate the cellular response to starvation are activated [1].

Other transcription pathways, including the aforementioned X receptor (FXR), contribute to regulating autophagy-lysosome function. in mammals, During feeding, bile acids stimulate FXR, which then binds to the promoters of multiple lysosomal and autophagic genes as well as the TFEB promoter, suppressing their expression [38]. In the case of fasting, the transcriptional co-activator CRTC2 is drawn to the promoters of autophagic-lysosomal genes by the cAMP response element-binding protein (CREB). However, during feeding, FXR binds to CREB and removes CRTC2, leading to the inactivation of CREB [38]. Additionally,

Peroxisomal proliferator-activated receptor-α (PPARα), which stimulates the expression of genes related to autophagy and lipid degradation, is deactivated by FXR [39].

It has been highlighted that autophagic gene subsets are controlled by numerous transcriptional factors, including p53, activating transcription factor 4 (ATF4) and the forkhead box O (FOXO) proteins [10, 40, 41] [10, 42].

Autophagy regulators in tissues have been observed. For instance, Foxk1/2 transcription factors were found to be negative regulators of autophagic gene expression in the case of muscle atrophy. However, mTORC1 controls Foxk1/2 proteins positively, leading to autophagy inhibition in nutrient-rich conditions [43].

1.1.7. Lysosomal membrane proteins

The lysosomal membrane is not just a simple barrier between the acidic lysosomal lumen and the cytoplasm, it also controls multiple functions, and contains many proteins [44]. As the lysosomal membrane is between 7 and 10 nm thick [1], and many organelles are transported through it, the membrane has several essential proteins known as lysosomal membrane proteins (LMPs) (Figure: 1.2) [44]. In addition to transport processes via the lysosomal membrane, these proteins maintain the acidity of the lysosome lumen. Consequently, LAMPs are commonly extremely glycosylated [45]. LAMP-1 and LAMP-2 are considered the most abundant type-1 transmembrane proteins of the lysosomal membrane, with more than 10 used glycosylation sites. Glycosylation is a form of co-translational and post-translational modification. It is the process by which carbohydrates are covalently attached to target polypeptides, polynucleotides, proteins, and lipids. This process is stimulated by glycosyltransferase enzymes, which act on specific substrates of sugar-

nucleotide donors [46]. Several different glycans are produced through glycosylation, and they play a regulatory role in cellular proteins and lipids. Glycosylation is regulated by glycosyltransferases and glycosidases, which compose the carbohydrate structures [46, 47]. Protein glycosylation includes N-glycans, O-glycosylation, and glycosaminoglycans (proteoglycans). N-glycans bind to asparagine residues of proteins, particularly a subset found in the Asn-X-Ser/Thr motif [47]. O-glycans are linked to a subgroup of serines and threonines. Glycosaminoglycans are linear and attached to serine and threonine, and they are produced by different biosynthetic pathways [47].

Protein glycosylation is covalently linked to single sugars, polysaccharides, or complex oligosaccharides at select target protein residues. Glycosylation affects protein function, stability, subcellular localization, and other traits. It has significant effects on the stability, activity, solubility, and folding of proteins, as well as protecting proteins from proteases and subcellular targeting. Additionally, it contributes to the formation of protein complexes [48].

The major post-translational alteration of proteins is glycosylation, and many biological processes at the cellular, tissue, and whole-organism levels are regulated by glycoproteins [49]. Glycosylation regulates several biological processes, including lysosomal function. Therefore, glycosylation affects the activity and stability of several lysosomal glycoproteins [50]. The lysosomal membrane is protected by these glycosylated proteins because lysosomal-associated membrane proteins (LAMPs), which are extensively glycosylated proteins, cover the inner side of the lysosomal membrane. These LAMPs stop the self-degrading of the lysosomal membrane by lysosomal hydrolases [51].

In several cells, LAMP molecules are considered the major carriers for poly-N-acetyllactosamines, and numerous N-glycosylation sites acquire poly-N-acetyllactosamines.

Because LAMP molecules have very complex carbohydrates like poly-N-acetyllactosamines, they counteract many lysosomal hydrolytic enzymes in the lysosomes [45]. LAMPs are highly abundant inside the lysosomal membrane, and they form a coat on the lysosomal membrane's inner surface that acts as a barrier to soluble hydrolases. Consequently, poly-N-acetyllactosamines are associated with glycoproteins in the lysosomal membrane are important for maintaining the stability of lysosomes [45]. Moreover, indirectly, during exocytosis, glycoproteins most likely control how lysosomes fuse with phagosomes, autophagosomes, or the plasma membrane [44].

The glycoprotein layer probably plays an important role in lysosome stability and integrity, in addition to that it might regulate the fusion of lysosomes with phagosomes, autophagosomes or with the plasma membrane in the case of exocytosis. While the direct transport processes across the membrane depend partly on the transmembrane sections of lysosomal membrane proteins, the connection between cytosolic proteins and proteins in other organelles depends on the short cytosolic parts of these proteins [44]. This probably explains why some lysosomal membrane proteins are necessary for some processes such as lysosomal motility, lysosomal exocytosis, membrane repair, autophagy, phagocytosis, MHC class II-dependent antigen presentation and macroautophagy. However, studies have indicated that cytosolic signals and adaptor proteins are needed for the transport of lysosomal membrane proteins to the target organelles [44].

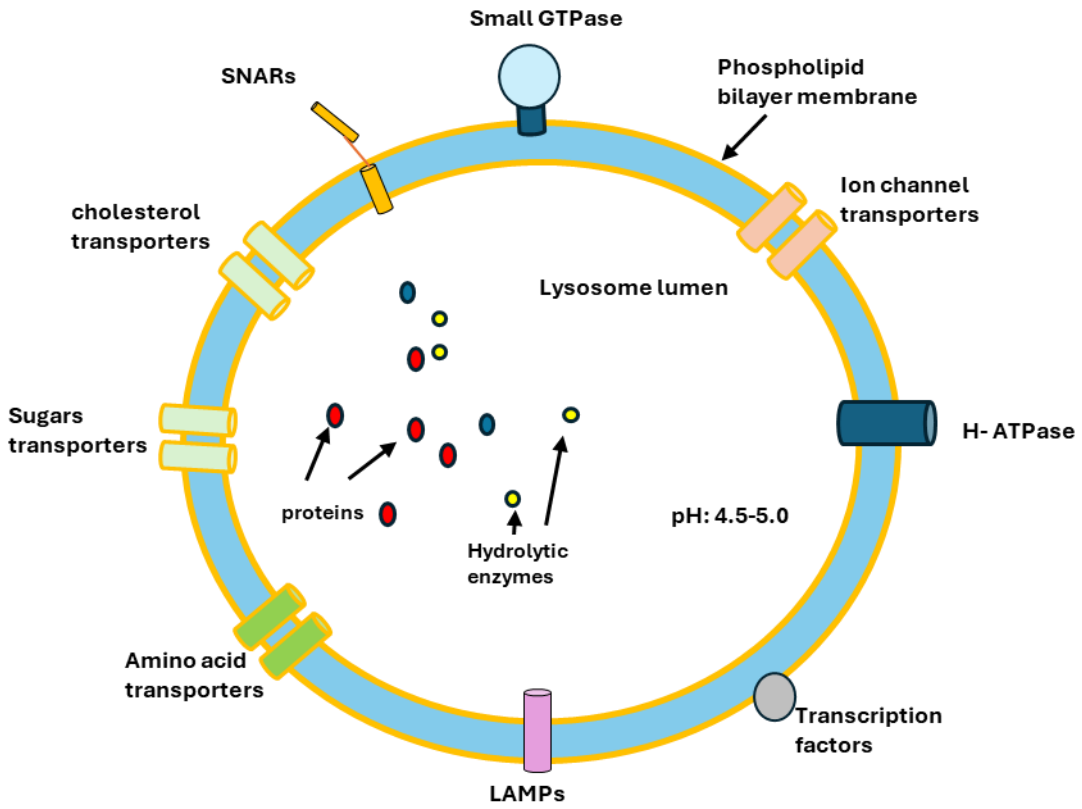

Figure 1. 2: The structure of lysosome with the lysosomal membrane proteins.

The lysosome is composed of a phospholipid bilayer membrane that contains membrane proteins and peripherally associated proteins. The lysosomal lumen has a highly acidic pH (4.5-5). The lysosomal membrane proteins include the highly glycosylated LAMPs proteins, which form a glycocalyx lining the organelle. Other membrane proteins include sugar, amino acid, cholesterol, and ion channel transporters. H-ATPase in the lysosomal membrane is used to pump H+ proton into the lysosome to maintain its acidity. There are other peripherally associated proteins, including SNAREs, small GTPases such as Rab7, and transcription factors like TFEB.

1.2. Lysosomal storage disorders

1.2.1. Lysosomal storage disorders overview

Lysosomal storage disorders (LSDs) are a group of heterogeneous and inherited metabolic disorders that result from lysosome enzyme deficiencies [6, 52, 53]. It has been estimated that LSDs occur in about 1 in 7000 live births [54]. Depending on the specific substrate and the accumulation site, this storage process leads to numerous clinical manifestations. Generally, although the rate of progression is variable, LSDs are progressive [53]. It is a common in all LSDs that specific macromolecules or monomeric compounds start to accumulate inside the lysosomal system, endosomal and autophagic [6]. A deficiency in acidic hydrolysis is a cause of many of LSDs [55]. However, a large number of these conditions are caused by defects in lysosomal membrane proteins [52-56].

1.2.2. The effect of Lysosome in LSDs

It has been observed that alterations in lysosomal function cause several disorders that are related to changes in the treatment and turnover of cellular constituents [6, 54]. As described above, mutations in lysosomal enzymes cause LSDs which are associated with severe neurodegenerative phenotypes. In addition, some mutations in endo-lysosomal genes related to LSDs are risk factors for late-onset neurodegenerative disorders such as Huntington's disease, Alzheimer's disease, Parkinson's disease, and frontotemporal dementia [6, 54].

The accumulation of biological macromolecules in the lysosomes, which results in the creation of sizable intracellular precipitates that impair cellular function, is what defines LSDs. These metabolic hereditary diseases occur from defects in proteins and enzymes

required in the biosynthesis and/or degradative function of lysosomes [57]. Proteins involved in lysosomal trafficking and transport, as well as the breakdown of lipids, proteoglycans, and proteins, may be impacted by lysosomal dysfunction in LSDs [57].

LSDs could be due to enzyme defects. Lysosomal enzyme deficiencies can lead to undegraded macromolecules, such as carbohydrates, lipids, and glycolipids. These substances are consequently stored. Perhaps LSDs occur due to activator defects. For example, the activity of hexosaminidases A and B was higher in the brain of patients with Tay-Sachs disease, indicating that this problem was not due to a hydrolysis defect, but rather an activator defect [52].

1.2.2.1. Different pathologies associated with lysosomal dysfunction

Lysosomal diseases are associated with defects in lysosomal function, deficiencies in lysosomal hydrolases, and deficiencies in lysosomal membrane-associated transporters [58].

The lysosome is important for maintaining cellular homeostasis as it protects cells against toxic agents and promotes immune regulation. Therefore, lysosomes are essential in protecting cells from death or damage due to their quick response to changing conditions [8]. Lysosomes have different sizes and shapes and depending on their positions in the cytosol and their structure, they can act and affect cells differently. There are many functions of lysosomes in the cell, and any dysregulation of their activity could affect cellular metabolic machinery, such as the transport and biogenesis of sugars, lipids, proteins, and nucleic acids. This might impair metabolic pathways, endocytosis, phagocytosis, and autophagy [8]. Lysosomal dysfunction or defects in fusion with vesicles containing cargo

result in neurodegenerative diseases. Lysosomal dysfunctions affect the activity of some organelles, including peroxisomes and mitochondria, increasing reactive oxygen species with pathological properties related to cancer, aging, neurological diseases, chronic inflammation, male infertility, and infections [8].

Mutations associated with most lysosomal storage diseases (LSDs) lead to various lysosomal dysfunctions, such as deficiencies in lysosomal hydrolases, resulting in the accumulation of their substrates [8].

Defects in lysosomal transit cause tiny molecules to collect inside the lysosomes, as opposed to lysosomal enzyme deficits, which cause the accumulation of undegraded macromolecules. These lysosomal transport defects include cystinosis, Salla disease, cobalamin F disease, J diseases, and mucolipidosis type IV [52].

Neurodegenerative diseases are characterised by the accumulation of aberrant proteins and organelles. Non-dividing neurons rely on the autophagy-lysosome pathway (ALP), which removes the aggregation of abnormal proteins and organelles. Defects in ALP and the accumulation of abnormal proteins cause several neurodegenerative diseases, including Huntington's disease (HD), Parkinson's disease (PD), and Alzheimer's disease (AD)[59].

Amyloid-beta (Aβ) peptides precipitating in extracellular amyloid plaques and neurofibrillary tangles accumulating in cells with phosphorylated microtubule-associated protein tau are two characteristics of Alzheimer's disease (AD) pathogenesis. ALP dysfunction is likely important for AD [59]. The cleavage of amyloid precursor protein (APP) depends on two pathways: the non-amyloidogenic pathway, which prevents Aβ formation, and the amyloidogenic pathway, which produces Aβ40 and Aβ42. Defects in lysosomal function or increased Aβ production lead to Aβ accumulation in neurons, resulting in in cell death and

the clinical signs of AD [59]. Neuronal axons include the microtubule-associated phosphoprotein tau, which promotes microtubule stabilisation and assembly. Tau accumulation is caused by ALP dysfunction, which results in hyperphosphorylated tau that builds up and creates neurofibrillary tangles in neurones, ultimately contributing to the development of neurodegeneration in AD patients. Hyperphosphorylation of tau likely leads to autophagy dysfunction due to neuronal microtubule instability, impairing the positioning and function of lysosomes [59].

To highlight the connection between lysosomes and AD disease, dysfunction in the autophagy-lysosome pathway (ALP) due to genetic variations leads to AD pathogenesis. Cathepsin B cleaves Aβ42, and in cases of genetic inactivation of that cathepsin in mice, it leads to increased Aβ42 deposition. Conversely, overexpression of cathepsin B decreases pre-existing amyloid protein deposition [60]. Additionally, it has been demonstrated that an increased AD risk is connected to the T allele of cathepsin D rs17571. Presenilin 1 (PS1) mutations cause early-onset familial AD. Consequently, the v-ATPase Voa1 subunit is dysregulated by the PS1 mutation, which leads to inactivated autophagy, elevated lysosomal pH, reduced proton pump activity, and lysosomal proteolysis failure. In the AD brain, there is a decrease in the expression of Beclin 1, an initiator of the autophagy pathway [60]. Consequently, neuronal autophagy is reduced, leading to Aβ deposition. However, Beclin 1 overexpression decreases Aβ accumulation 1. Transcriptional upregulation of lysosomal function by TFEB leads to APP dysfunction by lysosomes, which reduces Aβ levels in a mouse model of familial AD disease [60].

For Parkinson's disease (PD), the accumulation of misfolded proteins causes PD pathogenesis and reduces lysosomal function. Lewy bodies are mainly composed of alpha-

synuclein (α-syn), and when the aggregated proteins accumulate in these bodies, it leads to PD. Lysosomes play a crucial role in the degradation of α-syn in neurons via the chaperone-mediated autophagy (CMA) and macroautophagy pathways [61]. However, inhibition of either pathway results in an increase in α-syn levels. One of the genetic causes of PD is a mutation in α-syn, which leads to familial PD through protein fibrilization or accelerated oligomerization. Depletion of the ATPase cation transporter 13A2 (ATP13A2) results in the accumulation of α-syn due to lysosomal dysfunction. PD is affected by numerous gene mutations associated with lysosomal storage disorders [61], including in α/β-subunits of β hexosaminidase (Tay-Sachs and Sandhoff, respectively), glucocerebrosidase (found in Gaucher disease), Niemann-Pick type C1 protein, and sphingomyelin phosphodiesterase 1 (Niemann-Pick type A/B), α-galactosidase (Fabry), acid β-galactosidase (GM1 gangliosidosis), and CLN12/ATP13A2/PARK9 (NCL12) [62]. Additionally, PD is influenced by several risk factors, including mutations in lysosomal hydrolases such as mutated glucocerebrosidase (found in Gaucher disease) [59].

Mutations in the huntingtin (HTT) gene cause Huntington disease (HD), a rare autosomal dominant neurodegenerative disease. The CAG trinucleotide repeats in exon 1 of the HTT gene expands abnormally as a result of these mutations. A lengthy polyglutamine (polyQ) region that is repeated close to the N-terminus of the mutant HTT protein causes toxic oligomers to develop in the cytoplasm and nucleus of neurones. Huntingtin recruits several autophagy proteins, and the accumulation of mutant huntingtin (mHTT) causes lysosomal and autophagy dysfunctions [59].

Neurones with Huntingtin disease (HD) exhibit elevated autophagosome counts and sustain autophagy flux levels. Autophagy initiation and autophagic vesicle production are enhanced

by mTOR inhibition. However, the aggregated mutant huntingtin (mHTT) and damaged organelles are not moved to autophagosomes, leading to their accumulation in the cytoplasm and resulting in toxicity [59]. Macroautophagy removes the HTT mutant aggregates, with the autophagy-linked FYVE protein (ALFY) playing an important role in mHTT aggregation clearance. The autophagy receptor protein p62 is also crucial, as its dysfunction leads to increased neuron death induced by mHTT [59].

It has been demonstrated that lysosomal storage material accumulates in neurons throughout the brain [63]. Since most neurons cannot remove unwanted or damaged organelles and macromolecules through cell division, they heavily rely on lysosomal function and autophagy to clear these materials [64]. Autophagic defects have been identified in many LSDs, including mucopolysaccharidosis I, Niemann-Pick disease type C (NPC), Pompe disease, neuronal ceroid lipofuscinoses (NCLs), and Gaucher disease [64]. Additionally, lysosomal membrane permeability (LMP) has been detected in several LSDs, including mucopolysaccharidosis I and late-infantile NCL [65]. Aberrant autophagy associated with LMP may lead to protein aggregates and potentially enhance neurodegeneration [66].

Demyelination affects neuronal survival and function in both the central nervous system (CNS) and the peripheral nervous system (PNS), which is also a characteristic of lysosomal storage disorders (LSDs). The axons in both the CNS and PNS are covered by a myelin sheath, which consists of specialized neuroglia in the CNS and nonneuronal cells in the PNS. This sheath isolates the axon, allowing it to transmit electrical signals in neurons. LSDs impact myelination, leading to demyelination and severe neurological impairments [63, 67].

Numerous LSDs are linked to neurodegeneration, resulting in moderate to severe loss in the hippocampus, cerebellum, thalamus, and cerebral cortex, among other parts of the brain

[63]. The loss of neurons is often associated with reactive astrocytosis, which likely exacerbates neuronal abnormalities [63, 68].

1.2.2.2. Altered lysosomal activity in disease.

Some of LSDs feature severe neurodegenerative disease and others also feature neurological pathology [55, 56]. Changes in the endo-lysosomal system are increasingly being recognised as contributors to some late-onset neurodegenerative disorders like Alzheimer's disease, Huntington's, Parkinson's disease, and frontotemporal dementia and lysosomal gene mutations are risk factors. Hence, the central nervous system appears to be more vulnerable to lysosomal failure than other systems [59]. In several brain regions, most LSDs exhibit a neurodegenerative phenotype associated with the progressive accumulation of heterogeneous materials. While lysosomal proteins are expressed in most cells, neurons are particularly vulnerable to damage in LSDs because they do not divide. This means they cannot dilute storage material or replace it when lost. Additionally, neurons regulate large amounts of gangliosides, which are glycosphingolipids crucial for neuronal membrane composition and synapses. Gangliosides accumulate in all LSDs [69, 70].

Glycosphingolipids represent a significant portion of brain lipids. They are found in the form of glucosylceramide (GlcCer) and gangliosides, where the group of oligosaccharides of GlcCer is modified with sialic acid. Through lysosomal hydrolysis, these lipids undergo catabolism in the lysosome. When lysosomal hydrolysis is reduced, it results in the accumulation of glycosphingolipids, which form a subgroup of lysosomal storage disorders (LSDs) directly affecting neuronal function [69, 71].

The effects of psychosine and other abnormally accumulated sphingolipids on signal transduction pathways are considered important components in the development of LSDs. These pathogenic changes include the strange activation of Toll-like receptor 4, which stimulates neuroinflammation, as well as a decrease in fibroblast growth factor 2 signalling, crucial for neural stem cell proliferation. Additionally, there are alterations in insulin and insulin-like growth factor I signalling [66, 72].

Due to the high metabolic demands in neurons, especially Purkinje cells, they are vulnerable to aberrations in signalling pathways that support cellular metabolism. This can lead to increased cellular stress, excitotoxicity, and cell death [69].

Furthermore, the activity of TRPML1 is blocked by sphingomyelins, resulting in disrupted lysosomal Ca2+ release. This leads to lysosomal trafficking blockage and impaired autophagic removal in lipid storage disorders [69, 73].

Many LSDs lead to early neurological defects, developmental delays, behavioural abnormalities, and metabolic imbalances, which often lead to early death. These disorders are due to changes in the morphology, motility and number of lysosomes, undigested materials accumulation within the lysosomal lumen and abnormalities in intracellular trafficking that lead to enlarged and dysfunctional lysosomes [59]. Most LSDs are associated with the central nervous system which leads to degeneration and early death [67, 74].

1.2.2.3. Dysfunctions of lysosomal membrane proteins

Mutations in genes of LMPs have been demonstrated to cause several diseases whether severe visceral symptoms, neurodegeneration, or other diseases (Tabel 1.1). There are more

than 12 different disorders that have been recognised to result from LMPs defects, and these numbers are likely to increase as there are more than 100 different LMPs. Mutations in several genes encoding LMPs lead to neuronal ceroid lipofuscinosis (NCL), which includes neuronal lipofuscin accumulation, neuroinflammation and neurodegeneration [44]. Bone fractures and growth abnormalities, osteopetrosis, anaemia and bleeding problems are typical features of malignant infantile osteopetrosis [44, 75]. The mutation in the gene encoding the cystinosin protein leads to cystinosis, which causes kidney failure, acidosis, photophobia, blindness and diabetes. Dannon disease which has been shown to result from LAMP-2 mutations, features muscle atrophy, cardiomyopathy, and mental retardation [75]. Epilepsy, kidney failure and glomerulosclerosis diseases associated with the syndrome of action myoclonus-renal failure have been demonstrated to result from mutations in the gene encoding the LAMP-2/SCARB2 lysosomal membrane protein. Salla disease results from mutations in the sialin gene and includes nystagmus, hypotonia, and cognitive impairment diseases. There are feature diseases related to mucopolysaccharidosis type IIIC disorder comprising progressive dementia, neurological symptoms, aggressive behaviour, hyperactivity, deafness, seizures, and loss of vision [44]. Table 1.1 including those protein mutations, their diseases and clinical features.

Transmembrane protein 175 (TMEM175) is a lysosomal membrane protein and an ion channel that maintains the acidity in the lysosome. It is associated with neurological disorders [76]. Mutations in the *TMEM175* gene are associated with Parkinson's disease (PD), specifically correlated with the p.M393T variant in TMEM175. TMEM175 knockout (KO) in mouse neurons causes hyper-acidification of lysosomes, impairment of lysosomal hydrolytic activity, and α-synuclein accumulation in the brain, a typical pathological feature of PD [77]. Currents are started on the plasma membrane when human TMEM175 is

overexpressed in HEK293T cells or mouse TMEM175 is overexpressed in Xenopus laevis oocytes [78]. Mutations in the *TMEM175* gene affect protein function, which might alter lysosome function [79].

Defective free sialic acid export from the lysosome is the cause of Infantile Sialic Acid Storage Disorder (ISSD) and Salla disease. *SLC17A5* gene mutations are linked to both disorders. The membrane transporter protein sialin, which is encoded by this gene, is similar to glutamate transporters found in synaptic vesicles [75]. Salla disease is linked to a missense mutation (R39C) of the arginine residue present in the whole SLC17 family. Large deletions, a small in-frame deletion (ΔSSLRN), and missense and nonsense mutations are characteristics of mutations linked to ISSD. Compared to ISSD mutations, the R39C mutation may have a less severe impact on sialin function. Also, sialic acid transport in Salla and ISSD lysosomes was not detectable [75]. The function and expression of sialin are altered by ISSD-associated mutations. Sialic acid transport is deleted while lysosomal localization is preserved partially or fully. On the other hand, lysosomal localization and sialic acid transport are partially preserved in the R39C mutation [75].

The first recognised storage condition, cystinosis, is brought on by the lysosomal accumulation of cystine in numerous tissues. Inherited defects in cystinosin, a seven-transmembrane domain protein, lead to cystinosis [75, 80]. It is associated with bi-allelic mutations in the *CTNS* gene [80]. The promoter region and the first ten exons of the *CTNS* gene are eliminated when 57 kb are deleted, which is considered the most common mutation [75]. Two signals—a signal in the intracellular loop between the fifth and sixth TM and a tyrosine-based sorting motif in the C-terminal tail—are necessary for cystinosin to localise to lysosomes and late endosomes. On the other hand, cystinosin is moved to the

plasma membrane while maintaining lysosomal localisation when either signal is deleted. Cytosin is redirected to the cell surface when both signals are imperfect [75].

Juvenile neuronal ceroid lipofuscinosis is associated with defects in Ceroid Lipofuscinosis Neuronal 3 (CLN3), a lysosomal transmembrane protein [44]. Mutations in the *CLN3* gene cause this severe neurodegenerative autosomal recessive condition [80]. Additionally, juvenile neuronal ceroid lipofuscinosis is characterized by the accumulation of neuronal lipofuscin [44, 75]. The function of CLN3 is still unclear [44]. Protein palmitoylation is impacted by the deficiency of CLN3 [81].

The mutation in the *MFSD* gene encoding CLN7 causes late infantile neuronal ceroid lipofuscinosis (INCLs) or Batten disease, characterized by neurodegeneration and neuronal lipofuscin accumulation [75]. This disease is considered an autosomal recessive inherited lysosomal storage disorder [75, 80]. Mutation in the *MFSD* gene disrupts the lysosomal transmembrane protein CLN7. Recently, it has been identified that CLN7 functions as a novel lysosomal chloride channel. Lower levels of CLN7 expression in both central and peripheral neurones are associated with an increase in neuronal lysosomal activity and a decrease in lysosomal storage [77].

Mutations in the genes encoding OSTM1 and CLC7 result in malignant infantile osteopetrosis, leading to bone fractures, growth abnormalities, osteopetrosis, anemia, and bleeding problems [75]. CLC7 belongs to the family of CLC proteins [77], which are chloride channels and transporters [75]. It is a lysosomal membrane protein [75, 77]. Its appropriate expression, localisation, and transport activity depend on the beta subunit and osteoporosis-associated transmembrane protein 1 (OSTM1)[77]. Loss of CLCN7 function, caused by either recessive or dominant inherited variants in CLCN7, is associated with

osteopetrosis. Both the central and peripheral neurological systems exhibit significant levels of CLC7/Ostm1 expression, which is mostly found in lysosomes [77]. Additionally, they are found in osteoclasts. In both humans and mice, mutations in CLC7 and Ostm1 lead to osteopetrosis, neurodegeneration, and lysosomal storage disorders [77]. Loss of CLCN7 function leads to decreased or absent function of the Cl− channel, which causes osteopetrosis [80]. Osteopetrosis autosomal recessive type 4 (OPTB4), also known as autosomal recessive osteopetrosis or osteopetrosis infantile malignant 2, is caused by bi-allelic mutations in CLCN7, while osteopetrosis autosomal dominant type 2 (OPTA2), or autosomal dominant osteopetrosis type II, is caused by heterozygous mutations in CLCN7. Dominant OPTA2 is similar to recessive inherited OPTB4 [80].

The protein in the late endosomal/lysosomal membrane is known as Niemann-Pick Disease type C1 (NPC1) [77]. Bi-allelic mutations in the *NPC1* gene, which codes for the NPC1 protein, cause the lysosomal cholesterol export machinery autosomal recessive disorder [80]. Loss of NPC1 function causes lysosomal storage of cholesterol and other lipophilic compounds [80], resulting in Niemann-Pick type C disease (NPC), characterized by ataxia, dysarthria, hepatosplenomegaly, thrombocytopenia, and dysphagia [44, 75].

HGSNAT (Heparan-Alpha-Glucosaminide N-Acetyltransferase) is a lysosomal membrane protein probably involved in lysosomal acetyl import and transfer to heparan sulfate [44, 75]. Bi-allelic mutations in the *HGSNAT* gene, which encodes HGSNAT, cause impaired lysosomal degradation of the glycosaminoglycan heparan sulfate, leading to Mucopolysaccharidosis type IIIC, also known as Sanfilippo syndrome, an autosomal recessive inherited lysosomal storage disease [80]. HGSNAT missense variants lead to protein misfolding and retention in the endoplasmic reticulum. The storage of heparan

sulfate in microglial cells was observed in MPSIIIC mouse models, which might cause neuroinflammation and neuronal death [80].

A class of essential lysosomal membrane proteins is known as lysosome-associated membrane proteins (LAMPs), including LAMP-1 and LAMP-2, which are expressed in all cell lines. 50% of all lysosomal membrane proteins are LAMP-1 and LAMP-2, and they contribute to the maintenance of lysosomal pH, catabolism, and integrity [77]. Lysosomal associated membrane protein-2 (LAMP-2) belongs to the glycoprotein family [44, 75]. Danon disease is caused by mutations in the *LAMP2* gene. The deficiency of LAMP-2 in myocytes causes the accumulation of autophagic vacuoles, which is the pathological feature of Danon disease [44]. There are many LAMP2 mutations leading to splicing defects or protein truncation [75]. There are three splicing isoforms: LAMP2A, LAMP2B, and LAMP2C [75, 77]. LAMP2 influences endosomal/lysosomal-mediated cholesterol exportation, and overexpression of any of its isoforms reduces the amount of cholesterol that aggregates in late endosomes/lysosomes [77]. When the *LAMP2* gene is disrupted in mice, the disease mimics that of humans, becoming more severe and affecting more tissues [75].

Mucolipidosis type IV (MLIV), an autosomal recessive inherited neurodevelopmental lysosomal storage condition linked to lipid storage in lysosomes, is caused by mutations in the *MCOLN1* gene, which codes for the mucolipin-1 protein [75, 80]. Mucolipin-1, also known as TRPML1, is a lysosomal channel with six transmembrane domains that belongs to the transient receptor potential channel family [75]. MLIV is associated with the deficiency of TRPML1 function. Heterogeneous lipids and proteins build up in cytoplasmic vacuoles produced from lysosomes when mucolipin-1 function is impaired [80]. Mutations in the *Mcoln1* gene in mice were found to mimic the ophthalmic, neurological, and gastric defects

observed in MLIV patients [75]. TRPML1 is a cation channel that localizes to lysosomes and late endosomes [75, 80].

Bi-allelic mutations in the *LMBRD1* gene, which encodes the lipocalin membrane receptor domain containing 1 protein (LMBRD1), lead to Cobalamin F-type disease, an autosomal recessive inborn error of cobalamin (vitamin B12) metabolism [80]. LMBRD1 is a lysosomal transmembrane protein thought to be a cobalamin transporter [44, 75, 80]. The defect in cobalamin export from the lysosome is associated with Cobalamin F-type disease [75, 80]. Therefore, in this disease, free cobalamin accumulates in the lysosomes [75, 77].

The equilibrative nucleoside transporter 3 protein (ENT3) is a lysosomal transmembrane protein that depends on pH and controls the flow of nucleosides from lysosomes to the cytoplasm. H- syndrome is an autosomal recessive multisystem genodermatosis with systemic macrophage histiocytosis that is linked to bi-allelic mutations in the *SLC29A3* gene, which codes for ENT3. Loss of ENT3 function leads to the accumulation of lysosomal nucleosides, increasing the intra-lysosomal pH, impacting apoptotic cell clearance, and altering macrophage function [80]. ENT3 is highly expressed in tissue macrophages (histiocytes), which phagocytose and degrade dead cells and their nucleic acids in their lysosomes. ENT3 KO in mice causes the accumulation of intra-lysosomal nucleosides, which increases lysosomal pH, impacts apoptotic cell clearance, and alters macrophage function, leading to increased numbers of macrophages and histiocytosis. It has been demonstrated that ENT3 deficiency is associated with autophagic insufficiency, defective differentiation capacity, and adult stem cell exhaustion [80].

Hypopigmentation, organomegaly, and delayed myelination and development (HOD) are associated with a de novo missense variant in the *CLCN7* gene. Two children were reported

with HOD, both carrying the same de novo heterozygous CLCN7 variant, p. Tyr715Cys. An orthologous CLCN7 p. Tyr715Cys knock-in mouse model demonstrated the same human HOD phenotype. Expression of CLCN7 p. Tyr715Cys in Xenopus oocytes leads to elevated (gain-of-function) chloride current, which causes an increase in chloride ion transport into lysosomes [80].

The lysosomal transmembrane protein SLC17A5, also known as SIALIN, transports sialic acid and glucuronic acid. Mutations in the *SLC17A5* gene, which encodes this protein, are associated with Free Sialic Acid Storage Disease (FSASD). It is a multisystem neurodegenerative lysosomal storage disorder that is inherited in an autosomal recessive manner [80]. The accumulation of intra-lysosomal free sialic acid and glucuronic acid is caused by defects in SLC17A5. It has been detected that SLC17A5 works as a non-lysosomal glutamic acid-aspartate transporter in brain synaptic vesicles, which might cause the neurodegenerative phenotype in FSASD [80]. There are three types of FSASD: infantile sialic acid storage disease, caused by truncating SLC17A5 mutations; the intermediate form, associated with at least one mild SLC17A5 variant; and Salla disease, related to non-truncating SLC17A5 variants. Mature myelinating oligodendrocytes are reduced in mice with SLC17A5 knockout (KO) because of death and downregulation of polysialic acid-neural cell adhesion molecule (PSA-NCAM) [80].

Lysosomal integral membrane protein 2 (LIMP-2) is a chaperone and transporter of beta-glucocerebrosidase [44, 77]. It regulates the transport of glucosidase from the ER to the lysosome through endolysosomal compartments [77]. The defects in LIMP-2 are associated with β-glucosidase (GCase) activity in several tissues. One particular clinical spectrum of Gaucher's disease (GD) is action myoclonus-renal failure syndrome, which is brought on by

mutations in the SCARB2 gene that codes for LIMP-2 [44, 77]. Recently, it has been found that LIMP-2 is a lysosomal lipid transporter. LIMP-2 functions in lysosomal GCase import and lipid export may govern lipid storage and autophagy-lysosomal dysfunction in LIMP-2 defective mice, resulting in α-synuclein buildup and neuronal toxicity. Exogenous expression of LIMP-2 in *GD* gene therapy may be feasible, as overexpression of LIMP-2 in human glioma cells and murine neuroblastoma cells expedited the clearance of α-synuclein [77].

Other diseases have been recorded in cases of mutations in the genes encoding LMPs, including developmental delay, hepatosplenomegaly thrombocytopenia, ataxia, psychomotor retardation corneal opacity, and ophthalmological abnormalities (Tabel 1.1) [44, 75].

Table 1. 1. The LMP gene mutations and their diseases

Mutated protein	Disease associated	Clinical symptoms
Sialin	- Salla disease - Infantile sialic acid storage disorder	- Nystagmus, hypotonia, cognitive impairment, ataxia and psychomotor retardation. - Hepatosplenomegaly, severe motor impairment, facial dysmorphism, inability to thrive, and premature mortality.
Cystinosin	Cystinosis	Kidney failure, acidosis, photophobia, blindness, diabetes
CLN3 (Battenin)	Juvenile neuronal ceroid lipofuscinosis	Neurodegeneration, neuronal lipofuscin accumulations
CLN7	Late infantile neuronal ceroid lipofuscinosis	Neurodegeneration, neuronal lipofuscin accumulations
CLC7; OSTM1	Malignant infantile osteopetrosis	Osteopetrosis, bone fractures and growth abnormalities, anemia, bleeding problems
HGSNAT	Mucopolysaccharidosis type IIIC	Aggressive behaviour, neurological symptoms, , hyperactivity, seizures, progressive dementia, deafness and loss of vision.
LAMP-2	Danon disease	Muscle atrophy, cardiomyopathy and mental retardation
MCOLN1	Mucolipidosis type IV	Corneal opacity, psychomotor retardation, retinal degeneration and ophthalmological abnormalities.
NPC1	Niemann-pick type C	Thrombocytopenia, dysarthria, ataxia, dysphagia, and hepatosplenomegaly.
LMBRD1	Cobalamin F-type disease	seizures, methylmalonic aciduria, stomatitis, glossitis, and developmental delay.
Sialin	Free sialic acid symptoms disease (FSASD)	Neurodegenerative symptoms, which include cognitive impairment, cerebellar ataxia, and muscle hypotonia, in addition to organomegaly, coarse facial features.
ENT3	H-syndrome	Sensorineural hearing loss, flexion contractions of the fingers and toes, hyperpigmentation, induration, and hypertrichosis, short stature and hepatosplenomegaly.
HOD	Hypopigmentation, Organomegaly, and Delayed Myelination and Development (HOD) (HOD)	Hypopigmentation of skin and hair and organomegaly including liver, spleen and kidneys
LIMP-2/SCARB2	Action myoclonus renal faluoir disease (Gaucher disease)	Epilepsy, glomerulosclerosis and kidney failure
Transmembrane protein 175 (TMEM175)	Neurodegenerative diseases	Parkinson disease, Alzheimer disease, Lewy body dementia, alpha-synucleinopathies prodromal syndrome, and rapid eye movement sleep behaviour disorder.
CLCN7	- Osteopetrosis, Autosomal Recessive type 4 (OPTB4). - Osteopetrosis, Autosomal Dominant type 2 (OPTA2)	- Severe hematological deficits, primary neurodegeneration, and cerebral and retinal atrophy, severe spasticity, axial hypotonia and peripheral hypertonia, visual impairment. - A progressive segmentary osteosclerosis, bone problems including severe pain, fractures, scoliosis, hip osteoarthritis, and osteomyelitis of the mandible or septic osteitis and the hardness and the brittleness of the skeletons

1.2.3. LSDs and neurodegenerative disease

One well-studied LSD characterised by progressive neurodegeneration is Niemann-Pick type C (NPC) disease which is associated with the accumulation of de-esterified cholesterol within lysosomes. Progressive cerebellar ataxia has been shown in NPC patients [82, 83]. In Gaucher disease, which is considered the most common LSD, glucosylceramide accumulation results from the mutations of homozygous loss-of-function in the lysosomal enzyme β-glucocerebrosidase (GBA). Severe progressive neurodegeneration is associated with types II and III Gaucher disease [84, 85]. Heterozygous mutations in GBA have been more recently identified as the most common risk factor for Parkinson's disease [85].

1.3. Autophagy

1.3.1. Autophagy overview

Normal cellular development and growth are associated with the balance between protein synthesis and degradation. One major pathway for degradation is autophagy, which literally means a self-digestive process [86-89]. In eukaryotes, autophagy is a cellular degradation and recycling route that is extremely conserved [88]. There are three main types of autophagy in mammalian cells, microautophagy, macroautophagy and chaperone-mediated autophagy (CMA) [88, 89], while microautophagy and macroautophagy only operating in yeast cells (Figure 1.2) [90]. For all of them, the lysosomal function is essential for the degradation of cellular constituents [86-89]. In most tissues autophagy functions at low baseline levels and is induced in response to several stimulations through the activity changes of adenosine monophosphate-activated protein kinase (AMPK) and the master nutrient-responsive kinases mTORC1 [89]. Therefore, changes in extracellular and cytosolic

nutrient levels directly affect autolysosomal digestion levels to restore cellular homeostasis [87, 89]. Additionally, autophagy function to remove misfolded proteins, protein aggregates, foreign pathogens and damaged organelles is considered an autophagy function [86]. Abolishment of these protective functions of autophagy can lead to cancer, disorders of the immune system, neurodegeneration, and ageing [87, 91].

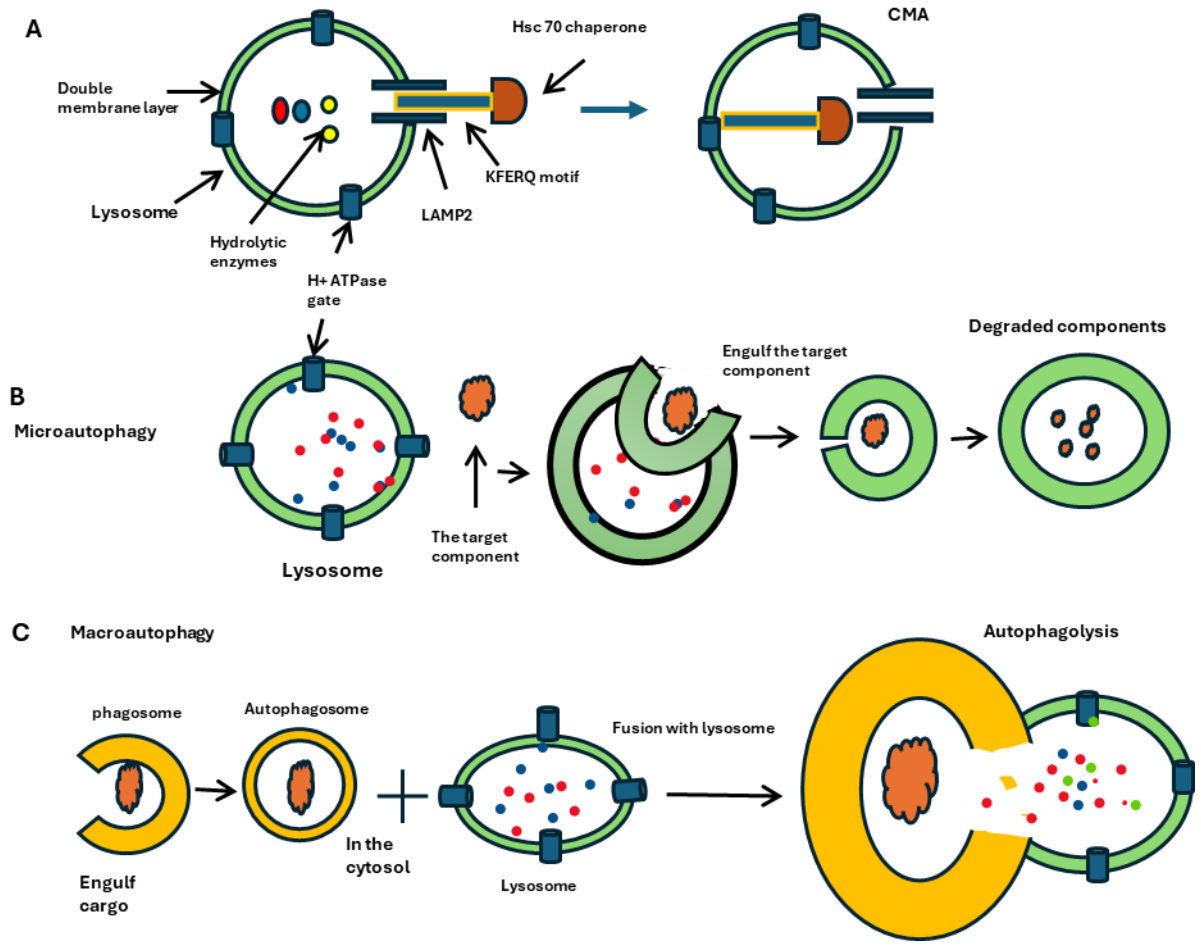

Figure 1. 3: Types of Autophagy process.

Autophagy is the process of degradation in body cells. **(A)** Chaperone-mediated autophagy (CMA) is involved in degrading soluble cytosolic proteins in the lysosome and is different from microautophagy and macroautophagy as it features the bulk sequestration of cytosolic components. It is highly selectiv, frequently breaks down target proteins with a distinct five-peptide motif (KFERQ-like) by using the chaperone protein HSC70. The target protein is drawn into the lysosome for breakdown after the receptor protein LAMP2A on the lysosomal membrane identifies the binding protein's exposed KFERQ group. **(B)** In the microautophagy process, the lysosome engulfs the target components before the degradation process. **(C)** Macroautophagy forms an isolation membrane to engulf cargos selected for degradation, then creates a double membrane autophagosome before fusion with the lysosome.

1.3.1.1. Microautophagy pathway

Microautophagy refers to the process of cytoplasmic contents entering the lysosome via lysosomal membrane deformation or invagination [88, 92]. Both microautophagy and macroautophagy include dynamic membrane rearrangements that terminate at the lysosome/vacuole which are different from proteasomal degradation [87]. Microautophagy comprises the direct cytoplasm engulfment at the degradative organelle surface by septation, protrusion and/or the limiting membrane invagination (Figure 1.2) [87, 90]. Studies have shown that endosomal microautophagy is a microautophagy-like process and transports the proteins of the cytosolic to the endosomal multi-vesicular bodies. Microautophagy needs further study to understand its regulation and its roles in human health and diseases [88].

1.3.1.2. Macroautophagy pathway

In the macroautophagy pathway, the initial site of sequestration does not happen in the lysosome limiting membrane, which makes it partially different from the microautophagy and CMA pathways [87, 88]. In macroautophagy, substrates are isolated within cytosolic double-membrane vesicles called autophagosomes which are associated with lysosomes to make autophagolysosomes. These are then acidified. Its substrates are damaged and superfluous organelles, cytosolic proteins, and invasive microbes (Figure 1.2) [93]. After the degradation process the breakdown products are returned into the cytosol in order to recycle the constituents of macromolecules to create energy to continue cell viability under unfavourable conditions and to protect the cell during situations of stress [87, 88], such as nutrient starvation, the absence insulin or absence of other growth factors, the stress of

endoplasmic reticulum and hypoxia [94]. Nutrient starvation is controlled by two pathways including the cAMP-dependent protein kinase A (PKA) and TOR, and both of them primarily sense carbon and nitrogen respectively [88, 95]. In yeast, under nutrient-rich circumstances, PKA is a macroautophagy inhibitor, and this inhibition occurs in mammalian cells partially via the phosphorylation of LC3 by PKA. In the nitrogen sensing process, amino acids regulate mTORC1 in addition to regulating the RAG proteins, RAS-related small GTPases which activate mTORC1 [88]. It has been shown that, macroautophagy is stimulated by an increase in cytosolic Ca^{2+} concentrations which are associated with endoplasmic reticulum stress (ER stress) [96]. ER stress can also induce macroautophagy via unfolded protein response (UPR) signalling in both yeast and mammalian [97, 98].

1.3.1.3. Chaperone-mediated autophagy pathway

The chaperone-mediated autophagy (CMA) pathway can be involved in the degradation of soluble cytosolic proteins in lysosomes, which is different from macro- and microautophagy. Unlike those forms, CAM features the in-bulk sequestration of cytosolic components. Additionally, CAM is able to selectively recognize cargo through cytosolic chaperones. Instead of engulfing substrates, they are translocated across the lysosomal membrane in a receptor-mediated manner, which distinguishes it from other autophagy forms [99]. So far, CMA has been described only in mammalian cells (Figure 1.2) [88, 99]. CMA substrates are not engulfed, but they are transported across the membrane of the lysosome into the lysosomal lumen. A pentapeptide KFERQ motif is common to all CMA substrates. Target proteins related to the KFERQ consensus motif are unfolded via the cytosolic chaperone action and transported across the membrane of the lysosome for degradation into the

lumen [100]. A variety of substrate proteins are degraded by CMA, including transcription factors and their inhibitors, certain glycolytic, the proteins of calcium and lipid binding, proteins involved vascular trafficking and proteasome subunits [100, 101].

1.3.2. The endo-lysosomal and autophagic pathways of degradation

The lysosome is considered the organelle of terminal degradation and cellular clearance. The degradation process occurs when materials are delivered to the lysosome from several locations and this process is performed through two pathways. The first is the endocytosis pathway, through which material enters the lysosome from outside the cell by using endocytic vesicles from in plasma membrane (Figure 1. 3) [28]. The second pathway is autophagy, which is responsible for the materials within the cell that are transported to the lysosome through autophagosomes (Figure 1. 3) [28, 102]. It has been noted that the dysregulation of autophagy is associated with many LSDs including many NCLs and other neurodegenerative diseases. The pathway of endo-lysosome is essential for cellular function and homeostasis [99]. This pathway facilitates the internalization of extracellular macromolecules and fluids with the protein of plasma membrane, and it is important in the sorting of the internalized membrane and its constituent proteins. The early and late-endosomes, pleiomorphic organelles and multi-vesicular domains are the important sorting stations in this pathway. Endosomal cargo is delivered to the lysosome as the acid hydrolases stimulate degradation, or cargo is recycled back to the plasma membrane through the endosomes recycling or transported to the Golgi by the complex of retromer. Endosomes that combine with the plasma membrane and discharge cargo into the extracellular space are known as exosomes [99, 100].

Rab GTPases are a large family of proteins that regulate vesicular trafficking, sorting dynamics and membrane remodelling within the endocytic pathway. Recently, it has been demonstrated that mitochondrial fission is regulated by lysosomal contact with mitochondria via Rab7 hydrolysis which allows bidirectional regulation of the dynamics of mitochondrial-lysosome [103]. This potentially explains the frequent observation of lysosomal and mitochondria dysfunction in many human diseases, including neurodegenerative disorders and LSDs such as the NCLs which feature neurodegeneration [104].

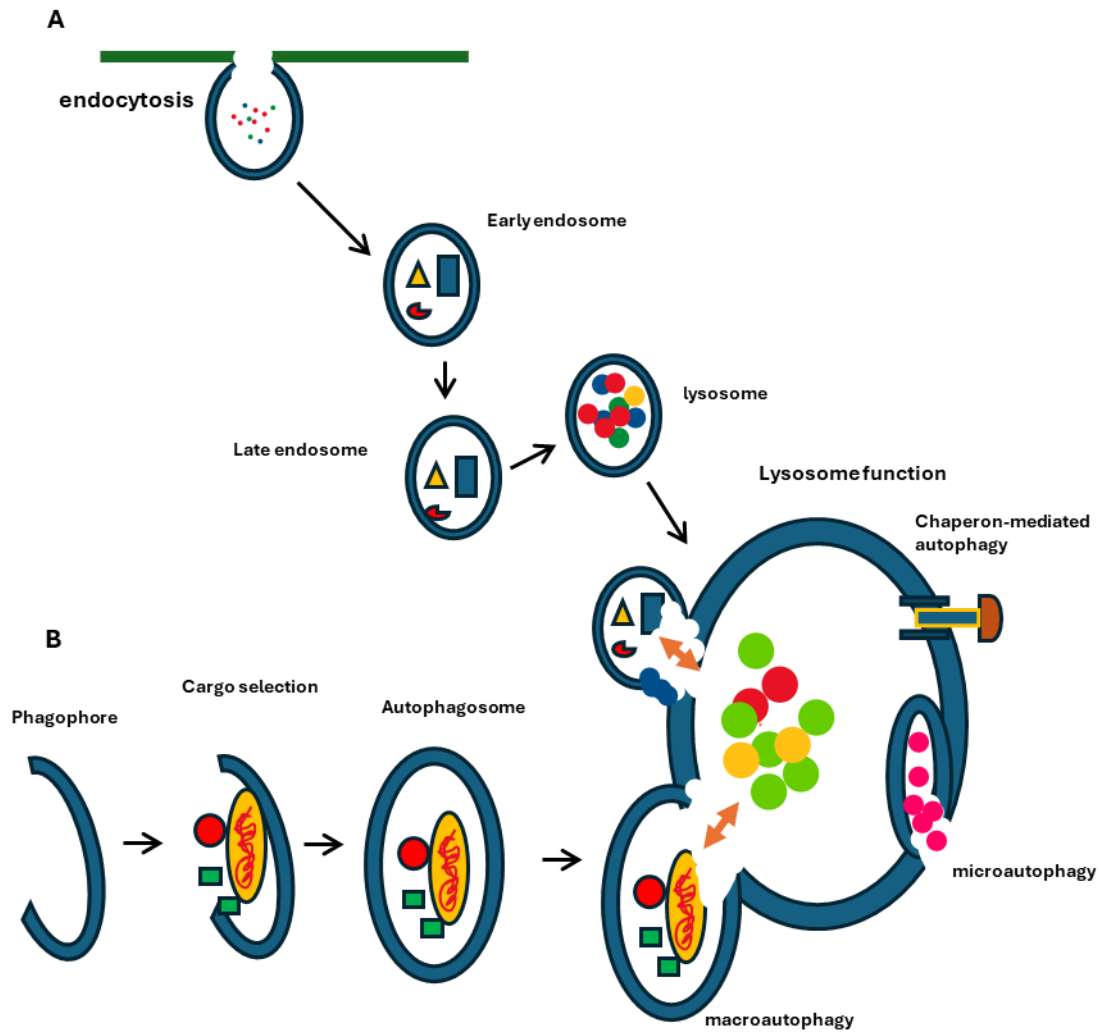

Figure 1. 4: Endolysosme and autophagy pathways.

Macromolecules are delivered from several locations to the lysosome for degradation, and this is performed in two ways. **(A)** The endocytosis pathway, where materials enter the lysosome from outside the cell via endocytic vesicles in the plasma membrane. **(B)** The second pathway is autophagy, where materials within the cell are transported to the lysosome through an autophagosome.

1.4. Neuromuscular junction

1.4.1. Neuromuscular junction

The neuromuscular junction (NMJ) is the connection between the motor nerves and skeletal muscle fibres, and it is one of the most studied synapses. In this part, the nerve action potential is converted to muscle contraction which is the essential role of the NMJ [105, 106]. Muscle contraction is associated with an increase in intracellular calcium concentration [107].

In the process of neuromuscular transmission, the target muscle cells receive the chemical transmitter released from the electrical activity in a motor neuron which leads to localised electrical depolarization and contraction activation [105]. Any problem that impairs the process of signal transmission might cause muscle weakness or paralysis and perhaps affect the quality of life [105, 108]. NMJ can be divided in to three phases depending on its structure and function including presynaptic, synaptic, and postsynaptic [105, 109].

1.4.2. Synapse

In the case of the NMJ, the synaptic cleft, which measures about 50 nm is the space between the nerve terminal and the postsynaptic membrane [109]. Through the synaptic cleft, acetylcholine (ACh) diffuses to the postsynaptic membrane after being released from the nerve terminal. About 50% released of Ach is hydrolysed by acetylcholinesterase (AChE) or transfers out of the cleft. AChE within the cleft terminates the Ach action when Ach unbinds from the Ach receptors (AChRs). As a result, the released choline is backed into the nerve terminal by a specific absorption protein to use again to synthesis a new transmitter in the nerve terminal (figure 1. 4) [105, 109].

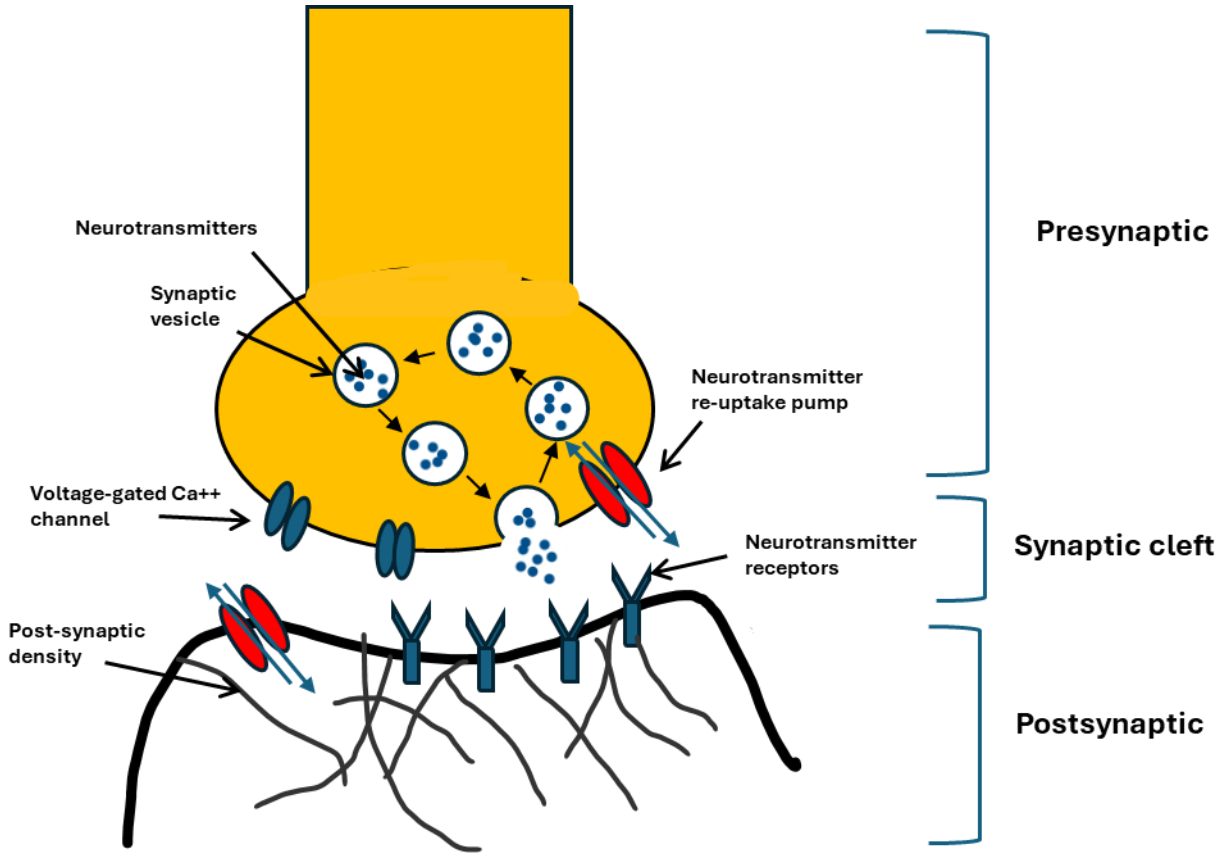

Figure 1. 5: Synaptic structure.

The synapse consists of three parts. The presynaptic part includes synaptic vesicles that store the neurotransmitter. Voltage-gated Ca^{2+} channels in the presynaptic membrane open due to the action potential, leading to the release of the neurotransmitter into the synaptic cleft. The second part is the synaptic cleft, through which the neurotransmitter diffuses to the postsynaptic membrane. The third part is the postsynaptic membrane, which contains the neurotransmitter receptors in its folds. Voltage-gated sodium channels in the postsynaptic part lead to the initiation of the action potential (AP). The postsynaptic density is also included in this part.

1.4.2.1. Presynaptic

It is the unmyelinated terminal fibre that is divided from a myelinated motor axon, and it is separated from its target (neuron or muscle cells) by a gap called the synaptic cleft (figure 1. 4) [109]. In the NMJ the voltage-gated Ca^{2+} channels are opened by the action potential effect in the presynaptic membrane which leads to the neurotransmitter Ach releasing [109, 110]. ACh is stored in vesicles called synaptic vesicles (SV) in presynaptic. These SV fuse with the cell membrane to release Ach into the synaptic cleft by exocytosis [109, 111]. The range of Ca^{2+} influx into the nerve terminal and the duration of nerve depolarization controls the amount of released ACh. However, the amount of ACh releases from SV is more than the amount needed to absorb in the postsynaptic ACh receptors [109].

1.4.2.2. Postsynaptic

The postsynaptic part is the receiving part of the synapses connection whose membrane is folded into secondary synaptic folds with a high density of AChRs essential for neuromuscular transmission. Nicotinic acetylcholine receptors (nAchRs) are included in postsynaptic folds. There are five subunits in a pentameric unit that are included in the transmembrane protein nAchR. In the deep membrane of postsynaptic folds, there are voltage-gated sodium channels that lead to the initiation of the action potential (AP). Ach action after entering the folds leads to the folds membrane depolarization and opens the channels of sodium voltage-gated (figure 1. 4) [105, 109].

1.4.2.2.1. Postsynaptic density

Postsynaptic densities (PSDs) were identified by electronic microscopy in the 1950s as an electron-dense part underneath the postsynaptic membrane (figure 1. 4) [112]. The

postsynaptic membrane is thickened and more electron-dense in excitatory or type 1 synapses than in other neuronal substructures. PSDs include a dense network of hundreds of proteins that serve a wide range of functions [112, 113]. These proteins are generally divided into cell-adhesion proteins, G-proteins, and modulators, the proteins of scaffolding and adaptor, cytoskeletal proteins, the receptors of membrane-bound, and channels and the molecules of signalling including kinases and phosphatases [112].

1.4.2.3. Pathology of the synapse

It has been proven that there is a relationship between synaptopathy and neurodegenerative diseases and this has been observed in NCL models. A problem with synaptic connections is considered an initiation event in several neurodegenerative diseases in the CNS and PNS. Studies support that, the changes in neuronal homeostasis affect the synapses and the involvement of synapses at early stages of disease development is associated with neurodegeneration [114-116]. It has been suggested that CLN genes that are mutated in the NCLs are associated with the development of the synapses and that abnormal neural development underpins the early onset of neuronal pathology of the NCLs [117].

In specific neural networks, synapses work as groups to regulate neuronal activity levels, which is important for learning, memory, and behaviour. Therefore, synaptic disturbances might have detrimental consequences. Changes in cell-intrinsic molecular mechanisms or biochemical processes in the surrounding environment can lead to synaptic dysfunction [115, 118]. Early or late synaptic dysfunction is associated with several diseases known as synaptopathies [118, 119]. These include neurodegenerative disorders like Huntington's disease (HD), Parkinson's disease (PD), and Alzheimer's disease (AD). These conditions are

characterized by progressive neuronal tissue loss and a simultaneous decline in cognitive and behavioural function. This slow decline is likely attributed to the accumulation of protein aggregates that affect neuronal integrity [115, 120, 121].

Although synaptopathy is an essential problem in neurodegenerative diseases, it is thought to be a result of an ongoing degenerative process in the brain. Consequently, the increasing loss of cortical neurones in Alzheimer's disease (AD), nigrostriatal neurones in Parkinson's disease (PD), and striatal medium spiny neurones in Huntington's disease (HD) all contribute to the weakening and loss of integrity in synapses [14]. However, several PD cases are linked to inherited mutations in synaptic genes, such as α-synuclein. In the case of HD, it is due to a CAG repeat expansion in HTT 1. Moreover, significant cognitive symptoms in neurodegenerative diseases are observed early, and subtle differences in higher functions are detected during the pre-symptomatic phase [115].

Synapse loss is a hallmark feature in several neurodegenerative disorders associated with cognitive decline. Neurodegeneration is linked to the loss of presynaptic terminals and dendritic spines, which in turn affects cognitive function. Changes in the structural and functional aspects of synapses lead to synapse loss, and these defects are related to motor, sensory, and cognitive impairments observed in a variety of neurodegenerative conditions such as ageing, amyotrophic lateral sclerosis, depressive disorders, Huntington's disease, Alzheimer's disease, and schizophrenia[122, 123]. In Alzheimer’s disease (AD), the loss of excitatory synapses is associated with cognitive impairments [123].

Synapses play a critical role in normal neurophysiology; therefore, the loss of synaptic integrity might occur in several neurodegenerative disorders. Many neurological disorders, such as Parkinson's disease, Alzheimer's disease, motor neurone disease, Huntington's

disease, and multiple sclerosis, sometimes present with the loss or malfunctioning of synapses as a late-stage symptom [124].

Synaptic dysfunction contributes to PD progression, affecting autophagy, protein trafficking, and mitochondrial function [119]. Synaptic dystrophy is considered an early stage of PD. The complexes of SNARE proteins undergo misfolding and non-specific interactions. Chaperones play a crucial role in removing these complexes from the synapse. α-synuclein, an oligomerization-prone chaperone, causes mislocalization of SNARE complexes, leading to decreased dopamine release and synaptic dystrophy. Consequently, dysfunctional dopaminergic synapses might contribute to disease development even before the appearance of neurodegeneration [119]. Synaptic defects have also been associated with neurodevelopmental disorders, including intellectual disability (ID), schizophrenia (SCZ), and autism spectrum disorder (ASD), which are characterized by abnormal behavioral or cognitive phenotypes[125].

The big multidomain protein known as leucine-rich repeat kinase 2 (LRRK2) is one of the prominent familial PD factors [126]. Decreases in synaptic plasticity and neurogenesis have been associated with the LRRK2 mutation. LRRK2 has been found to interacts with proteins that stimulate vesicle removal through the autophagy-lysosome pathway. Synaptic dysfunction appears to be affected by defective autophagy in the Parkinson's disease (PD) neurodegenerative cascade, leading to changes in synapse structure and function. Moreover, several PD-related proteins, including PINK1 and α-synuclein, are linked to autophagy [119].

In Alzheimer's disease (AD), it has been shown that synaptic and cognitive impairments in AD transgenic animal models are linked to an increase in soluble oligomeric amyloid beta

(Aβ) species before the appearance of plaques and tangles [119]. Aβ is a fragment peptide from Amyloid precursor protein (APP), by γ-secretase and β-site amyloid precursor protein-cleaving enzyme (BACE) [126]. Soluble Aβ increases neurotransmitter release at excitatory synapses, resulting in postsynaptic neurotoxicity and synapse failure. Depending on the appearance of cognitive decline before neuronal loss, synapse dysfunction probably contributes to memory loss in AD [126].

The neurofibrillary tangle (NFT) is hallmark of AD, is formed by Tau protein aggregation. Tau is an important in the synaptic protein stability and it involved in the structural support to form and maintain synapses. Therefore, the Tue strongly contributes to synaptic dysfunction [126].

Huntington's disease is associated with progressive deterioration of psychiatric, motor, and cognitive abilities, which precede the loss of neurons in all the neocortex and striatum. It has been observed that the size and density of postsynaptic spines are reduced in patients with HD [114]. Additionally, presynaptic proteins such as complexin 2 and rabphilin 3A are lost. Studies have shown that synaptic transmission defects occur in both the central and peripheral nervous systems, including increased resistance of neuronal input, decreased facilitation of paired-pulse responses, and increased acetylcholine sensitivity at the neuromuscular junction[114].

1.5. Neuronal ceroid lipofuscinosis

1.5.1. Neuronal ceroid lipofuscinosis overview

Many of the 50 lysosomal storage diseases are affected by lysosomal membrane proteins defect, including cystinosis, Danon disease, and some of the neuronal ceroid lipofuscinoses

(NCLs) [75, 127]. NCLs include a group of inherited neurodegenerative disorders of childhood that primarily affect the brain and retina. The cerebral, cerebellar cortex and retina are destructed selectively in addition to the loss of neurons in those organs because of NCLs [127, 128]. All but an ultra-rare form of NCL demonstrate an autosomal recessive mode of inheritance [129]. NCLs are classified depending on the severity of mutations and the onset ages which range from prenatal, infantile, and juvenile to adult. Numerous clinical features such as progressive loss of vision, seizures, deterioration of mental and motor, and the death of premature are related to NCLs. There are thirteen genetically different NCL variants have been identified. NCL mutated proteins represent the enzymes of soluble lysosomal, the proteins of polytopic membrane in lysosomes or the ER or the vesicle of synapse linked to proteins [129-132].

1.5.2. NCLs characterizations and clinical features

Histopathological and clinical characteristics were shared in the NCLs. NCLs characteristics include the accumulation of autofluorescent ceroid lipopigments, neuroinflammation and neurodegeneration. Autofluorescent ceroid lipopigment accumulation is found in both neural and peripheral tissues, but degeneration of nerve cells is restricted primarily to the cerebral and cerebellar cortices [77, 129]. Neuronal degradation primarily occurs in the cerebral and cerebellar cortices, and the accumulation of autofluorescent ceroid lipopigments serves as one of the most prominent markers in all NCLs [127].

The accumulation of intracellular lipopigments and neuronal degradation are two important features in NCL neuropathology. Neuronal degradation is thought to lead to clinical symptoms, disease progression, and premature death. It may initiate in the dendritic tree and continue until final neuronal loss predominates in the cerebral and cerebellar cortical

regions [133]. The extent of neuronal depletion is influenced by the age of onset and disease duration. Notably, in the cerebral cortex, layer II small neurons and layer V pyramidal neurons are more affected than nerve cell populations in other cortical layers, indicating a progressive neuronal damage pattern among different groups of nerve cells[133].

The common clinical features are retinopathy, leading to visual failure and blindness, seizures, physical deterioration, dementia and premature death [127, 129].

1.5.3. Lysosome and NCLs

The accumulation of autofluorescent materials in the lysosome, dysregulated autophagy, neurodegeneration, increased neuronal apoptosis and reduced lifespan are common features of all NCLs. It is a possible that lysosomal functions can be used to understand the pathogenic mechanisms of NCLs because of their role as a nutrient sensor and signalling hub in cells. The lysosome is a major degradative and recycling organelle in the cell, and it acts as a regulatory hub in cellular metabolism. In addition to its emerging new roles in cellular proliferation or quiescence [20], the lysosome is the essential component of preserving cellular homeostasis. The pathway of endo-lysosome requires expression and action of several components to control the processes of acid hydrolysis, lysosomal membrane proteins and lysosomal acidification machinery [20].

Through the sequence analysis of the promoters of lysosomal genes, it was observed that a palindromic motif (TCACGTGA) is enriched near their transcription start sites. A genome-wide search confirmed that this motif is linked to lysosomal function genes, and these genes exhibit coordinated expression. The coordinated lysosomal expression and regulation

(CLEAR) element was the name given to the enriched motif[134]. Recently, it has been detected that the element coordinated lysosomal expression and regulation (CLEAR) which is near the site of transcription initiation of numerous genes controls the genes expression that encode several lysosomal proteins. The transcription factor EB (TFEB) binds to CLEAR elements and stimulates numerous expression genes that encode lysosomal proteins. CLEAR elements are found in numerous genes encoding non-lysosomal and lysosomal proteins [134, 135].

Within 200 base pairs of the transcription initiation site, lysosomal genes share a 10-base E-box-like palindromic sequence (GTCACGTGAC). The MIT/TFE family of transcription factors identified the E-box (CANNTG) that is part of this motif, which is called the CLEAR element [136]. By directly binding to particular E-box sites via their promoters, TFEB has been shown to trigger transcription of numerous lysosomal genes; this gene network is known as CLEAR [137]. TFEB's overexpression leads to an increase in lysosomal biogenesis processes and enhances their ability for degrading lysosomal substrates, including autophagy substrates and glycosaminoglycans [136].

It has been observed that in LSDs, TFEB activates its target genes after it moves from the cytoplasm to the nucleus. However, translocation is prevented by the phosphorylation of TFEB by mTORC1 [134, 135]. Moreover, in common neurodegenerative diseases such as Alzheimer's, mTORC1 activation and the dysregulation of lysosomal acidification impair autophagy. It has been suggested that the dysregulation of autophagy leads to the pathogenesis of the LDSs including the NCLs [134, 135]. Moreover, even though mTORC1 signalling in NCL disease is not yet clear, it has recently been noticed that CLN7 gene

mutations lead to soluble lysosomal protein depletion which impairs mTOR reactivation [20, 138].

1.5.4. NCLs and LSDs

NCLs are considered lysosomal storage disorders (LSDs) [75, 127], which are characterized by a heterogeneous origin of the material of storage [130]. NCLs are considered LSDs because of accumulation of autoflourescent ceroid lipopigment, subunit c of mitochondrial ATP synthase or the proteins A and D activator of sphingolipid in lysosomes [131]. However, in classical LSDs, lysosomal enzymes or transporters deficiency or dysfunction causes specific undegraded substrates or metabolites accumulation respectively [139].

1.5.5. NCLs genes and related proteins

Depending on the clinical onset of symptoms, the NCLs were classified into four board of age include infantile, late infantile, juvenile, and adult[129-132].

Several NCL-associated proteins (CLN1 – CLN14) have been identified and they are characterised by the age of onset and pathological features. They are distinct in their intracellular localization and function. Several of them were found mostly in lysosomes including CLN1, CLN2, CLN3, CLN5, CLN7, CLN10 CLN12 and CLN13. However, CLN6 and CLN8 are localized in the endoplasmic reticulum (ER) and CLN4 and CLN14 were detected in the cytosol which is linked to the vesicular membrane (Figure 1.5) and (Table 1.2) [129-132].

Lysosomal soluble proteins include CLN1, which encodes palmitoyl protein thioesterase 1(PPT1), and CLN2 which encodes tripeptidyl-peptidase 1 (TPP1). However, the lysosomal soluble protein CLN5 function is unknown, while CLN10 and CLN13 encode cathepsin D and

cathepsin F respectively. Lysosomal transmembrane proteins are encoded by CLN3, CLN7 and CLN12 (Table 1.2) [130].

Mutations in NCLs proteins lead to different forms of NCL diseases. Studies have been indicated that, cellular processes including lipid and protein trafficking in the pathway of endocytic and the transport regulation of endosomal and lysosomal are shared points from several NCL protein deficiencies. For most NCL disease genes there is a typical disease phenotype linked to complete loss of function [132].

Table 1. 2: Function of NCL proteins

NCLs related protein	Size and protein features	Localization	Function	Disease
CLN1	306 amino acid, soluble protein	Lysosomal matrix, extra-lysosomal vesicles, extracellular	Palmitoyl thioesterase	Infantile, also late infantile, juvenile, and adult
CLN2	563 amino acid, soluble protein	Lysosomal matrix	Serine protease	Late infantile, juvenile
CLN3	438 amino acid, transmembrane protein	Late endosomal/lysosomal membrane, presynaptic vesicles	Unknown	Juvenile
CLN4	198 amino acid, soluble protein	Cytosol, associated to vesicular membranes	Hsc70 co-chaperone, used in exocytosis and endocytosis	Adult
CLN5	407 amino acid, soluble protein	Lysosomal matrix	Unknown	Late infantile, Finnish variant
CLN6	311 amino acid, transmembrane protein	Endoplasmic reticulum	Unknown	Late infantile
CLN7	512 amino acid, transmembrane protein	Lysosomal membrane	Chloride channel	Late infantile, Turkish variant
CLN8	286 amino acid, transmembrane protein	Endoplasmic reticulum	Unknown	Late infantile, Northern epilepsy
CLN9	-	-	Unknown	Juvenile
CLN10	462 amino acid, soluble protein	Lysosomal matrix, extracellular	Aspartyl endopeptidase	late infantile, Congenital
CLN11	593 amino acid, soluble protein	Extracellular	Unknown	Adult
CLN12	1180 amino acid, transmembrane protein	Lysosomal membrane	Unknown	Juvenil
CLN13	484 amino acid, soluble protein	Lysosomal matrix	Cysteine protease	Adult
CLN14	289 amino acid, soluble protein	Cytosol, associated to membrane.	Unknown	Infantile

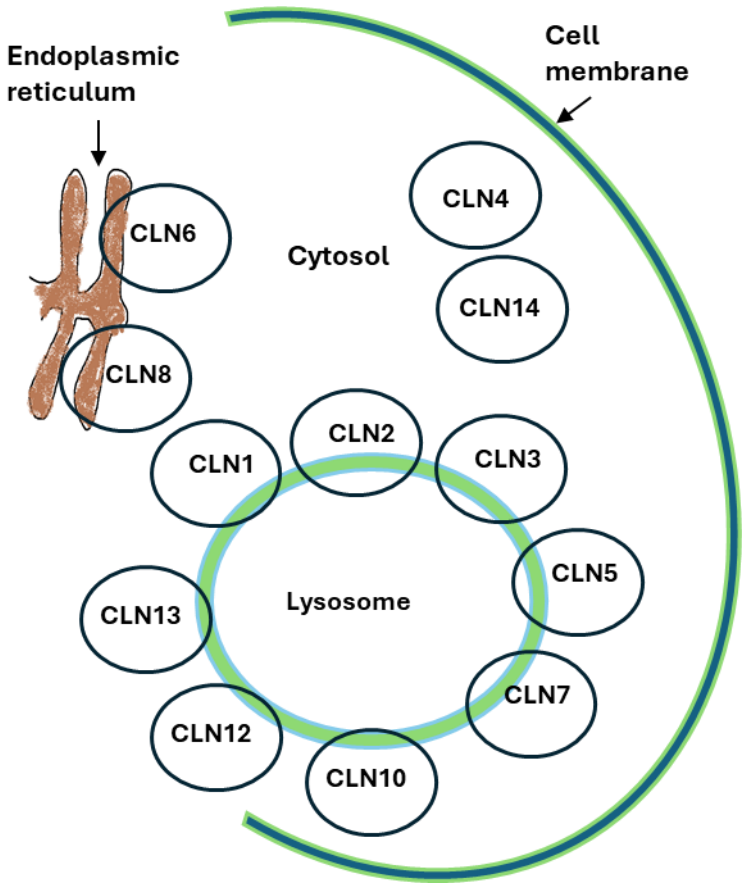

Figure 1. 6: The subcellular localizations of NCL proteins in the cell.

The diagrame shows the positions of NCL proteins (CLN1-CLN14) in the cell. Several NCL proteins including CLN1, CLN2, CLN3, CLN5, CLN7, CLN10, CLN12 and CLN13 are mainly localized in the lysosome. Some proteins localize in the lysosomal membrane such as CLN7. CLN6 and CLN8 are found in endoplasmic reticulum (ER), while other found in the cell cytosol like CLN4 and CLN14.

1.6. CLN7

1.6.1. CLN7 Structure

CLN7 is a polytopic lysosomal membrane glycoprotein that is localized in the lysosomal membrane [75, 127, 140]. The CLN7 size is 518 amino acids, with 12 predicted transmembrane domains (Figure 1.6) [75, 127]. Expression is higher in the rat brain than in other organs, with the highest concentration in the cerebellar cortex granular layer and in the hippocampus pyramidal layer which links to the distribution of degenerate neuron in CLN7 patients [140, 141]. In luminal loop 9, CLN7 is proteolytically cleaved to the N-glycosylation sites, proximally and distally. The lysosomal localisation is not altered by the substitution of the N-glycosylation sites for non-glycosylatable residues [140, 141]. Cysteine proteases cleave the CLN7 membrane glycoprotein proteolytically in acidic compartments. They are involved in two cleavage events in CLN7: one in the N-glycosylated fragment and another in the non-glycosylated fragment. In addition, studies have mentioned that the cysteine protease cathepsin L (Ctsl) is used for one of the two CLN7 proteolytic cleavage events [140]. CLN7 is encoded by the major facilitator superfamily domain containing 8 (MFSD8 gene) which is ubiquitously expressed in numerous alternative splice variants. It is part of the major MFS transporting specific modules of substrates involving drugs, sugars, organic and inorganic cations, and various metabolites. Mutations in CLN7/MFSD8 lead to late infantile onset NCL (CLN7 disease) at 1.5-5 years of age [140, 141]. Lysosomal proteinases cleave CLN7 protein, which leads to N- and C- terminal fragments that are released in the extracellular space [20, 140].

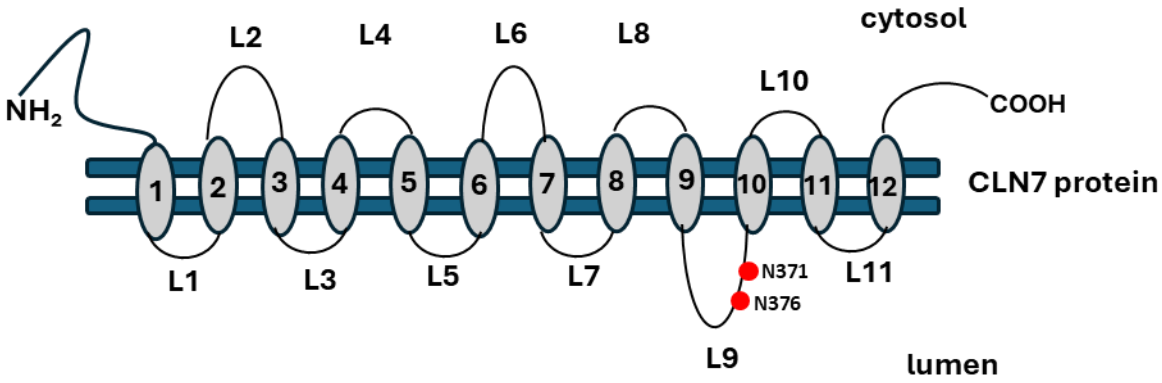

Figure 1. 7: The structure of CLN7 protein.

CLN7 is a lysosomal transmembrane protein (double membrane) comprising 518 amino acids and 12 predicted transmembrane domains. Luminal loops L1 to L11 and the N-terminus is predicted to be in cytosol (NH_2), Also C-terminus is in cytosol side (COOH). N-glycosylation consensus sites are present in the luminal loop 9 (L9) in two positions N371 and N376 (red colour). Two proteolytic cleavage sites for CLN7, one proximal to N-glycosylation sites in luminal loop 9 and another distal to these sites.

1.6.2. CLN7 localization

CLN7 is localized in the lysosomal membrane (Figure 1.5) [127]. Human CLN7 localizes to lysosomes/late endosomes at steady state [142], depending mainly on the N-terminal dileucine motif. Also, it colocalizes with LAMP1 puncta [143].

In the outer plexiform layer of mouse retinae, CLN7 colocalizes with the postsynaptic density protein 95, which is equivalent to the expression of pre-synaptic terminals in photoreceptors [144-146].

The expression of CLN7 has been observed throughout the brain, but its higher levels are shown in the hippocampal pyramidal cell layers and in the cerebellar granular layer. Additionally, in the rat brain, CLN7 is expressed abundantly in the hippocampus, more than in the midbrain, cerebellum, or striatum. An intermediate level of expression is seen in the cerebral cortices [143]. Moreover, in rat and mouse brains, CLN7is primarily expressed in neuronal cells, with the highest expression in the dentate gyrus, cornu ammonis 1 (CA1), and CA3 regions of the hippocampus, as well as in granule and Purkinje cells in the cerebellum [143, 147].

The CLN7 protein in *Drosophila* localizes to lysosomes, similar to the mammalian form, but it is prominently localized at the plasma membrane [128]. A clear orthologue of CLN7 has been found in *Drosophila* [137], which is broadly distributed throughout the central nervous system (CNS) and other tissues [128].

Even though CLN7 is expressed at higher levels in the glial surface near the entire CNS, it has been observed that, CLN7 expressed is in the glial peripheral surface which form the

blood brain barrier (BBB) in insects and this study needs more research [128]. Additionally, CLN7 is expressed in the developing visual system neurons in the *Drosophila larvae* eye disc, and in the brain optic lobe, which is consistent with expression in the retina in mice and with the visual system early degeneration in CLN7 disease patients. Moreover, and of relevance to this study, it has been shown that CLN7 is localised to the post-synaptic density in the neuromuscular junction (NMJ) of the *Drosophila* larval body wall muscle where it is required for the development of normal synapse [117, 128].

1.6.3. CLN7 and synapse

Studies mentioned the localization of CLN7 in the synapses and confirmed its localization in the post-synaptic cells body wall muscle of the NMJ where it makes a high level in the PSD. Consequently, there was a study suggested that the levels of CLN7 protein affect some significant processes of NMJ development and NMJ normal development requires CLN7 protein [117]. Theoretically, the dysfunction of the synapse is linked with the loss of CLN7, and its function is essential in the NMJ post-synaptic side [117].

1.6.4. CLN7 disease

The CLN7 gene mutations lead to the Turkish variant of late infantile neuronal ceroid lipofuscinosis (vLINCL), with the age of onset from 2 to 7 years. Severe epileptic seizures

are the initial symptom, followed by motor deterioration, myoclonus, psychiatric behavioural changes, blindness, dementia and premature death [141]. It has been shown by electron microscopic analysis that CLN7 patients have lysosomal storage material with a condensed fingerprint profile (FPP) or rectilinear profile (RLP) in circulating lymphocytes [127].

1.6.5. CLN7 mutations

1.6.5.1 CLN7/MFD8 mutations

The interruption of the *MFSD8/CLN7* gene has been recognised as the cause of the LINCL form of the NCLs [144]. Clinical data were identified from 25 patients, who were found to have the CLN7/MFSD8 novel mutations and 24 cases with a late-infantile onset phenotype with onset age between 1.5 – 5 years. Most patients have developmental regression or seizures. Studies demonstrated that, in the case of motor regression, mental, developing seizures and impact on speech, the disease progression was rapid, and the age of patient death ranged from 6.5 to 18 years [117, 127, 140, 141]. To date, more than 30 different mutations of human CLN7 have been identified including the mutations of missense, nonsense, or deletion/ frameshift that lead to a dysfunctional or non-functional CLN7 protein [117, 148, 149]. Seizures and developmental regression are the most common initial symptoms. Additionally, ataxia or visual impairment may be observed as initial symptoms in other patients. The disease rapidly progresses, with motor and mental regression, vision loss, and early-onset seizures in the majority of

patients. Moreover, they lose the ability to walk within 2 years after disease onset and die prematurely [149].

The CLN7 protein is encoded by the *MFSD8* gene, which is expressed in numerous alternative splice variants [131]. Immunofluorescence analysis observed that MFSD8 colocalizes with lysosomal markers, which means it is a novel integral lysosomal membrane protein [142], and it is therefore believed to function as a lysosomal transporter [149]. MFSD8 is targeted to lysosomes through a dileucine-based motif at the protein's N-terminal portion. However, it is thought that MFSD8 is partially directed to the lysosome via additional, presumably unconventional motifs. MFSD8 belongs to the MFS proteins based on homology analyses [149]. The MFS is a very large family of proteins found ubiquitously in all classes of organisms. These proteins act as carriers of single polypeptides, transporting small solutes through chemiosmotic ion gradients [142]. Depending on sequence homology, CLN7 belongs to the major facilitator superfamily (MFS), although the exact function of CLN7 remains unclear [131].

A study used a SNP-based homozygosity mapping approach with 10 families to localize the disease gene. Six homozygous mutations in MFSD8 were identified, and all of these six mutations cosegregated with the disease phenotype in the respective families [142]. Six nucleotide changes in MFSD8 were observed, one in each of the six families, which probably cause diseases as they alter the predicted amino acid composition of the MFSD8 protein is not clear whether the identified nonsense mutation leads to a truncated, nonfunctional protein or causes mRNA degradation via nonsense-mediated decay [142].

Missense mutations change conserved glycines that reside in the predicted transmembrane domains to aspartic acids, but this alteration does not affect the protein localization. This indicates that the defect in these mutants is caused more by the functional properties of the mutated protein than by altered localization [142]. However, mutations may also alter amino acids, potentially changing the structure and/or function of the protein. Alternatively, they may affect transcript splicing because they alter sequences at the junctions of exon-intron boundaries in the 3' ends of exons 7 and 11, which could lead to the production of abnormal mRNA and/or proteins [142].

The mutations affect the protein's function, as they might cause a frameshift in the protein and/or premature translation termination, leading to nonfunctional proteins [141].

It has been observed that lysosomal localization of CLN7 is not affected by the missense mutations associated with vLINCL, which means that vLINCL is affected by the loss or impaired function of CLN7 and is not a result of disturbed protein trafficking [143].

To detect CLN7 expression in mice brains and verify CLN7 absence in CLN7 KO mice, different brain regions were analysed. The resulting data showed that CLN7 was present in the whole membrane homogenates of the control mice's cerebral cortex, cerebellum, hippocampus, medulla, and olfactory bulb, but not in the homogenates of the CLN7 KO mice [150].

In the absence of CLN7, the brain and retina exhibit autofluorescence and lysosomal storage of saposin D and mitochondrial ATP synthase subunit c. Neurodegeneration also

occurs in the retina, olfactory bulb, cortex, and cerebellum. Furthermore, there is evidence of neuroinflammation and a reduction in the lifespan of mutant mice [138, 150].

1.6.5.2. Cerebellar granule and Muse Embryonic Fibroblast (MEF) models

In the human brain, cerebellar cortex granule neurons represent 80% of all neurons [141, 151]. The most affected part of the brain is the cerebellar cortex in CLN7 patients, and the cerebellar granular layer is completely lost at end stage disease. Because CLN7 is highly expressed in the cerebellum granule cell layer, cerebellar granule cells are a good model for studying CLN7 functions in neurons [143].

The neuronal cell line of an immortalized cerebellar (CB) isolated from *Cln7*$^{-/-}$ mice has been established to study CLN7 disease pathomechanisms [150, 152]. It has been shown that the *Cln7*$^{-/-}$ mouse represents a model of CLN7 disease in human as the clinical feature of the disease including neuroinflammation, the accumulation of lysosomal material in the brain and neurodegeneration have been observed [150]. Late endosomes (LEs) and lysosomes are enlarged in the *Cln7*$^{-/-}$ neurons, in addition to the defective outward movement of LEs/ lysosomes and the lysosomal exocytosis impairment [153].

As lysosomes are reported to be expanded in CLN7 disease, the late endosomal/ lysosomal vesicles size in the *Cln7* deletion CB cells was measured by fluorescence image analysis. In comparison with the control, in *Cln7* deleted CB cells there was an

enlargement in Lamp 1 –positive LEs/lysosomes. There were no significant differences in the amounts of Rab7 and Lamp1 between *Cln7* $^{-}/^{-}$ CB cells and wild-type controls, which means the LEs/ lysosomes enlargement was not affected by changes in these protein activities in the absence of CLN7 [153].

A western blotting experiment was used to analyse the levels of various enzymes of soluble lysosome including CLN5, LAMP 2, Cathepsin B, Cathepsin D and Cathepsin L in *Cln7* deletion CB cells *vs*. wild-type controls. It has been observed that the CLN5 and cathepsin D levels were reduced in CLN7 deletions compared to the wild-type control, while the amounts of cathepsin B, cathepsin L and Lamp 2 remained unchanged in the absence of CLN7 [153].

The autophagic substrates LC3-II and p62 accumulation in the tissue of brain has been detected in *Cln7* $^{-}/^{-}$ mice indicating impaired autophagy [150].

In CLN7 KO mice, the high levels of the microtubule-associated protein 1 light chain 3-II (LC3-II) neurona and the accumulation of p62 indicate constitutive macroautophagic impairment [150].

It has been tested whether CLN7 absence causes aberrant autophagy in cultured cells. To quantify autophagic flux, Cln7-absent CB and control cells were incubated in complete or amino acid- and serum-free EBSS media with or without bafilomycin A1 for 0.5 or 2 hours. Bafilomycin A1, a potent inhibitor of lysosomal acidification, stops protein degradation in lysosomes, leading to LC3-II and p62 accumulation, thus reflecting autophagic flux [153].

WB experiments on cln7-1- and wild-type cells detected no significant differences in the levels of LC3-II or p62 in cells treated with bafilomycin, indicating that the deletion of CLN7 had no effect on the basal or starvation-induced autophagic flux in CB cells. Moreover, wild-type and *Cln7−/−* cells starved for 2 hours in the absence of bafilomycin showed decreased p62 levels compared to fed states, indicating efficient proteolytic degradation of p62 by autophagy [153]. These data were confirmed by measuring autophagic flux, counting LC3-positive autophagosomes per cell with and without NH4Cl, another inhibitor of lysosomal proteolysis. In agreement with the results from WB experiments, the number of autophagosomes in *Cln7−/−* and wild-type cells was comparable, suggesting that the autophagy process is competitive in *Cln7−/−* CB cells. Additionally, lysosomal pH measurements in CB cells of both genotypes demonstrated that the loss of CLN7 does not alter lysosomal acidification[153].

However, there were no significant differences in the LC3-II and p62 levels in bafilomycin-treated cells between wild-type control and *Cln7* deletion CB cells, indicating that CLN7 deletion has no effects on basal or starvation-induced autophagic flux in the CB cells [153].

To identify the role of CLN7 in the outward transport of LEs/ lysosomes, *Cln7* deletion CB cells and wild-type control were incubated in a buffered solution at pH 6.8 or pH 7.3. However, the acidification of cytoplasm led to stimulation of the movement of the outward lysosome to the cell periphery [154]. Immunofluorescence microscopy was used to analyses the intracellular localization of LEs/ lysosomes. Decreasing the pH of cytoplasm stimulated LEs/ lysosomes outward transport in wild-type cells by about 70%,

as reflected by LAMP 1-postive vesicles becoming clustered peripherally. However, in the case of CLN7 loss, only 30% of cells revealed LEs/ lysosomes clustering at the peripheral site. However, mTOR kinase activity was inhibited by Torin 1 and decreased the wild-type vesicles outward movement to *Cln7* $^{-/-}$ CB cells levels and CLN7 deletion did not improve this effect [153]. It has been observed that Ca^{2+} plays a significant role in lysosomes motility regulation [155], so the Ca^{2+} concentrations have been measured in CB cells and there were no significant variances observed between *Cln7* $^{-/-}$ CB cells and wild-type control which indicates to the reduction of lysosomal outward movement in the case of CLN7 loss is not dependent on the lysosomal calcium. Moreover, to observe the effect of CLN7 in lysosomal exocytosis the CB cells were incubated in a calcium ionophore called ionomycin which leads to an increase in Ca^{2+} influx [153]

Impaired reactivation of mTORC1 was tested in *Cln7* $^{-/-}$ CB cells in response to starvation. However, mTORC1 time-dependent reactivation has not been observed in *Cln7* $^{-/-}$ CB cells and wild-type control. Although autophagy was induced in neuronal CB cells, mTORC1 reactivation was not affected by prolonged starvation followed by a re-supply of growth factors and nutrients. The data suggest that in the starvation case the absence of CLN7 affects AKT signalling and the decrease of AKT Ser473 phosphorylation in *Cln7* $^{-/-}$ CB cells leads to reduced viability [153].

For CLN7 MEF, quantitative proteomic data used the analysis of mass spectrometry of isolated lysosome from CLN7 KO mouse fibroblasts via Stable Isotope Labelling by Amino acids in Cell culture (SILAC) have been observed that deficiency of CLN7 leads to alterations in lysosomal soluble proteins levels under the conditions of steady state in

CLN7 KO MEFs. These are cells that are less able to adapt to starvation conditions and have a clear impairment in mTORC1 reactivation when nutrients are re-supplied after starvation. [138].

Quantification demonstrated that in comparison with wild-type controls, about 12 different soluble lysosomal proteins were decreased in CLN7 KO MEFs including the proteins of soluble lysosome used in the glycans degradation (fatty acid-modified proteins (prenyl cysteine oxidase (Pcyox1)), lipids (N-acylethanolamine-hydrolyzing acid amidase (Naaa), group XV phospholipase A2 (Pla2g15)), peptides (lysosomal Pro-X carboxypeptidase (Prcp), carboxypeptidase Q (Cpq), dipeptidyl peptidase 2 (Dpp7)), and sialate O-acetylesterase (Siae), N-acetylglucosamine-6-sulfatase (Gns), and aspartylglucosaminidase (Aga)) [138]. The data also showed a decrease in the amounts of the unknown function of lysosomal proteins which containing neuronal ceroid-lipofuscin protein 5 (CLN5), Niemann Pick type C2 protein (NPC2) and mammalian ependymin-related protein 1 in CLN7 KO MEFs compared with control cells. However, in CLN7 KO MEFs cells the amount of three soluble lysosomal proteins was increased including cathepsin K (Ctsk), cathepsin S (CtsS) and prosaposin (Psap) [138].

When the function of CLN7 protein is absent the levels of several soluble lysosomal proteins are affected, and the proteomic data have been confirmed by the measurements of immunoblotting enzymatic activity and the quantification of mRNA [138].

Cell metabolism is regulated by mTORC1 in cases of environmental stimulations. Nutrient starvation inactivates mTOR signalling and the mTORC1 pathway is reactivated by amino acids, which are provided by the autophagic substrates degradation. The S6 ribosomal protein (S6) phosphorylation, which is a downstream target of the mTORC1 pathway, has been observed to assess the effects of CLN7 KO MEFs in mTORC1 inactivation and reactivation during prolonged starvation in both CLN7 KO MEFs and wild-type control cells. The levels of phosphor-S6 were reduced after 8 and 12 hours of starvation in CLN7 MEFs in comparison with control cells showing mTOR signalling impairment in the case of starvation [138]. However, mTORC1 recruitment to lysosomes normally occurs in the absence of CLN7 and is active and responds normally to stimuli [138].

To investigate the possibility of defect in basal and starvation-induced autophagy under starvation, the immunoblotting analysis was done for CLN7 KO MEFs and the control cells which undergo starved up to 12 h in amino acid and serum free medium, and it was observed that autophagy-mediated degradation was unchanged in CLN7 KO lysosomes. In addition, CLN7 KO and wild-type MEFs were incubated in bafilomycin A1 in complete or in amino acid and serum-free starvation medium and the result demonstrated that the autophagic flux was unaffected in the case of CLN7 deletion [138].

The specific role of CLN7 during prolonged starvation and its significance for neuronal cells requires further study.

To identify more details about the cell biology of the disease, CLN7-/-mice were used to create two cell-based models. The first model consists of immortalized mouse embryonic fibroblasts (MEFs) transduced with the SV40 large T antigen [156, 157]. The second model involves mouse granule neuron progenitor cells (GNPCs) from cerebella [158], also immortalized by transduction with the SV40 large T antigen. The results demonstrated that fibroblasts have the potential to describe a general lysosomal phenotype, while GNPCs serve as a suitable model for studying NCL7 [143].

In summary, the main conclusions from the Cerebellum and MEF model are as follows: there is enlargement of late endosomes (LEs) and lysosomes, along with defective outward movement of LEs/lysosomes and lysosomal exocytosis impairment. Moreover, the CLN5 and cathepsin D levels were reduced in CLN7 deletions [153]. Additionally, loss of CLN7 function leads to autophagy impairment, while lysosomal acidification remains unaffected by the loss of CLN7. Furthermore, mTOR signaling is impaired in cases of starvation, but autophagic flux is unaffected in CLN7 deletion scenarios [138] [153]. It has been suggested that the absence of CLN7 affects AKT signaling during starvation, resulting in reduced viability [153].

In the absence of CLN7, 12 different soluble lysosomal proteins used in glycan degradation, peptide modification, and lipid and fatty acid metabolism were decreased. Among the lysosomal proteins that decreased are CLN5, cathepsin D, Niemann Pick type C2 protein (NPC2), and mammalian ependymin-related protein 1. Additionally, three soluble lysosomal proteins increased in amount: cathepsin K (Ctsk), cathepsin S (CtsS), and prosaposin (Psap) [138].

1.6.5.3. Mouse model.

Lysosomal dysfunction and impaired autophagy have been observed in the mouse model for CLN7 disease which was generated by exon 2 deletion from the CLN7/MFSD8 gene. In CLN7 knockout (KO) mouse brain, the dysfunction of lysosome was detected by the accumulation of autofluorescent lipopigments in lysosomes, the amounts increase of cathepsin B (CtsB), CtsZ, CtsD, and β-hexosaminidase, Saposin D and storage of subunit c of mitochondrial ATPsae synthase (SCMAS) in the brain and retina. Moreover, it was shown that microgliosis occurs in the brain, in addition to neurodegeneration and strong and progressive astrogliosis [150]. The rates of mortality were increased in CLN7 KO mice and there were clear signs of neurological deterioration, including paralysis in the hind leg, tremor and myoclonus epilepsy. An Increase in the activities of β-hexosaminidase enzyme in the brain of 10-month-old CLN7 KO mice was observed by about 2.6-fold in comparison with age matched wild-type mice [150].

Autophagy impairment is considered an important feature of many lysosomal storage diseases [64]. In the CLN7 KO mice brain, the increased level of the autophagy marker LC3-II and the accumulation of the autophagy adaptor protein p62 and polyubiquitinated proteins in the brain indicated impaired autophagy [150].

This study suggested that CLN7 deletion in the brain leads to lysosomal and autophagy system defects and eventually leads to neurodegeneration in the olfactory bulb, cortex, cerebellum, and retina, reduced mutant mouse lifespan and neuroinflammation. However, the link between lysosomal dysfunction and the putative lysosomal transport CLN7 deficiency is still unclear in this data [150].

1.6.5.4. Dog and monkey models

Studies have been done to study the CLN7 disease phenotype in naturally occurring cases in Chihuahua dogs [159]. In addition, the Japanese macaque monkey has been identified as a model of childhood neurodegenerative disorder neuronal ceroid lipofuscinosis caused by CLN7 gene mutation [148]. However, naturally occurring mutations in dogs and engineered mutations in monkeys are available in higher models. These have proven useful in studying neuropathology but have not yet been used to study CLN7 function.

1.6.5.5. *Drosophila melanogaster* model

The *Drosophila* gene is thought to be the only *Drosophila* orthologue of CLN7, sharing 57% of its amino acid sequence with human CLN7[117].

Drosophila, with its short generation time and low maintenance cost, has become an attractive tool for modelling human diseases. Furthermore, approximately three-quarters of human genes linked to diseases are conserved in the *Drosophila* genome, and several inherited diseases have been successfully modelled in *Drosophila* [160]. Numerous fundamental properties of higher eukaryotes have been discovered in the *Drosophila* central nervous system (CNS). Moreover, *Drosophila* has been used to study the cell biology of several human neurodegenerative disorders, including gain-of-function disorders such as tauopathies and loss-of-function forms of Parkinson's disease [160].

The visual pathology that develops early in the disease of CLN7 is compatible with the fact that Cln7, a glial protein in the CNS of *Drosophila*, is also expressed in neurones of the visual system from the earliest stages to adult flies [128]. The loss of CLN7 function was generated to study its role in *Drosophila*. Two mutants have been generated: $Cln7^{84D}$, in which exons 1-5 were excised, and another allele, $Cln7^{36H}$, in which exons 1, 2, and part of exon 3 were excised [117].

Previous studies investigated the function of CLN7 in the *Drosophila* neuromuscular junction (NMJ). Cln7 has been discovered to be expressed in the glia that surround the motor neurones as well as in the body wall muscles, which compose the NMJ's post-synaptic cells [128]. Furthermore, Discrete vesicles containing CLN7 are found right next to the post-synaptic location [117]. The study observed a reduction in type Ib motoneuron terminals at muscle 4 in the Cln7 mutant larvae, and this reduction is linked to synapse growth reduction. Therefore, the levels of CLN7 protein are important for NMJ development, and these results suggest that normal synapse development depends on CLN7 [117].

The normal size of the NMJ is affected by the reduction of Cln7 protein. CLN7 controls TOR signalling in a vascular component located at the post-synaptic side of the junction. In *Drosophila*, TOR signalling has been linked to synaptic activity at both central and peripheral synapses in earlier research, as TOR signalling has a conserved post-synaptic role [117]. However, the study also observed that the $Cln7^{84D}$ mutant leads to dysregulation of TORC1 activity. In addition, loss of CLN7 function causes failure of development of synapses, which leads to decreased function and behavioural

changes [117]. Therefore, *Drosophila* was chosen as the appropriate model for this study due to its advantages mentioned above. Additionally, the function of CLN7 in the NMJ in *Drosophila* and the presence of CLN7 in the PSD were considered.

1.6.6. CLN7 function

As reviewed above, numerous studies have investigated CLN7 protein function, in a variety of model systems. The absence of CLN7 leads to the depletion of soluble proteins in lysosomes and impairs mTOR reactivation [138]. In addition, several studies have suggested a role for CLN7 demonstrated in lysosomal function, with effects on lysosomal chloride haemostasis, the potential of the lysosomal membrane and the pH of lysosome. Moreover, it was found that loss of CLN7 function causes autophagy impairment, which leads to the accumulation of dysfunctional mitochondria [161]. The synapse dysfunction is linked with loss of CLN7, and its function is essential in the post-synaptic side of the NMJ [117].

However, no study had identified the function of CLN7 until recently when CLN7 was shown to be a novel endo-lysosomal chloride channel [162]. CLN7 has been discovered as a novel endolysosomal chloride channel, and studies have shown its regulatory effects on lysosomal function. However, CLN7 mutations lead to reduced chloride permeability. Through a Ca2+/calmodulin-dependent mechanism, overexpression of CLN7 causes endolysosomes to expand and increases endolysosomal chloride currents [162]. Chloride channel characteristics that are susceptible to chloride channel blockers

are present in both human CLN7 and its homolog. Additionally, CLN7 controls the conductance of lysosomal chloride[162]. The next stage will be to identify how changes to Cl^- transport impact the lysosomal membrane processes.

1.7. Aims

It has been shown in previous studies within the group that Cln7 is localized to the post-synaptic density in a vesicular compartment. Based on this, the possibility of its function in synaptic development is very strong. Therefore, the overarching aims of my thesis were to help determine how Cln7 functions at synapses to regulate synaptic development and to regulate metabolism. We know from previous studies in the group that Cln7 is localised to the post-synaptic density in a vesicular compartment, but we do not know what function it preforms there. One way of addressing this question is to identify which other proteins are in a complex with CLN7. Hence, my thesis concentrated on the following objectives:

- The first objective of my thesis was to validate the proximity labelling experiments with CLN7 to identify candidate interacting proteins using *Drosophila* S2 cells.
- The second, was to validate if those candidate interaction proteins can interact with CLN7 using alternate methods such as IP.
- The third, to ask whether similar interacting proteins could be found *in vivo* at the *Drosophila* NMJ.
- Alongside, a fourth objective was to continue the study of CLN7 function in growth control in *Drosophila* to ask how loss of CLN7 function impacts on metabolism.

2. MATERIALS AND METHODS

2.1. Cell culture methods

2.1.1. Biotin

Biotin is a significant label for protein detection, purification, and immobilization because of its extraordinary strong connection to streptavidin and avidin. It is one of the strongest noncovalent interactions between a protein and a ligand. It is smaller than enzyme labels and depend on that is less likely to interfere with normal protein function [163, 164]. Biotin was soluble in 0.1 M NaOH at 10 mg/ml (40 mM) as stock and stored at 4 C˚.

2.1.2. *Drosophila* Schneider 2 cells

The source of the *Drosophila* Schneider 2 cells (S2 cells) line is a primary of late stage (20-24 hours) *Drosophila melanogaster* embryos. S2 cells grew in Schneider's Drosophila medium containing 10 % (v/v) FBS and 1% (v/v) penicillin streptomycin (10,000 units/mL of penicillin and 10,000 µg/mL of streptomycin) (Thermo fisher) and were stored in a humidified incubator at 27 ^{o}C. The cells were semi adherent in the flask and the medium was replaced regularly every 72 hours or depending on the turbidity of the cells.

2.1.3. Thawing frozen cells

A vial of frozen cells was warmed up in a 37 °C water bath with gentle agitation to speed up the melting process. Once thawed, the cells were pipetted gently out into 4 ml of Schneider's medium/10% FBS at room temperature and mixed gently. The cell mixture was centrifuged at 1000 rpm for 5 minutes and the supernatant was removed and replaced with fresh medium. Then, the cells were transferred to a small flask and checked the following day for viability.

2.1.4. S2 cell transfection

In a sterile centrifuge tube, 250 µl of serum free medium was added with 2.5 µg plasmid DNA and after gently mixing, 7.5 µl Trans IT-2020 reagent (Mirus) was added in a ratio of 3:1 to the DNA. The mixture was incubated at RT for 20 minutes to allow enough time for the complex, but not more than 30 min. The mixture was added to wells of S2 cells at approximately $3x10^5$ in a 6-well dish gently rocked to distributed evenly and incubated at 27 ^oC for 72 hours.

For the stable cell line, pCoHygro is the hygromycin resistance vector that was co-transfected with the DNA by ratio mass 1:1 and every 48 – 72 hours cells were harvested and pelleted and replaced in the same wells or flasks by fresh media containing 1% (v/v) hygromycin until the resistant colonies were observed.

2.2. Molecular biology methods

2.2.1. Cloning

2.2.1.1. Gateway cloning

Forward and reverse primers (Table 2.4) were used to amplify the open reading frame (ORF) of TurboID-CLN7 DNA. Afterward, it was loaded onto a 1% (w/v) gel for electrophoresis to confirm that it was the correct size. The ORF was then inserted into the pENTR/D-TOPO cloning vector (Invitrogen), and after the miniprep process, it was sent for sequencing (section 2.2.7). Finally, the ORF was transformed into the destination vector as described in the following paragraphs.

2.2.1.2. LR Clonase II Enzyme Mix (Invitrogen)

It stimulates recombination an entry clone gene attL-flanked with destination vector attR-flanked to generate expression clone containing attB (Figure 4. 4). The kit was stored at -20 ^{o}C.

2.2.1.3. Luria-Bertani (LB) broth medium

LB broth (35 gm) powder was dissolved in 1L d H_2O and autoclaved. After autoclaving, the mixture was cooled to 55 °C and antibiotic (50 µg/ml) was added, then poured into 90 m petri plates and stored at 4 °C in the dark until use.

2.2.1.4. LB broth

As there are several suppliers, each with their own instructions for the amount of LB broth to be used, the suitable amount of LB broth (25 g/ 100 ml) was dissolved in distilled water dH_2O and autoclaved. It was then stored at 4°C for future uses.

2.2.1.5. Agarose Gel electrophoresis (AGE)

Agarose (1% w/v) was dissolved in 1 X TBE buffer (130 mM Tris-HCl pH 7.6, 45 mM Boric acid and 2.5 mM EDTA) (Table2.3) by heating. After the gel polymerised, it was transferred to a running BioRad horizontal electrophoresis device and covered by 1 X TBE. The gel was run at 140 V for approximately 30 mins.

2.2.2. Polymerase chain reaction (PCR)

Between 1 and 10 ng DNA was added to the forward primer (10 µM) (Table 2.4), the reverse primer (10 µM) (Table 2.4), 5X buffer High fidelity (HF), 50X dNTPs (0.2µM) and the proofreading enzyme Taq DNA polymerase (Progemga). The mixture was then completed with sterile water to 50 µl. The mixture was put in the PCR machine at initial denaturation at 95°C for 30 seconds, then annealing at 56°C for 30 seconds and extension at 72°C for 2 min for 30 cycles and the last extension at 72°C for 10 min.

2.2.3. DNA detection in the gel electrophoresis

After the PCR process, the sample was analysed by 1 % agarose gel electrophoresis (AGE) to detect the target amplification and the right size of the DNA product. Then, all the PCR DNA volume was loaded in the gel to have the detected band of the desired DNA. The PCR DNA sample was mixed with 1x DNA loading dye buffer double blue (ThermoFisher scientific) and loaded into the gel and run at 130V for about 40 min. The bands were observed on a blue light transilluminator, and the correct bands were excised with a razor blade for purification.

2.2.4. Purifying the PCR-DNA gel

The desired DNA fragments were taken with a clean and sharp blade. The amount of surrounding agarose as excised with the fragment. The purification process was done for the gel fragments by centrifugation (Promega) following the Wizard plus SV Gel and PCR Clean up protocol. The gel slice was placed into a 1.5 ml microcentrifuge tube and per 10 mg gel slice 10µl of membrane binding solution was added and incubated at 60 ^{o}C with shaking until the gel slice completely dissolved. Once the binding of the DNA process was done, and the product was washed with membrane wash solution, the DNA product was eluted to a clean 1.5 ml microcentrifuge tube by adding 50 µl of nuclease-free water to the minicolumn and centrifuged at 16000 × g for 1 minute and the purified PCR product was stored at -20°C.

2.2.5. Cloning the DNA into pENTR clone

In 1.5 ml Eppendorf tube, 5 µl of PCR DNA product was added to H_2O, salt solution and pENTR D/TORO (2:1:1:1) and incubated for 30 minutes at room temperature then transferred to ice for 5 min. 20 µl of bacterial *E. coli* component was added to the sample and incubated in the ice for 30 min before a heat shock at 42°C for 30 seconds. The S.O.C medium was added, and the mixture was shaken at 200 rpm for 60 minutes at 37°C. The solution was spread on LB agar plates plus kanamycin and incubated at 37°C overnight. Each colony on the pENTR agar plate was taken by sterile tip and transferred to 2 ml of LB broth medium containing (50 µg/ml) kanamycin resistance. It was incubated at 200 rpm overnight at 37°C and the LB growth culture was isolated according to the miniprep process.

2.2.6. Miniprep isolation of DNA

Following the miniprep kit protocol (sigma), the process was started by centrifuging the LB broth medium which contains the bacteria. The bacterial pellet was resuspended in the resuspension solution until homogenous. A lysis buffer was added and mixed gently and kept for 5 minutes to have a clear solution. The neutralization/binding solution was added to precipitate the cell debris and mixed gently. The solution was centrifuged at 14000 rpm for 10 minutes and the supernatant was transferred to a GenElute miniprep binding column. That column was inserted into the microcentrifuge tube and about 500 µl of the column preparation solution was added to that column and centrifuged at

12000 rpm and the flow throw discarded. The DNA supernatant was then added to the column and centrifuged at 14000 rpm for 1 min and the flow through was discarded. The column was washed with the diluted wash solution and after the centrifuge process the flow throw was discarded. The column was transferred to a new centrifuge, 100 µl of elution solution was added to the column to elute the DNA (50 µl elution solution was added in case more DNA concentration needed), and the DNA was storage at -20 ˚C.

2.2.7. Sequencing

This process is important to determine the nucleotide and confirm whether the gene is cloned in the correct orientation. Plasmid DNA (100µg) was sent for Sanger sequencing, usually the sequencing process is approved with standard M13 forward and M13 reverse primes (Table 2.4). Custom primers were ordered from Eurofins for non-standard sequencing and sent with the DNA.

2.2.8. Transformation to a destination cloning (pDEST vector)

After the analysis and sequence process of the plasmid DNA, LR clonase II enzyme was used in this process. Following the LR clonase II enzyme kit (Invitrogen) protocol, 0.5 µl plasmid DNA was added to 0.5 µl pDEST clone and completed to 8µl by TE buffer (10 mM Tris-HCl pH8.0, 1mM EDTA, pH 8.0) (Table 2.1). Then 2µl was taken from the previous mixture, placed into a new 1.5 sterile centrifuge, mixed with 0.5 µl LR recombination reaction and incubated at room temperature for 1 to 3 hours. The 2.5 µl

mixture was added to 40 µl *E. coli* bacterial and incubated on ice for 30 min before a heat shock at 42 ^{o}C for 30 seconds. S.O.C solution (250 µl) was added and incubated at 37 ^{o}C with shaking at 200 rpm for 1 hour. 50 µl of the mixture was spread in the LB agar plate containing ampicillin and incubated at 37 ^{o}C overnight. One colony was picked up with a sterile pipette tip and added into 50 ml LB broth containing (50 µg/ml) ampicillin and incubated at 200 rpm and 37 ^{o}C overnight.

2.2.9. Midiprep for the expression colony

Following the Midiprep Kit protocol (Sigma), the 50 ml culture solution was centrifuged at 5000 × g for 10 min and the supernatant was discarded and the pellet was resuspended with resuspension RNase. After that lysis solution was added and inverted gently into the mixture and left for about 5 min to become clear. A neutralization solution was added to the lysed cells and inverted gently for mixing. The binding solution was added to the mixture and that mixture was transferred into the barrel of the filter and incubated for 5 min. Cleared lysate was expelled into the column and centrifuged at 3000 × g for 3 min and the flow through was discard. Wash solutions 1 and 2 were added to the column and centrifuged at 3000 × g for 2 min and the flow through was thrown. For the elution process the collection tube was changed and the elution solution was added and centrifuged at 3000 × g for 5 min. The DNA concentration was measured using a DNA Nanodrop, and the DNA was concentrated to

obtain a final concentration of 1 µg/ µl. Three DEST vectors used in this process pTW, pAMW and pTMW.

2.2.10. DNA concentration

A 0.1 volume of 3 M sodium acetate buffer solution pH 5.2 (Table 2.1) was added to the DNA solution, then 0.7 of isopropanol was added, and centrifuged at 14000 rpm for 30 min at 4 °C, and the supernatant was thrown. The pellet was rinsed with 1.5 ml of 70 % ethanol and centrifuged at 14000 rpm for 10 min at 4 °C, then the supernatant was discarded. The pellet was left to air-dry until the residual ethanol evaporated and then resuspended with a suitable volume of d H_2O.

2.2.11. Single fly Genomic DNA prep

To validate wither the UAS-BioID-CLN7 or UAS-TurboID-CLN7 transgenes (Table 2.7) were present in the flies, 1 µl of proteinase K was added to 50 µl of squishing buffer (SB) (10 mM Tris-HCl PH 8, 1 mM EDTA, 25 mM NaCl) (Table 2.1). The fly was crushed with a P200 pipette tip for 5- 10 seconds without expelling, then the buffer was added to the crushed fly and incubated at 37 °C for 1 hour. The proteinase K was then inactivated by heating at 95 °C for 3 min. The mixture was centrifuged, and the supernatant was taken to a new centrifuge tube and saved at – 20 ˚C. For DNA analysis the PCR was done using GW5f Fwd and SVr primers (Table 2.4).

2.3. Biochemistry

2.3.1. Immunoprecipitation from cells

BioID-CLN7 or TurboID-CLN7 expressed in S2 cells were transferred from the plate to a falcon tube and centrifuged at 1500 x g for 5 min. The supernatant was discarded, and the pellet was washed once with phosphate-buffered saline (PBS) (Table 2.1). Afterward, the lysis buffer (Table 2.1) was added to the washed pellet and incubated on ice for 5 minutes. Subsequently, the lysate was centrifuged at 14,000 rpm for 10 minutes at 4°C.The supernatant was transferred to a centrifuge tube and anti-myc antibody (Table 2.5) was added for 2-4 hours. Magnetic protein G beads were washed by TBST (Table 2.1) and then added to the sample for 60 min (or overnight). The beads were washed with wash buffer (25 mM Tris-HCL pH 7.5, 5 mM $MgCl_2$, 150 mM NaCl, 1mM EDTA pH 8, table 2.2) for 5 x 5 minutes. An elution buffer (1x Laemmli buffer and 20 mM DTT) was then added, and the beads incubated at 70 ^{o}C for 5 min. The magnetic beads were then pulled to the magnet and the eluate was transferred to a new 1.5 ml Eppendorf tube. Samples were loaded onto SDS-PAGE gels for western blotting or stored at -20 ^{o}C.

2.3.2. SMALPs and GFP-Trap beads

The pAVW-CLN7 expressed in S2 cells (1 ml) were added into the 15 ml falcon and centrifuged at 1500 rpm for 3 minutes then the supernatant was thrown. The pellet was washed once with the buffer 1 (50 mM Tris-HCl PH 7.4, 150 mM NaCl, 5mM EDTA), and

centrifuged at 1500 rpm for 3 minutes and the supernatant was disposable. The pellet was re-suspended in the SMALPs lysis buffer solution (1 % Styrene Maleic-Acid Lipid Particles (SMALPs) (w/v), 50 mM Tris-HCl PH 7.4, 150 mM NaCl, 5mM EDTA and 1:200 Protease inhibitors (PI) (Calbiochem) (1 µl PI for 200 µl volume) at room temperature and incubated at room temperature with gentle shaking for 1 hour. After that, the sample was centrifuged at 14000 rpm for 30 min at 4 °C and the supernatant was removed to a new centrifuge tube. GFP-Trap beads were resuspended and about 10 µl were transferred to a new centrifuge tube and washed by suspending in 500 µl of buffer 1. The supernatant solution was added to GFP-Trap beads. Then, the mixture was incubated for 1 hour at RT with gentle rocking. The beads were pulled to a magnet and the flow through was transferred into a new tube. The beads were washed in 500 µl SMALP buffer for 3 x 5 minutes. The beads were then resuspended in 100 µl of 1x Laemmli buffer to elute the desired proteins, heated at 70 ˚C for 1 min and kept at RT for 15 minutes. Finally, the beads were pulled to a magnet to allow the eluate to be removed to a new tube and stored at – 20 ˚C.

2.3.3. Immunoprecipitation of flies

The cold lysis buffer (25 mM Tris-HCl pH 7.5, 5 mM MgCl2, 150 mM NaCl, 1 mM EDTA pH 8, 2 % (w/v) DDM and 1:200 protease inhibitors (PI) (1 µl PI for 200 µl volume) (Calbiochem)) was added to larval or adult flies in a centrifuge tube, they were crushed and kept on ice for 5 to15 minutes. The lysate was centrifuged at 14000 rpm for 15

minutes at 4 ˚C. Then, the supernatant was transferred into a new centrifuge tube and stored at -20 ˚C.

2.3.4. Immunoblotting

2.3.4.1. Western blotting

Samples (1 µl – 35 µl depending on the experiment) were loaded onto SDS-PAGE gels with 5 µl PageRuler Plus pre-stained protein ladder and run at 115 V for 90 min in the loading buffer (Table 2.3). The PVDF membrane was inserted in 100 % methanol for 30 seconds to equilibrate and then in 10 ml dH_2O for 5 min, and then in a cold transfer buffer solution (Table 2.3) for 10 min with shaking. The proteins were transferred to the PVDF membrane at 1X transfer buffer (Table 2.3) at 30 V overnight. The PVDF membrane was incubated in 5% milk in TBST (Table 2.1) for 30 min at room temperature to block, then it was left in primary antibody overnight at 4 ^{o}C or for 1 hour at RT. The membrane was washed in TBST (Table 2.1) 5 x 5 minutes then the secondary antibody was added onto the membrane and incubated for 60 min with gentle rocking at RT. The PVDF membrane was washed by TBST for 5 x 5 min with gentle shaking. SuperSignal West Femto Maximum Sensitivity Substrate (Themo Fisher) detection reagents 1:1 were added to the PVDF membrane before observation by chemiluminescent detection using a Vilber digital scanner.

In the case of Streptavidin- Horseradish Peroxidase (HRP) Conjugate, the PVDF membrane was incubated in the block buffer (5% milk in TSB table 2.1) for 1 hour with

gentle agitation at room temperature, then the membrane was washed with TSBT twice time for 5 minutes with agitation and incubated into 1:10000 streptavidin-HRP conjugate (Table 2.5) overnight at 4°C or for 1 hour at room temperature. After that, the PVDF membrane was transferred into a tray with 20 ml TSBT and washed for 5 min with agitation 3 x 5 minutes, then washed with TBS (Table 2.1) 3 x 5 minutes and finally with dH2O for 3 x 5 minutes with agitation. Suitable reagent detection was added to detect the bands by chemiluminescent detection.

2.4. *Drosophila melanogaster*

2.4.1. *Drosophila melanogaster* husbandry

The Bloomington Stock Centre, University of Indiana was the source of *Drosophila melanogaster* genetic lines. The stocks of flies used in this thesis are indicated in table 2.7. Stocks were maintained on standard food (Table 2.8) at 18°C at low density and expanded or crossed on nutrient-rich food at 25°C to increase progeny yield.

2.4.2. Juice agar plates

For 1000 ml volume, 752 ml water, 252 ml grape juice, 30 g agar and 12 g sucrose were mixed and heated in a large flask until the agar dissolved and boiled. The mixture was cooled to 50 °C, and 10 ml ethanol with 5 ml acetic acid were added to that mixture, mixed thoroughly, and transferred to plates. After setting, the plates were stored at 4 °C.

2.4.3. SY Blue food

Coomassie 2 % (v/v) was diluted in 100 % ethanol. 5 ml of the diluted Coomassie was then added to 50 ml SY food (Table 2.7) and this solution was then divided into 7 x 7ml vials.

2.4.4. Fly mass assay.

Wild-type (*w*^{1118}) and other genotypes of flies (Table 2.7) were mated in embryo collection cages, allowed to lay eggs for 24 hrs on grape juice agar plates, then the plates were changed over, and the eggs incubated for a further 24 hours to hatch as first instar larvae. These were then picked up off the agar plate and transferred in groups of 100 into vials of SY food (Table 2.8) and incubated at 25°C. The masses of adult males and females were measured separately in groups of 10 in analytical balance, and then the mean mass was calculated.

2.4.5. Food consumption

One hundred 1st instar larvae were inserted in vials of blue food and incubated at 25 ˚C until become L3 instar larvae for three days, then 20 % (w/v) sucrose in water was added to the L3 larval vial to float the larvae out. The larvae were then taken into a dish, washed with d H_2O, transferred into a centrifuge tube (20 larvae in each tube), and 10 µl PBS was added (10 µl PBS/1 larvae). Then the larvae were crushed and centrifuged at 14000 rpm for 15 minutes. Finally, 100 µl of the supernatant was added to the wells of

96-well plates for measurement of blue dye absorption at A595 as a proxy for food consumption. For the standard measurement, the 2% Coomassie dye was diluted in PBS ratios of 0:100 to 40:100.

2.4.6. Mapping of transgenic insertions

Transgenic lines of UAS-TurboID-CLN7 were generated by BestGene through insertion the DNA into embryo wild-type fly. Male adults of UAS-TurboID-CLN7 with coloured eyes were crossed with virgin females of the double balancer strain: w/w; If/CyO; MKRS, Sb/ TM6B, Tb, Hu. From the first-generation results, the males with coloured eyes, If and Sb were backcrossed with female virgin double balancer flies to map the transgenic insertions to chromosomes. Stable stocks of UAS-TurboID-CLN7 were generated with balancers or made homozygous, depending on the insertion. Three lines were established number 10, 17 and 18.

2.4.7. Expression of TurboID-CLN7

Males of UAS-TurboID-CLN7 (Table 2.7) were crossed with virgin females of Mef2-gal4/TM6B, Tb, Hu (Table 2.7) to drive TurboID-CLN7 expression in the muscles. The larvae were scored for the absence of Tb to ensure only TurboID-CLN7 -expressing flies were dissected.

2.4.8. Larval dissection

Larva (L3) was selected and placed in cold PBS (Table 2.1) in a glass specimen dish on ice. The larva was transferred to a drop of cold PBS in a Sylgard dish, and the mouth hooks were pinned. Gently, each larva was stretched by pulling on the posterior spiracles and was then cut first along the dorsal surface and then along the dorsal midline in both directions. Some of the gut was carefully removed to allow the cuticle to be seen, then the four corners were pinned out to create a butterfly shape. The rest of the trachea, guts and imaginal discs were removed. The larva was washed with fresh cold PBS. A drop of PBS with 4% formaldehyde was added to the larva to fix for 20 mins at RT, and then the larva washed 3 times with PBS. The pins were removed carefully, and the larva was transferred to an Eppendorf with PBS/0.1 Triton X-100 to permeabilise the cells for at least 10 mins. Multiple larvae were dissected and then added to the permeabilization solution which was kept on ice. Once dissection was completed, the larvae were blocked in PBS/1% BSA for 30-60 mins at RT. The block was then discarded and replaced with primary antibodies (Gt anti- HRP – A 594 1:500, mouse anti-DLG 1:100, rat anti-myc 1:1500 (Table 2.5)) and incubated O/N at 4°C on a nutator. The primary antibodies were discarded and the larval was washed 5 x 10-15 mins in PBS/TX. Then the secondary antibodies (donkey anti-mouse- Dylight 405; donkey anti-rat- Alexa 488, both 1:500 (Table 2.6)) were added to the larvae and it was left to rotate at RT for approximately 2-4 hours or O/N at 4°C. The larvae washed after the secondary antibody for 5 x 10-15 mins in PBS/TX. Prolong Gold mounting medium was added to a new clean slide. The larval taken and dabbed gently onto tissue to

remove excess liquid, then the samples were placed open side upwards on the slide, covered with a 1.5mm thick rectangular coverslip and stored at 4 ˚C before being imaged by confocal microscopy (an inverted Zeiss LSM780 confocal using (software).

2.5. Proximity labelling

2.5.1. In vitro proximity labelling

The in vitro labelling protocol of Roux et al. 2012 [163] was used. S2 cells expressing BioID and BioID-CLN7 were grown in cell culture flasks (volume 5ml 25 C^2). Biotin, which was dissolved in 0.1 M NaOH (40 mM stock), was added to the cells at a concentration of 500 µM in the entire volume and incubated for 24 hours.

Next, the cells were washed in PBS three times to remove free biotin. A lysis buffer (Table 2.1) was then added to the cells to extract biotinylated proteins for 10 min, and then lysates were sonicated for 10 seconds. After that, Triton X-100 was added to 2% (w/w) final concentration and the samples were sonicated for 10 seconds. Finally, 1 volume of cold 50 mM Tris-HCl pH 7.4 was added, and the samples were sonicated again for 10 seconds. The lysates were centrifuged at 14000 x g for 10 min at 4^o C and lysate fractions were taken before the remaining volume was incubated with NanoLink streptavidin Magnetic Beads (TriLink Biotechnologies) (after washing with TBST three times) at 4^o C overnight with rotation. After that, the beads mixture was centrifuged at 3000 x g for 30 min at 4^o C and flow-through samples were taken, then the beads were washed with BioID wash 1 twice (Table 2.2), with BioID washes 2 and 3 once each and

finally twice with BioID wash 4 (all wash solutions are detailed in table 2.2). The elution buffer (Table 2.1) containing 50 µl Laemmli sample buffer, 2 mM biotin and 10 mM DTT was added to the beads and heated at 98 ^{o}C for 5 min followed by the collection of the beads using a magnet and the transfer of the elution to a new centrifuge tube for running on SDS-PAGE gels.

2.5.2. In vivo proximity labelling

UAS-BioID-CLN7 and UAS-TurboID-CLN7 flies were crossed with Mef2-Gal4 flies to drive Myc-BioID-CLN7 and Myc-TurboID-CLN7 expression in muscles as described (all flies genotypes indicated in table 2.7). Third instar larvae were selected for Tb+ as described. biotin was added to some of the vials of food to become 50 µM in all the volume and flies were grown in that biotin food for 3 days, but others were used without biotin. At 4 ^{o}C, a lysis buffer (Table 2.1) was added to the *Drosophila* larvae at 20 µl per larva, crushed with a pestle, and centrifuged at 14000 xg for 10 min. Laemmli buffer was added to the supernatants and heated at 70 ^{o}C for 5 min, then analysed by SDS-PAGE and western blotting. For the identification of biotinylated protein, the same procedure was used as in Section 2.5.1.

2.5.3. Identification of proximity labelled proteins

2.5.3.1. Coomassie

After running the samples into the SDS-PAGE gel, the gels were stained overnight in Coomassie Blue stain (Bio-Rad) at RT and then washed in sterile water for 10 min three times. Bands were detected in a light box with white light.

2.5.3.2. Mass-spectrometry

To wash all equipment and surfaces, 70% ethanol was used, and gloves were worn to minimize keratin contamination. After loading proteins (BioID, BioID-CLN7, or TurboID-CLN7) onto an SDS-PAGE gel, Coomassie stain was added to the gel overnight. The stained gel was washed with ddH_2O three times for 10 minutes each, and then it was illuminated on a light box using white light to indicate the biotinylated proteins. The gel slices containing BioID, BioID-CLN7, or TurboID-CLN7 were isolated, cut out of the gel with a new, clean razor blade, and transferred to clean 1.5 ml Eppendorf tubes. The identical bands of BioID-CLN7 were observed, numbered, and taken in addition to those related to BioID bands. The gel slices were numbered while the gel was on the light box, and each slice has its number even in the Eppendorf tube. These gel slices are stored at -4°C prior to protein extraction and analysis, which is performed by the Advanced Mass Spectrometry Facility at the University of Birmingham according to their standard protocol. Mass spectrometry was carried out by the Proteomics service at the School of Biosciences, University of Birmingham. The Orbitrap Elite and Q-Exactive HF mass

spectrometers are used for protein/peptide identification. Both devices are equipped with a nano-flow liquid chromatography (LC) system with a reverse-phase column.

To identify proteins by MS, the interested protein excised from the gel is reduced and then digested into peptides using trypsin. Liquid chromatography, coupled to the mass spectrometer, is involved in separating the peptides. The peptide masses are determined by the mass spectrometer, and via MS/MS, their sequences can be confirmed. The detected peptide sequences are matched against a protein database to confirm the derived protein, and which proteins were originally present in the sample. To verify its presence, more than two unique peptides need to be detected from the same protein. By measuring the resulting peptide abundances in the mass spectrometer, relative protein quantitation can be inferred.

The results were sent in Microsoft Excel for separation and analysis. The Microsoft Excel sheet includes protein FDR confidence, protein description, coverage percentage, number of peptides, number of peptide spectrum matches (PSMs), number of protein groups, source of Sequest HT, molecular weight (MW) in kilodaltons (KDa), and number of unique protein peptides. In addition to that the BioID-CLN7 and BioID include the results contaminated with keratin which not included in TurboID-CLN7 results.

The contaminant results were removed, as well as the shared proteins for BioID-CLN7 and BioID or TurboID-CLN7 and tubby. Additionally, unique proteins related to BioID-CLN7 orTurboID-CLN7 were isolated. Several pieces of information should be considered, including whether biotin was added, whether the protein was found in

more than one sample or in more than one independent experiment, and the number of peptides and PSMs for the protein.

The gene names in that Microsoft Excel sheet were taken to the Flybase website (section 2.5.3.4) to determine the protein names, their CG numbers, and their possible localizations. The Flybase website offers research possibilities for genes, alleles, aberrations, and other genetic objects, sequences, phenotypes, stocks, and more. It was used to identify the hit protein names, their CG numbers, and the localizations of those proteins. After the MS analysis, the genes of interest can be researched further to obtain their names and CG numbers.

2.5.3.3. STRING analysis

STRING website was used for more analyses and to identify the possible protein interactions. It is a database of known and anticipated protein-protein interactions. Depending on computational prediction, knowledge transfer across species, and aggregated interactions from other (primary) databases, the interactions include both direct (physical) and indirect (functional) binds. High-throughput laboratory experiments, (conserved) co-expression, automated text mining, genomic context predictions, and prior database knowledge are some of the STRING data sources for interactions Moreover, there are 59'309'604 proteins from 12'535 organisms covered by the STRING database.

Protein-protein interactions, both known and projected, are listed in the STRING database. STRING is a database that contains known and predicted protein-protein interactions. These interactions, which rely on knowledge transfer between organisms and computational predictions, encompass both direct (physical) and indirect (functional) relationships. In addition to providing a variety of data sources, such as Genomic Context Predictions, High-throughput Lab Experiments, (Conserved) Co-Expression, Automated Textmining, and Previous Knowledge, the database collects interactions from other core databases. Moreover, the STRING database covers 59,309,604 proteins from 12,535 organisms.

As there are many proteins need to analysis by this website, hit proteins were loaded by researching and using CG protein numbers to obtain their protein interaction results within the Drosophila melanogaster organism. Additionally, the website offers information about the loaded proteins, including details about their interactions within the network.

The STRING network displays current interactions, with edges representing both physical and functional protein associations. The type of interaction evidence is indicated by the line color. Furthermore, Biological process gene ontology (GO), molecular function (GO), cellular component (GO), and other functional enrichments in the network can be displayed.

In this STRING network, I focused on protein interactions to demonstrate how hit proteins interact with each other and whether they interact with CLN7. Additionally, I

concentrated on gene ontology to understand the localization and function of the hit proteins, providing insights into the predicted function or effect of CLN7 (https://string-db.org/).

2.5.3.4. Fly-base analysis

FlyBase is an online bioinformatics database that contains molecular and genetic information about the *Drosophila* family of insects. FlyBase's data comes from a range of sources, including primary scientific publications and extensive genomic projects. FlyBase can be navigated using query tools by gene or mutant name, DNA or protein sequence, or terms from the several ontologies used to record functional, phenotypic, and anatomical data. To enable effective access to the available data and make it easier to find important relationships within the database, the database provides a number of query tools (FlyBase Homepage).

2.5.3.5. Validation of the BioID hit protein

pAVW-CLN7 cells were co-transfected with pCo-hygromycin in S2 cells to have a stable cell line of pAVW-CLN7 and used to detect whether BioID hit proteins (Table 4.1) interact with CLN7. This was proved via immunoprecipitation using SMALPs lysis and GFP-Trap beads (Section 2. 3. 2).

Table 2. 1: Buffer solutions recipe

Buffer name	Recipe
Phosphate buffer saline (PBS)	137 mM NaCl, 10 mM Na2HPO4, 2.7 mM KCl, and 1.8 mM KH2PO4, pH 7.4
PBST	PBS + 0.1 % Tween-20 (v/v)
Tris Buffer Saline (TBS)	50 mM Tris, 150 mM NaCl, pH 7.6
TBST	TBS + 0.1 % (v/v) Tween-20
Squishing buffer (SB)	10 mM Tris-HCl pH 8.0, 25 mM NaCl, 1 mM EDTA and 4mg/ml proteinase K
Tris-EDTA buffer (TE)	10 mM Tris-HCl pH8.0, 1mM EDTA, pH 8.0
Sodium acetate buffer	3 M sodium acetate pH 5.2
Lysis buffer for labelling	50 mM Tris-HCl pH 7.4, 0.4 % SDS, 5 mM EDTA, 500 mM NaCl, 1 mM DTT and 1:200 Protease inhibitors
Lysis buffer	25 mM Tris-HCl pH 7.5, 5 mM MgCl2, 150 mM NaCl, 1 mM EDTA pH 8.0, 2 % (w/v) DDM and 1:200 protease inhibitors
SMALP lysis buffer	1 % SMALPs, 50 mM Tris-HCl pH 7.4, 150 mM NaCl, 5mM EDTA and 1:200 Protease inhibitors
BioID elution buffer	1x Laemelli buffer, 2 mM Biotin solution and 20 mM DTT.
TurboID binding buffer	20mM Tris-HCl pH 7.5, 500 mM NaCl and 1 mM EDTA
TurboID elution buffer	1x Laemelli buffer, 10 mM biotin

Table 2. 2: Wash solution buffer

Solution	Recipe
Wash buffer	25 mM Tris-HCl pH 7.5, 5 mM MgCl2, 150 mM NaCl and 1 mM EDTA pH 8.0
SMALPs wash buffer	50 mM Tris-HCl pH 7.4, 300 mM NaCl and 5 mM EDTA.
BioID wash 1	2 % SDS (v/v)
BioID wash 2	50 mM HEPS pH 7.5, 500 mM NaCl, 0.1 % deoxycholate (w/v), 1 % TritonX-100 and 1 mM EDTA pH 8.0
BioID wash 3	10 mM Tris-HCl pH 8.0, 250 mM LiCl, 0.5 % deoxycholate (w/v), 0.5 % NP-40 and 1mM EDTA pH 8.0
BioID wash 4	50 mM Tris-HCl pH 7.4, 50 mM NaCl and 0.1 % NP-40
TurboID wash	20mM Tris-HCl pH 7.5, 500 mM NaCl and 1 mM EDTA

Table 2. 3: Electrophoresis buffer

Buffer solution	Recipe
SDS-PAGE running buffer	ddH2O, 25 mM Tris, 192 mM glycine and 0.1 (w/v) SDS
Tris-glycine transfer buffer	ddH2O, 25 mM Tris, 192 mM glycine
Tris-borate EDTA buffer (TBE)	130 mM Tris-HCl pH 7.6, 45 mM Boric acid and 2.5 mM EDTA

Table 2. 4: Primers

Primer	Function	Sequence (5’ – 3’)
M 13 forward	Sequencing testing	GTAAAACGACGGCCAG
M 13 refers	Sequencing testing	CAGGAAACAGCTATGAC
TurboID_GW_fwd	PCR of TurboID-CLN7 DNA	CACCATGGGCAAGCCCATCC
Cln7_GW_rev	PCR of TurboID-CLN7 DNA	TTACGCATGTGAAATCGAGTGCTG
Cln7_3’_OUT	Cloning	TACGTTCTGGACCTTCGGC
TurboID_5’_OUT	Cloning	GTCCAGCTCCCAGAATC
TurboID_3’_OUT	Cloning	AATAACAGGCGATGCTGCAC
Cln7_5’_OUT	Cloning	CAGCAGTGGCAGACGAATC
GW5f	DNA test in the fly	ATCGAGGCCTGTCTAGAAGC
SVr	DNA Test in the Fly	GGCATTCCACCACTGCTCCC

Table 2. 5: primary antibody

Antibody	Species	Concentration	Company
Anti-myc	Rat	1:1000	Abcam
Anti-myc	Gout	1:1000	Cell Signaling Technologies
Anti-GFP	Rabbit	1:1000	Abcam
Coracle	Mouse	1:100	DSHB
Discs Large	Mouse	1:40	DSHB
A-specrin	Mouse	1:40	DSHB
Integrin alpha PS1	Mouse	1:20	DSHB
Integrin beta PS	Mouse	1:20	DSHB
ATPase	Mouse	1:20	DSHB
Nervana	Mouse	1:20	DSHB
Anti-HRP- A 594	Goat	1:500	Jackson immuno
Anti-DLG	Mouse	1:100	DSHB U. lowa
Anti-myc	Rat	1:1500	Chromotech
Streptavidin-HRP	-	1:5000	Jackson Immuno
488-streptavidin	-	1:1000	Jackson Immuno

Table 2. 6: secondary antibody

Antibody	Species	Concentration	Company
HRP anti-rat	Hours	1:3000	Jackson Immuno
HRP anti- mouse	Hours	1:3000	Jackson Immuno
HRP anti-GFP	Goat	1:5000	Jackson Immuno
HRP anti-Goat	Rabbit	1:3000	Jackson Immuno
Ant-mouse DyLight 404	Donkey	1:500	Jackson immuno
Anti-rat Alexa 488	Donkey	1:500	Jackson immuno

Table 2. 7: fly genotypes

Line	BDSC ID	Full genotype	Description
w^{1118}	5362	w^{1118}; +/+; +/+	white-eyed wild type strain.
$Cln7^{36H}$		w^{1118}; +/+; $Cln7^{36H}$	Deletions of exons 2 and 3.
$Cln7^{84D}$		w^{1118}; +/+; $Cln7^{84D}$	Deletion of exons 1-5
$Chico^{1}$/ CyO		w^{-}; $Chico^{1}$/ CyO; +/+	Chico mutation
$Chico^{1}$/ CyO, gfp; $Cln7^{84D}$		w^{-}; $Chico^{1}$/ cyo, gfp; +/+; $Cln7^{84D}$	Chico and Cln7 mutations
Elavgal4	458	UAS-venus-Cln7/TM6B, Tb, Hu	Positive control DNA
Mef2-Gal4; $Cln7^{36H}$		w^{-}; +/+; Mef2-Gal4; $Cln7^{36H}$	Muscle Gal4
w^{-}; If/CyO; MKRS/TM6B		w^{-}; If/CyO; MKRS,Sb/TM6B, Hu	Double balancer
UAS-TurboID-CLN7 (II)		w^{1118}; If/UAS-TurboID-CLN7; TM6B, Tb, Hu/+	
UAS-TurboID-CLN7 (III)		w^{1118}; If/CyO; UAS-TurboID-CLN7/TM6B, Tb, Hu	

Table 2. 8: Fly food (All the size and volumes per 1 L)

Ingredient	Standard food	SY food
Water	750 ml	1 L
Agar (g/l)	8 gm	15 gm
Glucose (g/l)	50 gm	-
Sucrose (g/l)	-	50 gm
Yeast (g/l)	50 gm	100 gm
Soy flour (g/l)	10 gm	-
Hydroxybenzoate (volume)	1:100 volume	1:100 volume
Propionic acid (volume)	3:1000 volume	3:1000 volume

3. USING PROXIMITY LABELLING TO RECOGNISE CLN7 PROTEIN INTERACTIONS

3.1. Introduction

3.1.1. Proximity labelling

Proximity-dependent labelling (PL) is an alternative method to immunoprecipitation for the detection of protein-protein interactions [165] and it uses enzymes that produce reactive molecules that interact with neighbouring proteins covalently. Protein labelling is the technique of site-specific labelling that refers to the covalent attachment of molecules like biotin, enzyme, fluorophore and radioactive isotopes to specific sites of the target protein. This technique is utilized to enable the detection and purification of the desired protein and to simplify the tracking of protein interaction, expression, localization, and activity and conformation variations in complicated cellular signalling events. The monitoring of biological processes, specific detection workflows and reliable quantification of compounds are the major purposes of protein labelling. Labelled proteins can be purified through conventional affinity and identified and analysed by immunoblotting or mass spectrometry (Figure 3.1) [163, 164].

3.1.2. GAL4-UAS system

The GAL4-UAS system is an important biochemical method for studying gene expression and function in organisms such as Drosophila melanogaster [166]. It involves a

Saccharomyces cerevisiae transcription activator protein (GAL4) that is associated with an upstream activation sequence (UAS) and leads to the stimulation of downstream gene expression. The enhancer controls GAL4 expression in specific cells at specific times. When UAS is bound to GAL4, it promotes the transcription of the reporter gene[166, 167].

The driver line contains the GAL4 gene inserted into the DNA of the fly under the control of its native enhancer. This enhancer is tissue-specific, meaning it only activates GAL4 gene transcription in specific cell types of the fly [168]. The other line is the reporter line, which contains UAS and a reporter gene, controlling the expression of the reporter gene of choice [167, 168].

The GAL4 and UAS components are both separated independent transgenic lines. After crossing, the new generation fly carriers both the GAL4 gene and the UAS-reporter gene. In cells where GAL4 is expressed, the GAL4 protein will bind to UAS, triggering the expression of the reporter gene [169]. A common reporter is the GFP gene, which encodes Green Fluorescent Protein—a protein that glows [168, 169]. Using the reporter line that produces the glowing protein allows researchers to precisely identify which cells are expressing GAL4. In the cells where GAL4 was expressed, it will bind to UAS, which will then promote the expression of GFP, producing the glow protein that is easily visualized in the organism [169].

To begin, start with two separate lines: the driver and the promoter. When the enhancer of GAL4 is active, cross the driver line with other reporters to investigate cell and gene function in those specific cells [169].

The GAL4-UAS system can be used to produce cell-specific knockdown of gene function by combining this system with RNA interference (RNAi). GAL4 drives UAS, which is upstream of an inverted sequence separated by 10-100 bp of DNA. When the inverted sequences transcribe, double-stranded RNA hairpin loop structures are formed, leading to gene expression silencing via the RNAi pathway. This tool can be used in mutants to rescue phenotypes or observe the effects of knocking down gene functions in a tissue-dependent manner[170]. In *Drosophila,* depending on the P-element the UAS/GAL4 system is widely used for transgenes expression because its extremely versatile nature [171].

3.1.3. The reason for using PL instead of immunoprecipitation in the case of the CLN7 protein.

The standard method used to detect protein-protein interaction is immunoprecipitation, which in standard protocols requires the lysis of cells with detergents. As had been shown previously in the lab, the CLN7 protein is sensitive to detergent use, with standard detergents such as Triton X-100 potentially denaturing the protein or disrupting the protein complexes containing *Cln7*. Moreover, CLN7 is a membrane protein [172], and the purification of membrane proteins can be difficult

because most membrane proteins are found in low levels, and they are embedded in the lipid bilayer. Therefore, they need suitable detergents for solubilization and purification [173].

For the detection of protein-protein interactions it is important to keep those proteins during extraction and that can be difficult especially with membrane proteins. For the protein solubility, detergents are required but they disruption to the membrane environment which might change the protein fold and interfere with hydrophobic interactions for the proteins.

To avoid these difficulties, methods were developed as proteins can be labelled covalently in situ depend on their proximity to a target protein. Therefore, choosing another technique that does not depend on detergents to identify CLN7 protein interactions was vital. However, alternative methods had been developed previously in the group to label CLN7 partners including APEX2 and BioID. No result obtained with APEX2, but BioID was sufficient for CLN7 protein purification in particular in vitro labelling.

The BioID technique is utilized for proximity-dependent labelling of proteins in eukaryotic cells [163]. This approach is dependent on the fusion of a promiscuous *Escherichia coli* biotin protein ligase with a target protein [174]. BioID displays proximity-dependent biotinylation of proteins that are near-neighbours of the fusion protein (10 nm) i.e. proteins likely to be within the same complex. It is a useful and generally applicable technique for screening for both interacting and neighbouring proteins in

their native cellular environment. Because of the small size of biotin, it is simple, rapid, specific and unlikely to disturb the natural function of the protein [163]. In this method, promiscuous biotin ligase adds the biotin to proteins within 10 nm i.e. proteins likely to be within the same complex. As this labelling is performed in living cells, all protein complexes should remain intact [174]. When the labelling process is complete, cells are lysed and biotin-labelled proteins are extracted by binding to streptavidin beads (Figure 3.1) [163, 164]. Depending on its mechanism of action, BioID is active and suitable for application to insoluble and membrane proteins. Streptavidin can bind biotin in the presence of SDS, meaning strong lysis and denaturing conditions can be used. BioID can be used when fused to membrane proteins, which makes it an attractive option for identifying *Cln7* complexes.

Moreover, the BioID method able to detect weak and transient interactions, monitor the interactions in a relatively natural cellular setting, and provide temporal stimulation of biotin labelling [163].

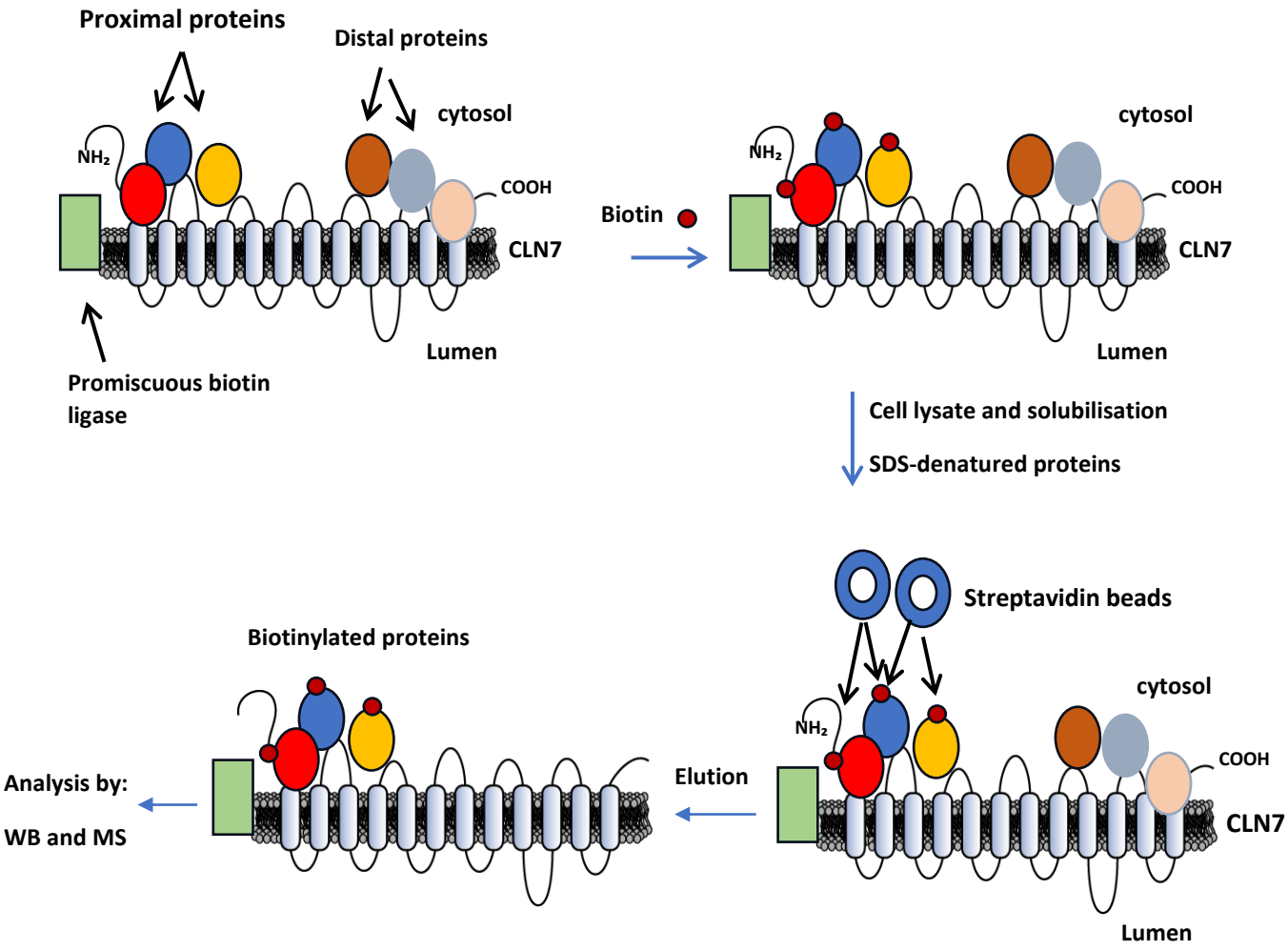

Figure 3. 1: The steps of proximity labelling.

The steps of proximity labelling started with the insert of promiscuous *E. coli* biotin protein ligase to a target protein in N-terminal side. After adding the suitable concentration biotin and incubate for 18-24 hours, so the promiscuous ligase biotin adds the biotin to the protein within 10 nm in the same complex (to the proximal proteins). The lysis process is done by using SDS detergent and after that wash processes were done and streptavidin-beads were added to the lysate. The biotin extracted by streptavidin beads and after beads eluate the elution sample analysed by western blotting (WB) or mass spectrometry (MS) to observe the biotinylated proteins.

Aim

To validate previous experiments using BioID-CLN7 to label and identify proteins interacting with *Cln7* in living *Drosophila* S2 cells. Then, to express BioID-CLN7 *in vivo* in the post-synaptic compartment of the neuromuscular junction to identify Cln7-containing complexes at the synapse.

3.2. Results.

3.2.1. Identification of CLN7 proteins binding in S2 cells and in fruit flies

A fusion protein of BioID fused at the N-terminus of *Cln7* with 6xMyc tags upstream was generated by Kyle Connolly. I expressed this construct in *Drosophila* S2 cells and used the labelling and extraction protocols established previously (Section 2.5.1).

3.2.1.1. In vitro BioID-CLN7 labelling.

S2 cells were transfected with BioID or BioID-CLN7 constructs expressed from a strong actin promoter and stably selected using hygromycin.

Large numbers of cells were needed for the labelling process (5 x 15 cm plates). They were incubated overnight in medium supplement with 500 µM biotin, then lysed in an SDS-containing buffer and biotinylated proteins affinity purified on streptavidin-conjugated beads (Figure 3. 1). Western blotting of cell lysates, the flow-throughs and eluates from the streptavidin beads were stained for rat anti-Myc primary antibody (1:1000) (Table 2.5). Clear bands correlating with the Myc-tagged BioID and BioID-CLN7 proteins were shown in eluates at 55 KDa and 130 KdDa respectively (Figure 3.2). The proteins were not detected within the cell lysates because they need to be extracted and purified from the beads.

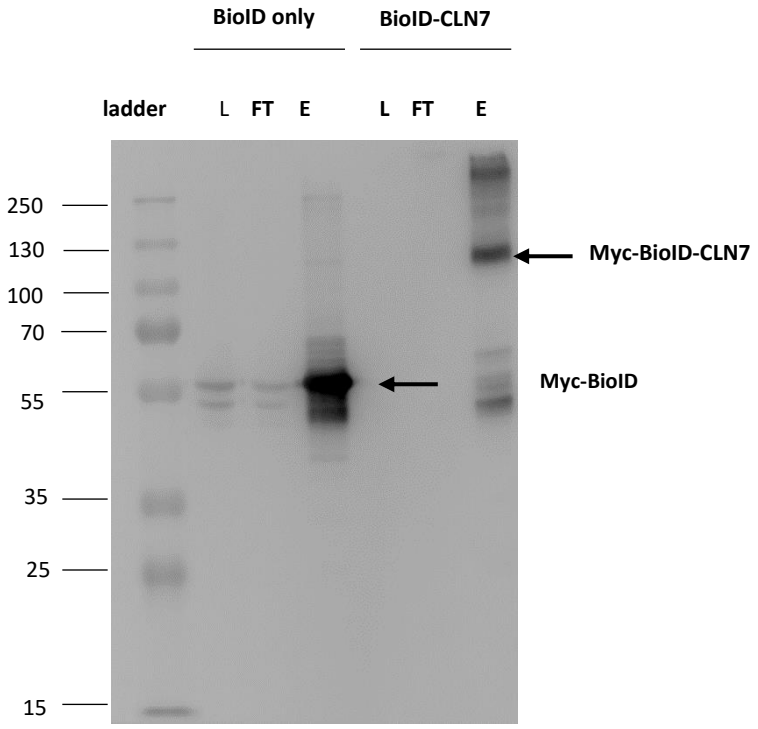

Figure 3. 2: In vitro labelling detecting myc-BioID and myc-BioID-CLN7 in S2 cells.

Western blotting of BioID and BioID-CLN7 expressing cells. Cell Lysate (L), Flow-through (FT) and Eluates (E). For the beads were run the gel for both BioID-CLN7 and BioID samples. 12% SDS-PAGE gel was used and 2 µl of protein was loaded in the gel. The membrane was stained with rat anti-Myc (1:1000) to reveal the Myc-BioID and Myc-BioID-CLN7 proteins. HRP-anti-rat (1:3000) secondary antibody was added to the membrane. The detected bands indicated by arrows in their right sizes.

Samples were then probed with 1:10000 streptavidin-HRP conjugate (Figure 3. 3). Self-labelling of BioID and BioID-Cln7 was visible (Figure 3. 3. A). In addition, labelling of proteins of multiple molecular weights were obvious in the elution from the BioID-CLN7 samples. A Coomassie stain of the samples showed a several number of bands in the BioID and BioID-CLN7 eluates (Figure 3.3. B).

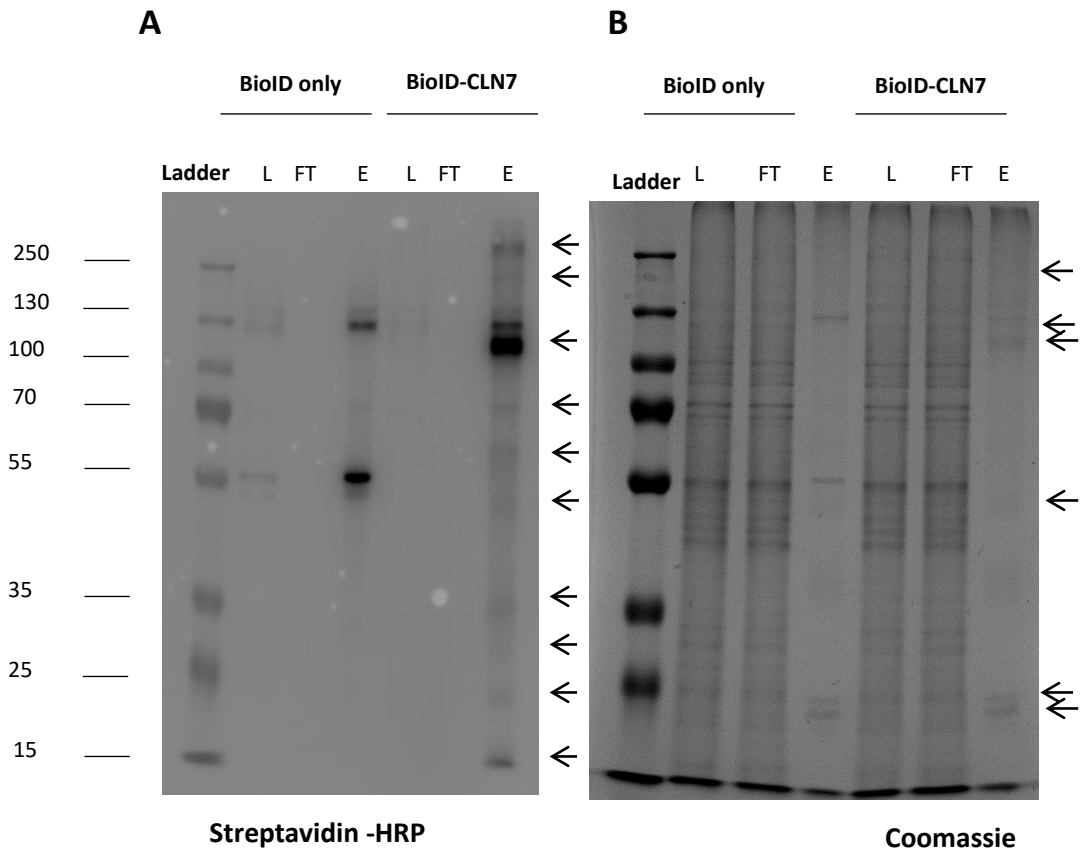

Figure 3. 3: In vitro labelling of BioID and BioID-CLN7 in S2 cells.

Western blotting experiment was done for BioID and BioID-CLN7 samples in 12% of SDS-PAGE gel to detect the biotinylated proteins in S2 cells. 2 µl of protein loaded in the gel for streptavidin experiment and 5µl loaded for Coomassie. (**A)** streptavidin-HRP conjugate (1:10000) revealing biotinylated proteins for BioID and BioID-CLN7 expressing cells. In comparison with BioID, arrows indicate the identical bands labelled in BioID-CLN7 samples, with no obvious correlate in BioID which only control samples. **(B)** Coomassie stain added for the same samples as in **A**. Arrows indicate the identical bands of BioID-CLN7 which not observed in BioID control samples. Lysate (L), flow-through (FT) and eluates (E).

3.2.1.2. Mass spectrometry analysis for BioID-CLN7 labelling.

Seventeen slices of prominently labelled bands from the BioID-CLN7 protein-interaction samples were cut out of the Coomassie gel and sent for analysis by mass-spectrometry (MS). Also, 5 samples of BioID were sent for MS analysis as a control. 5 slices were also cut from the BioID controls where prominently labelled bands at the same size as the BioID-CLN7 samples were present, with the assumption that these were endogenously biotinylated proteins.

Proteins can be labelled by both BioID and BioID-CLN7. Therefore, Common proteins found in both BioID and BioID-CLN7, as well as the unique proteins from the BioID samples, were excluded to focus solely on those unique proteins associated with BioID-CLN7.

To avoid contamination by keratin, the mass spectrometry (MS) processes were conducted under sterile conditions, as explained in section 2.5.3.2. The mass spectrometry results were exported to Microsoft Excel, including protein descriptions, to determine whether they were contaminated with keratin or uncontaminated. Consequently, all contaminated results were removed, and I focused on the uncontaminated results from the BioID-CLN7 experiment. Additionally, five samples of BioID were sent as controls, and the same procedures were applied to their results, removing any contaminated data due to keratin contamination. The BioID results were then compared with the BioID-CLN7 results, and similar proteins were excluded to isolate the unique results specific to BioID-CLN7. After eliminating both contaminated

results and proteins shared with BioID, a total of 388 identified proteins were associated with BioID-CLN7.

About 121 proteins ≥ 4 peptides, and the highest value was 67 peptides for one protein which was A-spectrin. Several proteins were repeated in more than one sample and more than one independent experiment. Moreover, peptide-spectrum matches (PSMs) serve as a collective measure of the number of peptides and modifications, including redundantly identified ones, associated with a master protein. PSMs are used as an approximate measure of protein abundance. 102 identified proteins had ≥ 5 PSMs.

Many proteins have been identified in an independent experiment and some proteins were repeated in several samples even in some independent experiments, such as Formin-like protein (fri), lethal giant larvae (l(2)gl), insulin receptor substrate 1 (chico), protein hu-li tai shao (hts), heat shock protein 83 (Hsp83), coracle, alpha-spectrin, protein slit (sli), protein draper (drpr), integrin alpha PS1 (mew) and so on (Tables 3. 1-3).

BioID-mediated biotinylation can be used as a screen to observe candidates that can later be systematically validated or investigated in a hypothesis-based manner. Depending on the BioID mechanism, biotinylated proteins can be divided into three categories. Firstly, direct interactions, which can be either transient or stable. Secondly, indirect interactions. Thirdly, vicinal proteins that interact directly or indirectly. Consequently, BioID is used as a screen for potential interactors or vicinal proteins[163].

3.2.1.3. The existence of BioID-CLN7 hit proteins.

In further explanation, numerous hit proteins were found after MS analysis. Several proteins were repeated in more than one sample and in more than an independent experiment. Tables 3.1- 3-3 include all hit BioID-CLN7 proteins in S2 cells with their molecular weights (Mw), number of peptides, number of samples, their identical experiments and corresponding Mw.

In sample 1 (Figure 3. 4. A), five proteins were identified, with the most interesting being Slit and Fused (Fu). In the same experiment, sample 2 (Figure 3. 4. A) revealed 19 proteins, with important hits including Formin-link, a glial protein; Lethal giant larvae, a cytoskeletal protein; and Draper, which is responsible for apoptotic cell phagocytosis in Drosophila[175]. Other proteins found in this sample with fewer than three peptides included Integrin alpha PS1, Integrin beta PS, Nirvana, Fu, and Hits. Sample 3 had 15 hit proteins (Figure 3.4.B), with important proteins including Slit, α-Spectrin (a cytoskeletal protein), Laminin γ-subunit, and Fused. For sample 4 (Figure 3.4.B), five proteins were found, with key hits being Formin-like protein, Lethal giant larvae, and Draper protein. In sample 5, 16 proteins were identified (Figure 3.4.B), with significant proteins including Formin-like protein, Draper, Lethal giant larvae, Slit, Integrin alpha PS1, and Integrin beta PS (Table 3.1). However, samples 3, 4, and 5 were all part of one independent experiment.

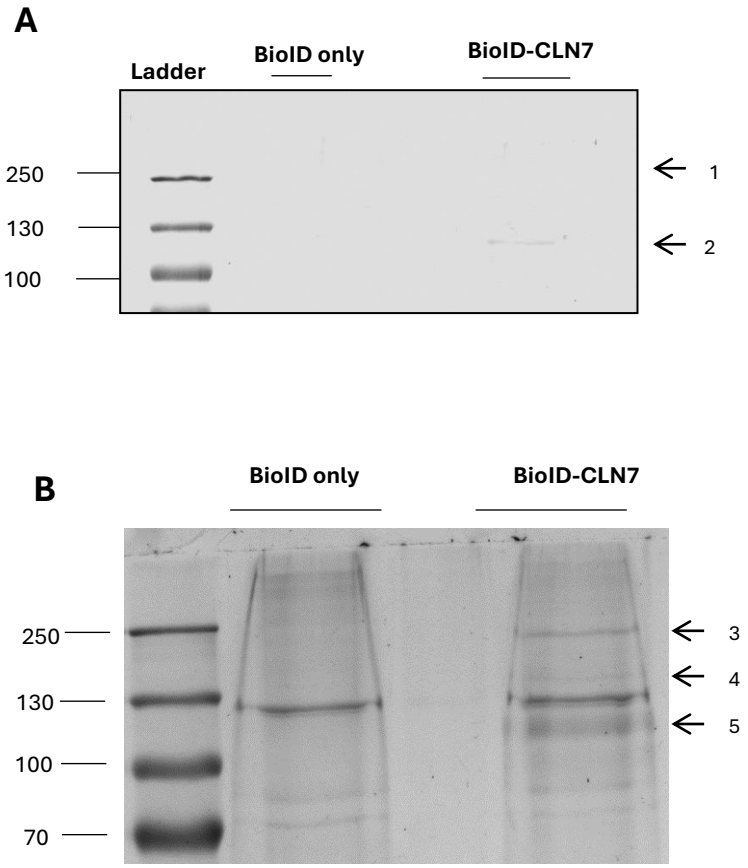

Figure 3. 4: In vitro labelling of BioID and BioID-CLN7 in S2 cells (Coomassie staining).

Coomassie stain added to the 12% of SDS-PAGE gel in **(A)** and **(B)** which were two independent experiments. In both experiments 5 µl of BioID-CLN7 sample was loaded into the gel. In addition, in **(A)** experiment, two bands of BioID-CLN7 were detected, and in **(B)** experiment, there were three bands of BioID-CLN7 found. The BioID sample was loaded as a control and the gel slices of the bands of BioID-CLN7 were taken for MS analysis. Arrows and numbers indicate the gel slices bands which cut to MS analysis. The bands present in both BioID and BioID-CLN7 samples at similar molecular weight were assumed to be endogenously labelled bands and were not extracted.

Table 3. 1: Potential BioID-CLN7 interacting proteins (Samples 1-5).

Sample number	Independent experimental repeat number	Mw of gel slice	Protein identified with peptide number	Corresponding predicted Mw
1	Once	250 KDa	- Slit (5 peptides) - Fue (2 peptides)	- 168 KDa - 90 KDa
2	Once	130 KDa	- Formin-link (11 peptides) - lethal giant larvae (5 peptides) - Draper (5 peptides)	- 133 KDa - 127KDa
3	Once	250 KDa	- Slit (14 peptides) - A-spectrin () - Laminin g unit (4 peptides)	- 168 KDa - 182 KDa
4	Once	>130 KDa	- Formin-link (35 peptides) - Lethal giant larva (13 peptides) - Draper (4 peptdes)	- 133 KDa - 113KDa
5	Once	<130 KDa	- Fomin-link (17 peptides) - Draper (6 peptides) - Lethal giant larva (4 peptides)	- 133KDa - 113KDa - 127KDa

In the third experiment, 117 proteins were found in sample 6 (Figure 3. 5). This sample contained several important proteins, including α-Spectrin, Coracle, Sodium/Potassium subunit alpha, Slit, Rho GTPase-activating protein, Zipper, Lethal giant larvae, Neuroglian, Integrin alpha PS1, Formin-like protein, Laminin γ-subunit, Gale, Pyk, and Fused. Sample 7 (Figure 3. 5) had 55 hit proteins, with important proteins identified as α-Spectrin, Lethal giant larvae, Formin-like protein, Coracle, Integrin alpha PS1, Na pump alpha, Ca-P60A, NorpA, and Fused. In sample 8 (Figure 3.5), 27 proteins were identified, with important hits including Integrin beta PS, Hits, Coracle, and Lethal giant larvae. Sample 9 contained 32 hit proteins (Figure 3.5), with the most interesting being Fax, Formin-like protein, Orct2, Chico, Hits, Lethal giant larvae, and Fused. Sample 10 had 69 identified proteins (Figure 3.5), including Gale, Taldo, Nirvana, Vaps60, Hits, Chico, Syb, Fused, Lethal giant larvae, and Scra. Sample 11 contained 28 hit proteins (Figure 3.5), with the most important being Synaptobrevin, Bia, Hits, and Slit (Table 3.2). Slit was found in samples 6 and 11, corresponding to molecular weights (Mw) of 250 kDa and 15 kDa, respectively. However, its expected Mw is 168 kDa, but it was detected in two different bands with very different Mw, indicating that this protein has multiple possible biotinylation sites. Additionally, as a high Mw protein (168 kDa), it may generate many fragments, which were found in two different bands. The higher band at 250 kDa corresponds to the Slit protein's Mw. Table 3.2 includes all proteins identified in this independent experiment.

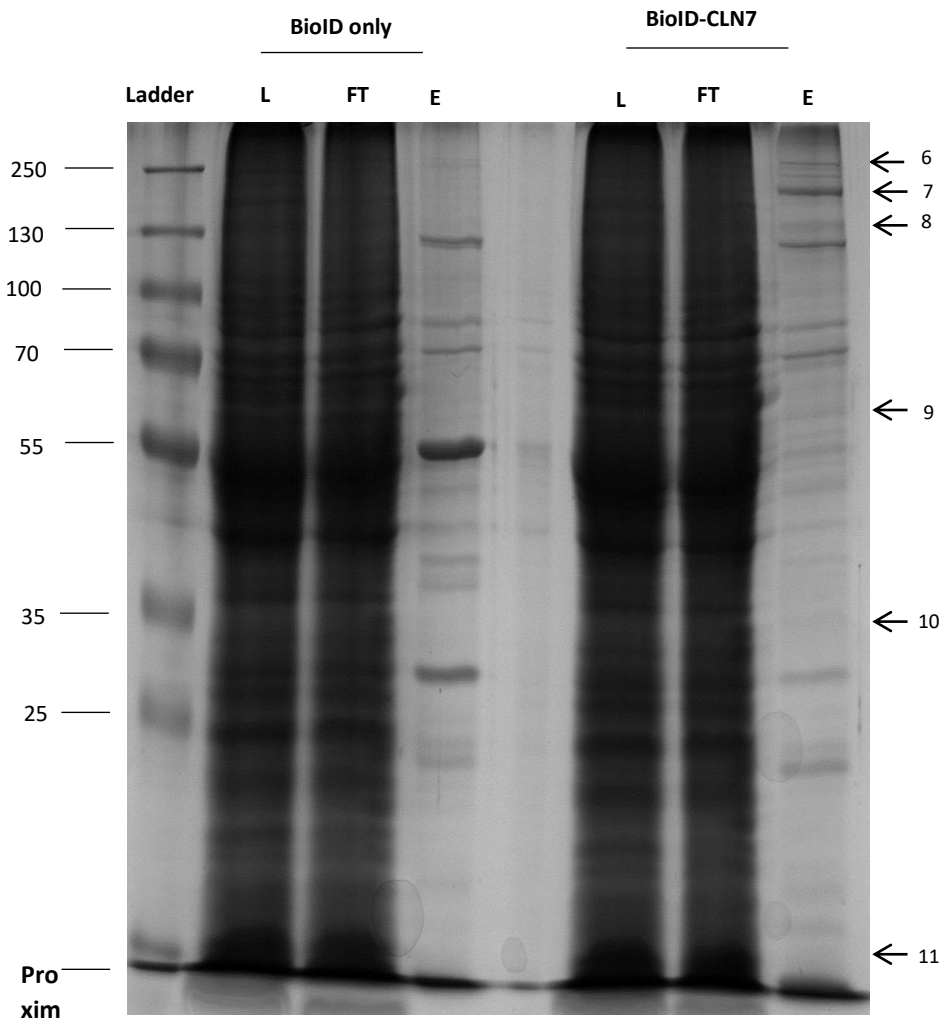

Figure 3. 5: In vitro labelling of BioID and BioID-CLN7 in S2 cells (Coomassie staining).

Coomassie stain added to the 12% of SDS-PAGE gel. 35 µl of eluates loaded into the gel. The arrows from 6 – 11 indicate the bands of BioID-CLN7. the gel slices were cut to MS analysis. The BioID sample was loaded as a control. The bands present in both BioID and BioID-CLN7 samples at similar molecular weight were assumed to be endogenously labelled bands and were not extracted. Lysate (L), flow-through (FT) and eluate (E).

Table 3. 2: The potential BioID-CLN7 interacting protein in samples 6-11.

Sample number	Independent experimental repeat number	Mw of gel slice	Protein identified with peptide number	Corresponding predicted Mw
6	Once	250 KDa	- A-spectrin (49 peptides) - Coracle (45 peptides) - Slit (22 peptides) - RhoGAPp 190 (18 peptides) - Zipper (25 peptides) - L(2)gl (16 peptides) - Neuroglian (13 peptides) - Mew (6 peptides) - Formin-link (5 peptides) - Laminin g subunit () - Gale () - Pyk (2 peptides)	- 278KDa - 184KDa - 168KDa - 180KDa - 237KDa - 182KDa
7	Once	<250 KDa	- A-spectrin (67 peptides) - L(2)gl (47 peptides) - Formin-link (48 peptides) - Coracle (34 peptides) - Mew (10 peptides) - Na pump alpha (17 peptides) - Ca-P60A () - Norp A (7 peptides) - Fu ()	- 278KDa - 184KDa
8	Once	>130 KDa	- Integrin beta PS() - Coracle (3 peptides) - L(2)gl(3 peptides)	 - 127KDa
9	Once	>55 KDA	- Fax (15 peptides) - Formin-link (7 peptides) - Orct2 (6 peptides) - Chico (8 peptides) - Hits (4 peptides) - L(2)gl() - Fu ()	- 47KDa - 63KDa
10	Once	35 KDa	- Gale (9 peptides) - Taldo (6 peptides) - Nirvana (7 peptides) - Vaps60 (5 peptides) - Hits (6 peptides) - Chico (4 peptides) - Syb () - Fu () - L(2)gl () - Scra (	- 39KDa - 36.7KDa - 35KDa - 25KDa
11	Once	15 KDa	- Syb (7 peptides) - Bia (3 peptides) - Hits () - Slit ()	- 17KDa - 23.7KDa

For sample 12 in the fourth experiment (Figure 4. 6. A), five proteins were found, with three interesting proteins including Lethal giant larvae, Formin-like protein, Synaptobrevin, Fused, and NorpA. Only four proteins were found in sample 13 (Figure 3. 6. A), with the important protein being Integrin beta PS. In sample 14 (Figure 3. 6. A), only three proteins were identified, with two interesting proteins being Fax and Formin-like protein. The fifth experiment contained three samples. In sample 15 (Figure 3. 6. B), four proteins were found, including two interesting proteins: Formin-like protein with 22 peptides and Lethal giant larvae with 3 peptides. In sample 16 (Figure 3. 6. B), three proteins were found, with two interesting proteins: Formin-like protein and Lethal giant larvae. Nine proteins were found in sample 17 (Figure 3. 6. B), with the important protein being Formin-like protein with 6 peptides. Table 3.3 includes all these proteins with their peptide numbers (≥ 3), their molecular weights (MW), and other details.

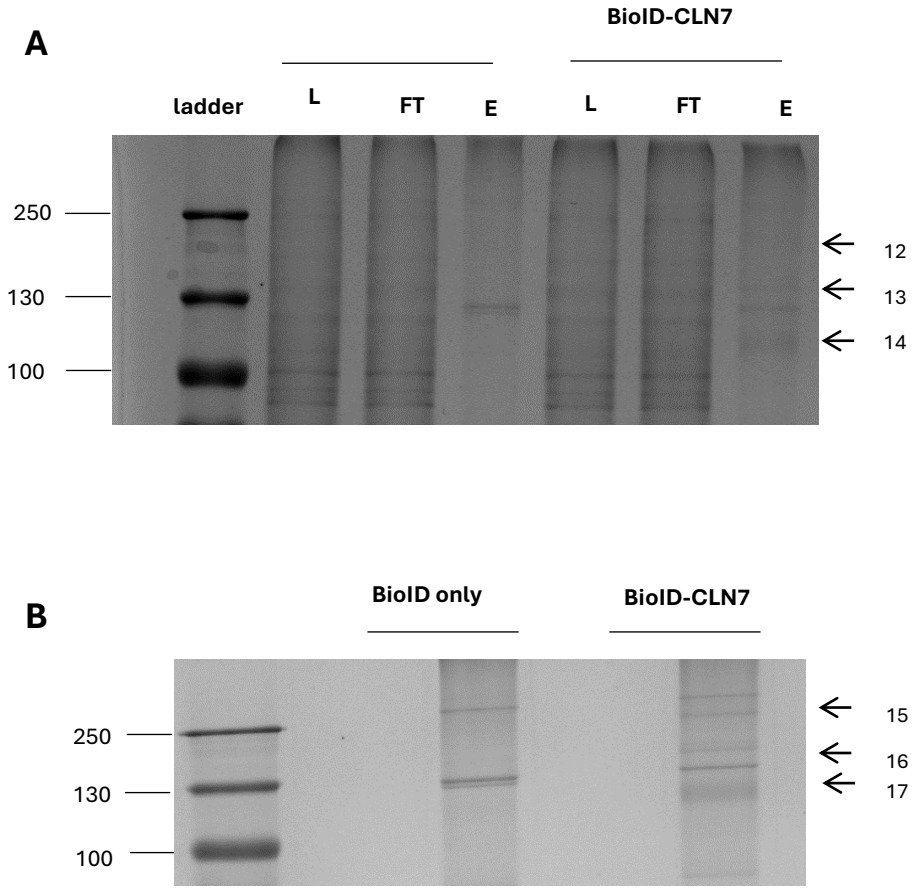

Figure 3. 6: In vitro labelling of BioID and BioID-CLN7 in S2 cells.

5 µl BioID-CLN7 loaded into 12% of SDS-PAGE gel in both **(A)** and **(B)** independent experiments and the gel stained by Coomassie. Arrows indicate the gel slices of BioID-CLN7 eluate bands which were taken for MS analysis, three bands for each experiment. The BioID sample was loaded as a control. The bands present in both BioID and BioID-CLN7 samples at similar molecular weight were assumed to be endogenously labelled bands and were not extracted. Lysate (L), flow-through (FT) and eluate (E).

Table 3. 3: The potential BioID-CLN7 interacting proteins samples 12-17

Sample number	Independent experimental repeat number	Mw of gel slice	Protein identified with peptide number	Corresponding predicted Mw
12	Once	<250 KDa	- Lethal giant larvae (32 peptides) - Formin-link (25 peptides) - Syb () - Fu () - norpA ()	
13	Once	130 KDa	- integrin-beta PS (	
14	Once	>100 KDa	- fax (4 peptides) - formin-link (3 peptides)	
15	250 KDa	250 KDa	- fomin-link (22 peptides) - lethal giant larvae (3 peptides)	
16	Once	>130 KDa	- Fomin-link (36 peptides) - Lethal giant larvae (10 peptides)	- 133KDa - 127KDa
17	Once	130 KDa	- Formin-link (6 peptides)	- 133KDa

3.2.1.4. Potential CLN7-interacting proteins identified in all experiments.

Several potential CLN7-interacting proteins were identified in more than one sample within the same experiment and were also found in more than one independent experiment. Experiment 3 included the highest number of identical proteins, particularly in samples 6, 7, 9, and 10. On the other hand, only one or two identical proteins were found in other samples. Several proteins, such as Coracle, α-Spectrin, Lethal giant larvae, Formin-like protein, Slit, and Integrin alpha PS1, were identified in multiple samples and independent experiments. Table 3.4 includes the BioID-CLN7 potential interacting proteins, the protein molecular weight (Mw), the sample number with the number of peptides in the same samples, repeated identically, and the principal localization. However, this table only includes proteins that are found in gel slices that correspond to their predicted Mw. Additionally, a number of hit proteins were found in samples with > peptides are included only. The principal cellular localizations were investigated using the FlyBase website, the STRING interaction database, gene ontology enrichment analysis tools.

Table 3. 4: BioID-CLN7 hit proteins in S2 cells.

Protein	MW	CG	No. of sample	No. of Peptide f*	Repeat identically	Principle Localization
Slit	168 KDa	CG43758	6 ,3,1	22,14,5	3 identical experiments	Cytoskeletal, cell projection
Coracle	184 KDa	CG11949	8,7,6	3,34,45	1	Cytoskeletal, cell junction, membrane
Formin-like protein	133 KDa	CG32138	17,16,15,14,12,9, 7,6,5,4,2	6,36,22,3,25,7,48, 5,17,35,11	5	Glial
Lethal giant larval	127 KDa	CG2671	16,15,12,8,7,6,5,4 ,3,2	10,3,32,3,47,16,4, 13,5,5	5	Cytoskeletal
a-spectrin	278 KDa	CG1977	7,6	67,49	1	Cytoskeletal, cell periphery, membrane, synapse
Integrin alpha-PS1	127 KDa	CG1771	7,6	10,6	1	Cytoskeletal
Integrin beta PS	93 KDa	CG1560			1	Cytoskeletal
Na+K+ATPas (alpha and beta)	112 KDa	CG5670	7,6	17,32	1	Cytoskeletal
Nirvana	35 KDa	CG9258	10	7	1	Glial
Chico	108 KDa	CG5686	10,9	4,8	1	Cytosol, membrane, cell periphery
Hts (hu li tai shao)	128 KDa	CG43443	10,9,8	6,4,7	1	Cytoskeletal
Draper	113 KDa	CG2086	5,4,2	6,4,5	2	Membrane, synapse
Fu (fused)	90 KDa	CG6551				Cytosol
Syb (synaptobrevin)	17 KDa	CG12210	11	7	1	Synaptic vesicles
Fax (failed axon connection)	47 KDa	CG4609	14,9	4,15	2	Membrane
Laminin g unit (LanB2)	182 KDa	CG3322	3	4	1	Cell periphery
Neruglian (Nrg)	143 KDa	CG1634	6	13	1	Membrane, cell junction
RhoGAPp190	180 KDa	CG32555	6	18	1	Cytosol
norpA	125 KDa	CG3620	7	7	1	Membrane, cell periphery, cell projection
Gale (Udp-galactose 4'-epimerase)	39 KDa	CG12030	10	9	1	Cytosol
Zipper	237 KDa	CG15792	6	25	1	Cytoskeleton, membrane, cell periphery
Pyk (Pyruvate kinase)	57,4 KDa	CG7070	6	2	1	Cytosol
Orct2 (Organic cation transporter 2)	63 KDa	CG13610	9,7,6	6,5,9	1	Membrane
Taldo (transaldolase)	36.7 KDa	CG2827	10	6	1	Other cellular components
Vps60 (vacuolar protein sorting 60)	25 KDa	CG6259	10	5	1	Membrane, endomembrane system
Scra (scraps)		CG2092			1	Cytoskeleton
Csp (Cysteine string protein)	27 KDa	CG6395	10	5	1	Synapse, cell projection
Mys (myospheroid)	92.6 KDa	CG1560	8	8	1	Membrane, cell periphery, cell junction, synapse
Hsp83 (Heat shock protein 83)	82 KDa	CG1242	7	10	1	Cell periphery, membrane, cytoskeleton
Bia (baiser)	23.7 KDa	CG11785	11	3	1	Membrane, endomembrane system

- The number of peptides is related to each sample respectively, e.g the slit in the first row the first number of sample is 6 and the number of peptides is 22 .

3.2.1.5. BioID-CLN7 hit proteins localized in Drosophila synapse NMJ

By concentration on the Drosophila nervous system, there are several proteins expressed in the nervous system of Drosophila, but the important proteins are related to cytoskeletal proteins of the neuro muscle junction and glial-specific proteins. The MS results showed that several interesting proteins interact with the CLN7 protein. This analysis identified cytoskeletal proteins of the neuro muscular junction (NMJ) including coracle, Na+K+ATPAse (alpha and beta subunit), PS1 integrin (alpha and beta subunit), discs large, lethal giant larvae and A-spectrin. Other proteins consisting of nirvana, formin-like and slit which are glial-specific proteins (Table 3.5).

Table 3. 5: The interesting BioID-CLN7 hit proteins in S2 cells

NO	Protein name	M.W	Drosophila organ
1	Coracle	184 KDa	NMJ Cytoskeleton
2	Integrin beta PS	93 KDa	NMJ Cytoskeleton
3	Integrin alpha PS1	127 KDa	NMJ Cytoskeleton
4	Na pump (alpha and beta subunit)	112KDa	NMJ Cytoskeleton
5	A-specrin	278 KDa	NMJ Cytoskeleton
6	Disc Large	106.7 KDa	NMJ Cytoskeleton
7	Lethal giant larvae	127 KDa	NMJ Cytoskeleton
8	Formin-like	133 KDa	Glial
9	Slit	168 KDa	Glial
10	Nirvana	35 KDa	Glial

3.2.2. Gene enrichment analysis

3.2.2.1. Network analysis of BioID-CLN7 hit proteins

To investigate potential links between the BioID-CLN7 interacting proteins, the STRING database of known and predicted protein-protein interactions was interrogated with the list of hits. STRING lists direct (physical) or indirect (functional) associations. (Figure 3. 7). Most Cln7-interacting hits were nodes with a least one other, suggesting CLN7 is part of a known, existing network. Interestingly, there was no empty node that confirmed the interactions between them. Moreover, the predicted functional associations were represented by edges that were demonstrated by up to seven coloured lines, and the predicted associations are represented by these lines colours. Moreover, there were five proteins even when their nodes were coloured, but they were not connected with other proteins as a coloured node indicates to the query proteins and first shell of interaction. In general, depending on the STRING analysis tool, there were 27 nodes and 37 edges (Figure 3. 7).

Integrin-beta PS (mys), α-spectrin, and coracle were linked with several proteins in addition to each other. Coracle interacted with eight proteins with different edges, integrin-beta PS was connected with eight proteins, while α-spectrin was linked with six proteins, and lethal giant larvae (l(2)gl) was connected with five proteins. CLN7 was included but was not linked with other proteins. This may be due to the lack of interaction information in the STRING analysis tool.

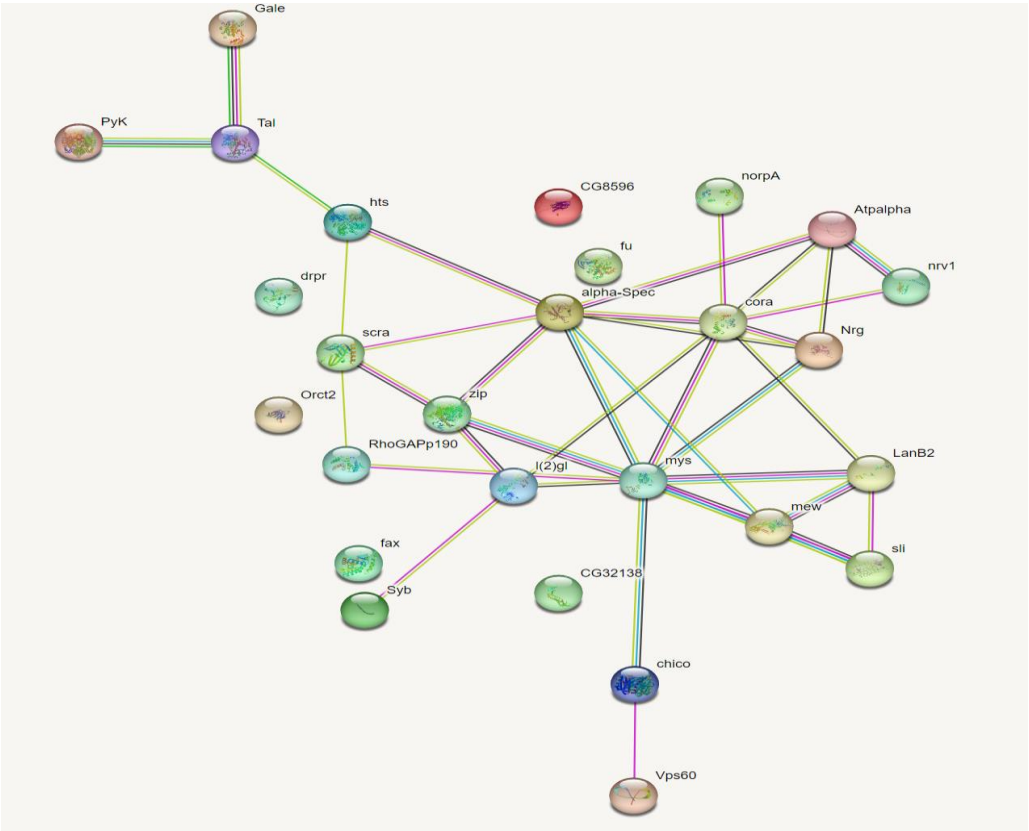

Figure 3. 7: The network of potential CLN7 interacting proteins.

BioID-CLN7 potential interacting proteins were analysed via the STRING database to identify the protein-protein interaction networks. According to the STRING analysis, the coloured nodes represent query proteins and the first shell of interaction, while the white nodes represent the second shell of interaction. There are no empty nodes, which would indicate proteins of unknown 3D structure, while filled nodes indicate that the 3D structure is known or predicted. CLN7 is shown as CG8596 in the network.

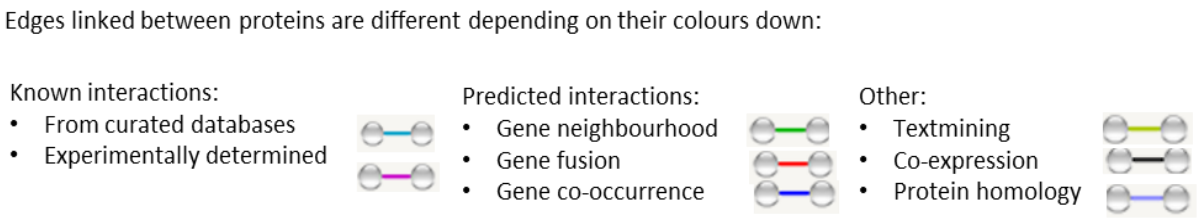

3.2.2.2. Functional enrichment analysis in the network

The STRING App was used to run functional enrichment analysis for Gene Ontologies (GO), including GO biological process, GO molecular function, and GO cellular component. Several important GO biological processes were enriched, including nervous system development, actin cytoskeleton, cell junction organization, cell membrane organization and cytoskeletal protein binding. Enriched GO cellular components including septate junction, post-synaptic, cell junction, synapse, plasma membrane and cortical actin cytoskeleton. In the case of GO molecular function, several categories were enriched which are included in Table 3. 6.

Table 3. 6: Functional enrichment analysis.

GO category	GO organization	Proteins
Biological process	Nervous system development	slit, coracle, integrin-alpha PS1, integrin-beta PS, a-spectrin, lethal giant larvae, hits, zipper, RhoGAPp190, atpalpha, neuronal, formin-like protein, fax and draper
	Actin cytoskeletal	coracle, integrin-alpah PS1, integrin-beta PS, hits, zipper, lethal giant larvae, scra and formin-like protein.
	Cell junction	coracle, a-spectrin, lethal giant larval, neuroglia and atpalpha
	Cell membrane	A-spectrin and scra
Molecular function	Cytoskeletal protein binding	coracle, a-spectrin, lethal giant larvae, formin-like protein, zipper, scra
Cellular component	Septate junction	coracle, lethal giant larval, neuroglia and atpalpha
	Post-synaptic	integrin-beta PS, hits, and draper
	Cell junction	integrin-beta PS, integrin-alpha PS1, atpalpha, norpA, coracle, a-spectrin, hits, lethal giant larvae, zipper, neuroglia, synaptobrevin and draper
	Synapse	a-spectrin, integrin-beta PS, lethal giant larvae, synaptobrevi, hits and draper
	Plasma membrane	coracle, integrin-alpha PS1, integrin-beta PS, a-spectrin, lethal giant larvae, synaptobrevin, neuroglia, nirvana, aptalpha, norpA, hits, zipper, scra, chico, draper, fused, and fax
	Cortical actin cytoskeleton	lethal giant larvae, zipper and scra

3.2.3. Validation of BioID-CLN7 interactions

3.2.3.1. co-immunoprecipitation.

It was important to validate the interactions identified by the BioID-Cln7 labelling. The rationale was originally to avoid the use of detergents to give the highest chance of native membrane complexes remaining intact. Previous work in the group found that the use of dodecyl maltoside, a very mild detergent often used for the purification of membrane proteins, might be suitable to prevent *Cln7* from denaturing. Therefore, standard co-immunoprecipitation from lysed cells was attempted with dodecyl maltoside used in place of the more commonly used Triton or NP-40 detergents.

Monoclonal antibodies were available for several of the interacting hits: Coracle, Na+K+ATPAse (alpha subunit), PS1 integrin beta, spectrin, DLG, and Nirvana. I started by investigating whether these proteins interact with CLN7. In the lysates, bands were detected for BioID-CLN7 as a control when the membrane probed with rat ant-myc (1:1000) primary antibody, in addition to Disc-large and Nirvana. However, the bands for Na+K+ATPAse and integrin-PBS were very low and difficult to observe (Figure 3. 8). There were no bands detected for Coracle and other proteins.

A standard co-immunoprecipitation experiment was then performed on Myc-BioID expressing S2 cells using an anti-Myc antibody. Elution from the protein G beads was probed with each of the monoclonal antibodies. When using rat anti-myc primary antibody, the bands of BioID-CLN7 were visualized in both lysate and elution samples as expected (Figure 3. 9. A). In this figure two bands observed in IP BioID-CLN7 which

Multiple nonspecific bands on the blot may be due to antibodies of poor quality or at too high a concentration, insufficient blocking, or nonspecific binding or the protein may be dimer.

However, for the hit proteins, only bands for Na+K+ATPAse and Nirvana were observed in their correct size for lysate samples, but there were no bands in the elution samples (Figure 3. 9. B-C). Additionally, there were no bands detected for other hit proteins, whether in the lysate or elution samples. Consequently, with this Co-IP method there was no potential proteins interact with CLN7 detected.

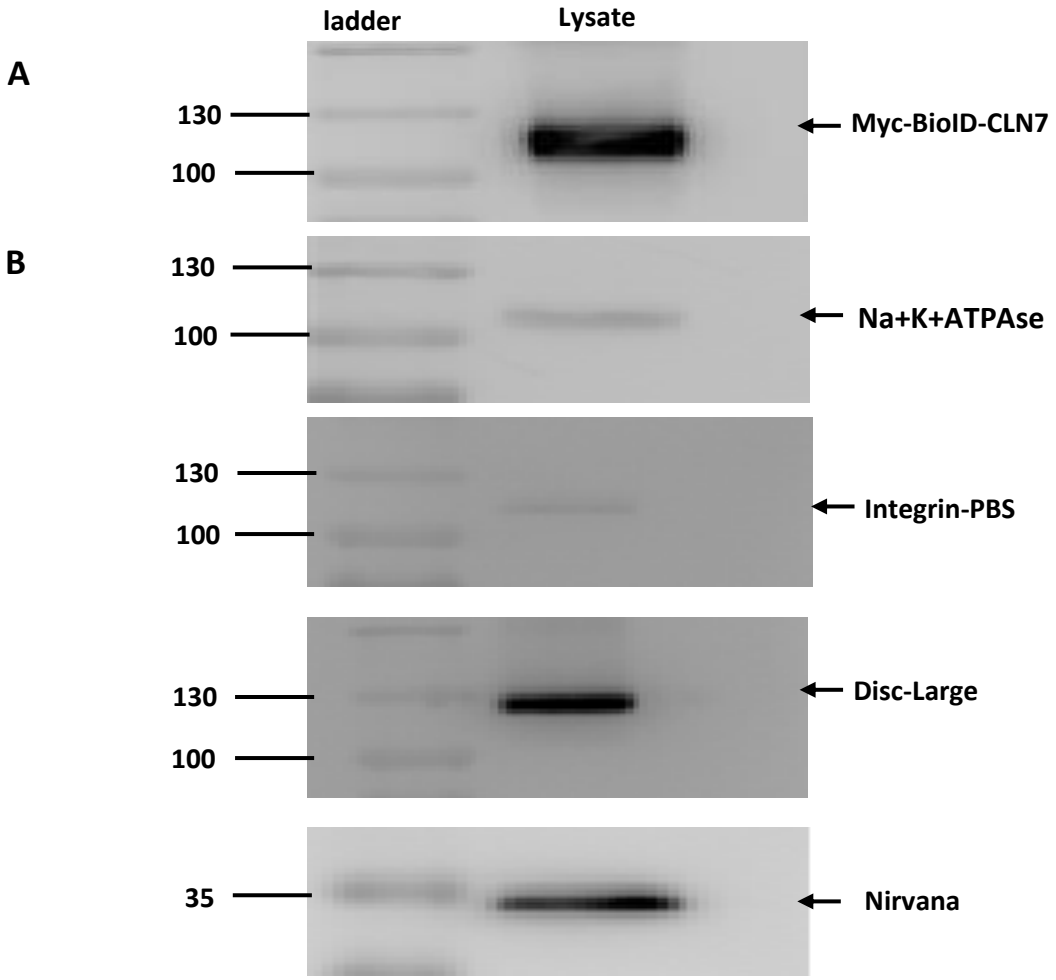

Figure 3. 8: Immunoprecipitation to validate potential BioID-Cln7 interacting proteins in S2 cells.

Western blotting of lysates of Myc-BioID-CLN7-expressing S2 cells. 12 % of SDS-PAGE gel used. 5µl of protein loaded into the gel. **(A)** As a control rat anti-myc (1:1000) used to detect myc-BioID-CLN7 band. **(B)** WB results for the BioID-CLN7 lysis buffer to detect BioID hit proteins and 1: 20 concentrations of primary anti-bodies were used for Na+K+ATPAse, integrin-PBS, Disc-Large and nirvana.

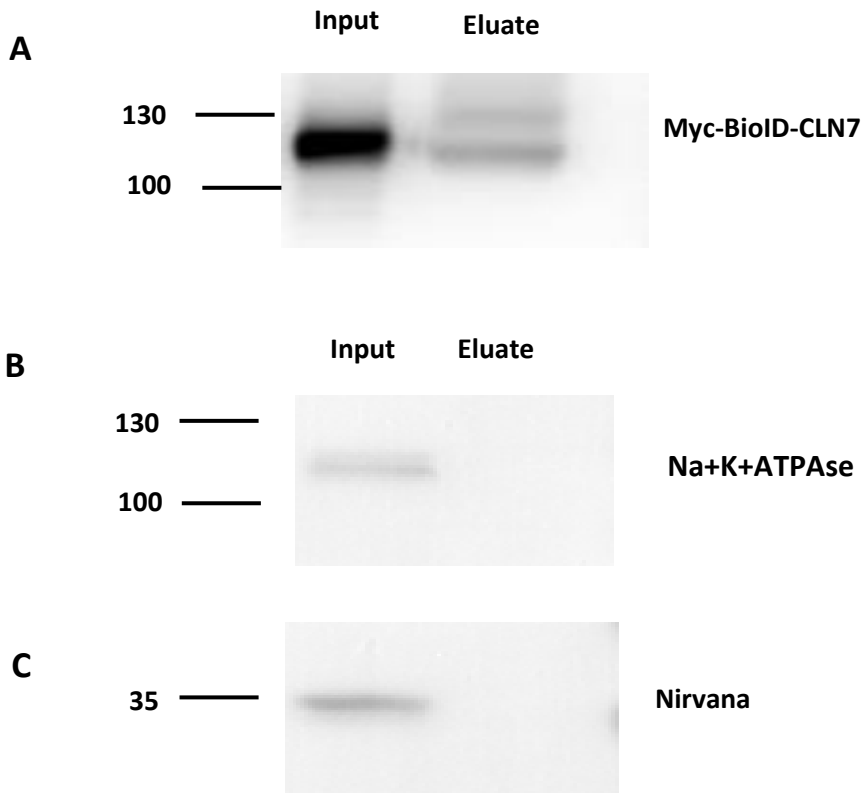

Figure 3. 9: Co-immunoprecipitation to detect potential interacting CLN7 proteins in S2 cells.

12% of SDS-PAGE gel used for co-Immunoprecipitations with rat anti-myc (1:1000) from Myc-BioID-Cln7-expressing S2 cells. 5µl proteins loaded into the gel for lysates and eluates. Lysate and elution of hit proteins were probed with the antibodies (1:20). **(A)** Myc-BioID-CLN7 which is detected in the right size in both lysate and eluate samples. **(B-C)** The lysate and Co-IP of hit proteins including Na+K+ ATPase and Nirvana.

3. 2. 3. 2. Co-immunoprecipitation with SMALPs.

A second approach for validating hits was attempted using Styrene Maleic-Acid Lipid Particles (SMALPs) in place of the n-Dodecyl-beta-Maltoside Detergent (DDM). SMALPs can be used to extract membrane proteins in native forms without the need for detergents [176]. We also decided to use the high-affinity GFP-trap to reduce the time needed to capture the *Cln7* target during precipitation. A previously generated pAVM-CLN7 plasmid that expresses Venus-YFP-CLN7 under the strong actin promoter was transfected into S2 cells and test extractions were run to identify minimal SMALP concentrations needed to extract YFP-Cln7 from cells and allow its precipitation on the GFP-Trap beads. The SMALPs concentration, the concentration of the hit proteins and the proficiency of the experimental process contributed to the perfect results. The minimal concentration 0.5% (w/v) SMALPs was started at the beginning and that was found to be effective as shown in (Figure 3. 10). YFP-Cln7 membrane stained by rabbit anti-GFP (1:1000) and the hit BioID proteins membrane stained by 1:20 of primary anti-body. The bands of YFP-Cln7 were clear for both lysate and elution in their right size (figure 3. 10. A). For BioID hits the bands of lysate for a-spectrin observed in the right size (figure 3. 10. B), in addition to nirvana (Figure 3. 10. F). No bands observed for coracle, Disc large and PS2 which might need more optimizing.

However, the same experiment has been repeated, and more proteins volumes were loaded into the gel (5 µl) and the bands for both extract and elution were clear in the right size with (1:1000) rabbit anti-GFP for YFP-Cln7 (Figure 3. 11. A). Regarding BioID hit

proteins only lysate bands were observed for coracle, nirvana, ATPase and integrin-alpha were observed in the right places (Figure 3.11).

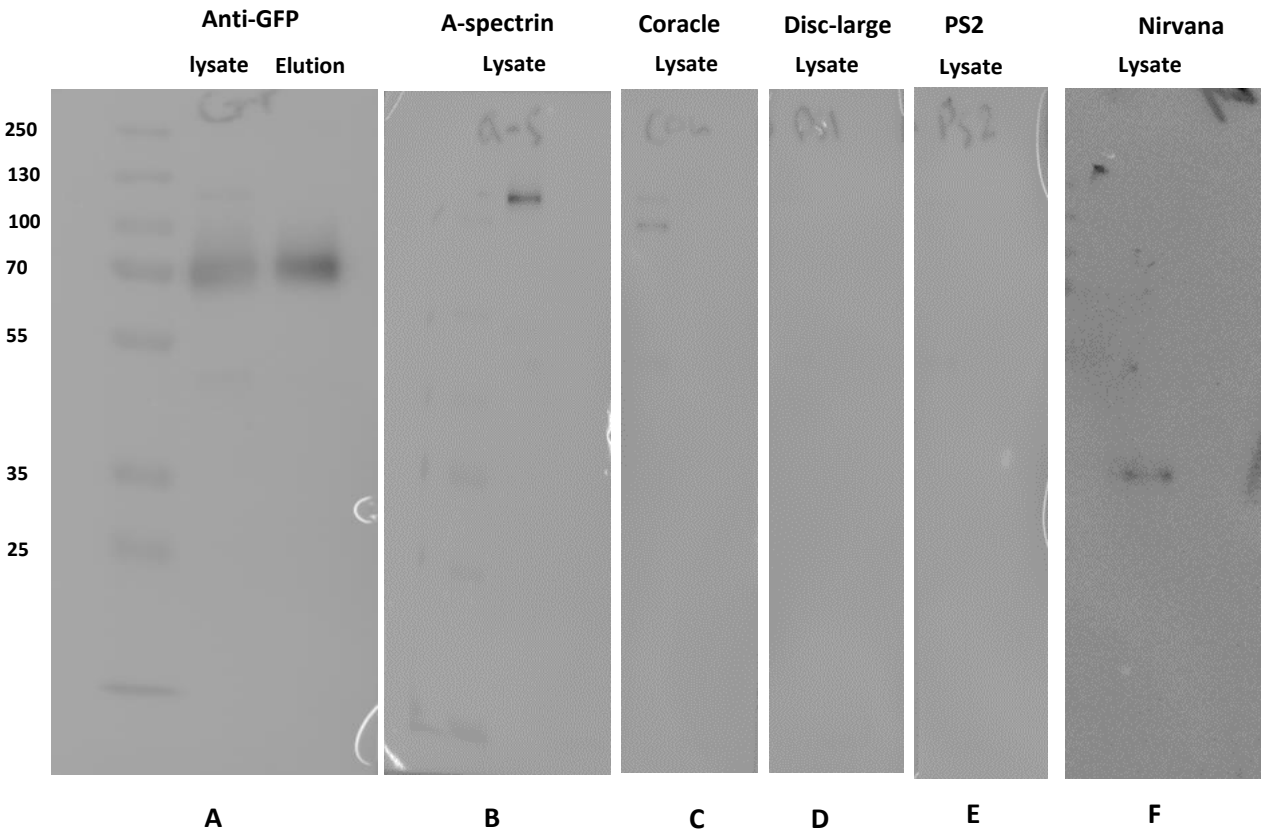

Figure 3. 10: Optimizing immunoprecipitation of YFP-CLN7 expressing cells and BioID hits with SMALPs.

Western blotting of immunoprecipitation experiments of YFP-CLN7 expressing S2 cells was performed using 0.5% (w/v) SMALPs instead of detergents. A 10% SDS-PAGE was used, and 2 µl of proteins were loaded into the gel. **(A)** A 1:1000 rabbit anti-GFP antibody was added to the membrane, and bands of the expected sizes for lysate and elution of YFP-CLN7 were observed. **(B-F)** The Western blot experiment was conducted only for extracts of BioID hits. **(B)** The band of α-spectrin (1:20) is shown at the expected Mw. **(C-E)** A 1:20 dilution of hit proteins coracle, Disc large, and PS2, respectively, was added, but no bands were detected. **(F)** A 1:20 dilution of Nirvana was added to the membrane, and its band appeared at the expected Mw.

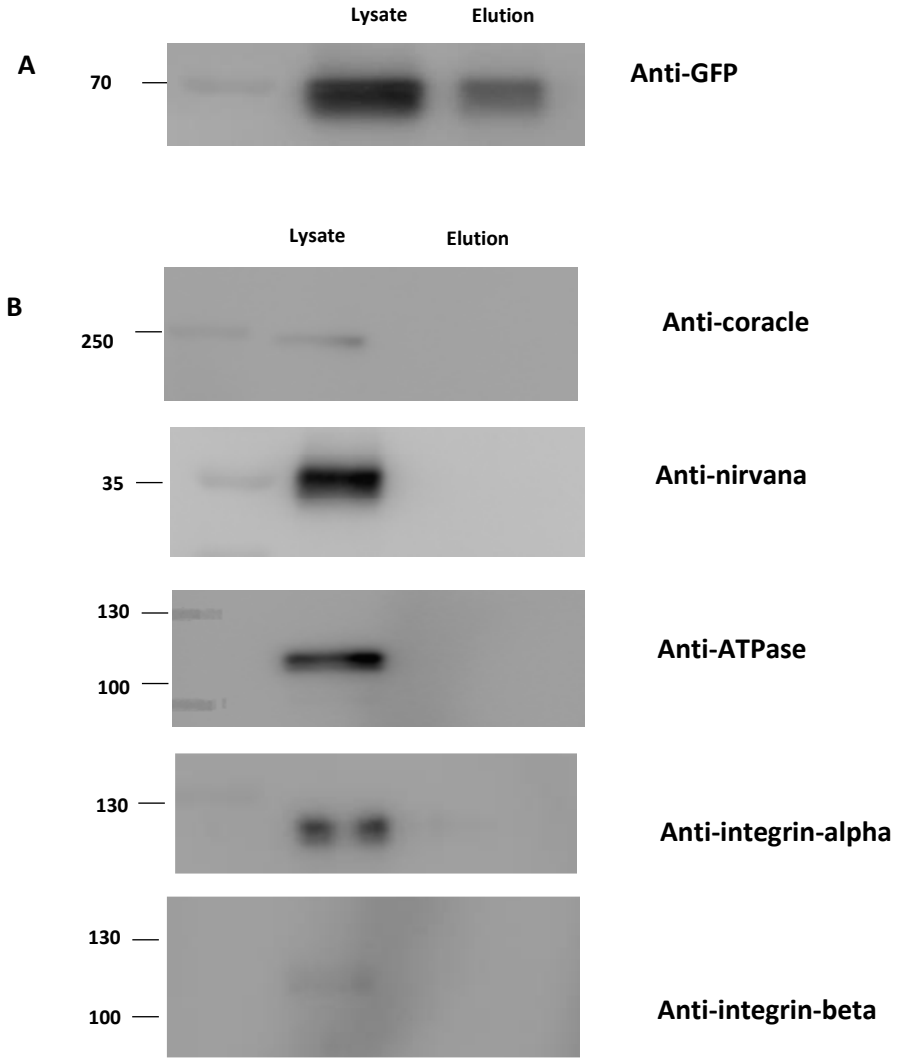

Figure 3. 11: Co-immunoprecipitation from YFP-CLN7 expressing S2 cells to validate potential interacting proteins using SMALPs.

Immunoprecipitation of YFP-Cln7 using SMALP extraction and GFP-Trap beads from S2 cells. 10 % SDS-PAGE gel used. 5µl of proteins were loaded into the gel. **(A)** YFP-Cln7 is detected in both the SMALP cell extract and after immunoprecipitation by using rabbit anti-GFP (1:1000) which used as a control. **(B)** Several BioID hits are detectable in SMALP extracts but not in eluates after co-immunoprecipitation.

As described above, I started by 0.5% (w/v) SMALPs within the lysis buffer and found that proper for YFP-CLN7 and other potential interacting proteins as shown in (Figure 3. 11). Both lysate and elution samples were detected with that SMALPs 0.5% concentration for YFP-CLN7. However, depending on this protocol, detection of the elution bands for hit proteins was impossible and there was not indicating for interaction. Therefore, to have appropriate results, changes in the protocol were initiated. The concentration of SMALPs was increased to 1% (w/v) and the NaCl concentration was increased from 150 mM to 300 mM in the wash buffer. YFP-Cln7 was clearly detectable in the extract and after immunoprecipitation (Figure 3. 11. A). However, no bands were detected for the elution of hit proteins. Consequently, I decided to heat the elution buffer containing beads for 1 minute. Heating is essential for releasing proteins from the GFP-trap beads, but it is not suitable for SMALPs. Therefore, I heated the sample for 1 minute at 60°C and found it to be appropriate for the samples. Two of the potential interactors were also detectable in both lysate and elution samples at the right size: Discs Large and a-Spectrin (Figure 3. 12. B). Several experiments were conducted to investigate other BioID hit proteins, including coracle, nirvana, integrin-beta, and Na+K+ATPAse but no positive results were obtained. One obvious conclusion is that Cln7 does not, in fact, interact with these proteins. However, further experiments will be needed to confirm that these were false positives in the BioID labelling experiments.

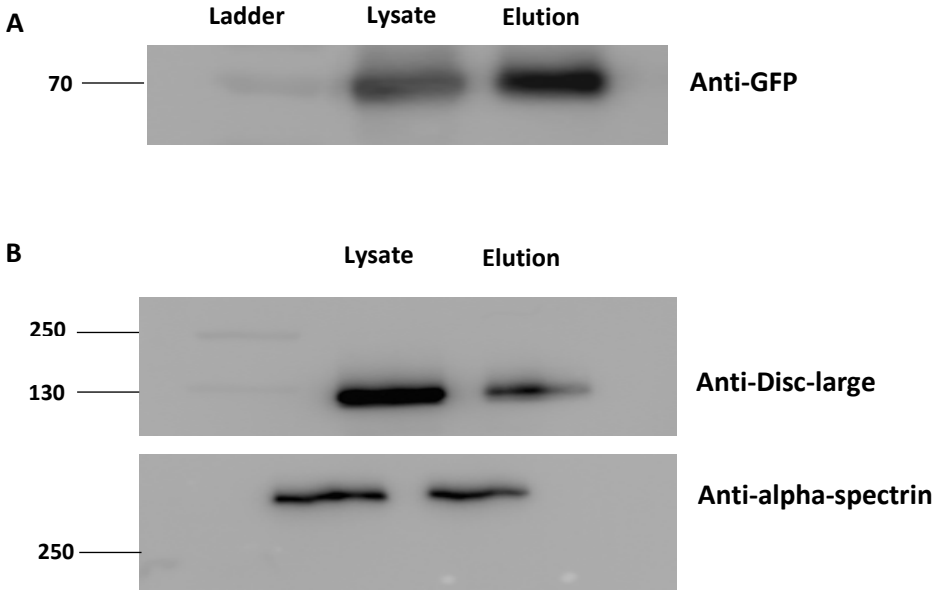

Figure 3. 12: Co-immunoprecipitation from YFP-CLN7 expressing S2 cells to validate potential interacting proteins using SMALPs.

10% SDS-PAGE gel was used. YFP-Cln7 was extracted using 1% SMALPs and immunoprecipitated with GFP-trap beads which was heated to 60 C˚ for 1 min. 5 µl proteins were loaded into the gel. **(A)** YFP-Cln7 is detected in both SMALP extract and immunoprecipitation elution by adding rabbit anti-GFP (1:1000) to the membrane and that was used as a control. **(B)** Discs large and α-Spectrin are detectable both extract and eluates samples at their expected sizes.

3.2.4. BioID-CLN7 interactions in *Drosophila melanogaster*.

Having validated the BioID-Cln7 approach in cells, I wanted to know if the same interaction could be detected at the post-synaptic compartment of the neuromuscular junction, where *Cln7* resides in an unidentified vesicular compartment. Of particular interest was the interaction with Discs large, a known scaffolding protein and organiser of the post-synaptic density. Myc-BioID-Cln7 was previously cloned with UAS elements upstream (section 3.1.2) by the group and transgenic flies generated. I crossed myc-BioID-CLN7 by a Mef2-Gal4 line to drive the expression of BioID-Cln7 to the fly muscles. Third instar larvae were dissected, fixed, stained and imaged by Richard Tuxworth to show the BioID-Cln7 fusion protein localises as at the post-synaptic density. Anti-myc antibody used to detect myc-BioID-CLN7 in the fly as it is clear in green colour with anti-HRP (red). Myc-BioID-CLN7 is recruited to the post-synaptic density, as expected (Figure 3. 13). Therefore, western blotting experiments were done to detect myc-BioID-CLN7 in flies and to show the biotinylated protein. Larvae were lysed and a Western blot was run and probed with anti-Myc and streptavidin-HRP, but no signal could be detected (Figure 3.14. A-B). Nor were they any bands detectable in eluates by Coomassie after a streptavidin-bead pull downs (Figure 3.14. C). it is clear that the BioID-CLN7 was recruited in the flies but having biotinylated protein was impossible as this technique did not work in flies.

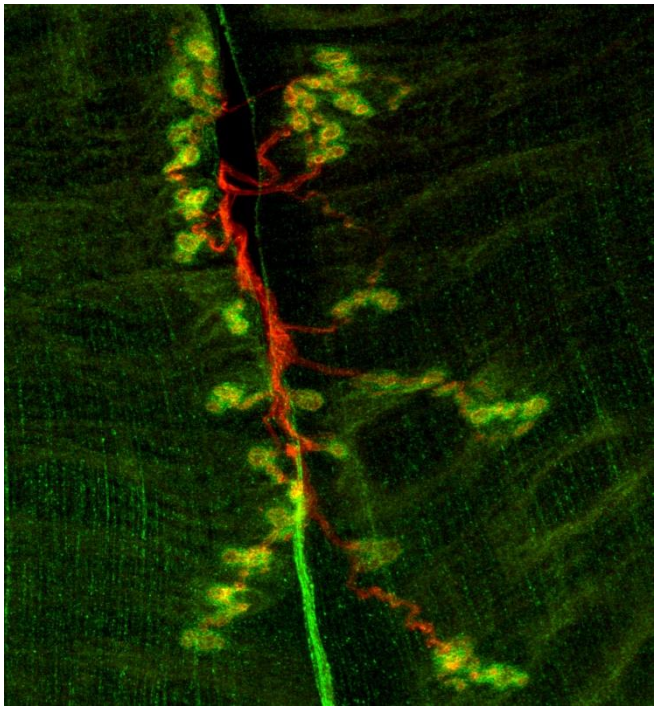

Cln7 HRP (neuronal membrane)

Figure 3. 13: BioID-CLN7 is recruited to post-synaptic density in *Drosophila melanogaster*.

The experiment was performed by Richard Tuxworth shown the expression of CLN7 in postsynaptic density in NMJ as third instar larvae were used to show the localization of the BioID-CLN7 fusion protein. UAS-BioID-CLN7 was transgenic in embryonic w^{1118} flies and crossed by Mef2-Gal4 to drive BioID-CLN7 to the fly muscle. Anti-myc antibody used to detect myc-BioID-CLN7 in the fly as it is clear in green colour with anti-HRP (red). Myc-BioID-CLN7 is recruited to the post-synaptic density, as expected.

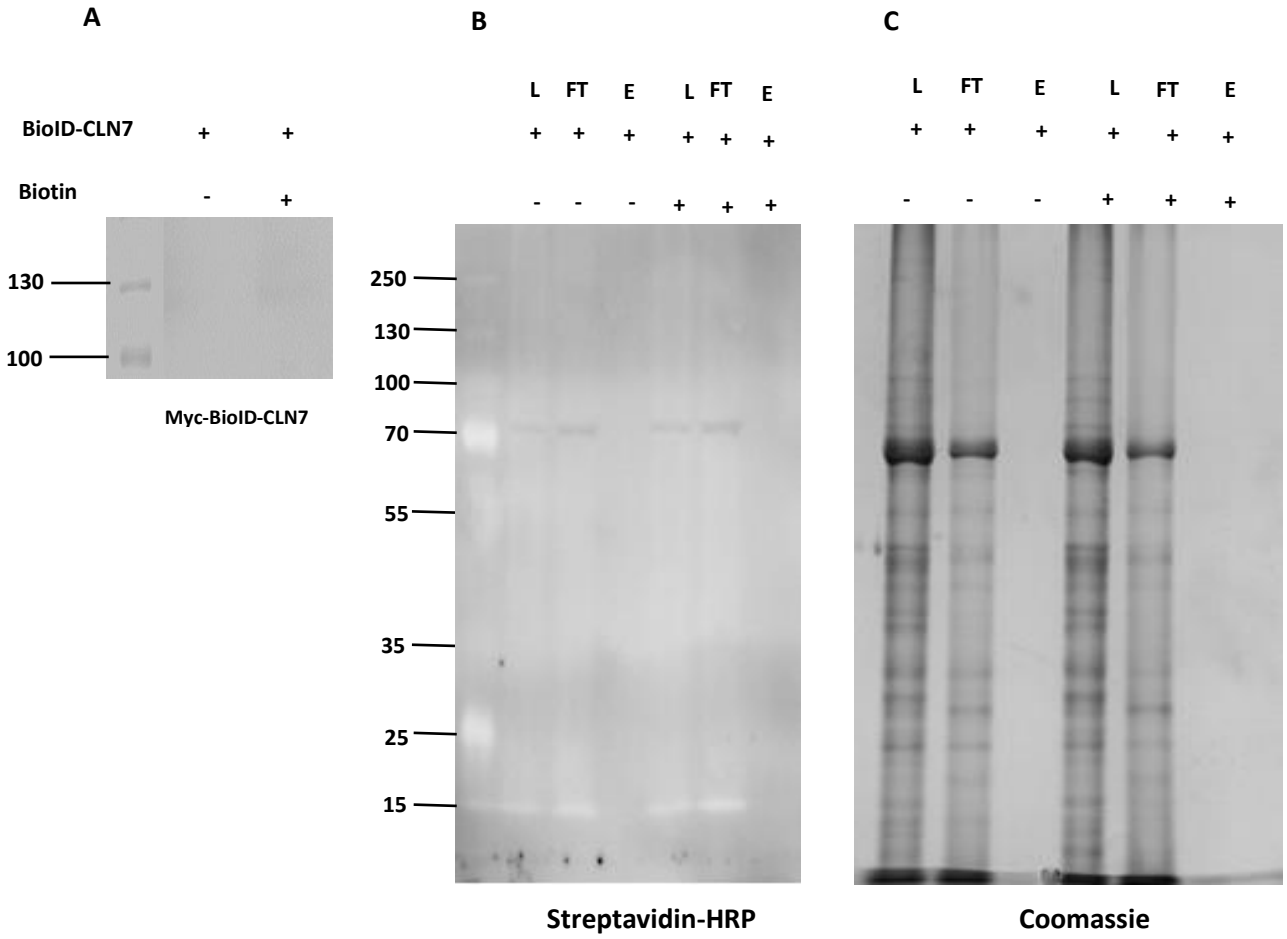

Figure 3. 14: In vivo BioID-CLN7 labelling in *Drosophila* Larvae.

UAS-BioID-CLN7 driven to the fly muscle by using Mef2-Gal4. Western blotting trail done for *Drosophila* larval to identify myc-BioID-CLN7 in the larval, with and without biotin. **(A)** Indicates no band detected for myc-BioID-CLN7 by using rat-anti-myc (1:1000). **(B)** pull-down of streptavidin HRP (1:5000) to identify biotinylated proteins. **(C)** Coomassie stain added to the SDS-PAGE gel and the result shows no band detected in elution samples. Cell lysate (L), flow-through (FT) and eluate (E).

To determine whether the UAS-BioID-Cln7 construct was present in the flies, the experiment of single fly genomic DNA preps followed by PCR (section 2.2.10) was performed on an adult fly. The analysis process utilized Gw5f Fw and SVr primers (refer to Table 2.4) to amplify BioID-CLN7 DNA. As a positive control, ElavGal4 adult fly was used (Table 2.7) and conducted PCR using the same primers. The UAS-BioID-CLN7 band was detected in the expected size, indicating the presence of the UAS-BioID-CLN7 transgene in the fly (Figure 3.15). Adult flies expressing the UAS-BioID-CLN7 under the control of Mef2-Gal4 were Western blotted and rat ant-myc (1:1000) added but no anti-myc signal was detectable (Figure 3. 16. A) and therefore, no biotinylated protein found with streptavidin-HRP (1:5000) (Figure 3. 16. B).

Although BioID-CLN7 had been correctly inserted in the fly (Figure 3. 13), proximity labelling using the BioID technique in the flies proved impossible due to its slow kinetics and low catalytic activity. This suggests the need for improvements in the proximity labelling technique to identify CLN7 interaction proteins in *Drosophila* larvae and adults.

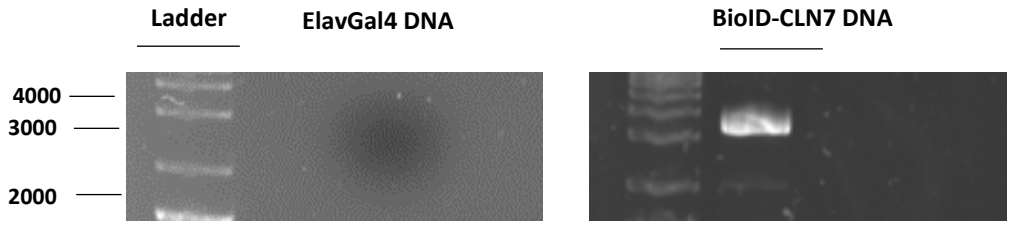

Figure 3. 15: Genomic DNA PCR to identify the BioID-CLN7 DNA transgene in *Drosophila melanogaster*.

A PCR from UAS-BioID-CLN7 genomic DNA to amplify the BioID-Cln7 construct. ElavGal4 DNA fly was used as a positive control. The BioID-CLN7 DNA is detected in the expected size while no band observed in the positive control elavGal4 which confirmed the existence of BioID-CLN7 DNA in the *Drosophila melanogaster*.

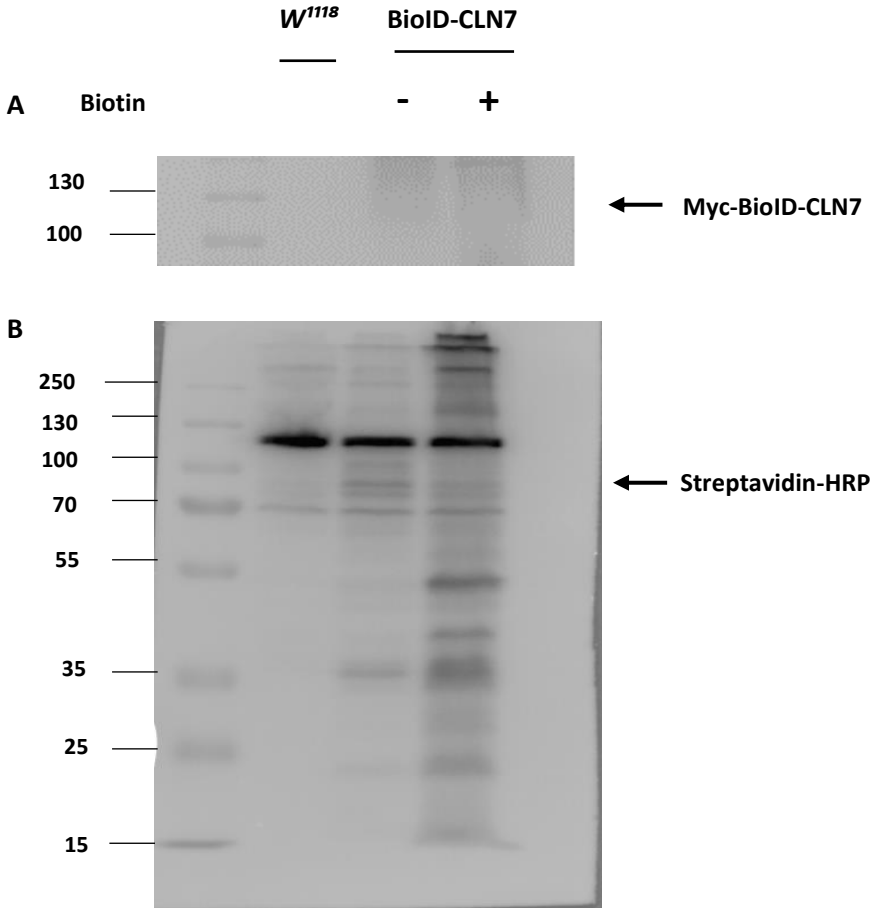

Figure 3. 16: In vivo BioID-CLN7 labelling expressing in the adult flies.

In vivo BioID-CLN7 labelling experiment of *Drosophila* adult flies. 100 µM biotin added to the fly food in addition to other food without biotin. 10 % SDS-PAGE gel was used and 5 µl of proteins loaded into the gel. w^{1118} flies were used as a control. **(A)** Rat anti-Myc (1:1000) used to identify Myc-BioID-CLN7 but there was no band detected in either -/+ biotin. **(B)** Streptavidin-HRP pull-down (1:5000) to identify the biotinylated proteins. The result highlights no protein biotinylated even in exogenous biotin.

3.3. Discussion

3.3.1. Proximity labelling BioID technique.

This part of the project aimed to validate the previous experiments and identify the CLN7 protein interactions in the cells by using BioID proximity labelling and trying to find if that could be applied in *Drosophila* flies and larval. This is a new technique that was developed in 2012 by labelling protein in eukaryotic cells [163]. This technique is suitable for CLN7 protein which is considered a cell membrane protein. This hydrophobic protein is sensitive, and Co-IP detergents affect this protein and lead to changes in the protein structure itself and other related compounds, and at the end there is no correct results will be obtained.

Applying proximity labelling in vitro by expressing BioID-CLN7 in S2 cells was indeed suitable for investigating candidate interacting proteins with CLN7. Numerous potential interacting proteins were identified using the BioID technique. However, similar results were expected when this technique was applied in flies. So, myc-BioID-CLN7 was recruited in the flies and larvae muscle to confirm the results obtained from S2 cells but no myc-BioID-CLN7 was detected in larval and no biotinylated proteins as well. Regarding adult flies, no band was detected for myc-BioID-CLN7, and no considerable biotinylated proteins were found by using the BioID proximity labelling technique even we know the BioID-CLN7 inserted in the right place and that was shown through IF (Figure 3.12) but labelling that was impossible.

However, BioID has its barriers, including slow kinetics and low activity, which make it impossible to apply in flies. Therefore, I turned to the second-generation proximity labelling systems which have higher activity and faster labelling kinetics to identify candidate CLN7 interacting proteins in flies (explained in sections 3.3.4 and 3.3.5).

3.3.2. BioID-CLN7 hit proteins.

By applying this BioID technique, many identical proteins were found after mass spectrometry analysis. By concentration on the Drosophila nervous system, there are several proteins expressed in the nervous system of Drosophila, but the important proteins are related to cytoskeletal proteins of the neuro muscle junction and glial-specific proteins. The MS results showed that several interesting proteins interact with the CLN7 protein. This analysis identified cytoskeletal proteins of the neuro muscular junction (NMJ) including coracle, Na+K+ATPAse (alpha and beta subunit), PS1 integrin (alpha and beta subunit), discs large, lethal giant larvae and A-spectrin. Other proteins consisting of nirvana, formin-like and slit which are glial-specific proteins (Table 3.2).

Coracle is a member of the protein 4.1 superfamily that establishes *Drosophila* glutamate receptors to the postsynaptic actin cytoskeleton and considered a component of the septate junction structure [177]. In addition, it has an essential function in the development of epithelial cells [178]. Another important protein related to the cytoskeleton NMJ is Na+K+ATPase (alpha and beta subunits) which is found in the cells membrane of neurons and other cells and is involved in sodium and potassium ions transport across the plasma membrane [179, 180]. Studies mentioned that, PS1 integrin (alpha and beta subunits) is enriched at the tip of a growing axon which suggests it has a role in axon guidance [181], in addition to that, laminin is known as a ligand for PS1 integrin, which is present along the embryonic axon pathways [181, 182]. Another important protein is lethal giant larvae, which plays a crucial role in cell polarity and asymmetric division, regulating exocytosis, mediating cytoskeletal and cancer suppressors [183]. Discs large protein is involved in connection septate junctions to the cytoskeleton [184, 185]. A-spectrin is the major constituent of the

cytoskeleton and plays an important role in the Drosophila NMJ through the regulation of the postsynaptic spectrin skeleton [186]. One study suggested that the existence of a postsynaptic, submembranous spectrin-actin network affects the organization of synapse development at Drosophila NMJ [187].

Regarding the proteins which related to the glia, the first one is formin-like which works with DAAM and Cdc42 and has a role in the neuronal development of mushroom bodies which suggests that protein has a role in neural growth [188]. It is also used with Cdc42 in the planar cell polarity establishment in the developing compound eye through its contribution to ommatidial rotation [188, 189]. The second protein is slit, which is important for cell migration and axon guidance during development [190]. It is a ligand for the guidance receptor roundabout (robo) and prevents unsuitable midline crossing by the Robo-expressing axon [191]. The nirvana protein stimulates ATP coupled hydrolysis with the change of Na and K ions across the plasma membrane [192]. However, the important point here is the place of CLN7 among those proteins and how this protein can regulate several functions through those hit proteins.

The hit proteins mentioned above are related to both the cytoskeleton and glia. Both the cytoskeleton and glia play important roles in regulating synaptic function, structure, plasticity, and development, which consequently impacts NMJ (neuromuscular junction) development. In *Drosophila*, cytoskeletal remodelling contributes to morphological and functional changes in synapses[193]. Cytoskeletal elements, including actin, intermediate filaments, and microtubules, are crucial for cell shape and size and contribute to developmental processes such as axon guidance, neuron division, and synapse formation

[194]. Both pre- and post-synaptic terminals contain the important cytoskeletal protein actin [195].

In the central and peripheral nervous systems (CNS and PNS) of animals, glia cells are essential components of synapses [196-198], regulate several aspects of synaptic development and function. In Drosophila, glia is essential for forming the blood-brain barrier to maintain ion homeostasis and for regulating neurotransmitter levels in adult muscles [199, 200]. Additionally, glia plays a role in chemical neurotransmission for synaptic communication [201].

Regarding the CLN7 protein, it has been observed that CLN7 functions at the Drosophila neuromuscular junction (NMJ). Furthermore, Cln7 is expressed in glia that ensheath motor neurons and in the muscles of the body wall, forming the post-synaptic cells of the NMJ. Consequently, it is possible that CLN7 regulates synapse function and plasticity through these hit proteins. Specifically, coracle, hit, and alpha-spectrin may be affected by CLN7, contributing to NMJ development. Conversely, any impairment in these proteins could lead to defects in CLN7 function, potentially dysregulating NMJ development.

3.3.3. Verification of protein interaction.

The important point in this issue is whether the BioID hit proteins really interact with CLN7. As with the PL experiment, there are proteins only neighbouring BioID or conjugated through this process. Consequently, an immunoprecipitation experiment was performed for the target proteins to identify which protein interacts with CLN7. The SMALPs sample and GFP-Trap beads were combined to have precise outcomes. From the experiment, a band of two candidate proteins was identified. The first one is Discs large protein which is involved

in connection septate junctions to the cytoskeleton [184, 185]. The second protein is A-spectrin which is the major constituent of the cytoskeleton and plays an important role in the Drosophila NMJ through the regulation of the postsynaptic spectrin skeleton [186].

DLG is the prototypic member of membrane-associated guanylate kinase homologs (MAGUKs) which are considered growing proteins [185, 202]. In Drosophila epithelia, DLG is important for cell polarity, septate junction, and the control of proliferation. The study demonstrated that, Dlg is localized at the septate junctions between epithelial cells and the neoplastic overgrowth of the imaginal discs resulted from that gene mutations. Consequently, it is considered a tumour suppressor gene. It is important in the regulation of the cytoskeleton, membrane proteins differential localization and apicobasal polarity of epithelial cells [185]. Other studies demonstrated the role of DIg in the regulation of the size, shape, and function of synaptic structures and in a new synapse formation DLG plays an important role in the expansion of postsynaptic membranes [202-204]. In addition, the Dlg mutation affects Drosophila NMJs as it leads to distribution in synaptic shaker potassium channels, fascilin II and larval synaptic growth [205, 206]. However, the interaction with *Cln7* need to be confirmed by more research in particular related to mutation to reveal the effect of *Cln7* in this protein function and how CLN7 might play a significant role in the synapse and septate junction and through Dlg protein.

Spectrin which includes alpha and beta subunits is a cytoskeletal and heterodimeric protein. It plays a significant role in the stability and structure of the cell membrane and the cell shape and contributes to diverse cell functions [207]. In Drosophila melanogaster, in addition to the above functions, it is crucial in larval morphogenesis, axon midline choice point recognition, the establishment of the nervous system, cell differentiation, endocytosis,

wound healing and egg formation [207]. The postsynaptic spectrin skeleton is important for the normal size and spacing of synapsis at the NMJ. It has been highlighted that β-Spectrin is important for the localization of α-Spectrin and ankyrin to the postsynaptic membrane while the appropriate localization of β-Spectrin and ankyrin within the subsynaptic reticulum (SSR) is regulated by α-Spectrin [187].

It has been shown that, the glial submembranous cytoskeleton produced by βII Spectrin plays a role in the assembly of paranodal junctions and nodes of Ranvior in the CNS and PNS [208].

As spectrins are important for membrane integrity and ultrastructure, it has been shown that the heart function is affected by β-Spectrin via the regulation of local signalling domains [209, 210]. Moreover, spectrin is the main component in the cytoskeleton and depending on that it has roles in the red blood cell (RBC) as the RBC biconcave shape, integrity and mechanical properties are marked by strange structural dynamics of their cytoskeleton [211]. However, the deficiency of spectrin causes hereditary red cell membrane disorders which probably leads to hemolytic anaemia [212].

DLG (Discs Large Homolog) is a central scaffolding protein at the post-synaptic density. Mutations in Dlg affect larval synapse growth, which in turn impacts NMJ (neuromuscular junction) development and function [172]. The critical question here is whether this effect occurs through an interaction with CLN7 and how it is mediated. Does loss of Dlg function lead to impairment of CLN7 and ultimately disrupt NMJ development? Additionally, how do mutations in Dlg influence CLN7's structure, function, localization, and expression?

Conversely, does CLN7 influence synapse function and plasticity via Dlg? It is also possible that CLN7's impact on NMJ development and function occurs through its effect on DLG and

if that directly or indirectly through other proteins. To understand this better, further studies are needed. One potential approach is to investigate CLN7 knockout or knockdown and observe the effect on DLG function, localization, or expression, either in vitro or in vivo using Drosophila larval models.

On the other hand, Dlg mutations may lead to alterations in CLN7's structure, function, or localization, potentially impairing synapse function and NMJ development. However, more research is necessary to fully understand the intricate interaction between these proteins.

Spectrin is essential for synapse stability, and the postsynaptic spectrin skeleton plays a crucial role in maintaining the normal size and spacing of synapses at the NMJ. When CLN7 experiences loss of function, how does it affect spectrin? Conversely, what happens to CLN7 in the case of a spectrin mutation? As mentioned earlier, further research is needed to explore the interaction between CLN7 and spectrin, specifically whether CLN7 impacts synapse and NMJ development through this hit protein. Additionally, investigating how spectrin functions in the absence of CLN7 is essential. Conducting more experiments in vitro and in vivo using Drosophila models will help uncover the true effect of CLN7 on synapse function, plasticity, and NMJ development in relation to spectrin.

3.3.4. Application of the proximity labelling technique in flies.

Labelling of BioID-CLN7 in vitro was interesting and several proteins were identified with the BioID proximity labelling technique. Therefore, applying proximity labelling in vivo is valuable to validate the previous results and identify the CLN7 protein-interactions and its effects in the *Drosophila melanogaster* nervous system, synapse, and lysosomal cell membrane.

Even the BioID technique was suitable for S2 cells and good results were obtained, but that was impossible in *Drosophila* flies and larvae. UAS-BioID-CLN7 was recruited to the post-synaptic density in the flies muscle cells but having bands after the proximity labelling trial was failed, even though many trials were done and optimized (Figure 3. 14 and 3. 16). BioID labelling is simple and non-toxic [163], but applying this technique in flies is impossible because the kinetics of BioID is slow requiring 18 to 24 or more hours for labelling with biotin to have sufficient biotinylated proteins. In addition, because of the low catalytic activity, applying BioID in some contexts such as flies, worms, or the endoplasmic reticulum lumen of cultured mammalian cells is difficult or impossible. Perhaps PL activity is affected by pH, redox environments and endogenous nucleophile concentrations of different organelles [213]. Consequently, it was crucial to try another second-generation proximity labelling technique (TurboID) to apply in vivo in the flies and discover the CLN7 interaction proteins.

3.3.5. An improvement of proximity labelling.

The improvement of proximity labelling started to overcome the difficulties that occurred in conventional screening methods for the identification of protein-protein associations in 2012. After applying the BioID method, the candidates identified can characterise direct or indirect interactors, and/or vicinal proteins that do not interact with the fusion protein physically. BioID has become widely used to study proteins and weak/ transient protein-protein associations (PPAs) in various experiments [163]. However, appropriate subcellular targeting is considered a challenge for any method that depends on the expression of fusion proteins. It has been observed that, the efficient targeting of certain fusion proteins was

prevented by fusion to BioID. Therefore, the same group who developed BioID, improved a new promiscuous biotin ligase variant, BioID2 which is smaller in size, more efficient at labelling proximate proteins and requires less biotin than BioID [164]. However, BioID2 still needs more time for labelling and another improvement for this method has been made the direct evolution of *E. coli* biotin ligase (BirA) to generate new promiscuous mutants, TurboID and miniTurbo [213]. In this study, the improvement of the new PL techniques is significant to labelling that in *Drosophila* larval and adult flies and revealing the CLN7 interaction proteins.

4. USE OF TurboID TO IDENTIFY THE CLN7 INTERACTING PROTEINS

4.1. Introduction

The proximity labelling technique BioID was impossible to apply in vivo in flies. one main reason was the slow kinetics which requires about 18-24 hours to label with biotin to produce appropriate biotinylated material for proteomic analysis. In addition, the low catalytic activity of BioID makes applying this technique in some contexts like flies, worms, or the endoplasmic reticulum lumen of cultured mammalian cells impossible [213]. To try to improve BioID, two improved versions carrying point mutations were introduced in 2018: TurboID is 35 KDa and has 15 mutations relative to wild-type BirA, while miniTurbo is 28 KDa with 13 mutations and an additional deletion within the N-terminal domain [213].

Both variants are capable of biotinylating endogenous proteins much more rapidly than BioID tested in mammalian cells, achieving 3 to 6-fold more biotinylation than BioID at early time points after labelling with exogenous biotin, and 15 to 23-fold greater than BioID at later time points, and are functional at lower levels of biotin. In 10 min TurboID produced similar biotinylation levels as BioID achieved in 18 hours. Moreover, TurboID was 1.5- to 2-fold more active than miniTurbo [213].

Aim

Given the failure of BioID-CLn7 labelling in vivo, I wanted to test whether using TurboID-CLN7 DNA or miniTurboID-CLN7 would allow *in vivo* proximity labelling of Cln7 interactions proteins.

4.2. Results

4.2.1. Developing TurboID and miniTurbo

4.2.1.1. Amplifying DNA

TurboID and miniTurbo were fused in *Cln7*, and the amplification process of the TurboID-CLN7 and miniTurbo-CLN7 DNAs was carried out using TurboID-GW forward and CLN7-GW reverse primers (Table 2.5) (Figure 4. 2. A). After the PCR process, gel electrophoresis analysis revealed accurate results for the DNA in the right sizes (Figure 4. 2. B). However, after amplifying the TurbiID-CLN7 and miniTurbo-CLN7, the PCR products were cloned into the pENTR vector and Sanger sequenced to ensure there were no errors introduced by the PCR.

The pENTR/D-TOPO Cloning Kit (Invitrogen) was used for efficient expression of the gene after recombination with the Gateway destination vector (Figure 4. 1). It is a fast and highly efficient 5-minute strategy to clone a blunt-end PCR product directly into a vector for entry into the Gateway system. In this technique, ligase, post-PCR procedures, and restriction enzymes are unnecessary. However, the PCR products were cloned into the pENTR vector and Sanger sequenced to ensure that no errors were introduced during PCR (Figure 4.1).

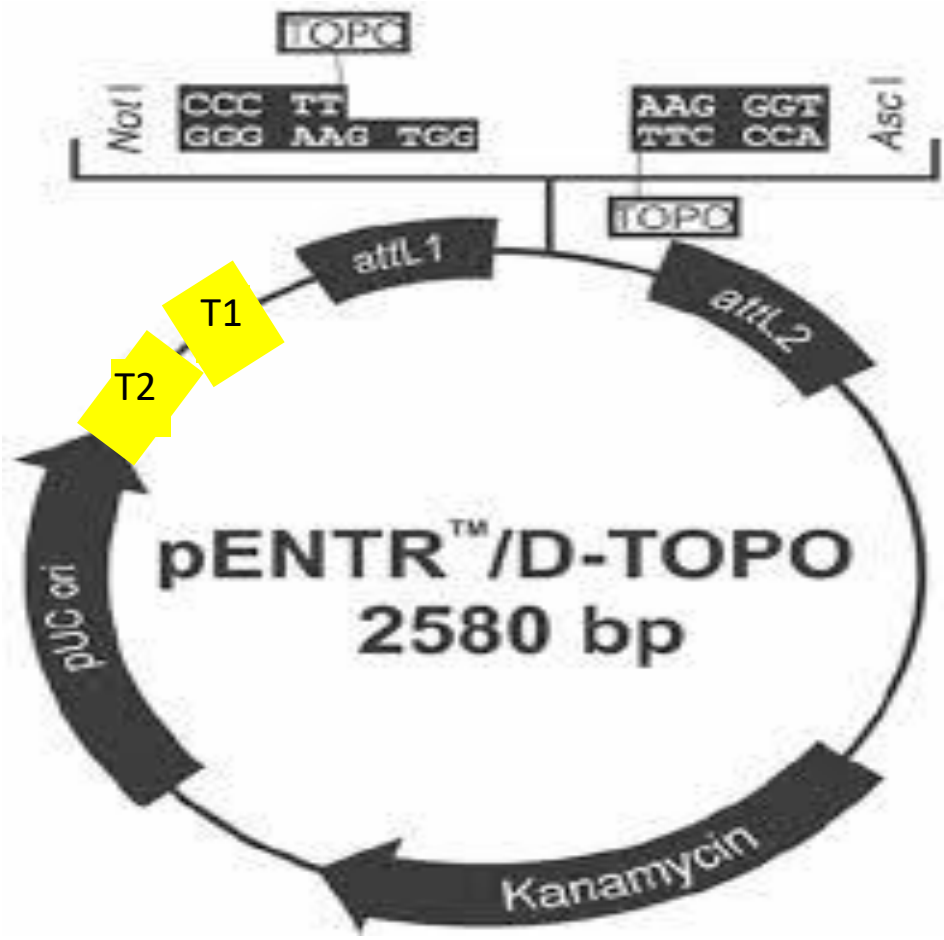

Figure 4. 1: Genetic Map of pENTR /D-TOPO Vector.

The pENTR™/D-TOPO™ vector contains 2580 base pairs (bp). It has attL recombination sites on either side of the PCR product insertion site, as well as M13 and T7 primer sequencing sites. It contains T1 and T2 transcription termination sequences. TOPO Cloning site (directional) for rapid, directional cloning of PCR product. Kanamycin resistance gene to selection of the plasmid in E. coli. pUC origin of replication for allowing high-copy replication and maintenance in E. coli (pENTR™ Directional TOPO® Cloning Kits).

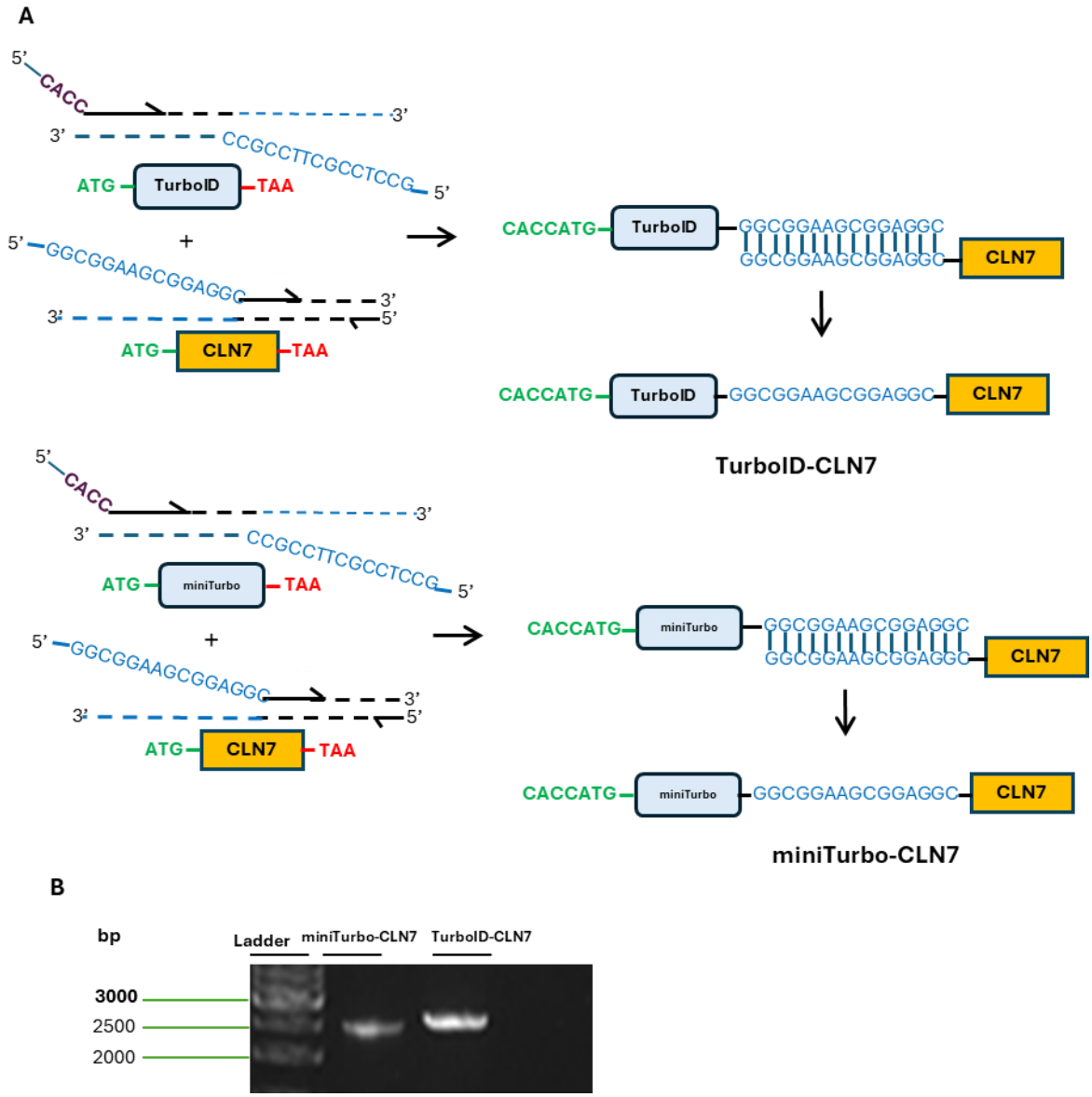

Figure 4. 2: Insertion and amplification of TurboID-CLN7 and miniTurbo-CLN7 DNAs.

Insertion and amplification of TurboID-CLN7 and miniTurbo-CLN7 DNA processes. **(A)** TurboID and minTurbo were fused in CLN7 to have TurboID-CLN7 DNA and miniTurbo-CLN7. Amplification process using TurboID_GW forward and Cln7_GW reveres primers. **(B)** Gel electrophoresis used to show TurboID-CLN7 DNA and miniTurbo-CLN7 DNA bands after PCR process and the bands detected in the right size (no template controls).

A CACC sequence included at 5’ end of the forward primer facilitates directional cloning into the pENTR/D-TOPO vector by topoisomerase, which also forms part of the Kozak sequence in the expression vector. Two phiC31 recombination sites, *att*L1 and *att*L2, allow for the transfer of the PCR product from the pENTR vector to any Gateway destination vector.

Both TuboID-CLN7 and miniTurbo-CLN7 DNAs were cloned into the pENTR/D-TOPO vector (Figure 4. 3) depending on the Gateway *Drosophila* vector collection (section 2.5).

The miniprep process (section 2.5.3) was then performed to purify the desired DNAs. After that, samples were sent for Sanger sequencing analysis, and the sequencing results confirmed that the gene was cloned in the correct orientation.

A collection of Drosophila-specific Gateway Destination vectors are available to allow for expression in cells or flies, with a variety of different epitope tags or fluorescent proteins that can be fused to the sequence at either the N- or C-terminus.

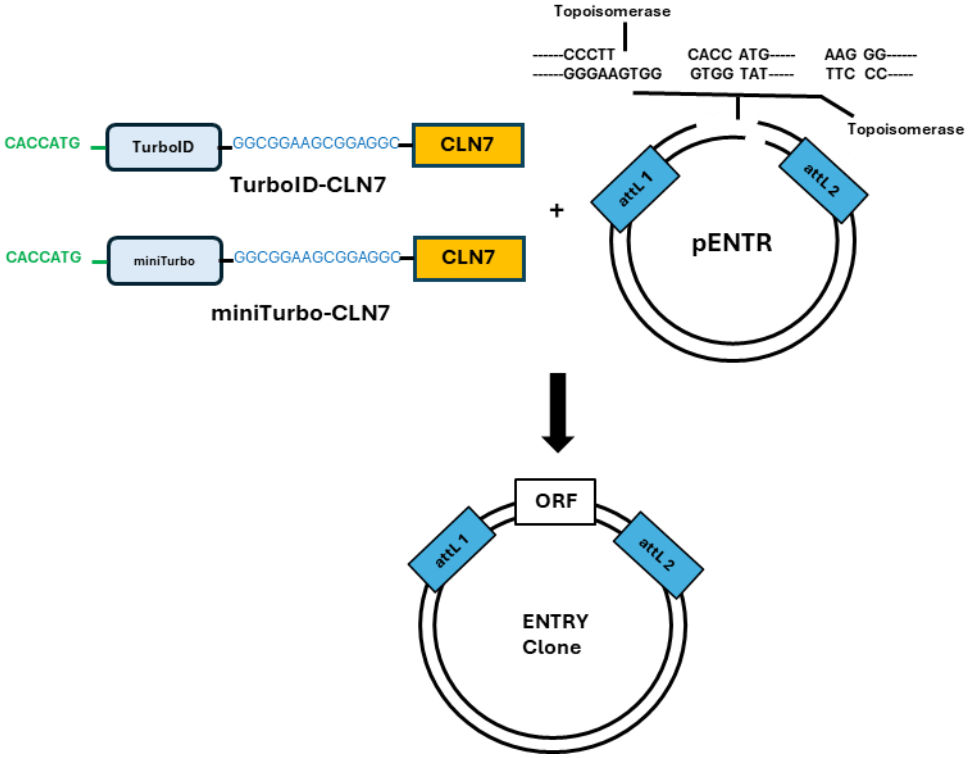

Figure 4. 3: Cloning of TurboID-CLN7 and miniturbo-CLN7 into pENTR vector.

The process of cloning started with inserting the amplified DNA (TurboID-CLN7 and miniTurbo-CLN7) into the pENTR clone which has kanamycin resistance. Depending on the Gateway drosophila vector collection, the CACC sequences are cloned into the pENTR/D-TOPO vector by Topoisomerase to form an open reading frame (ORF). After cloning, the Entry clone carried the ORF to transfer it into the destination vector, as depending on the gateway cloning method the ORF linked by attL1 and AttL2 recombination sites is recombined with the recombination sites attR1 and attR2 of a destination vector.

The Gateway cloning method involves recombining an Open Reading Frame (ORF) of interest into any vector using a simple and efficient reaction. The gene is combined with the ORF placed in the frame. In the Gateway technique, lambda integrase is used to recombine the ORF linked by attL1 and attL2 recombination sites with the recombination sites attR1 and attR2 of a destination vector. This process replaces the ORF with the cassette containing the ccdB gene in the destination vector (Figure 4. 4). The expression clone is generated using an LR recombination reaction (LR Clonase II enzyme mix from Invitrogen) between the entry clone and the destination vector. This enzyme stimulates recombination, resulting in an entry clone gene attL-flanked with a destination vector attR-flanked to generate an expression clone containing attB (Figure 4. 4).

Consequently, pure TurboID-CLN7 was translated into the pDEST vectors using Gateway™ LR Clonase™ II Enzyme Mix. Three pDEST vectors—pAMW, pTW, and pTMW—were used for the transformation of the TurboID-CLN7 DNA. All these Gateway destination vectors are resistant to ampicillin in the vector backbone and have two recombinant sites, attR1 and attR2. pAMW has an actin promoter (Actin5C) for use in tissue culture cells and 6xMyc tags at the N-terminus. pTMW has a UASt promoter for use in flies with a Gal4 driver and N-terminal 6xMyc tags. pTW has a UASt promoter for use in flies and no tag (The Drosophila Gateway™ Vector Collection | Carnegie Science).

After the transformation process, three expression clones were obtained: pAMW-TurboID-CLN7, pTMW-TurboID-CLN7, and pTW-TurboID-CLN7. The midiprep isolation process (section 2.6) was performed for all DNA expressions to obtain the desired plasmids. Subsequently, concentration processes were carried out for all three samples.

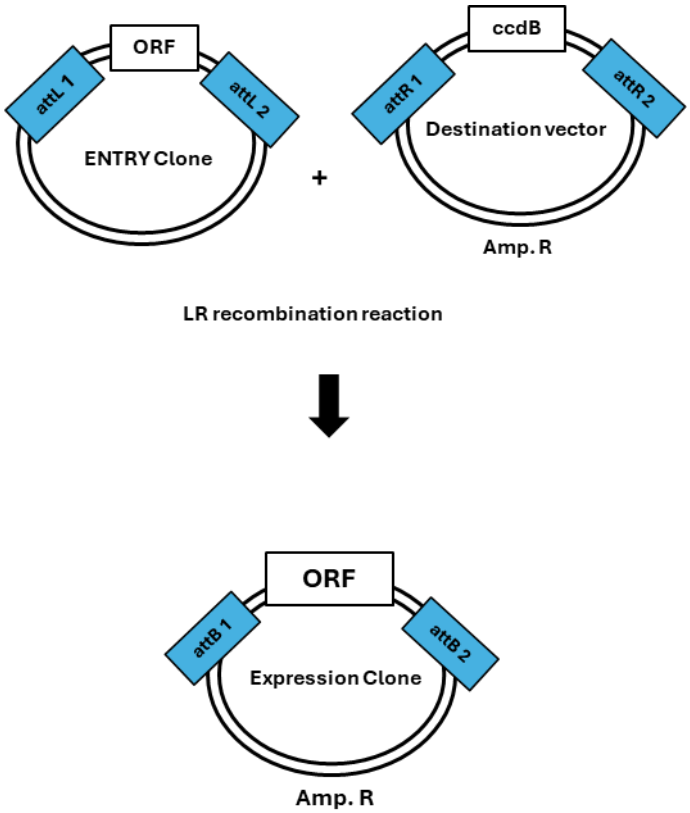

Figure 4. 4: Transformation of ORF from ENTRY clone into destination vector to have expression clone.

In the Gateway technique, LR recombination reaction used to recombine the ORF linked by attL1 and attL2 recombination sites with the recombination sites attR1 and attR2 of a destination vector. This process replaces the ORF with the cassette containing the ccdB gene in the destination vector to have the expression clone.

4.2.2. Identification of TurboID-CLN7 in S2 cells.

4.2.2.1. Transfection of pAMW-TurboID-CLN7.

S2 cells were transfected with the pAMW-TurboID-CLN7 plasmid using the TransIT-2020 transfection reagent and instructions. After approximately 72 hours, the cells had continued grown and appeared healthy, reaching 70-80% confluence, indicating that they were ready for the experiments.

4.2.2.2. Identification the expression of myc-TurboID-CLN7 in S2 cells.

To verify the development of TurboID-CLN7, a western blotting experiment was conducted initially to detect the expression of the myc-TurboID-CLN7 signal after transfection with S2 cells. The TurboID-CLN7 expressing cells were incubated without exogenous biotin. Then, the cells were lysed by using a lysis buffer (Table 2.1) which includes 2% w/v DDM detergent and 1:200 protease inhibitors. Rat anti-myc (1:1000) was used to detect myc-TuroID-CLN7 and even though no exogenous biotin was added a strong band signal has been detected for myc-TurboID-CLN7 at its right size (Figure 4. 5. A). However, having a clear band in the expected size, indicating that the TurboID expressing was accurate. The results encouraged the application of TurboID-CLN7 labelling, whether in vitro or in vivo.

Coomassie staining was used to assess the expression of TurboID labelling in S2 cells (Figure 4. 5. B) and multiple bands in the SDS-PAGE gel were shown, even no exogenous biotin. A comparison with BioID indicates that TurboID is more effective than BioID and is capable of biotinylating endogenous proteins to a greater extent than BioID tested in mammalian cells [213]. This conclusion is further supported by applying TurboID in the S2 cells and in *Drosophila* flies.

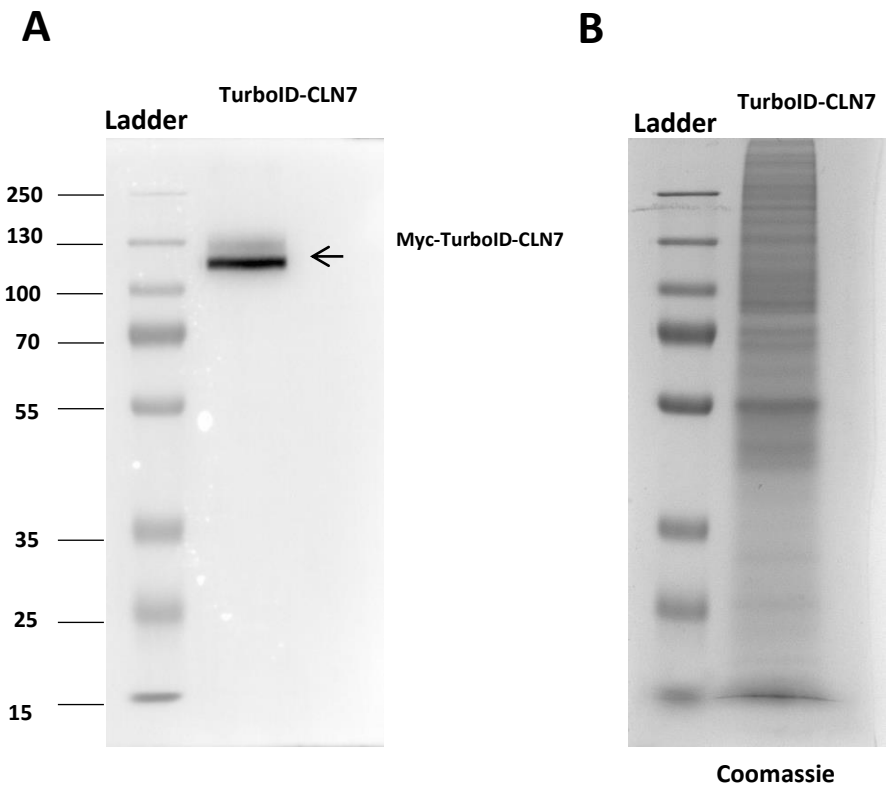

Figure 4. 5: Detection the myc-TurboID-CLN7 expression in S2 cells by Western blot.

Western blotting analysis of S2 cells to confirm the expression of Myc-tagged TurboID-CLN7 in S2 cells. 10 % of SDS-PAGE gel used and 10 µl of protein loaded into the gel. **(A)** Rat anti-myc (1:1000) confirms expression of Myc-tagged TurboID-CLN7 at the expected molecular weight. **(B)** Coomassie staining added to the SDS-PAGE gel to assess the protein biotinylation within S2 cells expressing Myc-TurboID-CLN7.

4.2.2.3. In vitro labelling TurboID-CLN7

To test for labelling by TurboID-Cln7, S2 cells were transfected with the pAMW-TurboID-CLN7. A stable cell line was generated by co-transformation of a hygromycin-resistant vector, pCoHygro, at the same time, followed by selection with hygromycin for 7 days. However, since TurboID requires less exogenous biotin and a shorter incubation time than BioID, 50 µM biotin was sufficient with TurboID to yield accurate results which were better than those obtained with BioID. Therefore, 50 µM biotin was added to the medium for 1 hour before lysis and overnight pulldown with streptavidin beads. Clear biotinylation was visible in TurboID-Cln7-expressing cells but not in control non-transfected cells. Labelling was clearly more intense after the addition of exogenous biotin (Figure 4. 6). There was clear evidence of self-labelling of the TurboID-Cln7 protein, without additional biotin but with biotin added, both self-labelling and labelling of other bands were clearly more intense.

Consequently, the appropriate results obtained from in vitro labelling of TurboID-CLN7 in S2 cells strongly encourage the application of TurboID-CLN7 DNA in genetics, which is expected to yield precise results in *Drosophila melanogaster*.

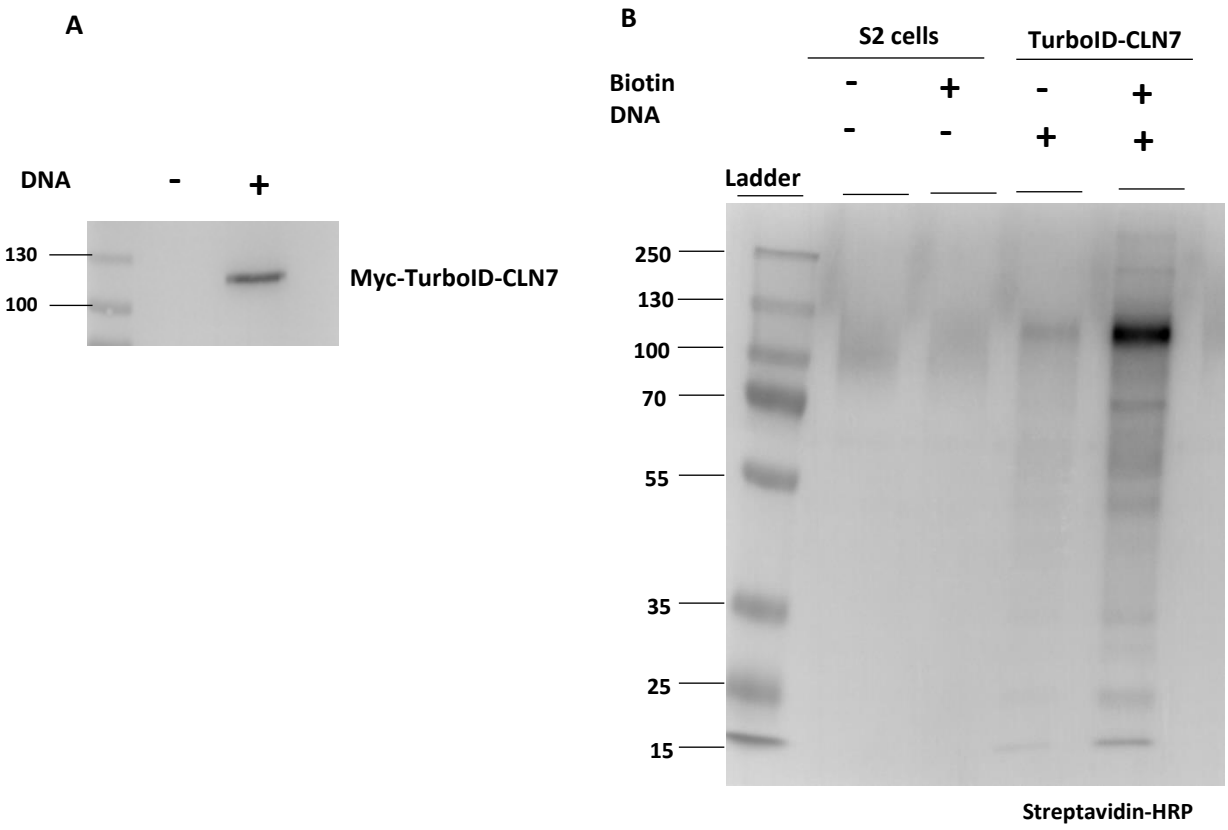

Figure 4. 6: In vitro labelling of TurboID-CLN7 in S2 cells.

In vitro labelling of myc-TurboID-CLN7 expressed in S2 cells. 10% SDS-PAGE gel used and 15 µl of proteins loaded into the gel. S2 cells were used as control. **(A)** Western blot of Myc-TurboID-CLN7 in S2 cells probed with rat anti-myc (1:1000). Un-transfected (-DNA) and transfected (+DNA) cells. the signal band of myc-TurboID-CLN7 is detected in the right size. **(B)** Western blot stained with streptavidin-HRP of a pull-down of biotin-labelled proteins using streptavidin-beads. Transfected status vs control cells and 50 µM biotin addition to the cell medium 1 hr before lysis is indicated as **–** and **+** above the figure. Biotinylated proteins bands are clear in TurboID-CLN7 within biotin.

4.2.3. In vivo labelling TurboID-CLN7

Having seen promising *in vitro* labelling, the TurboID-CLN7 construct was transferred to the pTMW Gateway Destination vector to allow for expression in flies under the control of a Gal4 driver. DNA was sent for injection into w^{1118} embryos to generate a transgenic line. Ten independent lines were generated and mapped to chromosomes by a standard crossing (Sections 2. 4. 6 and 2. 4. 7).

4.2.3.1. Expression of UAS-TurboID-CLN7 in flies

To test for the expression of TurboID-CLN7, I chose to use the Mef2-Gal4 driver to drive expression in the muscle of three UAS-TurboID-Cln7 lines. Mef2-Gal4 drives expression in the muscle, which is the post-synaptic cell of the NMJ.

Western blotting and immunofluorescence experiments were then performed by selecting larvae that were Mef2-gal4 x UAS-Myc-TurboID-Cln7 and then analysed. In addition, streptavidin pull-down trials were applied to identify biotinylated proteins.

Progeny inheriting UAS-TurboID-CLN7 were selected by scoring for a balancer chromosome carrying the Tb dominant mutation. Larvae inheriting the UAS-TurboID-CLN7 chromosome were wild-type but those inheriting the balancer were short and fat. Flies were grown in normal food or food supplemented with 50 μM biotin.

Flies were lysed buffer containing 2 % DDM non-ionic detergent in an attempt to protect the CLN7 membrane protein from denaturation and maintain protein complexes. Samples prepared without heating failed to extract any CLN7 so the heating of lysates at different temperatures was then tested. By using gout ant-myc (1:1000), myc-TurboID-CLN7 signal

bands were detected at their expected size at 130 KDa after heating the elution buffer at 70˚C (Figure 4. 7), but by heating the elution buffer to 95˚C, more protein was extracted (Figure 4. 8).

The results indicated that in transgenic line number 10, no band was detected without biotin, while a very unclear band was observed when biotin was added to the food. This is different from lines number 17 and 18, where the results demonstrated bands of myc-TurboID-CLN7 at the correct size with or without biotin (Figure 4. 7). Therefore, after confirming that TurboID-CLN7 is expressed at the correct size in the larval muscle, I wanted to see whether it was able to label proteins by biotinylation. A western blot of the lysates probed with streptavidin-HRP (1:5000), detected multiple biotinylated proteins. As shown, the larvae developed on food supplemented with biotin and heated at 95 ˚C, resulting in many biotinylated protein bands. In cases where no biotin was present, there were no bands related to biotinylation proteins (Figure 4. 8).

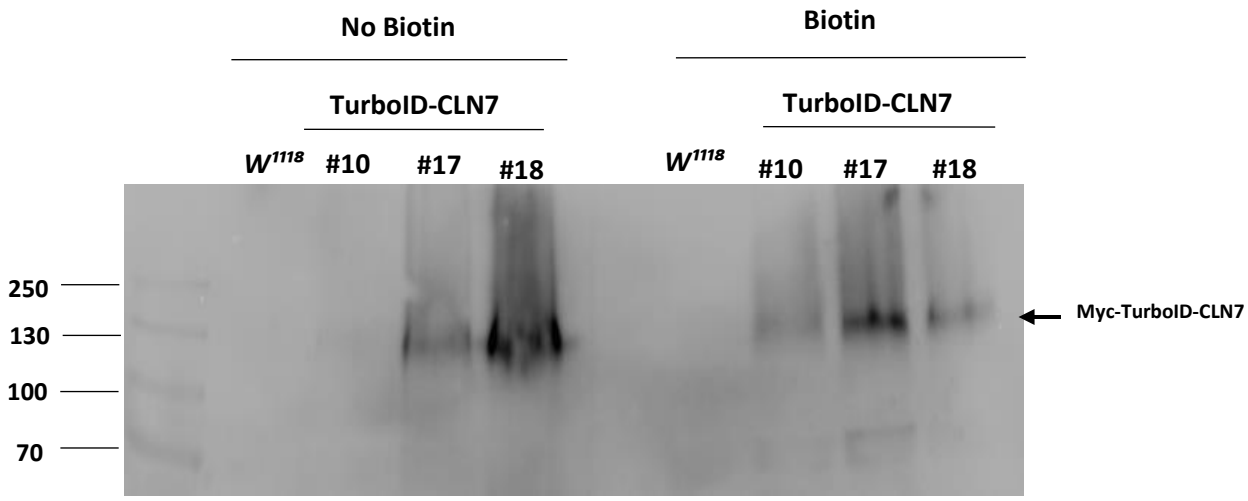

Figure 4. 7: Detection of myc-TurboID-CLN7 in *Drosophila* larvae by WB.

Western blotting experiment was done to detect TurboID-CLN7 expression in *Drosophila* larval. 10 % SDS-PAGE and 5 µl of proteins were loaded into the gel. Three independent lines of UAS-TurboID-CLN7 were crossed to Mef2-Gal4 used to drive expression in muscles then proteins extracted by lysis at third instar larval stage with and without biotin. w^{1118} was used as control larval. By using goat anti-myc (1:1000), a protein at the expected size of 130 kDa is detected in all lines but lines 17 and 18 show higher levels of expression.

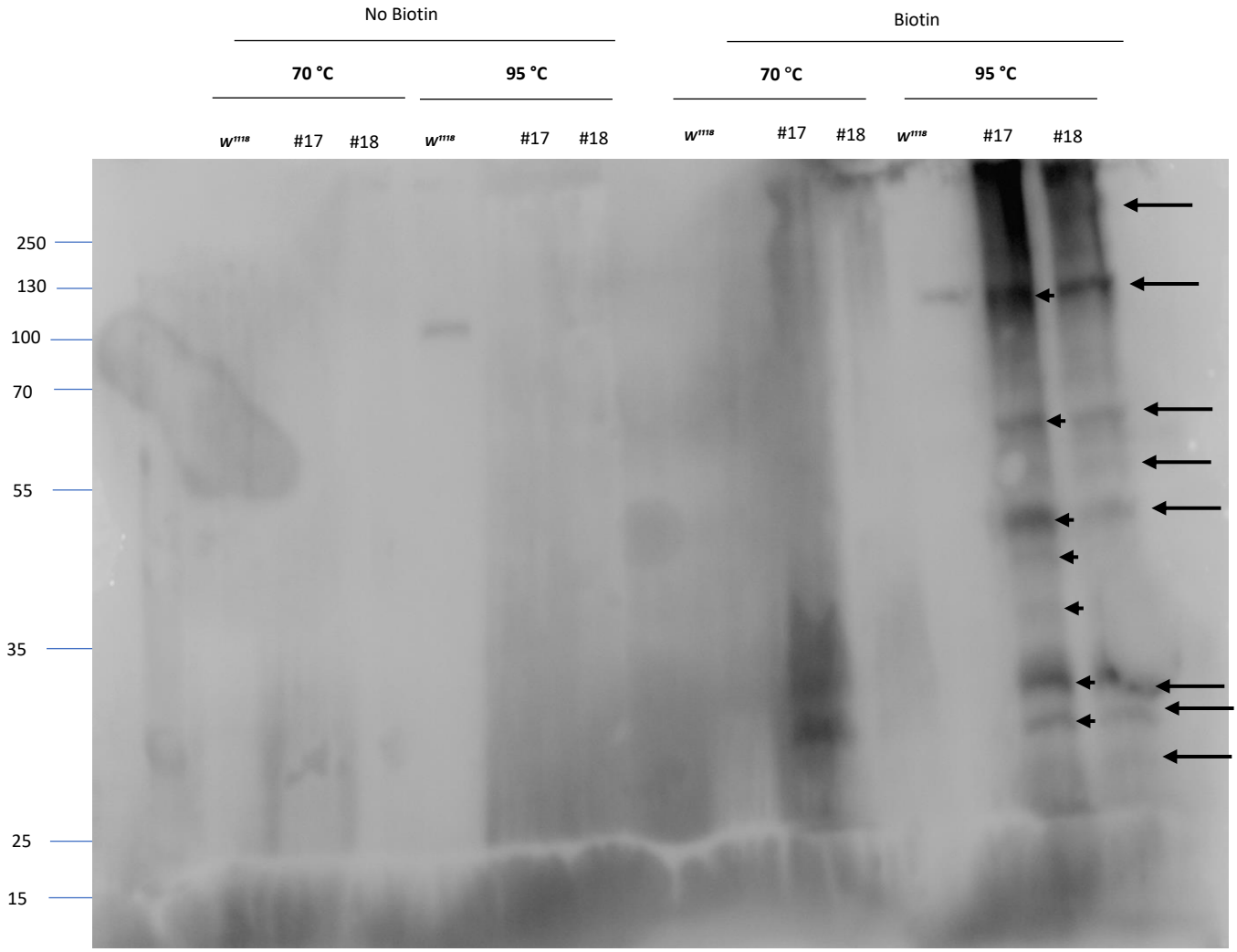

Figure 4. 8: Detection of biotinylated proteins by TurboID in *Drosophila* Larvae by WB.

5 µl proteins were loaded into 10 % SDS-PAGE gel to detect biotinylated proteins in *Drosophila* larvae for (-/+) biotin. A western blot of lysates from Mef2-Gal4 x UAS-Myc-TurboID-Cln7 larvae probed with streptavidin-HRP (1:5000) to identify biotinylated proteins. Biotinylated protein bands are detected from larvae developed in food supplemented with biotin more than without biotin. Heating to 95 Cª is more perfect than 70 Cª. Biotinylated proteins are evident by arrows. w^{1118} flies used as a control.

4.2.3.2. Immunofluorescence.

To test whether the TurboID-Cln7 protein localises correctly to the post-synaptic density, expressing 3rd instar larvae were dissected, fixed and stained by Richard Tuxworth. Confocal microscopy indicated that the Myc-tagged TurboID-Cln7 protein was present in a vesicular compartment that overlapped with anti-discs large at the synapse (Figure 4. 9). This experiment highlighted that TurboID-CLN7 was correctly recruited to synapses at the NMJ as expected.

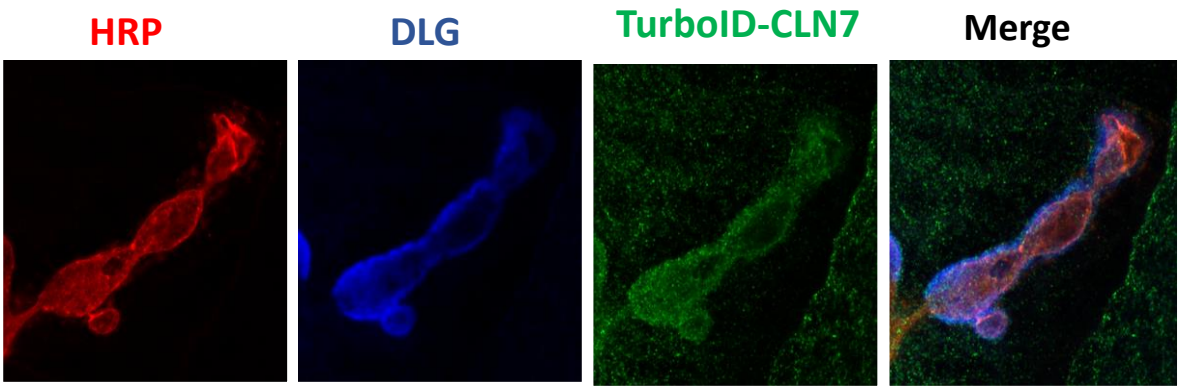

Figure 4. 9: Expression of TurboID-CLN7 into *Drosophila* larvae NMJ.

Confocal microscopy of third instar larval NMJ from Mef2-Gal4 x UAS-Myc-TurboID-Cln7 expressing flies. UAS-TurboID-CLN7 was transgenic in embryonic w^{1118} fly before crossing by Mef2-Gal4. Goat anti-HRP (red) highlights the neuronal plasma membrane and mouse anti-DLG (blue) the post-synaptic density. Rat anti-Myc (green) (1:1500) shows that Myc-TurboID-Cln7 overlaps with DLG in a vesicular pattern and in additional vesicles throughout the muscle cells.

4.2.4. Detection the TurboID-CLN7 expression in adult flies.

Proper results have been identified after the expression of TurboID-CLN7 in S2 cells and larval muscles, revealing numerous biotinylated protein bands in both samples. These bands are expected to represent many candidate interaction proteins. Consequently, it was interested to identify whether this technique would also label protein in adult flies.

To test for expression in adult flies, Mef2-Gal4 x UAS-Myc-TurboID-Cln7 flies were allowed to develop to adulthood and the visible dominant Hu marker carried by the balancer chromosome was used to select the correct genotypes.

Adult flies were transferred to food -/+ biotin for 3 days before lysates were made. After the lysis process, the eluates were heated to 70°C. Part of these elution samples was loaded to detect if their bands were in the correct positions. Meanwhile, the remaining elution samples were loaded, and streptavidin-HRP was added to the membrane to reveal the biotinylated proteins in flies.

A Western blot of lysates stained with Goat anti-Myc (1:1000) showed expression at 130 KDa for all the lines with or without biotin supplementation, indicating that the Mef2-Gal4 driver remains active in adult muscles (Figure 4. 10. A). Streptavidin-HRP (1:5000) also showed that the TurboID-CLN7 was able to label proteins when biotin was added to the food but not without biotin (Figure 4. 10. B).

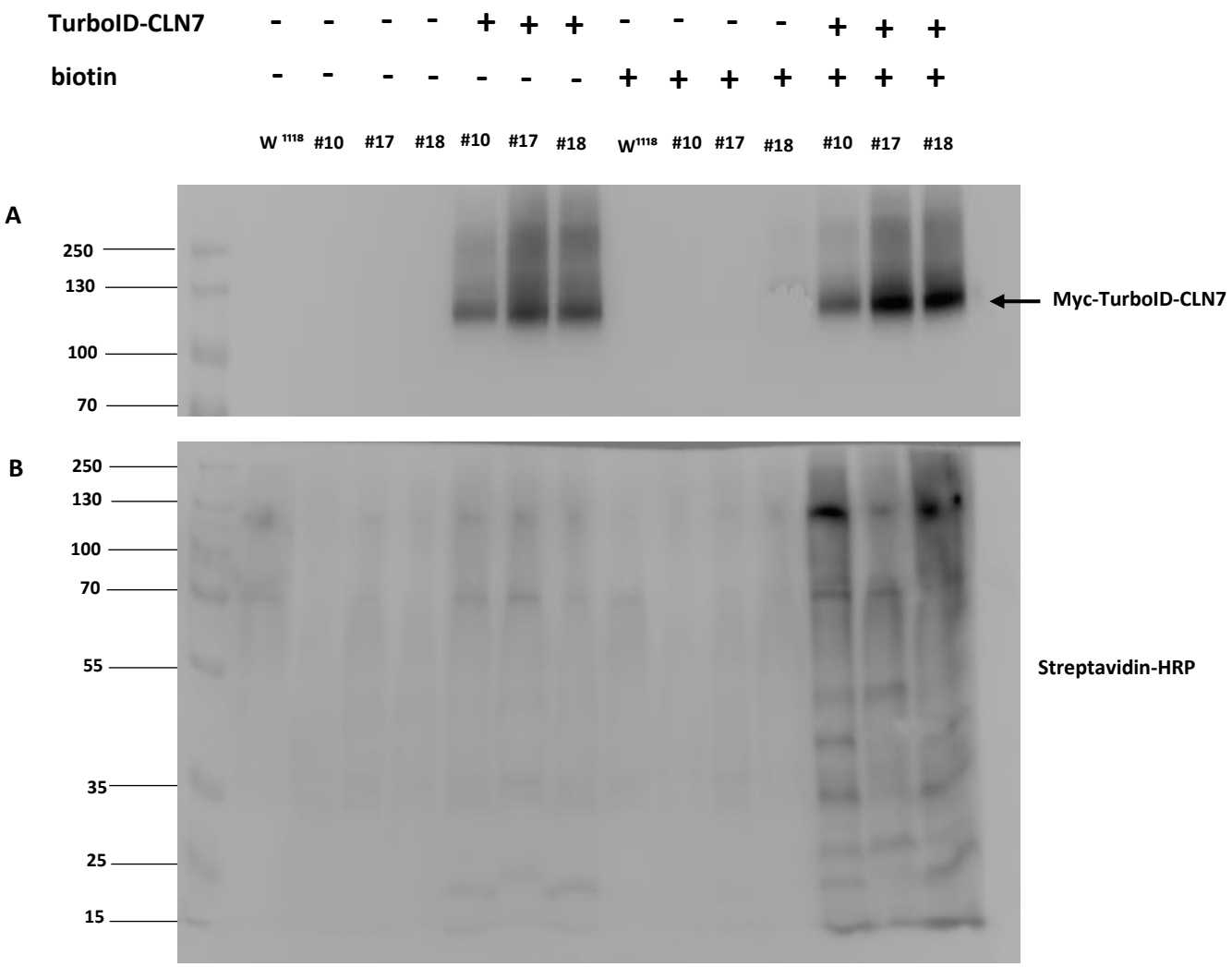

Figure 4. 10: Detection of myc-TurboID-CLN7 and biotinylated proteins in adult flies by WB.

Western blots of Mef2-Gal4 x UAS-MycTurbo-Cln7 expressing adult flies on food with or without biotin. 10 % SDS-PAGE gel was used and 5 µl proteins were loaded into the gel. Other humeral flies with no TurboID-CLN7 were used as a control and flies were fed (-/+) biotin. *W1118* adult fly used as a control and flies line numbers 10, 17 and 18 were used in this experiment. **(A)** Gout anti-myc (1:1000) detects expression of Myc-TurboID-CLN7 at the expected size. **(B)** Streptavidin-HRP (1:5000) was added into the membrane to identify biotinylated proteins. Labelling only occurs on flies fed food supplemented with biotin.

4.2.5. In vivo TurboID-CLN7 labelling.

Having achieved encouraging results with streptavidin-HRP, I wanted to identify which proteins were being labelled using mass spectrometry. Pull-down streptavidin experiments were performed for larval and adult flies using streptavidin-HRP beads.

Some flies (transgenic line number 18) were moved to food with 100 µM of biotin 3 days before the experiment. In the case of TurboID-CLN7 expression in flies, by adding Gout anti-myc (1:1000) the western blot trial demonstrated the myc-TurboID-CLN7 band in the right place at 130 KDa with and without biotin (Figure 4. 11. A). In addition, by adding Streptavidin-HRP (1:5000) to the membrane, TurboID-CLN7 shown labelled several proteins even with or without biotin (Figure 4. 11. B). Therefore, Coomassie staining was added to the SDS-PAGE gel and several identical bands were detected for UAS-TurboID-CLN7 (Figure 4. 12). Therefore, the labelled proteins from TurboID-CLN7 were isolated from the staining gel and sent for Mass-spectrometry analysis.

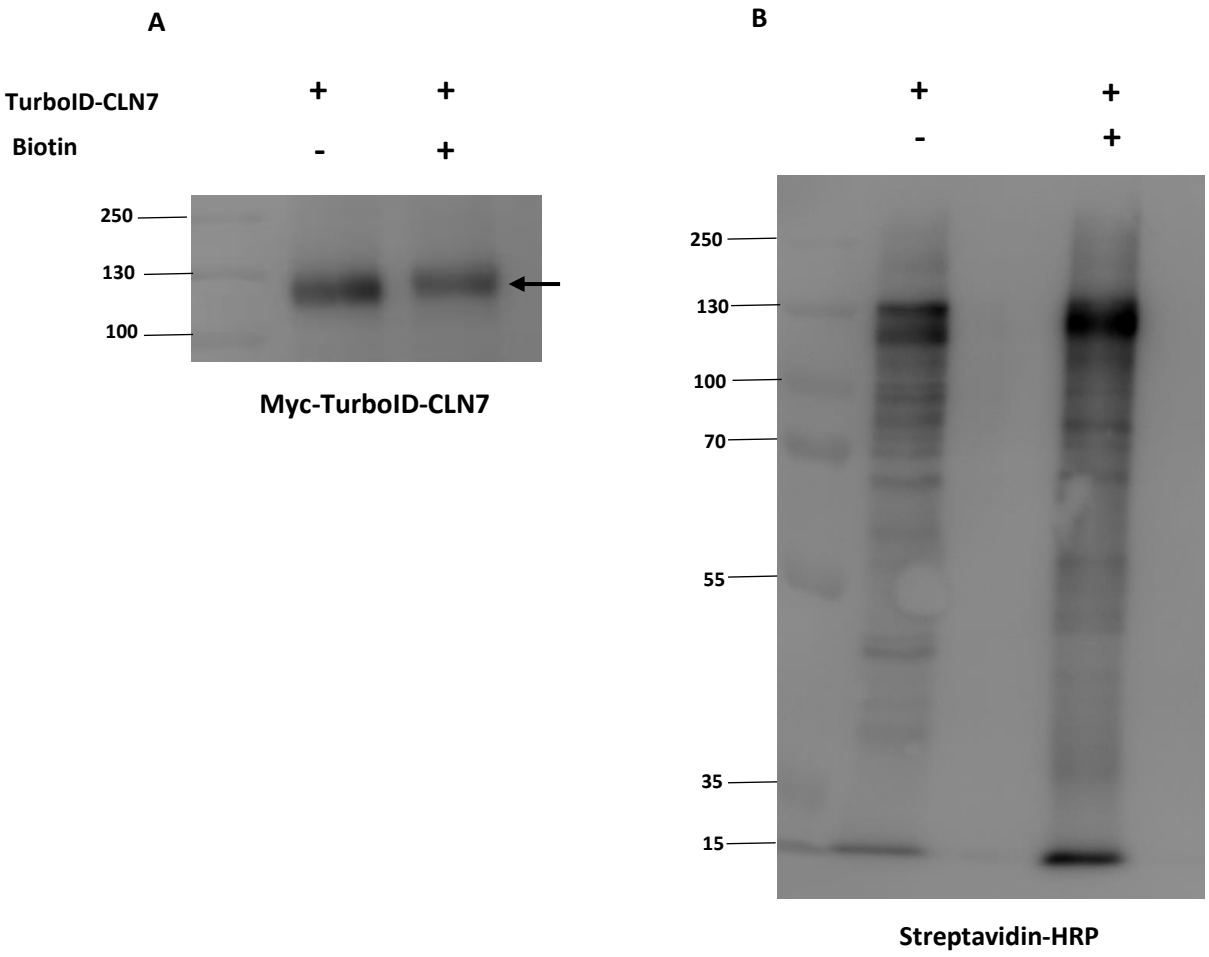

Figure 4. 11: In vivo labelling of TurboID-CLN7 from adult flies.

Western blotting analysis to test the PL in the flies. Mef2-Gal4 x UAS-MycTurbo-Cln7 expressing adult flies on food with or without biotin. 10 % SDS-PAGE gel was used and 5 µl proteins were loaded into the gel. Flies were moved to the food with 100 µM of biotin 3 days before the experiment **(A)** Gout anti-myc (1:1000) indicates Myc-TurboID-CLN7 expression at the correct molecular weight. **(B)** HRP-streptavidin (1:5000) shows biotinylated proteins extracted by streptavidin bead pulldown. Labelling is seen both with and without biotin addition to the food. Line number 18 used in this experiment.

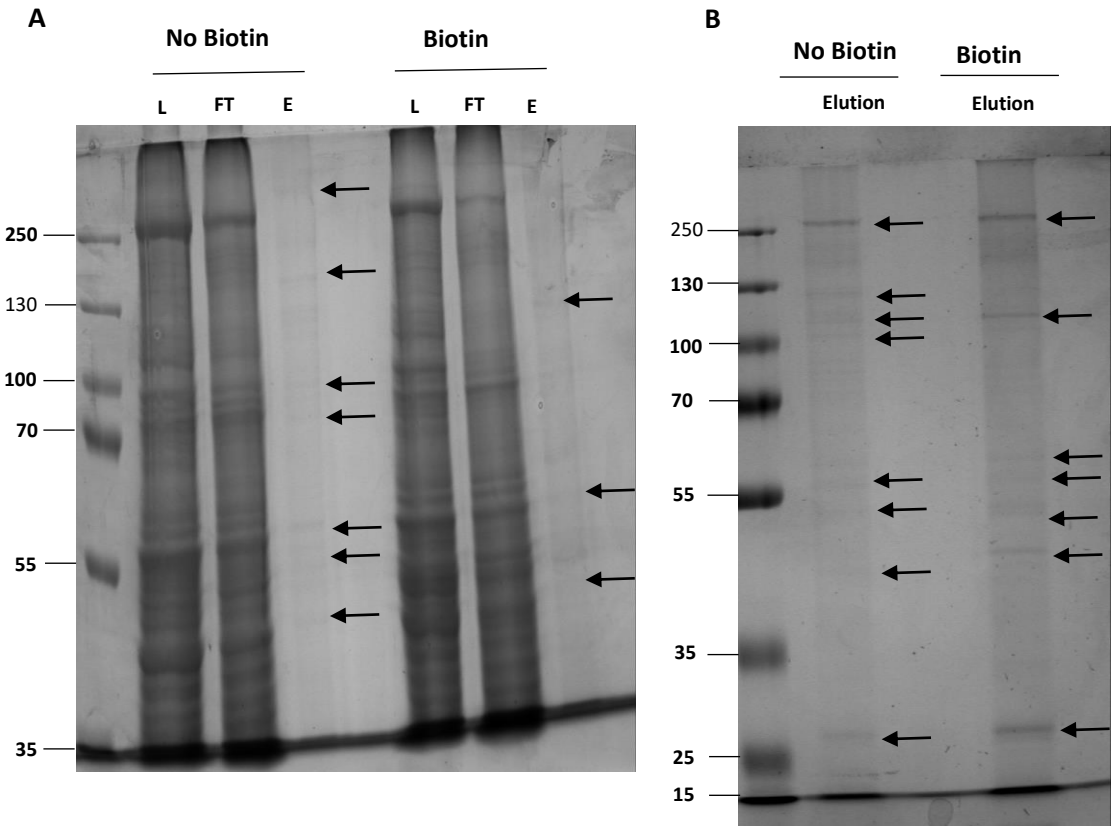

Figure 4. 12: In vivo labelling of TurboID-Cln7 expressing adult flies (Coomassie stain).

10 % SDS-PAGE gel was used and 5 µl and 10 µl of proteins were loaded into the gel. Coomassie staining of samples from streptavidin bead pulldown from Mef2-Gal4 x UAS-Myc-TurboID-Cln7 expressing adult flies on food -/+ biotin supplement. **(A)** 5 µl of proteins were loaded into the gel. Lysate (L), flow-through (FT) and eluate (E). (**B)** is repeated experiment, but 10 µl proteins were loaded into the gel. The identified biotinylated proteins detected and shown by arrows. Line number 18 used in this experiment.

4.2.6. Extraction of biotinylated proteins from TurboID-CLN7 expression larval.

The same streptavidin-pull-down experiments were done to identify the biotinylated proteins from the TurboID-CLN7 expression larval. Adding anti-myc (1:1000) demonstrated the bands for myc-TurboID-CLN7 in the right places and size in elution samples (Figure 4. 13. A). Moreover, it was shown that with TurboID-CLN7 expression, several biotinylated proteins were identified (Figure 4. 13. B)

To identify the identical bands of biotinylated proteins by TurboID, Coomassie stain was used in this case. In addition, Tubby larval were used as a control in addition to UAS-TurboID-CLN7 larval. After staining the gel with Coomassie, identical bands of TurboID-CLN7 eluates were detected with or without biotin (Figure 4. 14). Consequently, the gel slices of identical bands of UAS-TurboID-CLN7 in addition to the bands of tubby larval were extracted as a control and sent for MS analysis.

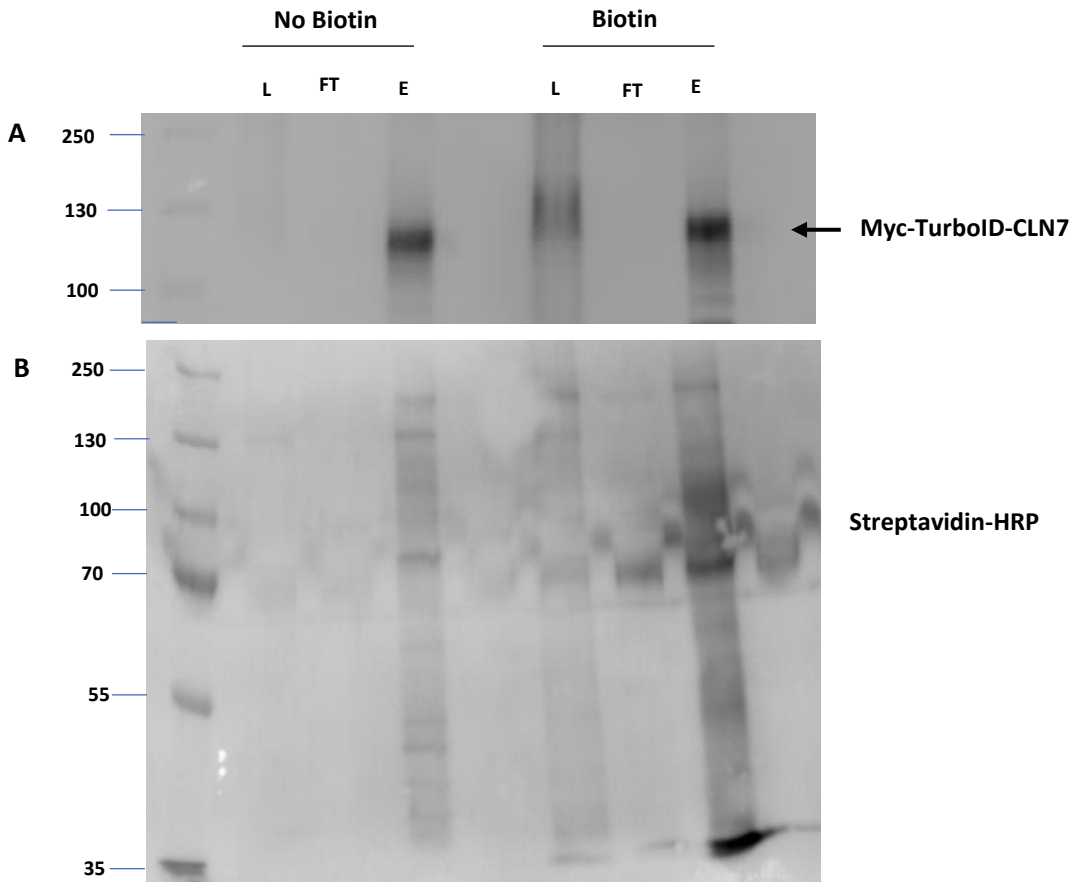

Figure 4. 13: In vivo labelling of TurboID-CLN7 from *Drosophila* larvae.

10% SDS-PAGE gel was used and 10 µl of proteins were loaded into the gel. Western blot of lysates from 3rd instar larva from Mef2-Gal4 x UAS-Myc-TurboID-Cln7 expressing flies line number 18. **(A)** Gout anti-myc (1:1000) was used to detect the expression of Myc-TurboID-CLN7 and the bands were detected in the right places for both (-/+) biotin. **(B)** Streptavidin-HRP (1:5000) reveals biotinylated proteins. Staining is more intense in flies developed on food supplemented with biotin. Lysates (L), flow-through (FT), and eluates (E).

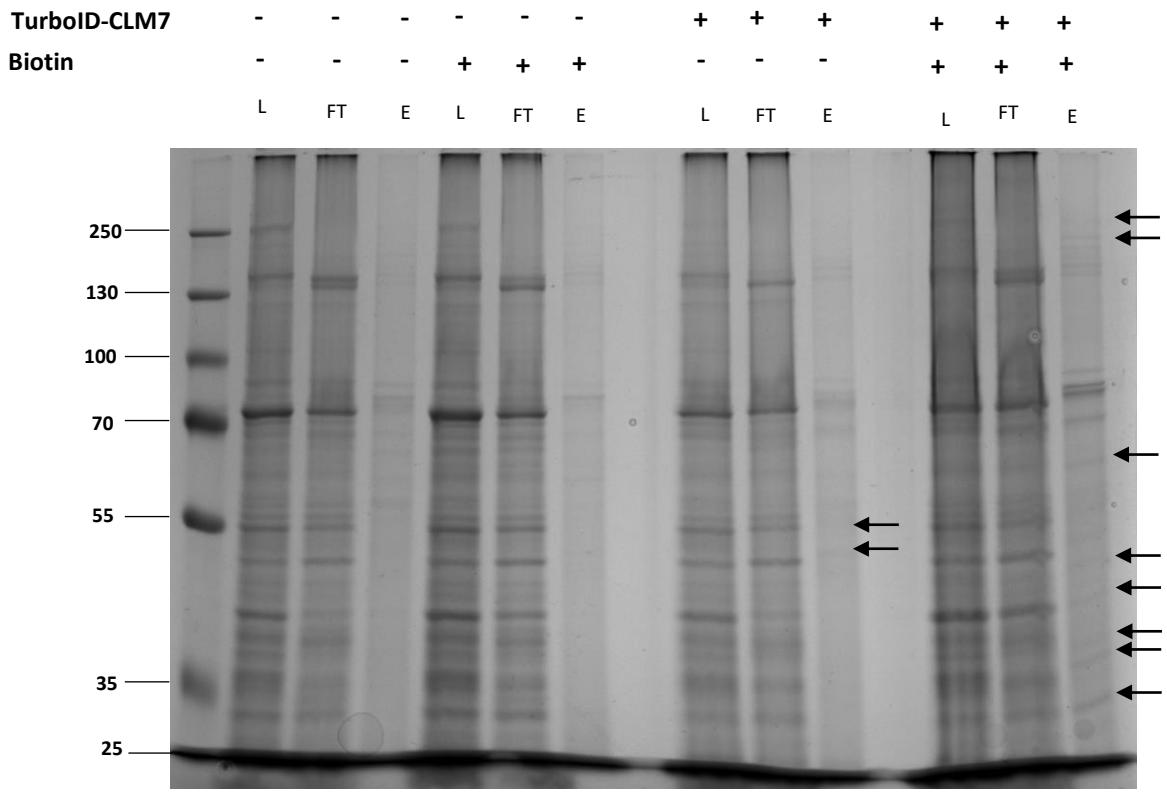

Figure 4. 14: In vivo labelling of TurboID-CLN7 from *Drosophila* larval (Coomassie stain).

10 % SDS-PAGE gel used and 20 µl of proteins were loaded to the gel. Western blot stained with Coomassie from lysates (L), flow-through (FT), and eluates (E) of larval samples. Tubby larval were used as a control and all larval were fed in (-/+) biotin food. The arrows shown unique bands from the Myc-TurboID-CLN7-expressing flies not found from control flies which inherited the balancer.

4.2.7. MS analysis of TurboID-CLN7.

The experiment was repeated twice more and four samples of TurboID-CLN7 gel slices related to larval were sent for MS analysis, in addition to one sample of tubby larval as a control to identify TurboID-CLN7 labelling proteins. Two of the gel slices were with biotin and two samples were without biotin. For the TurboID-CLN7 larval results there were 865 identified proteins consisting of 216 proteins ≥ 5 peptide spectrum matches (PSMs), 200 proteins ≥ 5 peptides and 190 proteins have ≥ 5 unique peptides. Numerous identified proteins were found in more than one sample. Both TurboID-CLN7 and the Tubby negative control shared frequently hit proteins because of the binding of some proteins to streptavidin beads or because endogenously biotinylated proteins could be identified in both samples. By concentrating on the identified proteins with ≥ 5 PSMs both samples shared multi proteins, and each sample had its unique proteins. There were 442 candidate proteins found in the Tubby larval and the number is probably very high because of the size of the gel slice taken for MS analysis. In this sample 128 proteins ≥ 5 PSMs and 112 proteins ≥ 5 peptides.

In the first experiment, two gel slices were sent for MS analysis. The first sample was related to Tubby larval and was used as a control for TurboID-CLN7. In the second sample, TurboID-CLN7 expression in larval (Figure 4. 15).

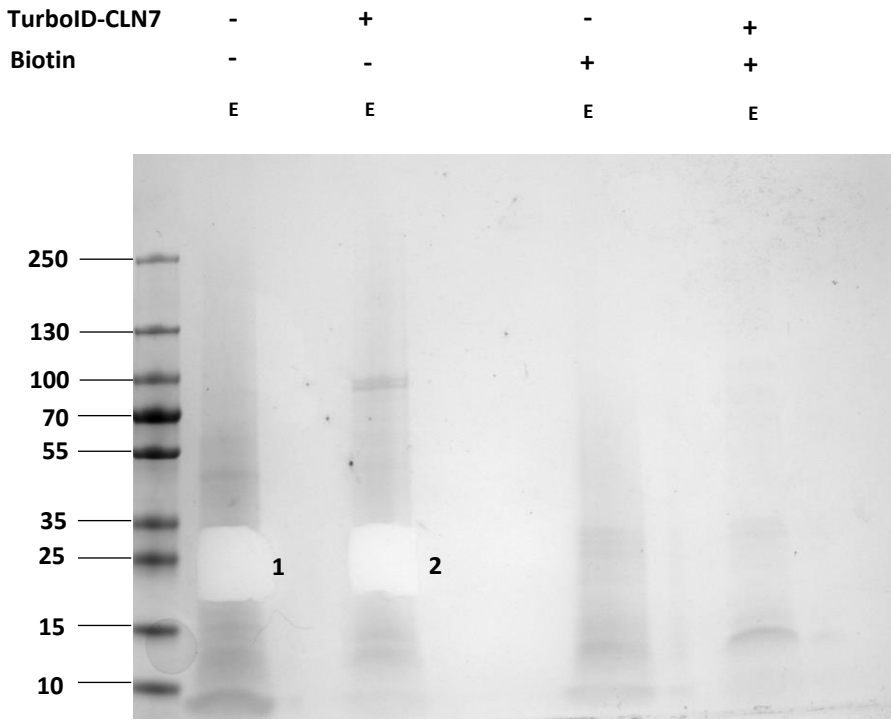

Figure 4. 15: In vivo labelling of TurboID-CLN7 from *Drosophila* larval (Coomassie stain).

Western blotting experiment done for Mef2-UAS x muc-TurboID-CLN7 *Drosophila* larval. 10% SDS-PAGE gel used and 20 µl of proteins were loaded into the gel and Coomassie staining added to the gel. Tubby larval used as a control and both types of larval fed in (-/+) biotin food. Coomassie-stained SDS-PAGE gel of proximity-labelled proteins extracted from control (1) and TurboID-Cln7-expressing larvae (2) and send for mass spectrometry.

The third repeat identified 352 uncontaminated proteins with 114 proteins ≥ 5 peptides and 119 proteins ≥ 5 PSMs from one gel slice; 39 uncontaminated proteins with 10 proteins ≥ 5 peptides and 11 ≥ PSMs from a second slice; and 32 uncontaminated proteins were found and there were 6 proteins ≥ 5 peptides and 7 ≥ PSMs and coracle protein was identified in this sample (Figure 4. 16).

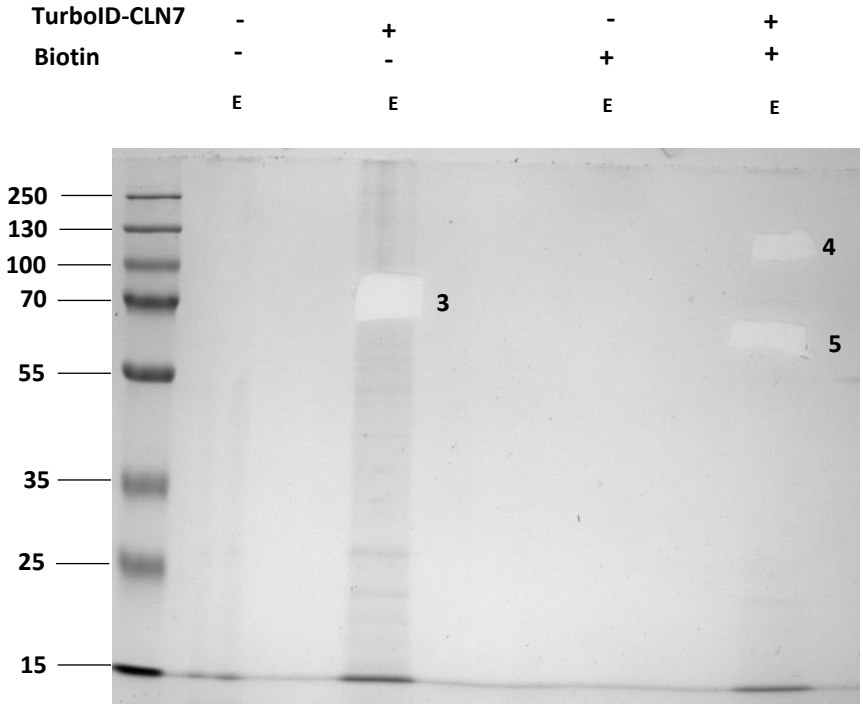

Figure 4. 16: In vivo labelling of TurboID-CLN7 from *Drosophila* larval (Coomassie stain).

Western blotting experiment done for Mef2-UAS x muc-TurboID-CLN7 *Drosophila* larval. 10% SDS-PAGE gel used and 20 µl of proteins were loaded into the gel and Coomassie staining added to the gel. Tubby larval used as a control and both types of larval fed in (-/+) biotin food. Coomassie-stained SDS-PAGE gel of TurboID-CLN7- expression larval without biotin (3) and TurboID-Cln7-expressing larvae with biotin (4) and (5) and send for mass spectrometry.

4. 2. 8. Potential interacting proteins after MS analysis.

Many hit proteins were identified after MS analysis in all the cellular components, and they are used in many cellular functions. By concentrating on protein with ≥ 3 peptides, many proteins were found in both TurboID-CLN7 expression and the control larvae (Table 4.1). Numerous proteins are located in the membrane in addition to other components in the particular cytoskeleton. Various proteins are found in other cellular parts such as cytosol, nucleus, cell projection and so on.

Table 4. 1: Hit proteins after MS analysis.

Protein	CG	Found in TurboID-CLN7 and control larval	Principle localization
Mhc (myosin heavy chain)	CG17927	✓	Cytoskeleton
Coracle	CG11949		Cytoskeleton, membrane, cell junction
Prm (Paramyosin)	CG5939	✓	Cytoskeleton
Moe (Moesin)	CG10701	✓	Cytoskeleton, membrane, cell junction, cell projection
Zasp52 (Z band alternatively spliced PDZ-motif protein 52)	CG30084	✓	Cytoskeleton, membrane, cell junction
Actn (α actinin)	CG4376		Cytoskeleton, membrane, cell junction
LamC (Lamin C)	CG10119	✓	Cytoskeleton, membrane
Bnk (bottleneck)	CG1480		Cytoskeleton
Ran	CG1404		Cytoskeleton
Shi (shibire)	CG18102		Cytoskeleton, membrane, synapse
Mlp84B (Muscle LIM protein at 84B)	CG1019	✓	Cytoskeleton
Dhc64C (Dynein heavy chain 64C)	CG7507		Cytoskeleton, cell projection
Gel (Gelsolin)	CG1106		Cytoskeleton
Up (upheld)	CG7107		Cytoskeleton
Cpa (capping protein alpha)	CG10540		Cytoskeleton, membrane, cell junction
Cpb (capping protein beta)	CG17158		Cytoskeleton, membrane
Rac1	CG2248		Cytoskeleton, membrane, cell projection
G (garnet)	CG10986		Membrane, synapse, cell projection
Rab8	CG8287	✓	Membrane, synapse
Rab5	CG3664	✓	Membrane, synapse
Mys (myospheroid)	CG1560		Membrane, cell junction, cell projection
Rab7	CG5915	✓	Membrane, synapse
Rab10	CG17060		Membrane, synapse
Rab14	CG4212		Synapse, endomembrane system
Fw (furrowed)	CG1500		Cell junction
Act42A (Actin 42A)	CG12051	✓	Nucleus, chromosome
SERCA (Sarco/endoplasmic reticulum Ca(2+)-ATPase)	CG3725	✓	Membrane
Apolpp (apolipophorin)	CG11064	✓	Extracellular region
ATPCL (ATP citrate lyase)	CG8322		Cytosol
GlyP (Glycogen phosphorylase)	CG7254	✓	Macromolecule complex, other cellular comp.
Bt (bent)	CG32019		Other cellular_ component
Sls (sallimus)	CG1915	✓	Nucleus
Vha68-2 (Vacuolar H^+ ATPase 68 kDa subunit 2)	CG3762	✓	Membrane
mAcon1 (Mitochondrial aconitase)	CG9244		Cytosol, mitochondria
Chc (Clathrin heavy chain)	CG9012	✓	Membrane
Hsc70-3 (Heat shock protein 70 cognate 3)	CG4147		Membrane
Sec23 (Secretory 23)	CG1250	✓	Membrane
sesB (stress-sensitive B)	CG16944	✓	Membrane
Acsl (Acyl-CoA synthetase long-chain)	CG8732		Membrane, cell projection
Neurochondrin	CG2330		Cell projection
ATPsyngamma (ATP synthase, γ subunit)	CG7610	✓	Membrane
Ank (Ankyrin)	CG1651		Membrane, cell projection
Blw (bellwether)	CG3612	✓	Membrane
Sec24CD (Secretory 24CD)	CG10882		Membrane
Pst (pastrel)	CG8588		Cytosol
Rab1	CG3320	✓	Membrane
PMCA (plasma membrane calcium ATPase)	CG42314		Membrane
ND-20 (NADH dehydrogenase 20 KDa subunit)	CG9172		Membrane
Surf4 (Surfeit 4)	CG6202	✓	Membrane
Nup358 (Nucleoporin 358kD)	CG11856		Membrane
Argk (Arginine kinase 1)	CG32031	✓	Membrane
Porin	CG6647	✓	Membrane
UQCR-C2 (Ubiquinol-cytochrome c reductase core protein 2)	CG4169	✓	Membrane
Vha68-2 (Vacuolar H^+ ATPase 68 kDa subunit 2)	CG3762		Membrane
Kr-h2 (Kruppel homolog 2)	CG9159	✓	Membrane
Ostgamma (Oligosaccharide transferase γ subunit)	CG7830		Membrane
Hsc70-3 (Heat shock protein 70 cognate 3)	CG4147	✓	Membrane
Surf4 (Surfeit 4)	CG6202		Membrane
Mpcp2 (Mitochondrial phosphate carrier protein 2)	CG4994		Membrane
rho-5 (rhomboid-5)	CG33304		Membrane
VhaSFD (Vacuolar H^+-ATPase SFD subunit)	CG17332	✓	Membrane
Sec61alpha (Sec61 α subunit)	CG9539		Membrane
Eglp4 (Entomoglyceroporin 4)	CG4019		Membrane
Cyt-c1 (Cytochrome c1)	CG4769		Membrane
SsRbeta (Signal sequence receptor β)	CG5474		Membrane
Sec23 (Secretory 23)	CG1250		Membrane
Spidey	CG1444	✓	Endomembrane system

4.2.9. The unique TurboID-CLn7 hit proteins.

By eliminating the control proteins from Table 4.1, the unique TurboID-CLN7 hit proteins were classified in Table 4.2. These important proteins are located in the cytoskeleton, synapse, cell junction, membrane, and other components. As can be seen in Table 4.2, several proteins are spread across many cellular components. Most proteins were found in sample 2 (Figure 4. 16), followed by sample 3. Additionally, several proteins were repeated in more than one sample and in both independent experiments. The number of peptide is related to the sample number respectively in the table 4.2.

Table 4. 2: The unique TurboID-CLN7 hit proteins in *Drosophila* larval.

Protein	MW	CG	No. of sample	No. of peptide	Repeated identically	Principle localization
Coracle	184 KDa	CG11949	5, 3	2, 33	1 independent experiment	Cytoskeleton, membrane, cell junction
Actn (α actinin)	107 KDa	CG4376	3	7	1	Cytoskeleton, membrane, cell junction
Bnk (bottleneck)	35.5	CG1480	3	1	1	Cytoskeleton
Ran	25 KDa	CG1404	3,2	4,9	2 independent experiment2	Cytoskeleton
Shi (shibire)	100 KDa	CG18102	3	3	1	Cytoskeleton, membrane, synapse
Dhc64C (Dynein heavy chain 64C)	532 KDa	CG7507	3	2	1	Cytoskeleton, cell projection
Gel (Gelsolin)	88 KDa	CG1106	2	5	1	Cytoskeleton
Up (upheld)	47.5 KDa	CG7107	2	4	1	Cytoskeleton
Cpa (capping protein alpha)	32 KDa	CG10540	2	2	1	Cytoskeleton, membrane, cell junction
Cpb (capping protein beta)	31.3 KDa	CG17158	2	2	1	Cytoskeleton, membrane
Rac1	21.3 KDa	CG2248	2	2	1	Cytoskeleton, membrane, cell projection
G (garnet)	115 KDa	CG10986	3	3	1	Membrane, synapse, cell projection
Mys (myospheroid)	92.6 KDa	CG1560	3	2	1	Membrane, cell junction, cell projection
(Na+K+ATPase)	115.5 KDa	CG5670	3	6	1	Membrane, cell periphery, cell junction
Rab10	23 KDa	CG17060	3,2	3,4	2	Membrane, synapse
Rab14	107.5 KDa	CG4212	2	2	1	Synapse, endomembrane system
Fw (furrowed)	107.5 KDa	CG1500	2	2	1	Cell junction
ATPCL (ATP citrate lyase)	120 KDa	CG8322	4,3	4,15	1	Cytosol
Bt (bent)	999.5 KDa	CG32019	4,3	5,32	1	Other cellular_ component
mAcon1 (Mitochondrial aconitase)	85	CG9244	3	18	1	Cytosol, mitochondria
Hsc70-3 (Heat shock protein 70 cognate 3)	72 KDa	CG4147	3.2	13,5	2	Membrane
Acsl (Acyl-CoA synthetase long-chain)	82 KDa	CG8732	3	12	1	Membrane, cell projection
Neurochondrin	81.6 KDa	CG2330	3	11	1	Cell projection
Ank (Ankyrin)	170 KDa	CG1651	3	8	1	Membrane, cell projection
Sec24CD (Secretory 24CD)	134 KDa	CG10882	3	7	1	Membrane
Pst (pastrel)	77.4 KDa	CG8588	3	5	1	Cytosol
PMCA (plasma membrane calcium ATPase)	138.6 KDa	CG42314	3	4	1	Membrane
ND-20 (NADH dehydrogenase 20 KDa subunit)	25 KDa	CG9172	3	3	1	Membrane
Nup358 (Nucleoporin 358kD)	299 KDa	CG11856	3	3	1	Membrane
Vha68-2 (Vacuolar H^+ ATPase 68 kDa subunit 2)	68	CG3762	3,2	19,9	2	Membrane
Ostgamma (Oligosaccharide transferase γ subunit)	37 KDa	CG7830	2	5	1	Membrane
Surf4 (Surfeit 4)	30.5 KDa	CG6202	3,2	3,6	2	Membrane
Mpcp2 (Mitochondrial phosphate carrier protein 2)	39 KDa	CG4994	2	4	1	Membrane
rho-5 (rhomboid-5)	52.4 KDa	CG33304	2	4	1	Membrane
Sec61alpha (Sec61 α subunit)	52 KDa	CG9539	2	4	1	Membrane
Eglp4 (Entomoglyceroporin 4)	32.4 KDa	CG4019	2	3	1	Membrane
Cyt-c1 (Cytochrome c1)	33.7 KDa	CG4769	2	3	1	Membrane
SsRbeta (Signal sequence receptor β)	21 KDa	CG5474	2	3	1	Membrane
Sec23 (Secretory 23)	87.5 KDa	CG1250	3,2	13,3	2	Membrane
Pyk	57 KDa	CG7070	3,2	12,17	2	Cytosol

4. 2. 10. Gene enrichment analysis

4. 2. 10. 1. TurboID-CLN7 hit proteins network

To investigate potential links between the TurboID-CLN7 hit proteins, the STRING database of known and predicted protein-protein interactions was queried with the list of hits. STRING lists direct (physical) or indirect (functional) associations (Figure 4. 17). Moreover, the predicted functional associations are represented by edges that are drawn with up to seven colored lines. Several proteins had colored nodes, but they were not connected to other proteins. A coloured node indicates to the query proteins and first shell of interaction. In general, according to the STRING analysis tool, there were 40 nodes and 73 edges. The data indicated that the network has significant interactions between proteins. CLN7 was included in this network (CG8596 node), but its node was not linked with any of those proteins, perhaps due to the lack of information related to CLN7 protein interactions in the STRING analysis tool. Coracle was shown connected to alpha integrin-beta and Na+K+ ATPase. Rab10 and rab14 were connected with each other by several linkages. Actin (alpha-actinin) which is localized in the cytoskeleton, membrane and cell junction was connected with most of the proteins in that network including integrin-beta protein. Na+K+ ATPase (Atpalpah) was strongly connected with two proteins vha68-2 and plasma membrane calcium ATPase (PMCA). Alpha integrin was shown to have a strong connection with actin and Ras-related protein (Rac1). It was connected with Coracle, Fw and Bt. All these proteins have essential functions, and they are linked with each other in this tool, indicating significant interactions. The interaction of CLN7 with several of them is strongly possible. The important point here is how CLN7 regulates their functions, which needs further studies.

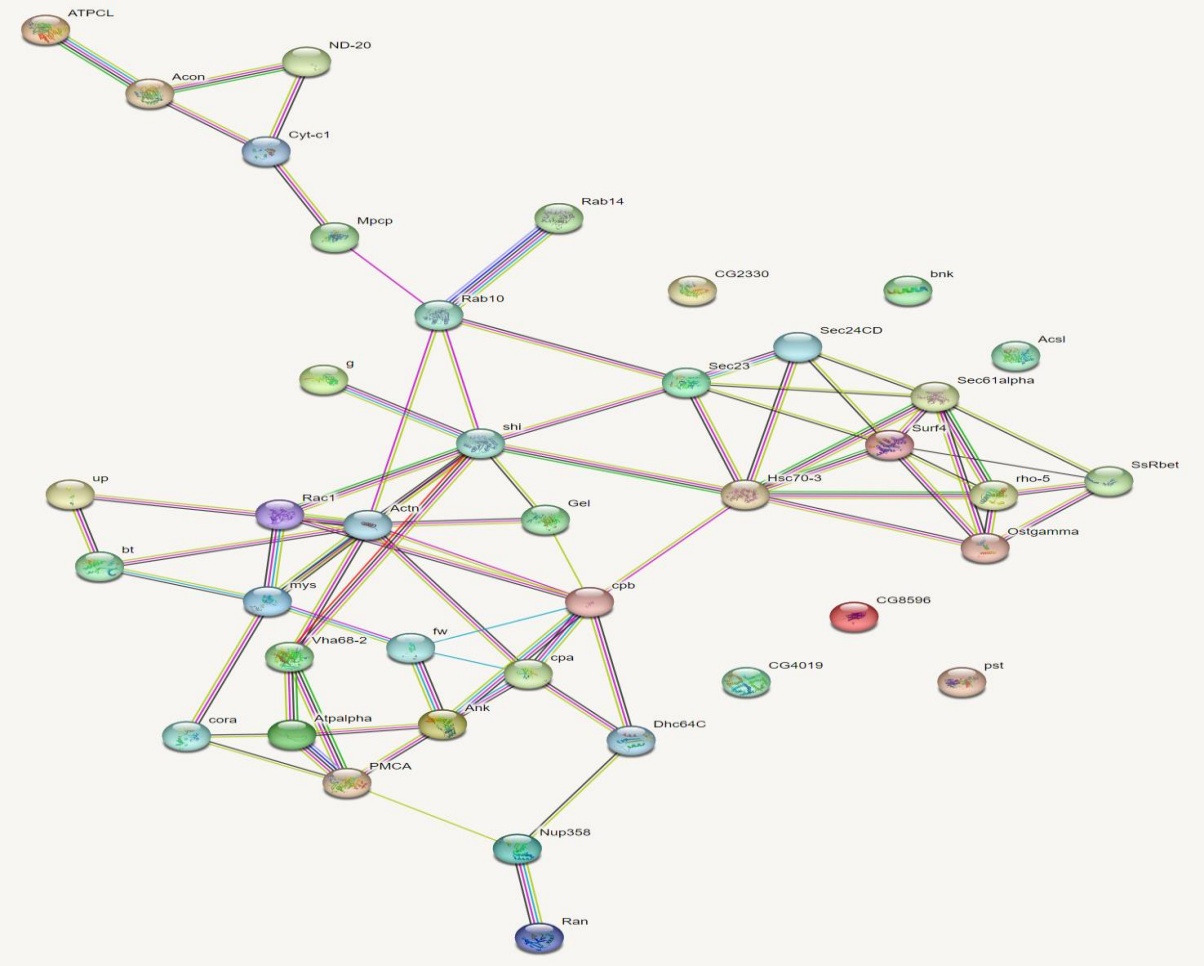

Figure 4. 17: The network of TurboID-CLN7 potential interacting proteins.

STRING analysis tool used to analyse TurboID-CLN7 potential interacting proteins to identify the protein-protein interaction networks. The coloured nodes represent query proteins and the first shell of interaction, while the white nodes mention the second shell interaction. There are no empty nodes which indicate to the proteins of unknown 3D structure, while filled nodes indicate that the 3D structure is known or predicted. CLN7 is shown as CG8596 in the network.

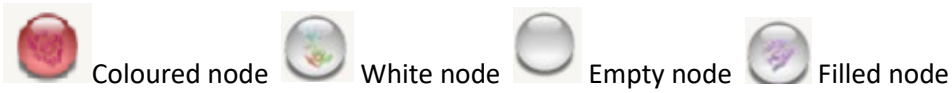

Edges linked between proteins are different depending on their colours down:

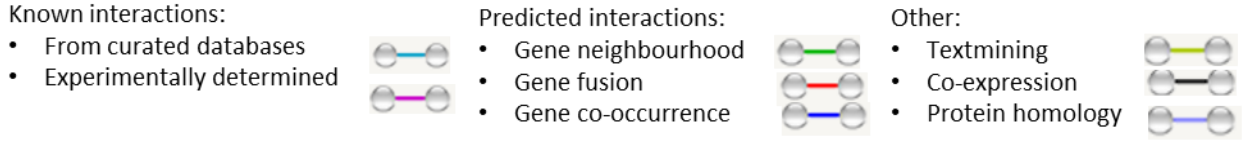

4. 2. 10. 2. Functional enrichment analysis in the network

The STRING analysis tool network was used to run functional enrichment analysis for Gene Ontologies (GO), including the terms GO biological process, GO molecular function, and GO cellular component.

The potential CLN7 interacting proteins contribute to several GO molecular functions. Six proteins can work in actin binding and eight proteins were recorded in cytoskeleton protein binding. For GTPase activity there were five proteins related to GTP binding. In the anion binding function, there were 14 proteins and 18 for ion binding (Table 4. 3).

For the cellular component GO, cytoskeletal component was found in ten proteins in that network, while synapse was noted in six proteins and plasma membrane in 13 proteins. Membrane was identified as a GO term for 26 proteins (Table 4. 3).

Table 4. 3: Functional enrichment analysis

GO category	GO organization	Protein
GO molecular function	Actin binding	Shi, gel, actin, cba, cbp and cora.
	Cytoskeleton protein binding	Cora, ank, cpa, cpb, gel, actn, shi and up.
	GTPase activity	Ran, rac1, shi, rad10 and rad14.
	GTP binding	Ran, rac1, shi, rad10 and rad14.
	anion binding function	Ran, PMCA, atpalph, Dhc64C, vha68-2, bt, rac1, gel, Hsc70-3, shi, bnk, rad10, rad14 and ATPCL.
	Ion binding	Ran, PMCA, atpalph, Dhc64C, vha68-2, bt, up gel, actn, rac1, Hsc70-3, shi, rad10, rad14, bnk, sec24CD, sec32 and ATPCL.
GO cellular component	Cytoskeleton	Cora, ran, Dhc64C, cpa, cpb, gel, rac1, up, shi and bnk.
	Synapse	Mys, Cln7, shi, g, rab10 and rab14.
	Cell junction	Cora, atpalpha, fw, Cln7, mys, actn, shi, g, rad10 and rad14.
	plasma membrane	Cln7, cora, PMCA, atpalpha, ank, cpa, vha68-2, mys, rac1, shi, acsl, rad10 and eglp4.
	Membrane	Cln7, eglp4, nup358, PMCA, cora, atpalpha, ank, cpa, vha68-2, mys, rac1, shi, hsc70-3, ostgamma, rho-5, SsRebt, surf4, sec61alpha, acsl, sec23, g, rab10, mpcp, cyt-c1 and ND-20.
GO Biological process	Cytoskeleton organization	Cora, ran, mys, dhc64C, cpa, cpb, bt, up, rac1, actn, gel, shi and bnk,
	CNS development	Nup358, cora, dhc64C, mys and rac1

4.3. Discussion

4.3.1. Development of Proximity Labelling TurboID

The aim for this chapter was to develop the proximity labelling TurboID technique and apply it *in vivo* to identify potential CLN7-interacting proteins. TurboID overcomes some of the limitations of the original BioID, including more efficient catalytic activity and much more rapid labelling kinetics, which make it more suitable for in vivo use. Additionally, TurboID achieves 3 to 6-fold more biotinylation than BioID and has a 10-fold lower requirement for biotin. When using low biotin concentration and shorter incubation time, TurboID achieves suitable labelling which BioID results in 18 hours.

TurboID-CLN7 and miniTurbo-CLN7 constructs were cloned and TurboID-Cln7 expressed in S2 cells for initial testing then transgenic flies were generated. TurboID-Cln7 was expressed in the muscles in larvae and adults and successful labelling was achieved. Mass spectrometry was used to identify labelled proteins from larvae. Validation of interactions by, for example, SMALP-mediated lysis followed by co-immunoprecipitation as used for the S2 cell experiments, remains outstanding.

4.3.2. Comparison between BioID and TurboID MS results.

By comparing with BioID-CLN7 hit proteins, several differences were observed between BioID and TurboID MS results. This may be because the current samples related to larvae, as the proteins were found more in larvae than in S2 cells. The number of samples in the case of BioID-CLN7 was 17, while in TurboID-CLN7 only 4 in TurboID-CLN7 sent for MS, but there were more identical proteins in the 4 TurboID-CLN7 larval samples than in the 17 BioID-CLN7 S2 cells. In the case of BioID-CLN7, 388 proteins were identified, while in TurboID-CLN7

865 proteins were found. With BioID-CLN7, BioID was the control used to distinguish the identical bands and proteins of BioID-CLN7, while tubby larvae sample was used as a control with TurboID-CLN7. However, in the case of BioID hit proteins, several proteins related to the cytoskeleton and glia were identified, while many proteins related to cytoskeleton post-synaptic density proteins were found in of TurboID hit proteins, one of them was coracle which was identified in two TurboID-CLN7 samples with and without biotin. Another protein was sodium/potassium subunit alpha in addition to Integrin-beta protein which was like BioID. However, the glial proteins that were identified in BioID-CLN7 including slit, formin-like and nirvana were not found in these samples possibly because few samples were analysed. Also, several proteins related to the cytoskeleton of NMJ which were found in BioID-CLN7 and were expected to be identified in TurboID-CLN7 samples were not found. Moreover, coracle was identified in two different samples one with biotin and another without biotin which strongly indicates the interaction of this protein with CLN7, this need to be confirmed with more experiments. Table 4. 4 includes a comparison between the most interesting BioID identified proteins and those found in TurboID.

Table 4. 4: Summary of interesting proteins found in BioID and TurboID.

NO	Protein name	Drosophila organ	BioID-CLN7 In cells	TurboID-CLN7 In flies
1	Coracle	NMJ cytoskeleton	✓	✓
2	Integrin beta PS	NMJ cytoskeleton	✓	✓
3	Integrin alpha PS1	NMJ cytoskeleton	✓	-
4	Na pump (alpha and beta subunit)	NMJ cytoskeleton	✓	✓
5	A-specrin	NMJ cytoskeleton	✓	-
6	Disc Large	NMJ cytoskeleton	✓	-
7	Lethal giant larvae	NMJ cytoskeleton	✓	-
8	Formin-like	Glial	✓	-
9	Slit	Glial	✓	-
10	Nirvana	Glial	✓	-

4.3.3. The most interesting hit proteins.

Applying proximity labelling TurboID-CLN7 in larval and adult flies was proper and the results were ideal as expected. With western blotting the adult flies demonstrated more and clearer results than the samples of larvae. This was clear in identical bands which were detected in the Coomassie gel results.

Even though numerous proteins were identified after MS analysis, only three most interesting cytoskeletal proteins were found like the BioID-CLN7, including coracle, Na+K+ ATPase and PS integrin beat (Table 4.2). PL work accurately in *Drosophila* larval and by analysing more samples other proteins will be identified. Furthermore, analysing adult *Drosophila* samples is strongly expected to yield more accurate results than analysing larvae samples. This expectation is based on the observation of clear bands in immunoblotting and the presence of multiple biotinylated protein bands in the streptavidin-HRP experiment. Additionally, when Coomassie stain is added to the gel, multiple bands are observed.

Coracle was identified in both experiments. It is a glial protein, a component of septate junctions and is required for synapse development. In the case of the coracle mutant, the glutamate receptors reduced from NMJ suggested that coracle is important for localization of NMJ glutamate receptors [177]. Coracle is one of the most important proteins related to cytoskeletal protein in NMJ which affects *Drosophila* glutamate receptors establishment in the postsynaptic actin cytoskeleton and the development of epithelial cells [177], and in addition to that it is a part of the septate junction structure [178]. CLN7 is a post-synaptic protein and also depending on the enrichment analysis (Table 4. 4) it is cell junction proteins suggesting it has an effect on the coracle and its function in NMJ, which can be tested by inducing a mutant in coracle or *Cln7*.

Another important protein related to the cytoskeleton NMJ is Na+K+ATPase (alpha and beta subunits) which is found in the cell membranes of neurons and other cells. It is involved in sodium and potassium ions transport through the plasma membrane, which creates an electrochemical gradient of sodium and potassium ions and makes energy for the active transport of several nutrients [179, 180]. From the STRING analysis of cellular components (Table 4. 3) Na+K+ATPaes belongs to cell junction category. CLN7 is a membrane protein, which suggests that the *Cln7* defect might disturb the action of sodium/ potassium transport.

For PS integrin-beta, the studies showed that it is enriched at the tip of a growing axon, which suggests it has a role in axon guidance [181], in addition, it contributes to endodermal integrity and adhesion between the midgut epithelium and the surrounding visceral muscle [181, 182]. the extracellular matrix and the intracellular cytoskeleton are connected by integrin transmembrane receptors [214]. Mys controls cellular adhesion, migration and survival [215]. From STRING analysis, the *mys* gene is localised in the synapse, cell junction and plasma membrane which strongly indicates the interaction with *Cln7*. in addition, it shares in cytoskeletal organisation and CNS development in the biological process GO (Table 4. 3). Based on the above, the interaction between integrin beta and CLN7 is strongly possible as both are cytoskeleton proteins which suggests a role for CLN7 in the connection of the extracellular matrix and the intracellular cytoskeleton and probably affect adhesion and migration through interaction with integrin beta. This needs to be confirmed with further experiments.

4.3.4. Validation of CLN7 proteins interaction.

Through the TurboID technique, many proteins were identified as strongly interacting with CLN7. However, validation of the interaction of CLN7 with the TurboID-CLN7 hit proteins is important to confirm the interaction, as PL conjugates the close-distance proteins and does not necessarily interact with a target protein. In addition, biotinylation of nonspecific proteins might occur with a long biotin treatment which leads to false positives. Furthermore, TurboID has higher activity and rapid proximity labelling which probably leads to nonspecific labelling in the PL process [213, 216]. Therefore, confirming the physical interactions of CLN7 with candidate proteins is important. Performing the TurboID labelling experiment in cells and identifying the candidate proteins, then applying that in flies, there is the possibility of repeating protein interaction with the target protein in both experiments. In addition, using immunoprecipitation in particular using SMALPs detergent is important to confirm the interaction of hit proteins. After that, testing the candidate proteins in *Cln7* mutation flies even with immunoblotting or immunofluorescence will highlight the effect of the absence of the *Cln7* function in the candidate interacting proteins and will confirm the exact interaction proteins.

5. IMPACT OF NUTRITION ON *DROSOPHILA* GROWTH AND DEVELOPMENT AND THE ROLE OF CLN7 IN THIS PROCESS

5.1. Introduction

In multicellular organisms, the combination of many genetic and environmental signals is important to regulate growth and one of those environmental signals is nutrient availability [217-219].

Nutrition plays an essential role in the growth and development of *Drosophila melanogaster* which determines their adult size, fecundity, and lifespan [220]. In addition, it is important to supply energy for body development and functioning. During food intake, nutrients are stored in the body as an energy source in case of starvation cases, and for activities that need more energy [221]. However, the performance of functions in the life stages may be affected by abnormalities in food intake during one life stage, which suggests a connection between adult biological functions and nutrient balance during developmental times [220, 222, 223]. Furthermore, nutrients are important for the body health including immune function, brain activity and digestion and absorption of food. Combining healthy nutrition with a healthy lifestyle at all ages prevents obesity and several metabolic diseases [224]. Body size is affected by larval nutrition, as many adult organs develop inside the larval body. When the larva eats, its body responds to the same signal that regulates body growth [221]. Observations have shown that nutrient restriction in larvae affects the metabolic status of mature adult flies. Additionally, higher fat levels in mature flies occur because of the reduction in using lipid stores during early adult stages of flies. Moreover, decreased

insulin signalling due to low nutrition in the larva leads to excess stored fat in adult flies [221].

The majority of adult fly structures, with the exception of the central nervous system, grow during the larval stage and take on their final shape during eclosion, the process by which the fly emerges from the pupal case [225].

The adult fly external structures develop from imaginal discs, histoblasts, and the imaginal ring. The clypeus and labrum develop from the clypeo-labral disc. The growth of the frons, eyes, and maxillary palps—the primary portion of the head—is aided by the eye-antennal disc [225]. The proboscis develops from the labial disc. The wing imaginal disc gives rise to the wing, notum, scutellum, and pleura. The prothoracic disc forms the prothorax, which supports the first leg. The haltere disc aids in the creation of the haltere, and the leg discs construct the legs. Histoblast nests that form as part of the embryonic epidermis give rise to the abdomen [225].

In terms of internal organs, imaginal rings that form during embryonic development give rise to the stomach, salivary glands, and trachea. Throughout adulthood, the larval Malpighian tubules persist. The imaginal discs' epithelial cells give rise to the adult muscles. Male and female genital discs and pole cells aid in the construction of the gonads, ovaries, and testes, while a nest of mesodermal follicle precursor cells forms the gonads, ovaries, and testes in females[225]. Controlling cell size and number leads to cell size regulation in developing multicellular organisms [226, 227].

The *Drosophila* life cycle has four morphologically distinct developmental stages: embryo, larva (which includes three instar stages), pupa and finally adult. The larval stage is followed by puparium formation, during which metamorphosis takes place over four days to form the

adult fly. All *Drosophila* growth occurs during the larval stages, with a remarkable increase in body mass. The final size of the adult is determined during the larval growth phase, and this is fixed when the larva enters metamorphosis [228, 229].

5. 1. 1. Insulin signalling pathway.

The insulin/insulin-like growth factor (IIS)/mechanistic Target of Rapamycin (mTOR) signalling pathway is a key regulator of growth in response to nutrition [230-232]. Insulin is a peptide hormone that plays important roles in regulating metabolic processes both at the cellular and systemic levels. The balance between lipid biosynthesis and breakdown is regulated by insulin signalling [233] and its defects lead to changes in growth, metabolism, fecundity and lifespan, as well as the stress response. The size and shape of the animal are determined by nutrition through the insulin/insulin-like growth factor (IIS)/Target of Rapamycin (TOR) signalling pathway. The IIS/TOR pathway controls growth in response to nutrition [230-232]. The deficiency of insulin in the fly leads to an increase in extracellular sugar, which may cause lipid storage by an insulin-independent mechanism [234, 235]. The lipid synthesis and breakdown are regulated by glucose and the peptide hormone insulin. In *Drosophila*, insulin signalling promotes fat storage in a cell-autonomous manner. It has been observed that triglyceride storage is stimulated in the *Drosophila* fat body by activating insulin signalling. Insulin signalling increases cell size and endoreplication in the larval fat body [234]. Higher lipid levels, greater tolerance to oxidative stress, and a longer lifespan are all indicators of reduced IIS activity in maturity [235]. The increase in lipid content is a shared feature in all long-lived II mutant flies. The function of IIS in the production and

storage of fat in the fat body of *Drosophila* is evolutionarily conserved because fat storage occurs primarily in this tissue [235].

In *Drosophila*, a high nutrition leads to the production of three insulin-like peptides (ILPs) in the CNS, including ILP2, ILP3 and ILP5 [230, 236, 237]. In the *Drosophila* central nervous system, neuroblast growth depends on local ILP production in the glia. In addition, tissue growth is continued via ILP6 secretion by the fat body when larvae stop feeding [230, 236, 237].

The IIS/TOR pathway controls *Drosophila* insulin-like peptides (DILPs) production in *Drosophila*. In the fat body, amino acid sensing in lysosomes regulates the recruitment of the TORC1 complex to the surface of the lysosomes where it is activated to regulate DILP synthesis and secretion in the insulin-producing cell (IPC). The IIS/TOR pathway has different effects on the growth of different organs, as in *Drosophila*, food intake regulates the size of the palps, wings, and legs in proportion to body size via IIS/TOR signalling activities. The DILPs probably link with the insulin-like receptor (InR) [230]. InR stimulates its substrate, chico, which recruits Dp110 (PI3 kinase) to the membrane through the protein p60 [238]. By Dp110, phosphatidylinositol-4,5-bisphophate (PIP2) is converted to PI-3,4,5-triphosphate (PIP3) [238-240]. The reverse – conversion of PIP3 to PIP2 is regulated by PTEN phosphatase [240].

Two nutrition sensitive pathways interact with the insulin pathway, the TOR and AMP-activated protein kinase (AMPK), to regulate growth. AMPK regulates *Drosophila* larvae growth and metabolism as this pathway senses energy levels by responding to the levels of intracellular adenosine nucleotide [230]. A rise in the AMP: ATP ratio in nutrient starved or stressed cells, triggers inhibition of the mTORC1 complex and inhibits cellular growth [241].

The nutritional input conveyed by the insulin/IGF and TOR signalling pathways is an important systemic signal [242]. Ligand linking to the insulin-like receptor plays an important role in recruitment and phosphorylation of the substrate of insulin receptor and activation of phosphoinositide 3-kinase (PI3K) and Akt [230]. TOR is activated by some extracellular signals such as amino acids, glucose and oxygen [243] (Figure 5. 1). However, an insulin receptor substrate is encoded by *Drosophila melanogaster* gene *chico*, however, *chico* is homologous to vertebrate insulin receptor substrate (IRS) [238, 244].

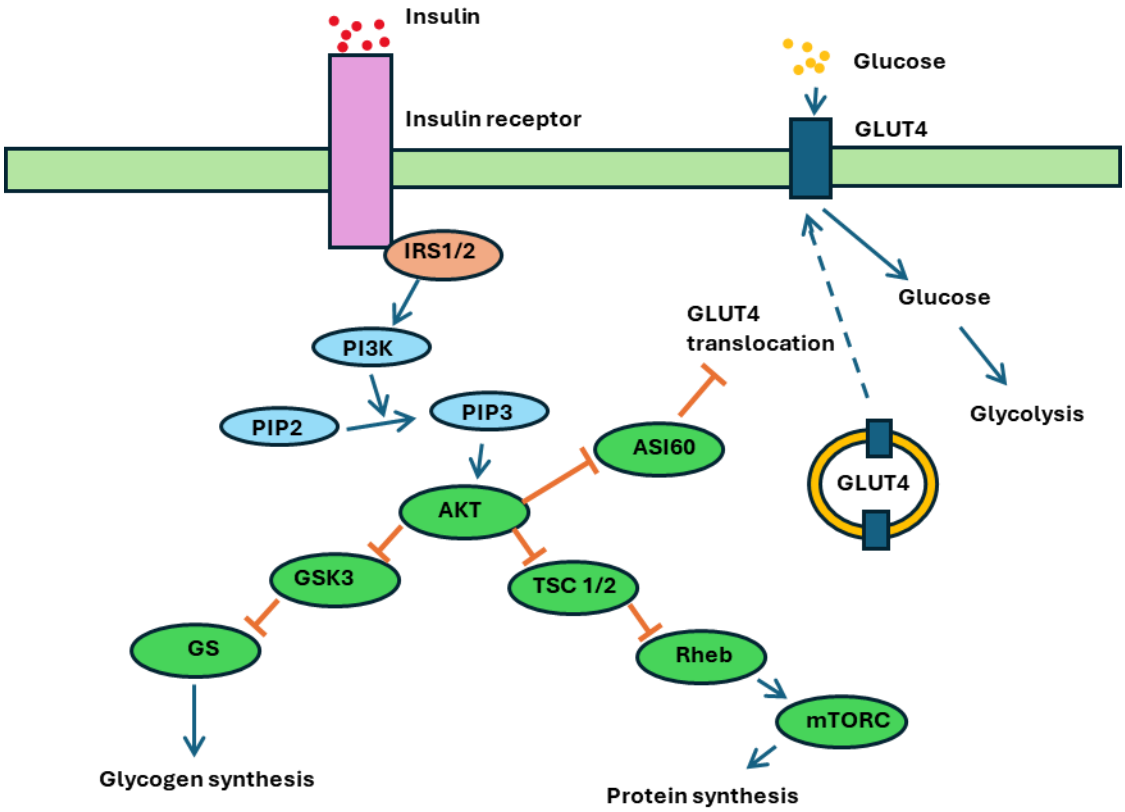

Figure 5. 1: The insulin signalling pathway.

The insulin signalling pathway starts with the binding of insulin to its receptor. This binding stimulates the association of the receptor with downstream mediators, including insulin receptor substrate-1 (IRS-1) (Chico in *Drosophila melanogaster*). The insulin receptor substrate activates PI3K directly by binding to the p85 regulatory subunit. PI3K stimulates the phosphorylation of PIP2, producing PIP3, which leads to the phosphorylation and activation of AKT. Subsequently, AKT phosphorylates GSK-3β and inhibits its activity, which activates glycogen synthase (GS) that regulates glycogen synthesis. AKT also inhibits AS160, leading to the translocation of GLUT4 to the cellular membrane. GLUT4 in the cell membrane facilitates glucose uptake into the cell, which is then converted to glycolysis in the presence of insulin. AKT activates mTORC, leading to protein synthesis and the regulation of autophagy and lipid synthesis.

5. 1. 2. mTOR signalling pathway

mTOR is an evolutionarily conserved serine/threonine protein kinase that regulates cellular growth and metabolism. It has two complexes, mTORC1 and mTORC2.The mTOR signalling pathway is crucial in cell growth, development, and ageing in response to changes in its surrounding environment. mTOR join signals initiate from changes in growth factors, energy status, nutrient and many physiological stresses. Therefore, mTOR regulates various cellular processes including cell survival, proliferation, growth, autophagy, transcription, and metabolism (Figure 5. 2) [9, 245, 246].

In all eukaryotes, mTOR kinases are found in two protein complexes, mTORC1 and mTORC2 and both complexes are used in cell growth [247]. TORC1 regulates ribosome biogenesis activity, protein synthesis and cell proliferation and cell differentiation inhibition. Both of them regulate cellular growth, lifespan and ageing and are implicated in several common disorders such as type 2 diabetes, cancer, obesity and neurodegeneration [245, 248].

Cell growth and metabolism are regulated by mTORC1, while mTORC2 controls proliferation and survival. mTORC1 play a central role in regulating the synthesis of proteins, lipids, and nucleotides, and regulates the balance between catabolism and anabolism in response to environmental conditions [249, 250]. mTORC1 regulates protein synthesis through modulation of S6K, mRNA translation initiation and ribosomal biogenesis [251]. Rapamycin is an inhibitor of mTORC1 (Figure 5. 2) [252, 253].

In *Drosophila*, dS6K was the first downstream effect of the TOR pathway to be identified. *Drosophila* S6K expressed in COS or NIH 3T3 cells was phosphorylated by mammalian 40S ribosomal protein 6 (RPS6) in a rapamycin sensitive, mitogen-dependent and wortmannin sensitive manner. Studies have demonstrated that the loss of dS6K function in the wing

leads to a decrease in cell size and an overall reduction in growth and body size but, importantly, this decrease in size was caused by a decrease in cell size, not in cell number [254].

Tuberous sclerosis 1 (Tsc1) and Tsc2 form a complex that is demonstrated to work with the insulin signalling pathway to inhibit TOR signalling [254]. The small GTPase Rheb (Ras homologue enriched in the brain) is targeted by Tsc2 directly. Rheb is regulated negatively by Tsc proteins via the GAP activity of Tsc2. Rheb mutations lead to a block in development from the first to second instar transition. It has been suggested that Rheb can regulate the nutritional control of cell growth as its overexpression can drive cell growth in starved animals [254].

Sterol regulatory element binding protein 1 (SREBP1) is a conserved lipid (sterol/ fatty acid) regulated transcription factor that controls the transcription of several genes used in lipid metabolism and the production of cell membrane (Figure 5. 2) [254, 255]. In *Drosophila*, SREBP is regulated by mTORC1 and used in the regulation of Akt-dependent cell growth [254, 256]. Dysregulation in mTOR signalling is linked to an increase in body weight and other diseases such as cancer and neurological diseases [249]. In addition, the metabolism of triglycerides is regulated by mTOR. It has been shown that TOR mutants lead to an increase in triglyceride levels.

Rapamycin forms a gain-of-function complex with FKBP12, and this complex specifically acts as an inhibitor of mTOR. Rapamycin acutely inhibits mTORC1, while mTORC2 inhibition can result from chronic exposure to rapamycin [257]. Rapamycin treatment increases fat stores and starvation survival. The mechanism of modulating of fat metabolism by TOR is still unclear [254].

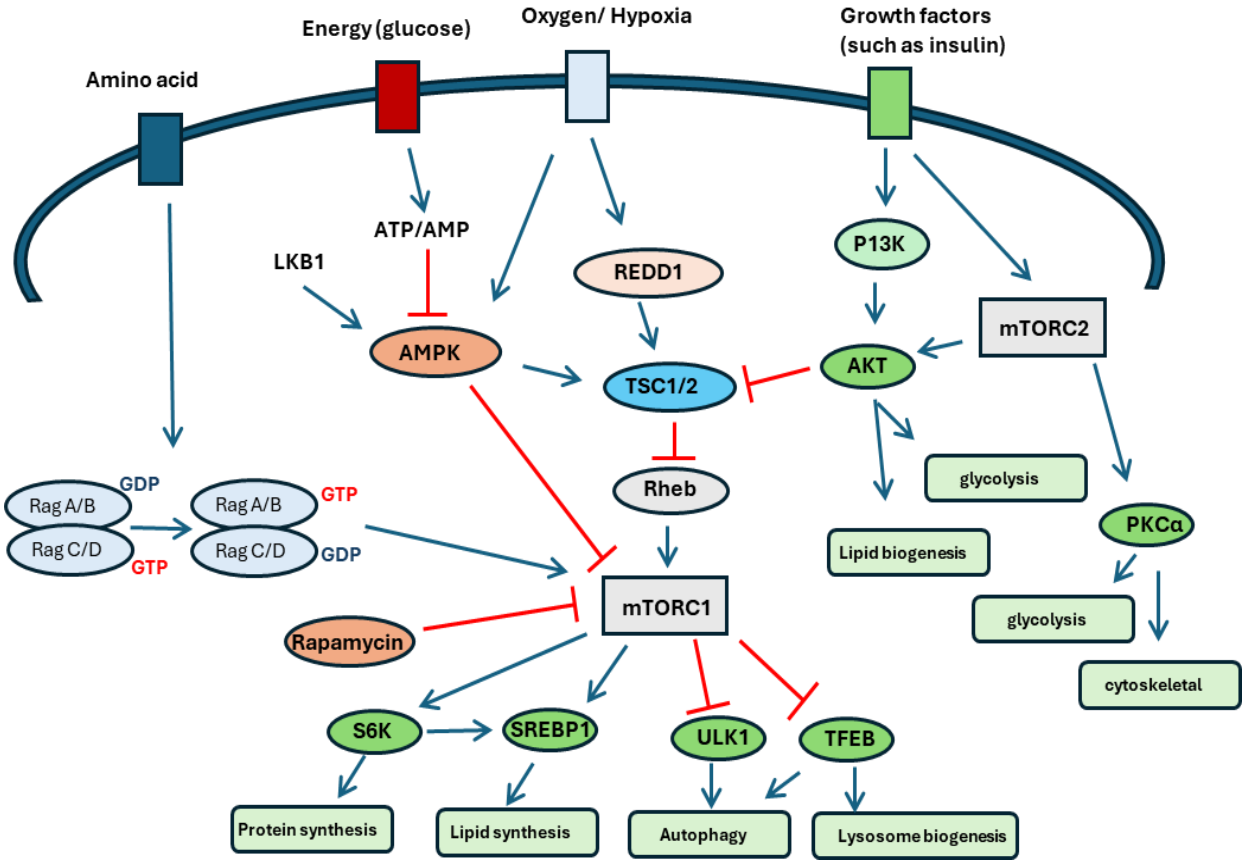

Figure 5. 2: The mTORC signalling pathway.

mTORC1 and mTORC2 signalling pathway processes. The sensors in the top of the figure including amino acids, energy, oxygen and growth factors. mTORC1 is regulated by all the sensors through several processes. Akt inhibits TSC1/2 and that enhances Rheb which stimulates mTORC1, while other processes including AMPK and REDD1 lead to TSC1/2 stimulation which inhibit Rheb and consequently inhibit mTORC1. mTORC1 regulates protein synthesis and lipid synthesis through enhancing S6K and SREP1, while control autophagy and lysosome biogenesis via the inhibition or decrease ULK1 and TFEP. mTORC2 regulated only by growth factors and stimulates PKCα and AKt to regulate cytoskeletal and glucose metabolism and lipid biogenesis. Blue arrows mean enhance or increase and orange arrows means inhibition or decrease.

5.1.3. Regulation of developmental time in *Drosophila*

In various metazoans, the rate and the duration of growth regulate the final size of adult which are affected by the environmental conditions [219, 258]. In several species, molecules of insulin/IGF family regulate the growth rate and the connection between the nutrition and growth [259].

In *Drosophila*, nutrition status controls the development time through acting on the prothoracic gland (PG) which secretes the moulting hormone ecdysone [260-262]. A decrease in mTORC activity in the PG leads to reduced ecdysone levels which in turn cause an increase in the growth time and in the size of animal.

The fat body of the insect plays an important role in energy storage and utilization. It serves as the central storage for excess nutrients. Additionally, it is considered an organ of great biosynthetic and metabolic activity [263].

Compared to vertebrate liver and adipose tissue, in insects, the fat body (FB) performs crucial humoral and storage roles linked to feeding. High amounts of proteins, lipids, and carbohydrates are accumulated by the FB during larval stages. During metamorphosis, autophagy degrades these materials to supply developing tissues [218, 264]. However, temporary nutrient deficiency can be compensated for by the FB. Moreover, the FB has endocrine activity and contributes to the stimulation DNA replication in larval brains and growth in imaginal disc explants During coculture trials [264, 265].

It has been shown that, the *Drosophila* larval tissue called fat body (FB) regulates the larval growth rate by using TOR pathway depending on the nutritional conditions [218, 258].

It has been suggested that the amino acid sensor mechanism is affected by dS6K. One of the main downstream targets of the TOR signalling pathway in flies is dS6K, and it has been shown that a hypomorphic dTOR heteroallelic combination is partially rescued by overexpression of an activated form of S6 kinase. Additionally, dTOR mutants exhibit growth defects and aggregation of fat body (FB) storage vesicles. Consequently, it is important to investigate how the TOR pathway contributes to the FB amino acid sensor mechanism [218].

The results have shown that overexpression of FB causes vesicle aggregation and restricts endoreduplication in FB cells, accompanied by growth defects and developmental delays. Therefore, inhibition of dTOR activity in the FB is sufficient to stimulate the amino acid sensor [218].

Furthermore, it has been demonstrated that the systemic regulation of larval growth originating from the FB is facilitated by the TOR nutritional checkpoint. Additionally, an amino acid sensor that functions in the FB regulates body size systemically [218].

Larvae undergo three size checkpoints to progress successfully to adulthood during *Drosophila* development, including the crucial weight, minimal viable weight, and metamorphosis threshold size. The next molt's likelihood of being metamorphic is determined by the threshold size for metamorphosis, which happens prior to the penultimate moult [228, 266]. While they reflect different outcomes, the minimal viable weight and critical weight both arise early in the last instar and simultaneously in *Drosophila*. The minimal viable weight, which is established by body fat storage levels adequate to provide the required energy, is the bare minimum needed to survive to adulthood without additional feeding [228, 266]. The critical weight describes the size at which entry into metamorphosis will not be delayed by starvation [267].

These checkpoints indicate a relationship between growth and maturation. It has been demonstrated that the pathways in the prothoracic gland (PG), *Drosophila* growth and maturation function as opposing forces, which regulates development time through ecdysone secretion in response to hormonal inputs. By modifying insulin/IGF (insulin-like growth factor) signaling (IIS) within the PG at various stages of larval development, a critical mass checkpoint reveals two phases of larval development. First, Larvae prefer rapid growth at the pre-checkpoint. Second, post-checkpoint, when maturation takes precedence. There are notable delays in maturation to pupation when the IIS pre-checkpoint is decreased, while reducing IIS post-checkpoint has no effect on development time [218, 258].

5.1.4. CLN7 regulates mTORC function

Cln7 is required to activate mTORC at the neuromuscular junction in neurodevelopment via a retrograde activity [117]. *Cln7* is required to activate mTORC at the neuromuscular junction during neurodevelopment via retrograde activity. The regulation of neural development by *Cln7* via TOR from a post-synaptic vesicular compartment is possible, as it has been observed that *Cln7* interacts molecularly with Rheb, an activator of the TOR complex [117].

Cln7-deficient MEFs show a defect in mTORC activation. In *Drosophila*, the absence of *Cln7* function leads to incomplete synapse development, resulting in decreased function and behavioural alterations due to TOR activity dysregulation. It has been shown that in *Drosophila* larvae, Cln7 mutants exhibit defects in TORC1 activity in the post-synaptic muscle [117].

An antibody to phosphorylated S6, a sign of TORC1 activity, was used to stain NMJs. Phosphorylated S6 was observed at active zones in the pre-synaptic boutons. However, pre-synaptic TORC1 activity remained normal [117].

Vesicles grouped close to the syncytial muscle nuclei in the post-synaptic muscle cell showed strong p6S staining, but the *Cln7* mutant showed lower vesicular staining, suggesting a decrease in TORC1 activity as a result of Cln7 function loss[117].

Previous work in the lab has identified that *Cln7* mutant adult *Drosophila* have a larger body mass than controls and that they are storing excessive triglyceride lipids. This is likely to be due to a failure to activate mTORC, leading to a stress-like response and excess lipid storage. In addition, mTORC1 is activated by Rheb which is small GTPase [117]. The expression of epitope-tagged forms of *Cln7* and Rheb in S2 cells demonstrated co-immunoprecipitation of two proteins which suggested a molecular interaction between the two proteins. In addition, it has been shown that they are colocalized when expressed in *Drosophila* S2 cells. Therefore, loss of *Cln7* function causes dysregulation of mTORC1 activity in the post-synaptic cells and that leads to developmental changes to the synapse and changes in the animal behaviour [117].

Aim

The aim of this chapter is to study the signalling pathways that lead to excessive mass of *Cln7* mutant adult *Drosophila*. Genetic epistasis will be used to ask whether *Cln7* sits within the IIS/mTORC1 pathway.

5.2. Results

5.2.1. The effect of *Cln7* mutations in the fly growth and development in comparison with other genotypes

Cln7 alleles were previously generated by the group [117]. The P-element NP0345 inserted upstream of the started codon was excised to generate two loss-of-function alleles, $Cln7^{84D}$ and $Cln7^{36H}$. In the $Cln7^{84D}$ allele exons 1-5 were excised and exon1, exon 2 and part of exon 3 were excised in the $Cln7^{36H}$ allele (Figure 5. 3) [117].

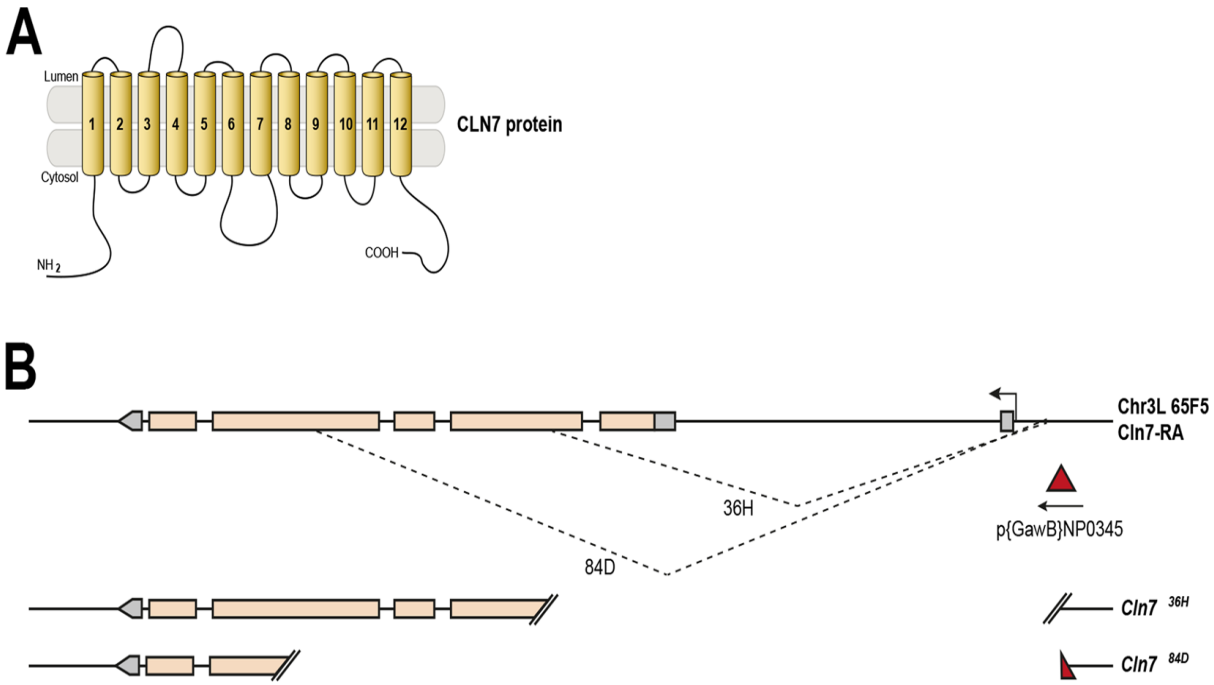

Figure 5. 3: Generation of *Cln7^{36H}* and *Cln7^{84D}* mutations.

Generation of *Cln7* mutations. (**A**) The CLN7 protein, a member of the multi-facilitator superfamily of solute transporters and a projected 12-span transmembrane protein. (**B**) The *Cln7* locus (CG8596) was deleted using P-element-mediated imprecise excision. Diagrammatic representations of two unidirectional deletion events, *Cln7^{84D}* and *Cln7^{36H}*, are provided. The *Cln7^{84D}* allele retains a portion of the P-element sequence [117].

The mass of adult flies carrying both *Cln7* mutants was measured using the same process as in the previous experiment. The mass of $Cln7^{36H}$ flies was recorded less than the flies of $Cln7^{84D}$ in both male and female flies (Figure 5. 4. A-B). The mean mass of $Cln7^{36H}$ adult males was 0.78 mg vs. 0.88 mg for $Cln7^{84D}$ males (n = 28 for $Cln7^{36H}$; 34 for $Cln7^{84D}$ and p-value <0.0001, 1- way ANOVA). For female flies the mean mass of adult $Cln7^{36H}$ was 0.9 mg vs. 1.23 mg for $Cln7^{84D}$ (p-value is 0.0003 and n= 33 for $Cln7^{36H}$; 37 for $Cln7^{84D}$, 1- way ANOVA). The mean mass of $Cln7^{36H}$ males was 0.78 mg vs. .76 mg for w^{1118} (n= 28 for $Cln7^{36H}$; 40 for w^{1118}; p-value > 0.07, 1- way ANOVA). For $Cln7^{36H}$ adult females the mean mass was 0.9 mg vs. 1.1 mg for the adult controls (n= 33 for $Cln7^{36H}$; 36 for the control and p-value > 0.07, 1- way ANOVA).

Even though the mean mass of $Cln7^{36H}$ flies was less than $Cln7^{84D}$ in both males and females, the mean mass of adult $Cln7^{36H}$ males recorded a slight increase compared to the control flies w^{1118} but depending on ordinary one-way ANOVA multiple comparisons there is no significant differences between the control mass and that $Cln7^{36H}$ flies for male and female flies. (Figure 5. 4).

As seen above, $Cln7^{84D}$ mutant flies recorded more mass than the controls in both males and females genotypes. Although $Cln7^{36H}$ recorded more mass than the controls, $Cln7^{84D}$ recorded more weight than the $Cln7^{36H}$ genotypes.

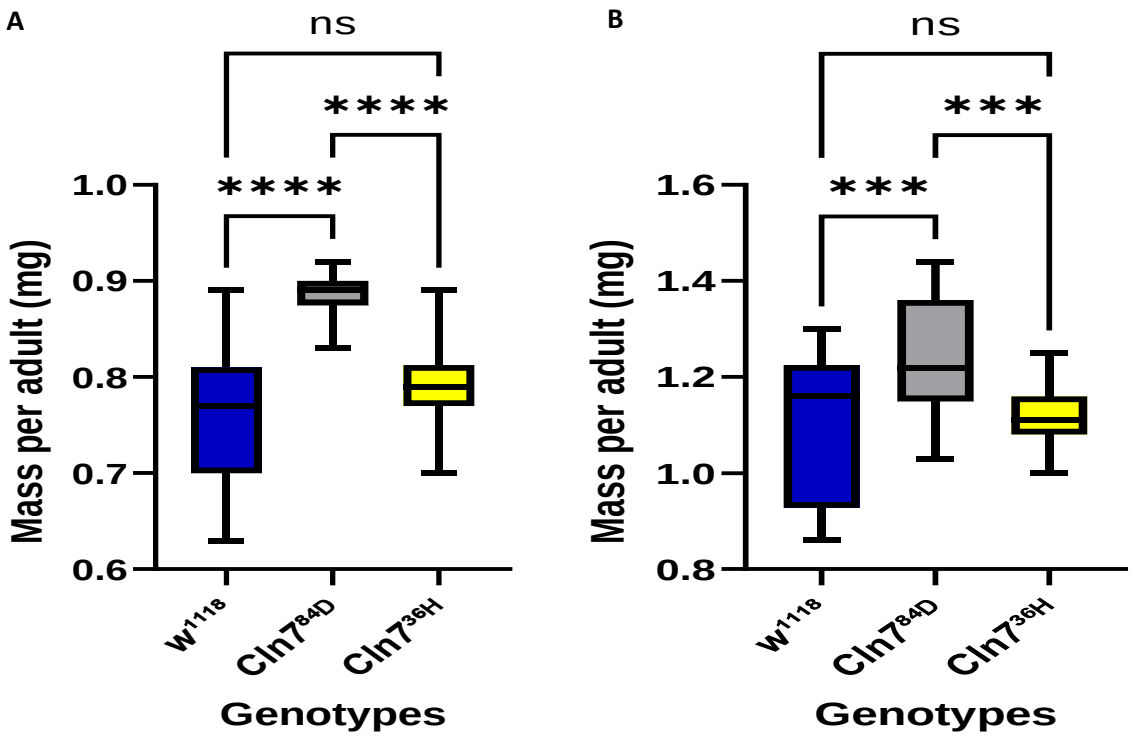

Figure 5. 4: The mean weight of *Cln7* alleles (*Cln7^{84D}* and *Cln7^{36H}*) which developed on SY food.

1 day age adult flies measured and compared with the control *w^{1118}*. **(A)** male adults and **(B)** female adults. The flies developed on SY food by taking the L1 instar and inserting them into the SY food vials. The vials saved at 25 ˚C during the development period. Each 10 flies weighted together, and the mean mass recorded for them, and the total dividend to 10 to have the mean mass for one fly. Boxes demonstrate the mean of means from n groups of 10 flies weighted together, and bars represent min-max values. X- values represent the weight of flies in mg and y-axis represent the genotype of flies. Depending on ordinary one-way ANOVA mutable comparisons, N.s p > 0.07, p value <0.0001. ****, p = 0.0003. ***. In this experiment the *Cln7* alleles compared with each other, and both compared with the control. The *Cln7^{84D}* mutants are significantly larger than the *w^{1118}* controls. while the *Cln7^{36H}* mutations were not significantly larger than the controls. The *Cln7^{84D}* flies are larger than the *Cln7^{36H}* flies which means more losing of Cln7 function leads to more weight for the flies. The weight of male genotypes between 0.6 - 1.0 mg in box **(A)** which less than the mass of females in box **(B)** which recorded between 0.8 – 1.6 mg.

Chico, which is homologous to vertebrate insulin receptor substrates (IRS), regulates cell proliferation, cell size, and overall body growth. Additionally, it plays a role in the regulation of cellular metabolism. The growth of homozygous mutant *chico* cells is slower than the normal flies, resulting in an autonomous reduction in cell size and the production of smaller organs. Although the size of *chico* flies is less than the normal flies, the lipid levels was observed more than their heterozygous siblings [238].

The regulation of protein synthesis is linked to growth. In mammalian cells, protein synthesis is regulated by two kinases: p70S6 kinase and mTOR. The PI3K/PKB signalling pathway activates these kinases, although the exact mechanism of this activation remains unknown. It has been shown that developmental delay and body size reduction result from the loss of *Drosophila* S6K activity. Protein kinase B, or PKB, is another name for the serine/threonine kinase Akt. Activated PKB controls growth and metabolism through different protein targets, including the fly homologs of Rheb, which activate TOR kinase. PKB also participates in the regulation of growth and metabolism by influencing TOR and S6K [268, 269].

PI3K/AKT-mediated mitogen-driven signalling is essential for the mTOR activation pathway [270]. mTOR is found downstream of PI3K and Akt. The PI3K/Akt/mTOR pathway is a major intracellular network that regulates cell proliferation. TSC1/2, a GTPase-activating protein for Rheb, is inhibited by Akt activation, which subsequently causes mTORC activation [271].

In *Drosophila,* the insulin receptor homolog (InR) is bound by the secreted insulin-like peptides (ILPs). Chico binding to InR initiates downstream signalling, which is then followed by PI3K recruitment and PIP2 conversion to PIP3. PIP3 is recognised by Akt kinase, which uses it to regulate cell growth by activating dTOR and proliferation by other means [272].

In *Drosophila* the *chico* gene encodes an insulin receptor substrate (IRS) which binds to the intracellular domain of the Insulin receptor and is required for activation of the IIS pathway [238]. Homozygous *chico* mutant cells experience a selective growth disadvantage, as their growth is slower than that of wild-type cells. This reduction in growth is evident in the size of discs and the adult eye, resulting in smaller cells compared to wild-type cells[238].

Heterozygous flies are smaller than controls, with reduced fecundity and enhanced stress response, consistent with reduced mTORC signalling [238]. Pervious study in the lab showed that, if *Cln7* mutant flies have increased mass because they fail to activate mTORC correctly, leading to triglyceride storage, this is likely to be downstream of *chico* has *Cln7* interacts with the mTORC activator Rheb.

In this experiment the mass of several adult fly genotypes were observed and recorded. In addition to the w^{1118} control strain, two loss-of-function alleles of *Cln7* were used: $Cln7^{84D}$ and $Cln7^{36H}$. The $chico^{1}$ alleles was combined with the *Cln7* alleles to test for genetic epistasis (Table 2. 7). Flies were developed on simple SY food (section 2.4.3) to maintain consistency with previous experiments. To ensure consistent culturing density between experiments, 100 of first instar larvae (L1) were taken from embryo collection agar plates and transferred to vials of SY food and allowed to develop to adult stages. The mass of flies was then measured 1 day after eclosion. 10 flies were measured and the mean number of them was recorded which repeated for all flies and all of them left in the same food and the same conditions.

As seen previously, the *Cln7* mutants were significantly heavier than the w^{1118} control flies, for both males and females. The mean mass of male $Cln7^{84D}$ flies was 0.88 mg vs. 0.76 mg for the control ($p< 0.0001$. n= 34 for $Cln7^{84D}$; 40 for w^{1118}, 1- way ANOVA) (n value means

group of 10 flies weighted together). For the *Cln7*^{84D} adult females, the mean mass was 1.23 mg vs. 1.1 mg for controls (p-value 0.0002. n= 37 for *Cln7*^{84D}; 36 for the control, 1- way ANOVA) (Figure 5. 5).

The same mass measurement was done for the *chico*^{1} heterozygous flies, plus *chico*^{1} in combination with *Cln7*^{84D}. As expected, the mean mass of *chico*^{1}*/+* males was 0.7 mg and female fly was 0.97 mg, both of which were significantly lower than control flies, (n= 35 for male *chico*^{1}*/+*; 40 for *w*^{1118} and p-value < 0.0001. For females n= 31 for *chico*^{1}*/+*; 36 for the control and p < 0.0001, 1- way ANOVA) (Figure 5. 5). Both male and female *chico*^{1}*/+; Cln7*$^{84D/84D}$ flies were, in contrast, significantly heavier than controls, although they did not reach the same mass as the *Cln7*^{84D} flies. The mean mass of *chico*^{1}*/+; Cln7*$^{84D/84D}$ males was 0.812 mg vs. 076 mg for the control, (n= 17 for *chico*^{1}*/+; Cln7*$^{84D/84D}$; 40 for *w*^{1118} p-value = 0.004, 1- way ANOVA). For the adult females mass of *chico*^{1}*/+; Cln7*$^{84D/84D}$ was 1.21 mg vs. 1.1 mg for the control females (p-value for = 0.0103 for *chico*^{1}*/+; Cln7*$^{84D/84D}$ females and n= 19; for the control n= 36, 1- way ANOVA). *Cln7*$^{84D/84D}$ recorded a significant increase mass than *chico*^{1}*/+; Cln7*$^{84D/84D}$ for male flies as that observed in the graph (Figure 5. 5. B). While for the females there is no significant difference between both genotypes.

As seen above, *Cln7*^{84D} mutant flies recorded more mass than the controls in both males and females genotypes.

Regarding the *chico* genotype, even though *chico* genotypes recorded less mass than the controls, when combined with the *Cln7* mutant (*chico*^{1}*/+; Cln7*$^{84D/84D}$), the mass of flies was greater than that of the controls. However, this combination genotype recorded less mass than *Cln7*^{84D}, indicating the effect of *Cln7* loss function on the weight of flies.

Additionally, it was observed that the wild-type and *Cln7* mutant genotypes produced more eggs and larvae than other genotypes related to *chico* and the *chico* combination with $Cln7^{84D}$. Although the *chico* genotypes were developed under the same conditions (food and temperature), the hatching time for these genotypes was slower compared to the wild-type and *Cln7* genotypes. While the number of eggs was not recorded, it became evident when the larvae were collected and transferred to the SY food vials. Wild-type and *Cln7* mutant larvae could be collected in one day, whereas *chico* genotypes required more time and days to collect 100 larvae for the SY food vials.

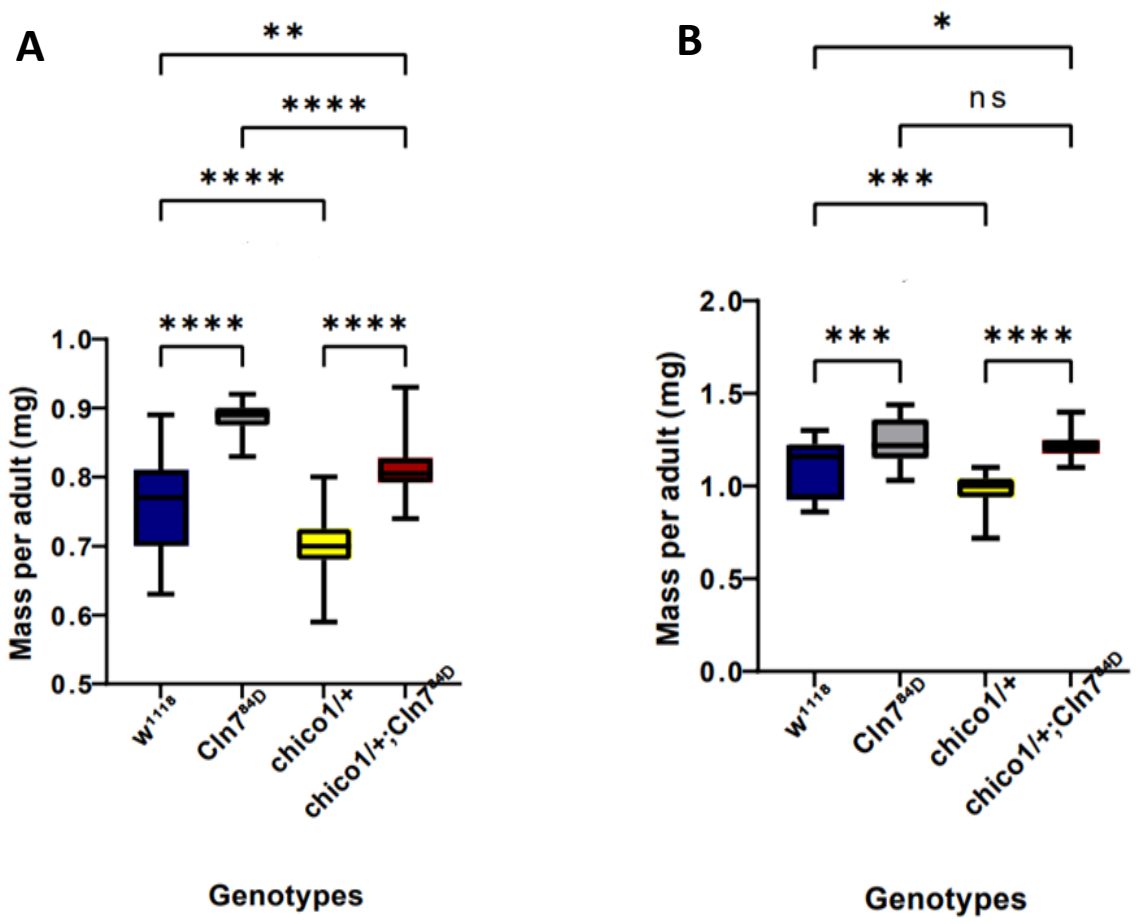

Figure 5. 5: The mean masses of adult *Drosophila* genotypes developed on SY food.

The weight comparisons between genotypes of adult flies (**A**) males and (**B**) females. The flies developed in SY food by taking the L1 instar and inserting them in the SY food. The vials saved at 25 ˚C during the development. 1 day old-adult flies weighted in group of 10 flies for all genotypes in addition to the control w^{1118} and the total dividend to 10 to have the mean mass for one fly. Boxes demonstrate the mean of means from n groups of 10 flies weighted together, and bars represent min-max values. X- values represent the weight of flies in mg and y-axis represent the genotype of flies. The weight of male genotypes between 0.5- 1.0 mg in box **(A)** which less than females mass in box **(B)** which between 0.5 – 2.0 mg. Statistical analysis was performed depending on ordinary one-way ANOVA mutable comparisons. N.s p> 0.05, p = 0.0103. *, p=0.0040. **, p = 0.0002 ***, p<0.0001. ****

5.2.2. The size of flies in larger cohorts

To validate the previous experiment, flies were cultured directly in large numbers in bottles rather than being transferred from embryo collection agar plates to small vials after hatching as first instar larvae. As a result, the flies started their growth and development from the embryo stage in the SY food, rather than on grape juice agar. One day after eclosion as adults, the mass of each genotype was measured as before. For all the flies, the same relationships between genotypes were seen, although the flies were generally larger than in the first experiments in vials (Figure 5. 6). The *chico*^{1}*/+; Cln7*$^{84D/84D}$ flies were no longer statistically significantly larger than controls for males, but they remained significantly different for females.

The mean mass of *Cln7*^{84D} males was 0.98 mg vs. 0.78 mg for *w*^{1118} males (p-value < 0.0001 and n= 53 for *Cln7*^{84D}; 39 for *w*^{1118}, 1- way ANOVA). About the female mass for the wild-type control was 1.02 mg vs. 1.35mg for the adult *Cln7*^{84D} females (p < 0.0001 and n= 53 for *Cln7*^{84D}; 38 for the control). For the males *chico*^{1}*/+; Cln7*$^{84D/84D}$ the mean mass was 0.823 mg vs. 0.78 mg for *w*^{1118}, (n= 30 for *chico*^{1}*/+; Cln7*$^{84D/84D}$; 39 for *w*^{1118} and p-value > 0.423, 1- way ANOVA). Also, the mean mass of adult females *chico*^{1}*/+; Cln7*$^{84D/84D}$ was 1.172 mg vs. 1.02 mg of the controls (n= 29 for *chico*^{1}*/+; Cln7*$^{84D/84D}$; 38 for *w*^{1118} and p-value <0.0001, 1- way ANOVA). For *chico*^{1}*/+* male flies, they recorded less mass than *w*^{1118} and that was 0.7 mg vs. 0.78 mg for the controls (n= 32 for *chico*^{1}*/+*; 39 for *w*^{1118} p-value <0.0001, 1- way ANOVA). However, for the adult *chico*^{1}*/+* females the mean mass was 0.97 mg vs. 1.02 mg for the controls (n= 33 for *chico*^{1}*/+*; 38 for *w*^{1118} p-value > 0.423, 1- way ANOVA).

As observed previously, *Cln7* mutants (*Cln7*^{84D}) recorded more mass than wild-type control genotypes. Additionally, the *chico* genotype mass was lower than the wild-type genotype,

but when combined with the Cln7 mutant (*chico*^{1}*/+; Cln7*$^{84D/84D}$), they recorded a greater weight than the control genotypes, even though it had less mass than the *Cln7*^{84D} genotypes. Chico genotypes recorded more weight than before in section 5. 2. 2. probably because they developed in SY food from the embryo stage which affected on their behaviour or the lipid storage or another unknown reason.

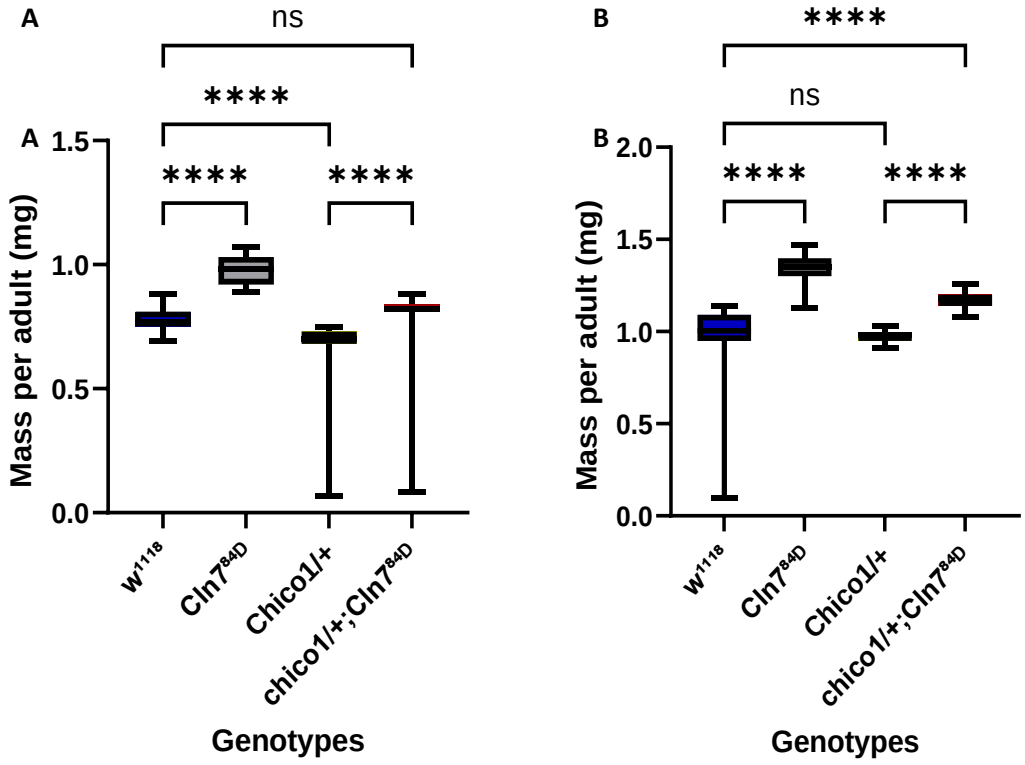

Figure 5. 6: The mean masses of the adult *Drosophila* genotypes developed in larger cohorts on SY food.

The comparisons between genotypes of adult flies (**A**) males and (**B**) females. 1 day old-adult flies weighted in group of 10 flies for all genotypes in addition to the control w^{1118}. The bottles saved at 25 ˚C during the development period. Each 10 flies weighted together, and the mean mass recorded for them, and the total dividend to 10 to have the mean mass for one fly. Boxes demonstrate the mean of means from n groups of 10 flies weighted together, and bars represent min-max values. X- values represent the weight of flies in mg and y-axis represent the genotype of flies. The weight of male genotypes between less than 0.5 - 1.5 mg in box **(A)** which less than the mass of females in box **(B)** which recorded between less than 0.5 – 2.0 mg. Statistical analysis was performed depending on ordinary one-way ANOVA mutable comparisons, N.s $p > 0.423$, $p<0.0001$. ****. Flies were directly cultured in large numbers in bottles and started their life in SY food from embryo stage to the eclosion. Consequently, the weight is different than before in particular for *chico* genotypes.

5.2.3. Food consumption for the control w^{1118} and $Cln7^{84D}$

There are several important reasons for the increased mass of the $Cln7^{84D}$ mutant. One possible reason why the $Cln7^{84D}$ mutants were larger was that they consumed more food during larval development. Flies were fed food supplemented with 2% Coomassie dye, crushed when emerging from the food to pupate at the late larvae stage and the OD595 recorded of the lysates. A standard curve of Coomassie concentrations was established to help quantify the level of food intake (Figure 5. 7. A).

Lysates were made from multiple larval for w^{1118} and $Cln7^{84D}$ genotypes. larval samples. The mean OD595 for the $Cln7^{84D}$ genotype was 0.4 nm higher than the control larvae w^{1118} which recorded 0.27 nm (Figure 5. 7. A). Interpolating from the standard curve, the value of food consumption concentration for the $Cln7^{84D}$ larval recorded 0.021 mg/ml, while the value of the wild-type control was 0.013 mg/ml (n= 13 for w^{1118} controls; 15 for $Cln7^{84D}$ larval, p-value 0.0187 and 2-tailed T test). This suggested that the $Cln7^{84D}$ mutation flies eat more than the wild-type flies or possibility excrete less.

The experiment assesses food intake directly, and the most relevant explanation for this issue is the food intake behaviour, which I focused on. Regarding the absorption of dye from the gut, it is possible, but this does not contradict the food intake behaviour for the larvae. As for gut transit times, they were taken into consideration, but as I mentioned above, the food intake was the main focus. The measurement of dye in the fly excretion probably answers some unclear points in this issue.

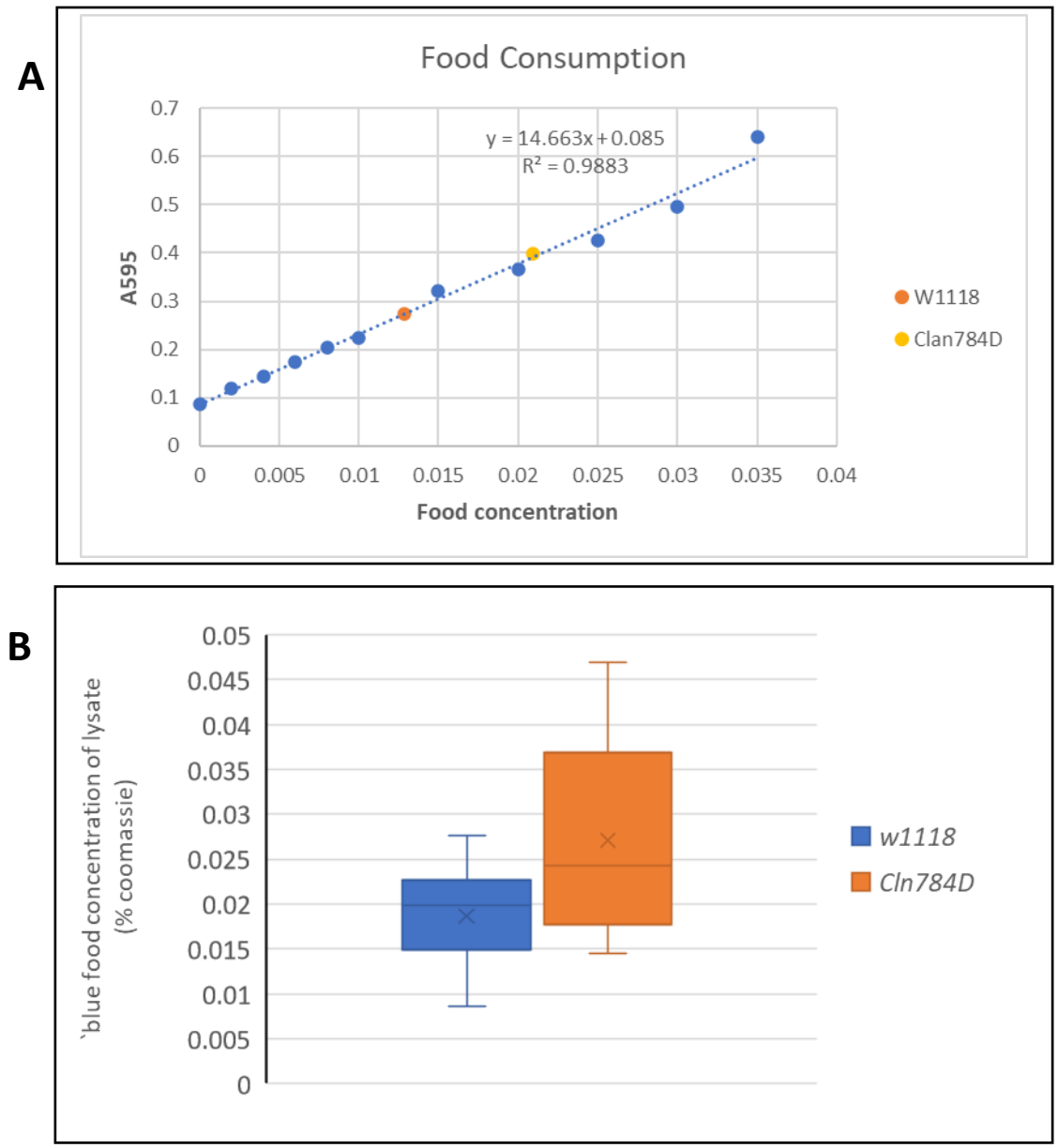

Figure 5. 7: Measurement of food consumption by *Cln7* mutants vs w^{1118} controls.

The concentration of the Coomassie-containing food consumed by larvae was measured by crushing larvae emerging from the food to pupate at late larval stage and measuring absorbance at 595nm. As larval were washed by water which means the dye colour represent the intake food by larvae and mainly the day absorbed from the gut (**A**) A standard of increasing Coomassie concentrations. The mean absorbance value for w^{1118} is shown in orange and $Cln7^{84D}$ samples in yellow. (**B**) The comparison of the individual blue food concentration values between w^{1118} (blue) and $Cln7^{84D}$ (brown). Lysates from $Cln7^{84D}$ have significantly higher concentrations of Coomassie dye then controls (p-value 0.0187, 2-tailed T test).

5.3. Discussion

5.3.1. The possible role of CLN7 in fly growth and development

It has been demonstrated here that the flies with a loss-of-function *Cln7* mutation are larger than controls, which matches what had been shown previously. It is not clear why the 36H mutation failed to replicate previous finding. One possibility is that the strain had become mixed up with another and was not correct.

There are several reasons to explain the increased weight of *Cln7* mutant flies, including an increase in nutrition storage and food consumption, increased muscle mass, decreased excretion and up-regulation of cell growth and/or proliferation [273].

The food consumption experiments data suggests the *Cln7* mutant flies do eat more food than control larvae or potentially fail to excrete the same rate. It has been shown in the lab that, there is a developmental delay in the *Cln7* mutant flies which may explain the additional food consumption. That additional food is then stored as lipids. Does this delay occur because the animals fail to recognise when they reach the correct mass to enter metamorphosis? More likely, the loss of Cln7 puts the fly into a stress responsive mode which drives higher levels of lipid storage as a protective mechanism. It is also clear from lipid metabolomics experiments carried out by the group that there is a change in sphingolipid metabolism that may also underpin the lipid storage phenotype.

5.3.2 *Cln7* and mTORC regulation

Cln7 has a role in regulating mTORC signalling at the neuromuscular junction during neural development [138]. Given that mTORC is central to growth signalling in cells, it seems

possible that loss of *Cln7* function leads to dysregulation of mTORC and a switch in stress signalling and lipid metabolism. Studies in *Cln7* deficient mouse embryonic fibroblasts (MEFs) have shown that mTORC1 re-activation is impaired after serum withdrawal and re-supply [138]. Moreover, a decrease in the TOR activity affects the prothoracic gland (PG) and thus causes a delay in development, affects the size of the animal [258], and affects triglyceride levels [254]. Furthermore, the TOR pathway is utilized by the *Drosophila* larval tissue called fat body (FB) to regulate larval growth rate depending on nutritional conditions through the control of IIS in all tissues. [218, 258]

In *Drosophila*, Chico is an insulin receptor substrate [238]. Mutations affects cell growth and lifespan by reducing IIS to mTORC1 resulting in smaller cells, extended lifespan and stress resistance [274]. One possibility is that *Cln7* acts downstream of Chico to regulate mTORC1 activity. Alternatively, it could be in a parallel pathway. In a *Chico/+;Cln7* double mutant, the mass was significantly increased. This suggests that Cln7 is not in the same pathway as mTORC1. To understand that, the cell size will need to be measured.

Is there lipid storage in *Chico* heterozygous flies? If not, this suggests *Cln7* not acting in the same way as *Chico* and IIS. There is a need to measure cell size in all genotypes. If cell size is not changed in *Cln7* mutations, then it is not likely to be the same pathway as Chico. In the Chico1/+;Cln7 combination, is there more lipid storage and smaller cells together? This might be expected if pathways are parallel.

Previously study in the lab, tested the interaction between $Cln7^{84D}$ and mTORC2. Therefore, TORC1 activity was blocked genetically using the $rictor^{\Delta 42}$ allele. The mass of $Cln7^{84D}$ flies was greater than the control, while the mass of $rictor^{\Delta 42}$ flies was smaller than w^{1118}. However, when combined, the mean mass of the mTORC1;Cln7 double mutant was the

same as the mass of *rictor*$^{\Delta 42}$ mutants, which suggested that *Cln7* is required to regulate mTORC2.

It has been demonstrated in the lab that, lifespan and stress resistance are affected by loss of *Cln7* function. *Cln7* mutant flies significantly extend the lifespan more than the w^{1118} flies, in particular the female mutants. However, one mechanism known to increase lifespan is TOR inhibition [275], which indicates that mTORC is likely to be inhibited. In addition, the Cln7 mutant flies showed resistance to oxidative stress and starvation.

The experiments indicated that, the mass of *chico*^{1} heterozygous flies was significantly less than the controls. *Chico* plays an important role in cell proliferation, cell size of individual cells and body growth in addition to controlling cellular metabolism. *Chico* mutations have been shown to reduce body size because of the reduction in cell size and cell number. *Chico* flies are fewer in number than normal flies, but they show increased lipid levels compared with their heterozygous siblings [238]. However, the combination of *chico*^{1}*/+; Cln7*$^{84D/84D}$ mutants indicated an increase in the mean mass over the controls for both males and females. Moreover, in this combination mutants there were two opposite effects, chico mutant which leads to a decrease in the fly mass and *Cln7* mutation which causes an increase in the fly mass. It was clear from the experiment that the loss of *Cln7* function outweighs the *chico* mutant in the fly body. The *Cln7* mutations leads to mTORC dysregulation. mTOR integrates signals from nutrients, amino acid, energy, and growth factors to regulate cell growth and cell cycle progression co-ordinately. mTORC1 enhances cell capacity to synthesis de novo proteins required for cell growth [276]. However, mTOR inhibition leads to an increase in cholesterol and triglyceride. [277]

Chico mutation perhaps leads to a reduction in cell size or cell number. Study mentioned that the loss of *chico* function leads to an increase in the lipid level, even though they had smaller size than the control [238].

One explanation is that the increase in fly mass is due to an increase in the lipid levels in the body as this lipid accumulation in the *chico* mutation and also in the case of TORC dysregulation. In addition, one side effect of rapamycin which is an mTORC1 inhibitor is hyperlipidaemia [9]. Also, mTORC dysregulation may lead to changes in feeding behaviour. However, both mutations possibly work individually in the fly body which also explains the increase of the fly mass with combination mutants while it decreased in the case of the *chico* mutation.

6. GENERAL DISCUSSION

6.1. The CLN7 function

The objective of this project is to identify the CLN7 function in the lysosomal membrane and synapses through reorganizing the partner proteins in CLN7 complexes from S2 cells and fruit flies. The proximity labelling method was used to identify candidate protein interactions. However, numerous proteins were found in S2 cells and *Drosophila* melanogaster flies. The BioID technique performed in S2 cells resulted in several hits, including coracle, DLG, a-spectrin, B-spectrin, lethal giant, nirvana, and others. By applying immunoprecipitation to confirm the interaction, particularly using SMALPs, two important proteins were obtained: DLG and a-spectrin. Both play crucial roles in synapse structure, function, and localization, as mentioned before (section 3.3.4). Identifying the partner proteins from flies is essential to confirm the S2 cells results and reveal the CLN7 function in flies. Consequently, the TurboID technique was developed and performed in S2 cells and flies. Many TurboID hits were obtained as candidate interacting proteins, and several BioID hits were repeated and observed in this technique. However, frequent proteins related to NMJ cytoskeleton, glial cells, synapses, and cell membranes were found, indicating the strong possibility of CLN7 contributing to synapse structure, function, and consequently NMJ function and development. This theory is supported by a previous study that showed Cln7 mutants in *Drosophila* are linked to synapse dysfunction and abnormal NMJ development [117].

Several proteins related to the plasma membrane and membrane, which indicate the possible function of CLN7 in the lysosomal membrane through those candidate proteins. CLN7 is a lysosomal membrane protein, and studies have mentioned that the absence of

CLN7 affected the levels of some lysosomal membrane proteins and other soluble lysosomal proteins [138]. Understanding how CLN7 regulates the lysosomal membrane requires more study to understand its specific role there. Recently, CLN7 was shown to be a novel endo-lysosomal chloride channel [162]. However, identifying its role in lysosomal function and the effects to Cl^- transport changes in the lysosomal membrane still need more studies.

In addition, this study observed the effect of *Cln7* loss of function on fly weight and development, as the weight of *Cln7* mutant flies was greater than that of wild-type flies. However, several reasons are related to this result. For instance, the mutants might eat more food, excrete less, or perhaps store a high level of lipids. Additionally, their feeding behaviour might change throughout the developmental period. It has been identified that Cln7-deficient MFEs affect mTORC activity [138]. Furthermore, the *Cln7* mutant reduces TORC1 activity [117]. This suggests that the loss of *Cln7* function causes a reduction in TORC activity, leading to changes in *Drosophila* nutritional behaviour and resulting in changes in fly weight and development.

6.2. The possible effects of CLN7 in *Drosophila* growth and development

The work in this thesis helped to reveal how CLN7 regulates the growth and development of flies and highlights its role in regulating mTORC signalling, in two different developmental contexts: neural development and general metabolism.

In flies carrying CLN7 mutations, there was an increase in mass through development. This appears backwards as an increase in mass would suggest overactive mTORC activity, despite previous studies indicating that CLN7 might be required for mTORC activation (at least after periods of nutrient starvation). Measuring the consumption of food showed that the *Cln7*

mutant flies had ingested more food than the controls, which likely explained the change in mass. Previous studies in the group had indicated developmental delay, which is also probably a contributing factor as the flies spent more time in the food before pupating. The possibility that the difference lies in excretion rather than ingestion has not yet been investigated. It is unclear how CLN7 might regulate the mTORC process, given that is it a Cl- transporting channel. Is mTORC regulated via changes in the internal Cl- in lysosomes? This is not known.

Another possibility is the effect of CLN7 on growth factors including insulin and insulin-like growth factors which regulate glucose metabolism, cell proliferation and cell survival [278, 279]. Therefore, the loss of CLN7 function probably dysregulates the insulin and insulin-like growth factor which increases the level of lipid storage in the fly body. Moreover, nuclear receptors which are a family of transcription factors contribute to cell proliferation, development, metabolism, and reproduction. However, ligand factors interact directly with nuclear receptors inside cells after crossing the cell membrane. How CLN7 may affect that as it is a lysosomal membrane protein, and as lysosomes can gather in the perinuclear region, create several metabolites and anchor signalling factors, signal transduction and transcription responses can be affected by the link of lysosomes with the nucleus [280].

All cellular functions are regulated by the metabolism which plays vital roles in cell growth, and development [281] and cell metabolism is regulated by mTORC1 in response to environmental changes. The structural and mechanical functions that are important regulations in cell metabolism depend on numerous proteins such as cytoskeleton proteins. The possibility of CLN7 interacting with several cytoskeleton proteins has been shown in this study. In addition, numerous soluble lysosomal proteins were depleted in the absence of

CLN7. How CLN7 regulates those proteins and what kinds of effects this has require further studies.

Chico is the insulin receptor substrate in *Drosophila* and has a regulation in cell size and growth [238]. What is interesting is that, *chico* was found labelled by BioID-CLN7 in S2 cells and there is a probability of interaction between CLN7 and *chico*, which suggests that insulin signalling is strongly regulated by CLN7. However, the interaction between CLN7 and *chico* and the effect of CLN7 on insulin signalling in this pathway need further studies.

6.3. Efficiency of proximity labelling to identify protein interaction

To identify the CLN7 function in synapses and lysosomal membrane, PL was applied to identify the protein-protein interactions and discover the candidate proteins in this issue.

Two methods of PL have been developed and used, APEX2 [282], which its proximal protein can be tagged in 1 min [283, 284], but it is toxic for living samples as it needs H2O2 for use [285]. Another PL enzyme is BioID which is a nontoxic and simple technique [163], but it has a disadvantage as its slow kinetics require at least 18 hours for labelling with biotin which makes it difficult to apply in flies [213]. However, BioID2 has been developed as a new promiscuous biotin ligase variant [164], but it also needs more time for labelling [213]. Therefore, two promiscuous ligases have been improved TurboID which is 35 KDa with 15 mutations relative to wild-type BirA and miniTurbo which is 28 KDa with 13 mutations with BirA and with N-terminal domain deleted. Both TurboID and miniTurbo can show detectable signals after less time with biotin than BoID, can also reveal high activity at 30 ˚C and can work without exogenous biotin [213]. In this study, using BioID proximity labelling in vitro showed high efficiency and numerous identified proteins were discovered via this

technique. However, applying and using PL in *Drosophila* was a significant objective. The BioID technique was impossible to use in flies due to its certain limitations. Therefore, TurboID was developed and inserted in the flies and immunoblotting showed appropriate outcomes. Its efficacy in flies was highlighted as a proper technique in addition it was a rapid technique in S2 cells compared with BioID. This confirms the proper use of this technique as a perfect way to discover the CLN7 interaction proteins.

6.4. The role of CLN7 in synapses

Previous studies had highlighted a role for CLN7 in regulating mTORC-based growth of synapses but there was no indication of how CLN7 might function in that process. This study has provided stronger evidence for a role for CLN7 at the synapse by demonstrating interactions with key proteins at the post-synaptic density. In addition, the loss of *Cln7* affects the autophagic flux within neurons and autophagy [117], which is important in the neuronal development and health and stimulate synapse development in *Drosophila* [286].

PL demonstrated that several considered candidate proteins interact with CLN7. CLN7 interacts both by proximity labelling and co-immunoprecipitation with spectrin which is essential in synapse stabilization and with discs-large (the *Drosophila* homologue of PSD-95), which is a central scaffolding protein at the post-synaptic density. It is unlikely to be a coincidence that the CLN7-PSD95 interaction was identified in both non-neuronal cells and *in vivo*. Similarly, it is unlikely to be a coincidence that CLN7 was shown to be in proximity to several glial proteins, with Coracle and with integrins, all of whom have roles to play in synapse development.

Moving forward, this thesis has provided real options for investigating the CLN7 function further. Mutations in interaction partners can be introduced to ask how CLN7 localisation changes. Does PSD-95/DLG anchor CLN7 in the post-synaptic density? Is the interaction with Coracle required for normal synapse development? These questions are relatively straightforward to answer and will provide valuable insight into the CLN7 function. However, comparing the in vitro and in vivo results will provide support, as several proteins will be repeated in all experiments. Additionally, loss of protein function, whether *Cln7* or the interacting proteins, via KD or KO, will highlight Cln7's regulation of those hit proteins and their existence or function. Subsequently, recognizing its effects on synapses and NMJ. Using other biochemistry methods is important for analysing and confirming the subsequent results. What is not clear from this study, and remains a key open question is what CLN7 does at the synapse, and how does it do ? How is a potential Cl- transport function required at the post-synaptic density? Is CLN7 in a lysosome-like location? It is clear that CLN7 is present in vesicles at the synapse, but are they low pH vesicles? Is lysosomal fusion with the plasma membrane as described in the introduction important for the development, growth, expansion and plasticity of the synapse? All of these questions remain outstanding, but the identification of likely players working alongside CLN7 will help to answer these questions.

6.5. The future plan

In conclusion, the objective of this project was to discover the functions of CLN7 in synapses and lysosomal cell membrane. The BioID technique highlighted precise results. Moreover, the developed PL TurboID demonstrated the efficacy of labelling in *Drosophila melanogaster*, and it was effective for obtaining appropriate results after immunoblotting

and identifying proteins after MS analysis. To confirm the protein interaction, other experiments need to be applied in both larval and adult flies in addition to in vitro labelling and comparing all results of the identified proteins. Moreover, optimizing specific steps to achieve perfect results is important. In addition, designing an appropriate control is important to eliminate false positives and have specific results as in this experiment using TurboID as a control with TurboID-CLN7. However, because there was no TurboID transgenic, tubby larval and humeral adult flies were used as controls in addition to the wild type in immunoblotting. Moreover, as proximity labelling conjugate the close distance proteins which probably not interact with the target protein, validation of CLN7 hit proteins is important to reveal the interaction and to know the effect of CLN7 on the interaction proteins.

To uncover the behaviours of the CLN7 protein, whether in vitro or in vivo, the combination of many experiments such as cellular methods, genetics, biochemistry, and so on is very important.

For accurate results, in vitro labelling for BioID and BioID-CLN7 should be applied to identify candidate interacting proteins from S2 cells. However, using BioID here as a control and to obtain unique proteins for BioID-CLN7, as was done in chapter 3, is crucial. For the TurboID technique, both TurboID and TurboID-CLN7 should be prepared and applied in vitro to obtain appropriate results after expression in S2 cells, similar to what was performed with the BioID technique. Both TurboID and TurboID-CLN7 should be transgenic in *Drosophila melanogaster* and crossed with Mef2-UAS flies to drive TurboID and TurboID-CLN7 expressions in the muscles. In vivo labelling of TurboID-CLN7 and TurboID should be done for larval and adult flies, and the unique candidate interacting proteins of TurboID should be

avoided for both of them to have only the TurboID-CLN7 hits in larval and adult flies. Consequently, comparing the results of all these experiments is important to detect the repeating proteins in all of them. Then, another confirming experiment will help identify the interacting proteins with CLN7, such as immunoprecipitation using SMALPs, even in S2 cells or larval and adult flies. After that, other genetic experiments are essential to observe the effect of loss of CLN7 function on the interacting proteins after IP and whether that will affect synapse structure, function, and plasticity in the Drosophila NMJ. Conversely, in the case of knockout or knockdown of those interacting proteins, what will happen to CLN7's existence, structure, function, and localization, and subsequently, whether it affects *Drosophila* synapse and NMJ.

The regulation of TORC signalling by *Cln7* was predictable, as the absence of *Cln7* function led to an increase in fly weight. CLN7 is a lysosomal membrane protein, and its effect on TOR is possible, but the mechanism remains unclear. This regulation needs to be revealed, such as through the function of insulin and insulin growth factors. Testing insulin and insulin growth factors is important to correlate them with the TORC effect. Additionally, studying the effect of *Cln7* on TOR through its signalling pathway, growth factors (such as Rheb, Akt, or TSC1/2), is essential to demonstrate the real mechanism. Furthermore, measuring food consumption and excretion will help identify larval behaviour during *Cln7* loss of function. Moreover, detecting the storage of glucose and lipids in larval tissue will contribute to understanding this regulation.

References:

1. Perera, R.M. and R. Zoncu, *The Lysosome as a Regulatory Hub.* Annu Rev Cell Dev Biol, 2016. **32**: p. 223-253.
2. Johnson, D.E., et al., *The position of lysosomes within the cell determines their luminal pH.* J Cell Biol, 2016. **212**(6): p. 677-92.
3. Luzio, J.P., et al., *The biogenesis of lysosomes and lysosome-related organelles.* Cold Spring Harb Perspect Biol, 2014. **6**(9): p. a016840.
4. Settembre, C., et al., *Signals from the lysosome: a control centre for cellular clearance and energy metabolism.* Nat Rev Mol Cell Biol, 2013. **14**(5): p. 283-96.
5. Kaushik, S. and A.M. Cuervo, *Chaperone-mediated autophagy: a unique way to enter the lysosome world.* Trends Cell Biol, 2012. **22**(8): p. 407-17.
6. Platt, F.M., B. Boland, and A.C. van der Spoel, *The cell biology of disease: lysosomal storage disorders: the cellular impact of lysosomal dysfunction.* J Cell Biol, 2012. **199**(5): p. 723-34.
7. Bajaj, L., et al., *Lysosome biogenesis in health and disease.* J Neurochem, 2019. **148**(5): p. 573-589.
8. Bonam, S.R., F. Wang, and S. Muller, *Lysosomes as a therapeutic target.* Nat Rev Drug Discov, 2019. **18**(12): p. 923-948.
9. Laplante, M. and D.M. Sabatini, *mTOR signaling in growth control and disease.* Cell, 2012. **149**(2): p. 274-93.
10. Inpanathan, S. and R.J. Botelho, *The Lysosome Signaling Platform: Adapting With the Times.* Front Cell Dev Biol, 2019. **7**: p. 113.
11. Kaur, J. and J. Debnath, *Autophagy at the crossroads of catabolism and anabolism.* Nat Rev Mol Cell Biol, 2015. **16**(8): p. 461-72.
12. Parmar, N. and F. Tamanoi, *Rheb G-Proteins and the Activation of mTORC1.* Enzymes, 2010. **27**: p. 39-56.
13. Betz, C. and M.N. Hall, *Where is mTOR and what is it doing there?* J Cell Biol, 2013. **203**(4): p. 563-74.
14. Hemmings, B.A. and D.F. Restuccia, *PI3K-PKB/Akt pathway.* Cold Spring Harb Perspect Biol, 2012. **4**(9): p. a011189.
15. Manning, B.D. and A. Toker, *AKT/PKB Signaling: Navigating the Network.* Cell, 2017. **169**(3): p. 381-405.
16. Huang, J., et al., *The TSC1-TSC2 complex is required for proper activation of mTOR complex 2.* Mol Cell Biol, 2008. **28**(12): p. 4104-15.
17. Zoncu, R., et al., *mTORC1 senses lysosomal amino acids through an inside-out mechanism that requires the vacuolar H(+)-ATPase.* Science, 2011. **334**(6056): p. 678-83.
18. Ogmundsdottir, M.H., et al., *Proton-assisted amino acid transporter PAT1 complexes with Rag GTPases and activates TORC1 on late endosomal and lysosomal membranes.* PLoS One, 2012. **7**(5): p. e36616.
19. Duran, R.V., et al., *Glutaminolysis activates Rag-mTORC1 signaling.* Mol Cell, 2012. **47**(3): p. 349-58.
20. Mukherjee, A.B., et al., *Emerging new roles of the lysosome and neuronal ceroid lipofuscinoses.* Mol Neurodegener, 2019. **14**(1): p. 4.
21. Song, Q., et al., *The emerging roles of vacuolar-type ATPase-dependent Lysosomal acidification in neurodegenerative diseases.* Transl Neurodegener, 2020. **9**(1): p. 17.
22. Zeng, J., O.S. Shirihai, and M.W. Grinstaff, *Modulating lysosomal pH: a molecular and nanoscale materials design perspective.* J Life Sci (Westlake Village), 2020. **2**(4): p. 25-37.
23. Tancini, B., et al., *Lysosomal Exocytosis: The Extracellular Role of an Intracellular Organelle.* Membranes (Basel), 2020. **10**(12).

24. Buratta, S., et al., *Lysosomal Exocytosis, Exosome Release and Secretory Autophagy: The Autophagic- and Endo-Lysosomal Systems Go Extracellular.* Int J Mol Sci, 2020. **21**(7).
25. Reddy, A., E.V. Caler, and N.W. Andrews, *Plasma membrane repair is mediated by Ca(2+)-regulated exocytosis of lysosomes.* Cell, 2001. **106**(2): p. 157-69.
26. Medina, D.L., et al., *Transcriptional activation of lysosomal exocytosis promotes cellular clearance.* Dev Cell, 2011. **21**(3): p. 421-30.
27. Wolfson, R.L., et al., *Sestrin2 is a leucine sensor for the mTORC1 pathway.* Science, 2016. **351**(6268): p. 43-8.
28. Xu, H. and D. Ren, *Lysosomal physiology.* Annu Rev Physiol, 2015. **77**: p. 57-80.
29. Cang, C., et al., *mTOR regulates lysosomal ATP-sensitive two-pore Na(+) channels to adapt to metabolic state.* Cell, 2013. **152**(4): p. 778-790.
30. Jin, N., M.J. Lang, and L.S. Weisman, *Phosphatidylinositol 3,5-bisphosphate: regulation of cellular events in space and time.* Biochem Soc Trans, 2016. **44**(1): p. 177-84.
31. Dong, X.P., et al., *The type IV mucolipidosis-associated protein TRPML1 is an endolysosomal iron release channel.* Nature, 2008. **455**(7215): p. 992-6.
32. Lamming, D.W. and L. Bar-Peled, *Lysosome: The metabolic signaling hub.* Traffic, 2019. **20**(1): p. 27-38.
33. Roczniak-Ferguson, A., et al., *The transcription factor TFEB links mTORC1 signaling to transcriptional control of lysosome homeostasis.* Sci Signal, 2012. **5**(228): p. ra42.
34. Settembre, C., et al., *A lysosome-to-nucleus signalling mechanism senses and regulates the lysosome via mTOR and TFEB.* EMBO J, 2012. **31**(5): p. 1095-108.
35. Palmieri, M., et al., *Characterization of the CLEAR network reveals an integrated control of cellular clearance pathways.* Hum Mol Genet, 2011. **20**(19): p. 3852-66.
36. Settembre, C., et al., *TFEB links autophagy to lysosomal biogenesis.* Science, 2011. **332**(6036): p. 1429-33.
37. Sambri, I., et al., *RagD auto-activating mutations impair MiT/TFE activity in kidney tubulopathy and cardiomyopathy syndrome.* Nat Commun, 2023. **14**(1): p. 2775.
38. Seok, S., et al., *Transcriptional regulation of autophagy by an FXR-CREB axis.* Nature, 2014. **516**(7529): p. 108-11.
39. Lee, J.M., et al., *Nutrient-sensing nuclear receptors coordinate autophagy.* Nature, 2014. **516**(7529): p. 112-5.
40. Napoli, M. and E.R. Flores, *The family that eats together stays together: new p53 family transcriptional targets in autophagy.* Genes Dev, 2013. **27**(9): p. 971-4.
41. Pike, L.R., et al., *Transcriptional up-regulation of ULK1 by ATF4 contributes to cancer cell survival.* Biochem J, 2013. **449**(2): p. 389-400.
42. Lim, C.Y. and R. Zoncu, *The lysosome as a command-and-control center for cellular metabolism.* J Cell Biol, 2016. **214**(6): p. 653-64.
43. Bowman, C.J., D.E. Ayer, and B.D. Dynlacht, *Foxk proteins repress the initiation of starvation-induced atrophy and autophagy programs.* Nat Cell Biol, 2014. **16**(12): p. 1202-14.
44. Schwake, M., B. Schroder, and P. Saftig, *Lysosomal membrane proteins and their central role in physiology.* Traffic, 2013. **14**(7): p. 739-48.
45. Fukuda, M., *Lysosomal membrane glycoproteins. Structure, biosynthesis, and intracellular trafficking.* J Biol Chem, 1991. **266**(32): p. 21327-30.
46. Loaeza-Reyes, K.J., et al., *An Overview of Glycosylation and its Impact on Cardiovascular Health and Disease.* Front Mol Biosci, 2021. **8**: p. 751637.
47. Ohtsubo, K. and J.D. Marth, *Glycosylation in cellular mechanisms of health and disease.* Cell, 2006. **126**(5): p. 855-67.
48. Eichler, J., *Protein glycosylation.* Curr Biol, 2019. **29**(7): p. R229-R231.
49. Pereira, M.S., et al., *Glycans as Key Checkpoints of T Cell Activity and Function.* Front Immunol, 2018. **9**: p. 2754.

50. Hiraoka, M., et al., *Role of N-glycosylation of human lysosomal phospholipase A2 for the formation of catalytically active enzyme.* J Lipid Res, 2013. **54**(11): p. 3098-105.
51. Henell, F., J.L. Ericsson, and H. Glaumann, *Degradation of phagocytosed lysosomes by Kupffer cell lysosomes.* Lab Invest, 1983. **48**(5): p. 556-64.
52. Ferreira, C.R. and W.A. Gahl, *Lysosomal storage diseases.* Transl Sci Rare Dis, 2017. **2**(1-2): p. 1-71.
53. Sun, A., *Lysosomal storage disease overview.* Ann Transl Med, 2018. **6**(24): p. 476.
54. Marques, A.R.A. and P. Saftig, *Lysosomal storage disorders - challenges, concepts and avenues for therapy: beyond rare diseases.* J Cell Sci, 2019. **132**(2).
55. Stepien, K.M., et al., *Secondary Mitochondrial Dysfunction as a Cause of Neurodegenerative Dysfunction in Lysosomal Storage Diseases and an Overview of Potential Therapies.* Int J Mol Sci, 2022. **23**(18).
56. Kielian, T., *Lysosomal storage disorders: pathology within the lysosome and beyond.* J Neurochem, 2019. **148**(5): p. 568-572.
57. Rebiai, R., et al., *Synaptic Function and Dysfunction in Lysosomal Storage Diseases.* Front Cell Neurosci, 2021. **15**: p. 619777.
58. Poswar, F.O., et al., *Lysosomal diseases: Overview on current diagnosis and treatment.* Genet Mol Biol, 2019. **42**(1 suppl 1): p. 165-177.
59. Zhang, Z., et al., *Role of lysosomes in physiological activities, diseases, and therapy.* J Hematol Oncol, 2021. **14**(1): p. 79.
60. Xiao, Q., et al., *Neuronal-Targeted TFEB Accelerates Lysosomal Degradation of APP, Reducing Abeta Generation and Amyloid Plaque Pathogenesis.* J Neurosci, 2015. **35**(35): p. 12137-51.
61. Schneider, L. and J. Zhang, *Lysosomal function in macromolecular homeostasis and bioenergetics in Parkinson's disease.* Mol Neurodegener, 2010. **5**: p. 14.
62. Deng, H., X. Xiu, and J. Jankovic, *Genetic convergence of Parkinson's disease and lysosomal storage disorders.* Mol Neurobiol, 2015. **51**(3): p. 1554-68.
63. Rama Rao, K.V. and T. Kielian, *Astrocytes and lysosomal storage diseases.* Neuroscience, 2016. **323**: p. 195-206.
64. Lieberman, A.P., et al., *Autophagy in lysosomal storage disorders.* Autophagy, 2012. **8**(5): p. 719-30.
65. Micsenyi, M.C., et al., *Lysosomal membrane permeability stimulates protein aggregate formation in neurons of a lysosomal disease.* J Neurosci, 2013. **33**(26): p. 10815-27.
66. Rodriguez-Muela, N., et al., *Lysosomal membrane permeabilization and autophagy blockade contribute to photoreceptor cell death in a mouse model of retinitis pigmentosa.* Cell Death Differ, 2015. **22**(3): p. 476-87.
67. Onyenwoke, R.U. and J.E. Brenman, *Lysosomal Storage Diseases-Regulating Neurodegeneration.* J Exp Neurosci, 2015. **9**(Suppl 2): p. 81-91.
68. Vitner, E.B., F.M. Platt, and A.H. Futerman, *Common and uncommon pathogenic cascades in lysosomal storage diseases.* J Biol Chem, 2010. **285**(27): p. 20423-7.
69. Sharma, J., et al., *Lysosomes and Brain Health.* Annu Rev Neurosci, 2018. **41**: p. 255-276.
70. Walkley, S.U., *Secondary accumulation of gangliosides in lysosomal storage disorders.* Semin Cell Dev Biol, 2004. **15**(4): p. 433-44.
71. Sandhoff, K. and T. Kolter, *Biosynthesis and degradation of mammalian glycosphingolipids.* Philos Trans R Soc Lond B Biol Sci, 2003. **358**(1433): p. 847-61.
72. Ballabio, A. and V. Gieselmann, *Lysosomal disorders: from storage to cellular damage.* Biochim Biophys Acta, 2009. **1793**(4): p. 684-96.
73. Shen, D., et al., *Lipid storage disorders block lysosomal trafficking by inhibiting a TRP channel and lysosomal calcium release.* Nat Commun, 2012. **3**: p. 731.
74. Prat Castro, S., et al., *Neurodegenerative Lysosomal Storage Disorders: TPC2 Comes to the Rescue!* Cells, 2022. **11**(18).

75. Ruivo, R., et al., *Molecular and cellular basis of lysosomal transmembrane protein dysfunction.* Biochim Biophys Acta, 2009. **1793**(4): p. 636-49.
76. Wu, L., et al., *TMEM175: A lysosomal ion channel associated with neurological diseases.* Neurobiol Dis, 2023. **185**: p. 106244.
77. Wang, H., et al., *Advances in Drug Discovery Targeting Lysosomal Membrane Proteins.* Pharmaceuticals (Basel), 2023. **16**(4).
78. Tang, T., B. Jian, and Z. Liu, *Transmembrane Protein 175, a Lysosomal Ion Channel Related to Parkinson's Disease.* Biomolecules, 2023. **13**(5).
79. Palomba, N.P., et al., *Common and Rare Variants in TMEM175 Gene Concur to the Pathogenesis of Parkinson's Disease in Italian Patients.* Mol Neurobiol, 2023. **60**(4): p. 2150-2173.
80. Huizing, M. and W.A. Gahl, *Inherited disorders of lysosomal membrane transporters.* Biochim Biophys Acta Biomembr, 2020. **1862**(12): p. 183336.
81. Mirza, M., et al., *The CLN3 gene and protein: What we know.* Mol Genet Genomic Med, 2019. **7**(12): p. e859.
82. Platt, N., et al., *Immune dysfunction in Niemann-Pick disease type C.* J Neurochem, 2016. **136 Suppl 1**: p. 74-80.
83. Bernardo, A., et al., *Myelin Defects in Niemann-Pick Type C Disease: Mechanisms and Possible Therapeutic Perspectives.* Int J Mol Sci, 2021. **22**(16).
84. Goyal, M. and A. Gupta, *Lysosomal Storage Disorders: Clinical, Biochemical and molecular profile from Rare disease centre, India.* Ann Indian Acad Neurol, 2021. **24**(5): p. 686-692.
85. Riboldi, G.M. and A.B. Di Fonzo, *GBA, Gaucher Disease, and Parkinson's Disease: From Genetic to Clinic to New Therapeutic Approaches.* Cells, 2019. **8**(4).
86. Glick, D., S. Barth, and K.F. Macleod, *Autophagy: cellular and molecular mechanisms.* J Pathol, 2010. **221**(1): p. 3-12.
87. Yorimitsu, T. and D.J. Klionsky, *Autophagy: molecular machinery for self-eating.* Cell Death Differ, 2005. **12 Suppl 2**: p. 1542-52.
88. Parzych, K.R. and D.J. Klionsky, *An overview of autophagy: morphology, mechanism, and regulation.* Antioxid Redox Signal, 2014. **20**(3): p. 460-73.
89. Yang, Z. and D.J. Klionsky, *Mammalian autophagy: core molecular machinery and signaling regulation.* Curr Opin Cell Biol, 2010. **22**(2): p. 124-31.
90. Wen, X. and D.J. Klionsky, *An overview of macroautophagy in yeast.* J Mol Biol, 2016. **428**(9 Pt A): p. 1681-99.
91. Park, H., J.H. Kang, and S. Lee, *Autophagy in Neurodegenerative Diseases: A Hunter for Aggregates.* Int J Mol Sci, 2020. **21**(9).
92. Marzella, L., J. Ahlberg, and H. Glaumann, *Autophagy, heterophagy, microautophagy and crinophagy as the means for intracellular degradation.* Virchows Arch B Cell Pathol Incl Mol Pathol, 1981. **36**(2-3): p. 219-34.
93. Feng, Y., et al., *The machinery of macroautophagy.* Cell Res, 2014. **24**(1): p. 24-41.
94. He, C. and D.J. Klionsky, *Regulation mechanisms and signaling pathways of autophagy.* Annu Rev Genet, 2009. **43**: p. 67-93.
95. Stephan, J.S., et al., *The Tor and cAMP-dependent protein kinase signaling pathways coordinately control autophagy in Saccharomyces cerevisiae.* Autophagy, 2010. **6**(2): p. 294-5.
96. Hoyer-Hansen, M., et al., *Control of macroautophagy by calcium, calmodulin-dependent kinase kinase-beta, and Bcl-2.* Mol Cell, 2007. **25**(2): p. 193-205.
97. Hoyer-Hansen, M. and M. Jaattela, *Connecting endoplasmic reticulum stress to autophagy by unfolded protein response and calcium.* Cell Death Differ, 2007. **14**(9): p. 1576-82.
98. Ding, W.X., et al., *Differential effects of endoplasmic reticulum stress-induced autophagy on cell survival.* J Biol Chem, 2007. **282**(7): p. 4702-4710.

99. Bejarano, E. and A.M. Cuervo, *Chaperone-mediated autophagy.* Proc Am Thorac Soc, 2010. **7**(1): p. 29-39.
100. Orenstein, S.J. and A.M. Cuervo, *Chaperone-mediated autophagy: molecular mechanisms and physiological relevance.* Semin Cell Dev Biol, 2010. **21**(7): p. 719-26.
101. Arias, E. and A.M. Cuervo, *Chaperone-mediated autophagy in protein quality control.* Curr Opin Cell Biol, 2011. **23**(2): p. 184-9.
102. Cao, J., et al., *Endo-lysosomal pathway and ubiquitin-proteasome system dysfunction in Alzheimer's disease pathogenesis.* Neurosci Lett, 2019. **703**: p. 68-78.
103. Wong, Y.C., D. Ysselstein, and D. Krainc, *Mitochondria-lysosome contacts regulate mitochondrial fission via RAB7 GTP hydrolysis.* Nature, 2018. **554**(7692): p. 382-386.
104. de la Mata, M., et al., *Mitochondrial Dysfunction in Lysosomal Storage Disorders.* Diseases, 2016. **4**(4).
105. Slater, C.R., *The Structure of Human Neuromuscular Junctions: Some Unanswered Molecular Questions.* Int J Mol Sci, 2017. **18**(10).
106. Ratliff, W.A., et al., *Neuromuscular Junction Morphology and Gene Dysregulation in the Wobbler Model of Spinal Neurodegeneration.* J Mol Neurosci, 2018. **66**(1): p. 114-120.
107. Kuo, I.Y. and B.E. Ehrlich, *Signaling in muscle contraction.* Cold Spring Harb Perspect Biol, 2015. **7**(2): p. a006023.
108. Rodriguez Cruz, P.M., et al., *The Neuromuscular Junction in Health and Disease: Molecular Mechanisms Governing Synaptic Formation and Homeostasis.* Front Mol Neurosci, 2020. **13**: p. 610964.
109. Hirsch, N.P., *Neuromuscular junction in health and disease.* Br J Anaesth, 2007. **99**(1): p. 132-8.
110. Badawi, Y. and H. Nishimune, *Presynaptic active zones of mammalian neuromuscular junctions: Nanoarchitecture and selective impairments in aging.* Neurosci Res, 2018. **127**: p. 78-88.
111. Rizzoli, S.O., *Synaptic vesicle recycling: steps and principles.* EMBO J, 2014. **33**(8): p. 788-822.
112. Boeckers, T.M., *The postsynaptic density.* Cell Tissue Res, 2006. **326**(2): p. 409-22.
113. Sheng, M. and E. Kim, *The postsynaptic organization of synapses.* Cold Spring Harb Perspect Biol, 2011. **3**(12).
114. Wishart, T.M., S.H. Parson, and T.H. Gillingwater, *Synaptic vulnerability in neurodegenerative disease.* J Neuropathol Exp Neurol, 2006. **65**(8): p. 733-9.
115. Taoufik, E., et al., *Synaptic dysfunction in neurodegenerative and neurodevelopmental diseases: an overview of induced pluripotent stem-cell-based disease models.* Open Biol, 2018. **8**(9).
116. Para, C., P. Bose, and A.V. Pshezhetsky, *Neuropathophysiology of Lysosomal Storage Diseases: Synaptic Dysfunction as a Starting Point for Disease Progression.* J Clin Med, 2020. **9**(3).
117. Connolly, K.J., et al., *The neuronal ceroid lipofuscinosis protein Cln7 functions in the postsynaptic cell to regulate synapse development.* Sci Rep, 2019. **9**(1): p. 15592.
118. Ardiles, A.O., et al., *Molecular and Cellular Mechanisms of Synaptopathies.* Neural Plast, 2017. **2017**: p. 2643943.
119. Lepeta, K., et al., *Synaptopathies: synaptic dysfunction in neurological disorders - A review from students to students.* J Neurochem, 2016. **138**(6): p. 785-805.
120. Lim, J. and Z. Yue, *Neuronal aggregates: formation, clearance, and spreading.* Dev Cell, 2015. **32**(4): p. 491-501.
121. Klaips, C.L., G.G. Jayaraj, and F.U. Hartl, *Pathways of cellular proteostasis in aging and disease.* J Cell Biol, 2018. **217**(1): p. 51-63.
122. Henstridge, C.M., M. Tzioras, and R.C. Paolicelli, *Glial Contribution to Excitatory and Inhibitory Synapse Loss in Neurodegeneration.* Front Cell Neurosci, 2019. **13**: p. 63.

123. Subramanian, J. and M.E. Tremblay, *Editorial: Synaptic Loss and Neurodegeneration.* Front Cell Neurosci, 2021. **15**: p. 681029.
124. Henstridge, C.M., E. Pickett, and T.L. Spires-Jones, *Synaptic pathology: A shared mechanism in neurological disease.* Ageing Res Rev, 2016. **28**: p. 72-84.
125. Zoghbi, H.Y. and M.F. Bear, *Synaptic dysfunction in neurodevelopmental disorders associated with autism and intellectual disabilities.* Cold Spring Harb Perspect Biol, 2012. **4**(3).
126. Bae, J.R. and S.H. Kim, *Synapses in neurodegenerative diseases.* BMB Rep, 2017. **50**(5): p. 237-246.
127. Jalanko, A. and T. Braulke, *Neuronal ceroid lipofuscinoses.* Biochim Biophys Acta, 2009. **1793**(4): p. 697-709.
128. Mohammed, A., et al., *in vivo localization of the neuronal ceroid lipofuscinosis proteins, CLN3 and CLN7, at endogenous expression levels.* Neurobiol Dis, 2017. **103**: p. 123-132.
129. Haltia, M., *The neuronal ceroid-lipofuscinoses.* J Neuropathol Exp Neurol, 2003. **62**(1): p. 1-13.
130. Carcel-Trullols, J., A.D. Kovacs, and D.A. Pearce, *Cell biology of the NCL proteins: What they do and don't do.* Biochim Biophys Acta, 2015. **1852**(10 Pt B): p. 2242-55.
131. Kollmann, K., et al., *Cell biology and function of neuronal ceroid lipofuscinosis-related proteins.* Biochim Biophys Acta, 2013. **1832**(11): p. 1866-81.
132. Mole, S.E. and S.L. Cotman, *Genetics of the neuronal ceroid lipofuscinoses (Batten disease).* Biochim Biophys Acta, 2015. **1852**(10 Pt B): p. 2237-41.
133. Williams, R.E., et al., *Diagnosis of the neuronal ceroid lipofuscinoses: an update.* Biochim Biophys Acta, 2006. **1762**(10): p. 865-72.
134. Sardiello, M., *Transcription factor EB: from master coordinator of lysosomal pathways to candidate therapeutic target in degenerative storage diseases.* Ann N Y Acad Sci, 2016. **1371**(1): p. 3-14.
135. Martini-Stoica, H., et al., *The Autophagy-Lysosomal Pathway in Neurodegeneration: A TFEB Perspective.* Trends Neurosci, 2016. **39**(4): p. 221-234.
136. Zhang, W., et al., *Regulation of TFEB activity and its potential as a therapeutic target against kidney diseases.* Cell Death Discov, 2020. **6**: p. 32.
137. Muzaffar, N.E. and D.A. Pearce, *Analysis of NCL Proteins from an Evolutionary Standpoint.* Curr Genomics, 2008. **9**(2): p. 115-36.
138. Danyukova, T., et al., *Loss of CLN7 results in depletion of soluble lysosomal proteins and impaired mTOR reactivation.* Hum Mol Genet, 2018. **27**(10): p. 1711-1722.
139. Filocamo, M. and A. Morrone, *Lysosomal storage disorders: molecular basis and laboratory testing.* Hum Genomics, 2011. **5**(3): p. 156-69.
140. Steenhuis, P., et al., *Proteolytic cleavage of the disease-related lysosomal membrane glycoprotein CLN7.* Biochim Biophys Acta, 2012. **1822**(10): p. 1617-28.
141. Kousi, M., et al., *Mutations in CLN7/MFSD8 are a common cause of variant late-infantile neuronal ceroid lipofuscinosis.* Brain, 2009. **132**(Pt 3): p. 810-9.
142. Siintola, E., et al., *The novel neuronal ceroid lipofuscinosis gene MFSD8 encodes a putative lysosomal transporter.* Am J Hum Genet, 2007. **81**(1): p. 136-46.
143. Sharifi, A., et al., *Expression and lysosomal targeting of CLN7, a major facilitator superfamily transporter associated with variant late-infantile neuronal ceroid lipofuscinosis.* Hum Mol Genet, 2010. **19**(22): p. 4497-514.
144. Khan, K.N., et al., *Specific Alleles of CLN7/MFSD8, a Protein That Localizes to Photoreceptor Synaptic Terminals, Cause a Spectrum of Nonsyndromic Retinal Dystrophy.* Invest Ophthalmol Vis Sci, 2017. **58**(7): p. 2906-2914.
145. Koulen, P., et al., *Immunocytochemical localization of the postsynaptic density protein PSD-95 in the mammalian retina.* J Neurosci, 1998. **18**(23): p. 10136-49.

146. Hamanaka, Y. and I.A. Meinertzhagen, *Immunocytochemical localization of synaptic proteins to photoreceptor synapses of Drosophila melanogaster.* J Comp Neurol, 2010. **518**(7): p. 1133-55.
147. Damme, M., et al., *Gene disruption of Mfsd8 in mice provides the first animal model for CLN7 disease.* Neurobiol Dis, 2014. **65**: p. 12-24.
148. McBride, J.L., et al., *Discovery of a CLN7 model of Batten disease in non-human primates.* Neurobiol Dis, 2018. **119**: p. 65-78.
149. Kousi, M., A.E. Lehesjoki, and S.E. Mole, *Update of the mutation spectrum and clinical correlations of over 360 mutations in eight genes that underlie the neuronal ceroid lipofuscinoses.* Hum Mutat, 2012. **33**(1): p. 42-63.
150. Brandenstein, L., et al., *Lysosomal dysfunction and impaired autophagy in a novel mouse model deficient for the lysosomal membrane protein Cln7.* Hum Mol Genet, 2016. **25**(4): p. 777-91.
151. Herculano-Houzel, S., *The human brain in numbers: a linearly scaled-up primate brain.* Front Hum Neurosci, 2009. **3**: p. 31.
152. Jankowiak, W., et al., *Retinal Degeneration in Mice Deficient in the Lysosomal Membrane Protein CLN7.* Invest Ophthalmol Vis Sci, 2016. **57**(11): p. 4989-4998.
153. von Kleist, L., et al., *A newly generated neuronal cell model of CLN7 disease reveals aberrant lysosome motility and impaired cell survival.* Mol Genet Metab, 2019. **126**(2): p. 196-205.
154. Heuser, J., *Changes in lysosome shape and distribution correlated with changes in cytoplasmic pH.* J Cell Biol, 1989. **108**(3): p. 855-64.
155. Li, X., et al., *A molecular mechanism to regulate lysosome motility for lysosome positioning and tubulation.* Nat Cell Biol, 2016. **18**(4): p. 404-17.
156. Esbjorner, E.K., et al., *Direct observations of amyloid beta self-assembly in live cells provide insights into differences in the kinetics of Abeta(1-40) and Abeta(1-42) aggregation.* Chem Biol, 2014. **21**(6): p. 732-42.
157. Kuperstein, I., et al., *Neurotoxicity of Alzheimer's disease Abeta peptides is induced by small changes in the Abeta42 to Abeta40 ratio.* EMBO J, 2010. **29**(19): p. 3408-20.
158. Kodam, A., et al., *Altered levels and distribution of amyloid precursor protein and its processing enzymes in Niemann-Pick type C1-deficient mouse brains.* Glia, 2010. **58**(11): p. 1267-81.
159. Ashwini, A., et al., *Neuronal ceroid lipofuscinosis associated with an MFSD8 mutation in Chihuahuas.* Mol Genet Metab, 2016. **118**(4): p. 326-32.
160. Faller, K.M., et al., *The neuronal ceroid lipofuscinoses: Opportunities from model systems.* Biochim Biophys Acta, 2015. **1852**(10 Pt B): p. 2267-78.
161. Lopez-Fabuel, I., et al., *Aberrant upregulation of the glycolytic enzyme PFKFB3 in CLN7 neuronal ceroid lipofuscinosis.* Nat Commun, 2022. **13**(1): p. 536.
162. Wang, Y., et al., *CLN7 is an organellar chloride channel regulating lysosomal function.* Sci Adv, 2021. **7**(51): p. eabj9608.
163. Roux, K.J., et al., *A promiscuous biotin ligase fusion protein identifies proximal and interacting proteins in mammalian cells.* J Cell Biol, 2012. **196**(6): p. 801-10.
164. Kim, D.I., et al., *An improved smaller biotin ligase for BioID proximity labeling.* Mol Biol Cell, 2016. **27**(8): p. 1188-96.
165. Kim, D.I. and K.J. Roux, *Filling the Void: Proximity-Based Labeling of Proteins in Living Cells.* Trends Cell Biol, 2016. **26**(11): p. 804-817.
166. Brand, A.H. and N. Perrimon, *Targeted gene expression as a means of altering cell fates and generating dominant phenotypes.* Development, 1993. **118**(2): p. 401-15.
167. Hahn, S. and E.T. Young, *Transcriptional regulation in Saccharomyces cerevisiae: transcription factor regulation and function, mechanisms of initiation, and roles of activators and coactivators.* Genetics, 2011. **189**(3): p. 705-36.

168. Casas-Tinto, S., M. Arnes, and A. Ferrus, *Drosophila enhancer-Gal4 lines show ectopic expression during development.* R Soc Open Sci, 2017. **4**(3): p. 170039.
169. Halpern, M.E., et al., *Gal4/UAS transgenic tools and their application to zebrafish.* Zebrafish, 2008. **5**(2): p. 97-110.
170. Perrimon, N., J.Q. Ni, and L. Perkins, *In vivo RNAi: today and tomorrow.* Cold Spring Harb Perspect Biol, 2010. **2**(8): p. a003640.
171. Phelps, C.B. and A.H. Brand, *Ectopic gene expression in Drosophila using GAL4 system.* Methods, 1998. **14**(4): p. 367-79.
172. Beumer, K., et al., *Integrins regulate DLG/FAS2 via a CaM kinase II-dependent pathway to mediate synapse elaboration and stabilization during postembryonic development.* Development, 2002. **129**(14): p. 3381-91.
173. Lin, S.H. and G. Guidotti, *Purification of membrane proteins.* Methods Enzymol, 2009. **463**: p. 619-29.
174. Choi-Rhee, E., H. Schulman, and J.E. Cronan, *Promiscuous protein biotinylation by Escherichia coli biotin protein ligase.* Protein Sci, 2004. **13**(11): p. 3043-50.
175. Manaka, J., et al., *Draper-mediated and phosphatidylserine-independent phagocytosis of apoptotic cells by Drosophila hemocytes/macrophages.* J Biol Chem, 2004. **279**(46): p. 48466-76.
176. Hesketh, S.J., et al., *Styrene maleic-acid lipid particles (SMALPs) into detergent or amphipols: An exchange protocol for membrane protein characterisation.* Biochim Biophys Acta Biomembr, 2020. **1862**(5): p. 183192.
177. Chen, K., et al., *The 4.1 protein coracle mediates subunit-selective anchoring of Drosophila glutamate receptors to the postsynaptic actin cytoskeleton.* J Neurosci, 2005. **25**(28): p. 6667-75.
178. Lamb, R.S., et al., *Drosophila coracle, a member of the protein 4.1 superfamily, has essential structural functions in the septate junctions and developmental functions in embryonic and adult epithelial cells.* Mol Biol Cell, 1998. **9**(12): p. 3505-19.
179. McDonough, A.A., K. Geering, and R.A. Farley, *The sodium pump needs its beta subunit.* FASEB J, 1990. **4**(6): p. 1598-605.
180. Roy, M., E. Sivan-Loukianova, and D.F. Eberl, *Cell-type-specific roles of Na+/K+ ATPase subunits in Drosophila auditory mechanosensation.* Proc Natl Acad Sci U S A, 2013. **110**(1): p. 181-6.
181. Hoang, B. and A. Chiba, *Genetic analysis on the role of integrin during axon guidance in Drosophila.* J Neurosci, 1998. **18**(19): p. 7847-55.
182. Urbano, J.M., et al., *PS integrins and laminins: key regulators of cell migration during Drosophila embryogenesis.* PLoS One, 2011. **6**(9): p. e23893.
183. Cao, F., et al., *Lethal (2) giant larvae: an indispensable regulator of cell polarity and cancer development.* Int J Biol Sci, 2015. **11**(4): p. 380-9.
184. Oshima, K. and R.G. Fehon, *Analysis of protein dynamics within the septate junction reveals a highly stable core protein complex that does not include the basolateral polarity protein Discs large.* J Cell Sci, 2011. **124**(Pt 16): p. 2861-71.
185. Woods, D.F., et al., *Dlg protein is required for junction structure, cell polarity, and proliferation control in Drosophila epithelia.* J Cell Biol, 1996. **134**(6): p. 1469-82.
186. Mallik, B., et al., *Regulation of neuromuscular junction organization by Rab2 and its effector ICA69 in Drosophila.* Development, 2017. **144**(11): p. 2032-2044.
187. Pielage, J., R.D. Fetter, and G.W. Davis, *A postsynaptic spectrin scaffold defines active zone size, spacing, and efficacy at the Drosophila neuromuscular junction.* J Cell Biol, 2006. **175**(3): p. 491-503.
188. Dollar, G., et al., *Unique and Overlapping Functions of Formins Frl and DAAM During Ommatidial Rotation and Neuronal Development in Drosophila.* Genetics, 2016. **202**(3): p. 1135-51.

189. Gombos, R., et al., *The Formin DAAM Functions as Molecular Effector of the Planar Cell Polarity Pathway during Axonal Development in Drosophila.* J Neurosci, 2015. **35**(28): p. 10154-67.
190. Havlioglu, N., et al., *Slit proteins, potential endogenous modulators of inflammation.* J Neurovirol, 2002. **8**(6): p. 486-95.
191. Tong, M., et al., *The Role of the Slit/Robo Signaling Pathway.* J Cancer, 2019. **10**(12): p. 2694-2705.
192. Sun, B. and P.M. Salvaterra, *Two Drosophila nervous system antigens, Nervana 1 and 2, are homologous to the beta subunit of Na+,K(+)-ATPase.* Proc Natl Acad Sci U S A, 1995. **92**(12): p. 5396-400.
193. Ojelade, S.A., S.F. Acevedo, and A. Rothenfluh, *The role of the actin cytoskeleton in regulating Drosophila behavior.* Rev Neurosci, 2013. **24**(5): p. 471-84.
194. Lamprecht, R. and J. LeDoux, *Structural plasticity and memory.* Nat Rev Neurosci, 2004. **5**(1): p. 45-54.
195. Landis, D.M. and T.S. Reese, *Cytoplasmic organization in cerebellar dendritic spines.* J Cell Biol, 1983. **97**(4): p. 1169-78.
196. Auld, V.J., et al., *Gliotactin, a novel transmembrane protein on peripheral glia, is required to form the blood-nerve barrier in Drosophila.* Cell, 1995. **81**(5): p. 757-67.
197. Baumgartner, S., et al., *A Drosophila neurexin is required for septate junction and blood-nerve barrier formation and function.* Cell, 1996. **87**(6): p. 1059-68.
198. Stork, T., et al., *Organization and function of the blood-brain barrier in Drosophila.* J Neurosci, 2008. **28**(3): p. 587-97.
199. Huang, Y. and M. Stern, *In vivo properties of the Drosophila inebriated-encoded neurotransmitter transporter.* J Neurosci, 2002. **22**(5): p. 1698-708.
200. Rival, T., et al., *Physiological requirement for the glutamate transporter dEAAT1 at the adult Drosophila neuromuscular junction.* J Neurobiol, 2006. **66**(10): p. 1061-74.
201. Pandey, U.B. and C.D. Nichols, *Human disease models in Drosophila melanogaster and the role of the fly in therapeutic drug discovery.* Pharmacol Rev, 2011. **63**(2): p. 411-36.
202. Chen, K. and D.E. Featherstone, *Discs-large (DLG) is clustered by presynaptic innervation and regulates postsynaptic glutamate receptor subunit composition in Drosophila.* BMC Biol, 2005. **3**: p. 1.
203. Gorczyca, D., et al., *Postsynaptic membrane addition depends on the Discs-Large-interacting t-SNARE Gtaxin.* J Neurosci, 2007. **27**(5): p. 1033-44.
204. Budnik, V., et al., *Regulation of synapse structure and function by the Drosophila tumor suppressor gene dlg.* Neuron, 1996. **17**(4): p. 627-40.
205. Guan, B., et al., *The Drosophila tumor suppressor gene, dlg, is involved in structural plasticity at a glutamatergic synapse.* Curr Biol, 1996. **6**(6): p. 695-706.
206. Thomas, U., et al., *Synaptic targeting and localization of discs-large is a stepwise process controlled by different domains of the protein.* Curr Biol, 2000. **10**(18): p. 1108-17.
207. Zhang, R., et al., *Spectrin: structure, function and disease.* Sci China Life Sci, 2013. **56**(12): p. 1076-85.
208. Susuki, K., et al., *Glial betaII Spectrin Contributes to Paranode Formation and Maintenance.* J Neurosci, 2018. **38**(27): p. 6063-6075.
209. Derbala, M.H., et al., *The role of betaII spectrin in cardiac health and disease.* Life Sci, 2018. **192**: p. 278-285.
210. Unudurthi, S.D., et al., *betaIV-Spectrin regulates STAT3 targeting to tune cardiac response to pressure overload.* J Clin Invest, 2018. **128**(12): p. 5561-5572.
211. Barbarino, F., et al., *Targeting spectrin redox switches to regulate the mechanoproperties of red blood cells.* Biol Chem, 2021. **402**(3): p. 317-331.

212. Ciullini Mannurita, S., et al., *Case Report: Signal Transducer and Activator of Transcription 3 Gain-of-Function and Spectrin Deficiency: A Life-Threatening Case of Severe Hemolytic Anemia.* Front Immunol, 2020. **11**: p. 620046.
213. Branon, T.C., et al., *Efficient proximity labeling in living cells and organisms with TurboID.* Nat Biotechnol, 2018. **36**(9): p. 880-887.
214. Schwartz, M.A., *Integrins and extracellular matrix in mechanotransduction.* Cold Spring Harb Perspect Biol, 2010. **2**(12): p. a005066.
215. Clyman, R.I., F. Mauray, and R.H. Kramer, *Beta 1 and beta 3 integrins have different roles in the adhesion and migration of vascular smooth muscle cells on extracellular matrix.* Exp Cell Res, 1992. **200**(2): p. 272-84.
216. Zhang, Y., et al., *TurboID-Based Proximity Labeling for In Planta Identification of Protein-Protein Interaction Networks.* J Vis Exp, 2020(159).
217. Conlon, I. and M. Raff, *Size control in animal development.* Cell, 1999. **96**(2): p. 235-44.
218. Colombani, J., et al., *A nutrient sensor mechanism controls Drosophila growth.* Cell, 2003. **114**(6): p. 739-49.
219. Texada, M.J., T. Koyama, and K. Rewitz, *Regulation of Body Size and Growth Control.* Genetics, 2020. **216**(2): p. 269-313.
220. May, C.M., A. Doroszuk, and B.J. Zwaan, *The effect of developmental nutrition on life span and fecundity depends on the adult reproductive environment in Drosophila melanogaster.* Ecol Evol, 2015. **5**(6): p. 1156-68.
221. Rehman, N. and J. Varghese, *Larval nutrition influences adult fat stores and starvation resistance in Drosophila.* PLoS One, 2021. **16**(2): p. e0247175.
222. Tu, M.P. and M. Tatar, *Juvenile diet restriction and the aging and reproduction of adult Drosophila melanogaster.* Aging Cell, 2003. **2**(6): p. 327-33.
223. Monaghan, P., *Early growth conditions, phenotypic development and environmental change.* Philos Trans R Soc Lond B Biol Sci, 2008. **363**(1497): p. 1635-45.
224. Botchlett, R., et al., *Nutritional approaches for managing obesity-associated metabolic diseases.* J Endocrinol, 2017. **233**(3): p. R145-R171.
225. Green, P., A.Y. Hartenstein, and V. Hartenstein, *The embryonic development of the Drosophila visual system.* Cell Tissue Res, 1993. **273**(3): p. 583-98.
226. Amodeo, A.A. and J.M. Skotheim, *Cell-Size Control.* Cold Spring Harb Perspect Biol, 2016. **8**(4): p. a019083.
227. Modi, S. and A. Singh, *Controlling organism size by regulating constituent cell numbers.* Proc IEEE Conf Decis Control, 2018. **2018**: p. 2685-2690.
228. Tennessen, J.M. and C.S. Thummel, *Coordinating growth and maturation - insights from Drosophila.* Curr Biol, 2011. **21**(18): p. R750-7.
229. Thummel, C.S., *Molecular mechanisms of developmental timing in C. elegans and Drosophila.* Dev Cell, 2001. **1**(4): p. 453-65.
230. Koyama, T., C.C. Mendes, and C.K. Mirth, *Mechanisms regulating nutrition-dependent developmental plasticity through organ-specific effects in insects.* Front Physiol, 2013. **4**: p. 263.
231. Michaelson, D., et al., *Insulin signaling promotes germline proliferation in C. elegans.* Development, 2010. **137**(4): p. 671-80.
232. Korta, D.Z., S. Tuck, and E.J. Hubbard, *S6K links cell fate, cell cycle and nutrient response in C. elegans germline stem/progenitor cells.* Development, 2012. **139**(5): p. 859-70.
233. Wilcox, G., *Insulin and insulin resistance.* Clin Biochem Rev, 2005. **26**(2): p. 19-39.
234. DiAngelo, J.R. and M.J. Birnbaum, *Regulation of fat cell mass by insulin in Drosophila melanogaster.* Mol Cell Biol, 2009. **29**(24): p. 6341-52.
235. Broughton, S.J., et al., *Longer lifespan, altered metabolism, and stress resistance in Drosophila from ablation of cells making insulin-like ligands.* Proc Natl Acad Sci U S A, 2005. **102**(8): p. 3105-10.

236. Brogiolo, W., et al., *An evolutionarily conserved function of the Drosophila insulin receptor and insulin-like peptides in growth control.* Curr Biol, 2001. **11**(4): p. 213-21.
237. Ikeya, T., et al., *Nutrient-dependent expression of insulin-like peptides from neuroendocrine cells in the CNS contributes to growth regulation in Drosophila.* Curr Biol, 2002. **12**(15): p. 1293-300.
238. Bohni, R., et al., *Autonomous control of cell and organ size by CHICO, a Drosophila homolog of vertebrate IRS1-4.* Cell, 1999. **97**(7): p. 865-75.
239. Britton, J.S., et al., *Drosophila's insulin/PI3-kinase pathway coordinates cellular metabolism with nutritional conditions.* Dev Cell, 2002. **2**(2): p. 239-49.
240. Matsuoka, S. and M. Ueda, *Mutual inhibition between PTEN and PIP3 generates bistability for polarity in motile cells.* Nat Commun, 2018. **9**(1): p. 4481.
241. Ling, N.X.Y., et al., *mTORC1 directly inhibits AMPK to promote cell proliferation under nutrient stress.* Nat Metab, 2020. **2**(1): p. 41-49.
242. Partridge, L., et al., *Ageing in Drosophila: the role of the insulin/Igf and TOR signalling network.* Exp Gerontol, 2011. **46**(5): p. 376-81.
243. Gonzalez, A. and M.N. Hall, *Nutrient sensing and TOR signaling in yeast and mammals.* EMBO J, 2017. **36**(4): p. 397-408.
244. Naganos, S., et al., *Learning defects in Drosophila growth restricted chico mutants are caused by attenuated adenylyl cyclase activity.* Mol Brain, 2016. **9**: p. 37.
245. Wullschleger, S., R. Loewith, and M.N. Hall, *TOR signaling in growth and metabolism.* Cell, 2006. **124**(3): p. 471-84.
246. Gough, N.R., *Focus issue: TOR signaling, a tale of two complexes.* Sci Signal, 2012. **5**(217): p. eg4.
247. Hill, A., et al., *Redesigning TOR Kinase to Explore the Structural Basis for TORC1 and TORC2 Assembly.* Biomolecules, 2018. **8**(2).
248. Gonzalez, S. and C. Rallis, *The TOR Signaling Pathway in Spatial and Temporal Control of Cell Size and Growth.* Front Cell Dev Biol, 2017. **5**: p. 61.
249. Saxton, R.A. and D.M. Sabatini, *mTOR Signaling in Growth, Metabolism, and Disease.* Cell, 2017. **168**(6): p. 960-976.
250. Hay, N. and N. Sonenberg, *Upstream and downstream of mTOR.* Genes Dev, 2004. **18**(16): p. 1926-45.
251. Kapahi, P., et al., *With TOR, less is more: a key role for the conserved nutrient-sensing TOR pathway in aging.* Cell Metab, 2010. **11**(6): p. 453-65.
252. Ballou, L.M. and R.Z. Lin, *Rapamycin and mTOR kinase inhibitors.* J Chem Biol, 2008. **1**(1-4): p. 27-36.
253. Lamming, D.W., *Inhibition of the Mechanistic Target of Rapamycin (mTOR)-Rapamycin and Beyond.* Cold Spring Harb Perspect Med, 2016. **6**(5).
254. Katewa, S.D. and P. Kapahi, *Role of TOR signaling in aging and related biological processes in Drosophila melanogaster.* Exp Gerontol, 2011. **46**(5): p. 382-90.
255. Bertolio, R., et al., *Sterol regulatory element binding protein 1 couples mechanical cues and lipid metabolism.* Nat Commun, 2019. **10**(1): p. 1326.
256. Porstmann, T., et al., *SREBP activity is regulated by mTORC1 and contributes to Akt-dependent cell growth.* Cell Metab, 2008. **8**(3): p. 224-36.
257. Li, J., S.G. Kim, and J. Blenis, *Rapamycin: one drug, many effects.* Cell Metab, 2014. **19**(3): p. 373-9.
258. Layalle, S., N. Arquier, and P. Leopold, *The TOR pathway couples nutrition and developmental timing in Drosophila.* Dev Cell, 2008. **15**(4): p. 568-77.
259. Livingstone, C., *The insulin-like growth factor system and nutritional assessment.* Scientifica (Cairo), 2012. **2012**: p. 768731.
260. Niwa, Y.S. and R. Niwa, *Neural control of steroid hormone biosynthesis during development in the fruit fly Drosophila melanogaster.* Genes Genet Syst, 2014. **89**(1): p. 27-34.

261. Kannangara, J.R., C.K. Mirth, and C.G. Warr, *Regulation of ecdysone production in Drosophila by neuropeptides and peptide hormones.* Open Biol, 2021. **11**(2): p. 200373.
262. Mirth, C., J.W. Truman, and L.M. Riddiford, *The role of the prothoracic gland in determining critical weight for metamorphosis in Drosophila melanogaster.* Curr Biol, 2005. **15**(20): p. 1796-807.
263. Arrese, E.L. and J.L. Soulages, *Insect fat body: energy, metabolism, and regulation.* Annu Rev Entomol, 2010. **55**: p. 207-25.
264. Skowronek, P., L. Wojcik, and A. Strachecka, *Fat Body-Multifunctional Insect Tissue.* Insects, 2021. **12**(6).
265. Britton, J.S. and B.A. Edgar, *Environmental control of the cell cycle in Drosophila: nutrition activates mitotic and endoreplicative cells by distinct mechanisms.* Development, 1998. **125**(11): p. 2149-58.
266. Nijhout, H.F. and C.M. Williams, *Control of moulting and metamorphosis in the tobacco hornworm, Manduca sexta (L.): cessation of juvenile hormone secretion as a trigger for pupation.* J Exp Biol, 1974. **61**(2): p. 493-501.
267. Shingleton, A.W., *The regulation of organ size in Drosophila: physiology, plasticity, patterning and physical force.* Organogenesis, 2010. **6**(2): p. 76-87.
268. Murillo-Maldonado, J.M., et al., *Drosophila insulin pathway mutants affect visual physiology and brain function besides growth, lipid, and carbohydrate metabolism.* Diabetes, 2011. **60**(5): p. 1632-6.
269. Teleman, A.A., *Molecular mechanisms of metabolic regulation by insulin in Drosophila.* Biochem J, 2009. **425**(1): p. 13-26.
270. Owonikoko, T.K. and F.R. Khuri, *Targeting the PI3K/AKT/mTOR pathway: biomarkers of success and tribulation.* Am Soc Clin Oncol Educ Book, 2013.
271. Paplomata, E. and R. O'Regan, *The PI3K/AKT/mTOR pathway in breast cancer: targets, trials and biomarkers.* Ther Adv Med Oncol, 2014. **6**(4): p. 154-66.
272. Ahmad, M., et al., *Evolutionary responses of Drosophila melanogaster under chronic malnutrition.* Front Ecol Evol, 2018. **6**.
273. Ward, C., et al., *Autophagy, lipophagy and lysosomal lipid storage disorders.* Biochim Biophys Acta, 2016. **1861**(4): p. 269-84.
274. Clancy, D.J., et al., *Extension of life-span by loss of CHICO, a Drosophila insulin receptor substrate protein.* Science, 2001. **292**(5514): p. 104-6.
275. Kenyon, C.J., *The genetics of ageing.* Nature, 2010. **464**(7288): p. 504-12.
276. Tee, A.R., *The Target of Rapamycin and Mechanisms of Cell Growth.* Int J Mol Sci, 2018. **19**(3).
277. Mulder, F.V.M., et al., *The long-term effect of mTOR inhibition on lipid and glucose metabolism in tuberous sclerosis complex: data from the Dutch TSC registry.* Orphanet J Rare Dis, 2022. **17**(1): p. 252.
278. Leroith, D., E.J. Scheinman, and K. Bitton-Worms, *The Role of Insulin and Insulin-like Growth Factors in the Increased Risk of Cancer in Diabetes.* Rambam Maimonides Med J, 2011. **2**(2): p. e0043.
279. Laron, Z., *Insulin-like growth factor 1 (IGF-1): a growth hormone.* Mol Pathol, 2001. **54**(5): p. 311-6.
280. Zhao, Q., S.M. Gao, and M.C. Wang, *Molecular Mechanisms of Lysosome and Nucleus Communication.* Trends Biochem Sci, 2020. **45**(11): p. 978-991.
281. Metallo, C.M. and M.G. Vander Heiden, *Understanding metabolic regulation and its influence on cell physiology.* Mol Cell, 2013. **49**(3): p. 388-98.
282. Rhee, H.W., et al., *Proteomic mapping of mitochondria in living cells via spatially restricted enzymatic tagging.* Science, 2013. **339**(6125): p. 1328-1331.
283. Paek, J., et al., *Multidimensional Tracking of GPCR Signaling via Peroxidase-Catalyzed Proximity Labeling.* Cell, 2017. **169**(2): p. 338-349 e11.

284. Lobingier, B.T., et al., *An Approach to Spatiotemporally Resolve Protein Interaction Networks in Living Cells.* Cell, 2017. **169**(2): p. 350-360 e12.
285. Martell, J.D., et al., *Engineered ascorbate peroxidase as a genetically encoded reporter for electron microscopy.* Nat Biotechnol, 2012. **30**(11): p. 1143-8.
286. Shen, W. and B. Ganetzky, *Autophagy promotes synapse development in Drosophila.* J Cell Biol, 2009. **187**(1): p. 71-9.